UC San Diego

UC San Diego Electronic Theses and Dissertations

Title

Characterization of Chromosomal Abnormalities Reveals Non-Canonical Hippo Kinase Functions in Hematologic Malignancy

Permalink

https://escholarship.org/uc/item/79k7f6zm

Author

Stoner, Samuel Alton

Publication Date

2019

Peer reviewed|Thesis/dissertation

eScholarship.org Powered by the California Digital Library
University of California

UNIVERSITY OF CALIFORNIA SAN DIEGO

Characterization of Chromosomal Abnormalities Reveals Non-Canonical Hippo Kinase Functions in Hematologic Malignancy

A dissertation submitted in partial satisfaction of the
requirements for the degree Doctor of Philosophy

in

Biomedical Sciences

by

Samuel Alton Stoner

Committee in charge:

Professor Dong-Er Zhang, Chair
Professor Rafael Bejar
Professor Steven Dowdy
Professor Kun-Liang Guan
Professor David Traver

2019

Copyright

Samuel Alton Stoner, 2019

All rights reserved.

The Dissertation of Samuel Alton Stoner is approved, and it is acceptable in quality and form for publication on microfilm and electronically:

Chair

University of California San Diego

2019

TABLE OF CONTENTS

Signature page iii

Table of Contents iv

List of Figures vi

List of Tables x

Acknowledgements xi

Vita xii

Abstract of the Dissertation xiii

Chapter 1. Introduction 1
1.1. Del(20q) chromosomal abnormality in hematological malignancy 1
1.1.1. Del(20q) in Myelodysplastic Syndrome 3
1.1.2. Del(20q) in classical Myeloproliferative Neoplasm 5
1.1.3. Del(20q) in additional hematological malignancies and clonal hematopoiesis 7
1.1.4. Genomic mapping of the minimal common deleted region 9
1.1.5. Functional characterization of del(20q)-relevant genes 13
1.1.6. Cooperating mutations in del(20q) malignancies 21
1.2. t(8;21) chromosomal translocation in AML 22

Chapter 2. Hippo Kinase Loss Contributes to Del(20q) Hematologic Malignancies through Chronic Innate Immune Activation 24
2.1. Introduction 26
2.2. Results 29
2.2.1. Hippo kinase *STK4* is transcriptionally downregulated in del(20q) MDS and MPN patients 29
2.2.2. Hematopoietic-specific Hippo kinase inactivation results in lethal bone marrow failure with clinical features of del(20q) MDS 34
2.2.3. Inducible Hippo kinase inactivation recapitulates features of MDS and MPN in adult mice 42
2.2.4. Hippo kinase inactivation promotes macrothrombocytopenia upon aging even in absence of malignant clonal HSC expansion 46
2.2.5. Heterozygous Hippo kinase inactivation cooperates with JAK2-V617F to promote lethal myelofibrosis 57
2.2.6.*Stk4* loss cooperates with JAK2-V617F to activate innate immune responses and proinflammatory cytokine production 58
2.2.7. MST1 negatively regulates IRAK1/TRAF6-mediated innate immune activation of NF-κB 62

2.2.8. IRAK1 inhibition rescues the aberrant inflammatory cytokine production associated with Hippo kinase loss in MPN 66
2.3. Discussion 71
2.4. Materials and Methods 75

Chapter 3. A non-canonical Hippo-RASSF2 signaling pathway controls Rac-GTPase activation and is therapeutically exploitable in hematologic cancer 92
3.1. Introduction 93
3.2. Results 96
3.2.1. *RASSF2* transcription is differentially-regulated across specific AML subtypes 96
3.2.2. Re-expression of RASSF2 is tumor-suppressive specifically in (t8;21) AML. 101
3.2.3. RASSF2 function is unrelated to oncogenic Ras signaling or nucleo-cytoplasmic shuttling in hematologic cancer 108
3.2.4. RASSF2-mediated functions are dependent on interaction with Hippo kinases MST1/2 111
3.2.5. SARAH domain-mediated stabilization of RASSF2 is a non-canonical MST1 signaling mechanism with functional consequences in leukemia.. 115
3.2.6. Proximity-dependent biotin labeling defines the endogenous RASSF2-proximal proteome and reveals a novel role in regulation of Rac GTPase activation via DOCK2 121
3.2.7. RASSF2 is a critical regulator of Rac GTPase activation in acute myeloid leukemia 129
3.2.8. RASSF2 expression predicts sensitivity to small-molecule inhibition of DOCK2 GEF activity as a therapeutic strategy in myeloid leukemia 137
3.3. Discussion 142
3.4. Materials and Methods 145

References 160

LIST OF FIGURES

Figure 1.1 Summary of genomic mapping of the del(20q) minimal common deleted region (CDR) in hematological malignancy patients and individuals with clonal hematopoiesis associated with aging 12

Figure 2.1 Hippo kinase *STK4* is located in the 20q CDR and downregulated in MDS and MPN patients with del(20q) 31

Figure 2.2 Assessment of 20q gene expression in myelofibrosis patients 32

Figure 2.3 Position of *STK4* within the del(20q) common deleted region 33

Figure 2.4 Conditional Hippo kinase inactivation in hematopoietic cells..... 36

Figure 2.5 Hematopoietic-specific inactivation of Hippo kinases results in lethal bone marrow failure with frequent extramedullary erythropoiesis in the spleen 37

Figure 2.6 Hypocellular bone marrow and pancytopenia in Hippo kinase knockout mice 39

Figure 2.7 Granulocytic skewing in bone marrow and spleen of Hippo kinase knockout mice 40

Figure 2.8 Frequent megakaryocytic abnormalities in Hippo kinase knockout mice 41

Figure 2.9 Experimental strategy for inducible somatic inactivation of Hippo kianses Stk4 and Stk3..... 43

Figure 2.10 Inducible somatic Hippo kinase inactivation recapitulates clinical features of del(20q) MDS and MPN 44

Figure 2.11 Selection pressure towards non-excised alleles upon aging in Mx1-Cre model 45

Figure 2.12 Hippo kinase inactivation does not provide a competitive HSC advantage 47

Figure 2.13 Hippo kinase-deficient hematopoietic cells fail to properly engraft in bone marrow 48

Figure 2.14 Heterozygous Hippo kinase inactivation does not promote malignant HSC expansion in the bone marrow..... 49

Figure 2.15 Heterozygous Hippo kinase inactivation promotes macrocytic thrombocytopenia upon aging 50

Figure 2.16 Modeling heterozygous Hippo kinase inactivation in a JAK2-V617F MPN model 53

Figure 2.17 Heterozygous Hippo kinase inactivation cooperates with JAK2-V617F to promote lethal myelofibrosis 54

Figure 2.18 Enhanced reticulin bone marrow fibrosis in JAK2-V617F;$Stk4^{+/-}$$Stk3^{+/-}$ mice 55

Figure 2.19 Additional characterization of bone marrow and splenic fibrosis in moribund JAK2-V617F;$Stk4^{+/-}$$Stk3^{+/-}$ mice 56

Figure 2.20 Hippo kinase deletion cooperates with JAK2-V617F to activate innate immune response and proinflammatory cytokine production 60

Figure 2.21 JAK2-V617F expression has a greater effect on serum cytokine variance than does genotype 61

Figure 2.22 MST1 negatively regulates NF-κB activation through IRAK1 64

Figure 2.23 MST1 negatively regulates innate immune activation through IRAK1/TRAF6 65

Figure 2.24 IRAK1 inhibition rescues the aberrant proinflammatory cytokine production associated with Hippo kinase loss in MPN 68

Figure 2.25 IRAK1 inhibition reduces aberrant NF-κB activation associated with *STK4* knockdown 69

Figure 2.26 IRAK1 inhibition does not rescue additional hematopoietic phenotypes associated with homozygous somatic Hippo kinase inactivation 70

Figure 3.1 Expression and transcriptional regulation of *RASSF2* in normal human hematopoiesis 98

Figure 3.2 Transcriptional repression of *RASSF2* specifically in t(8;21) AML patients 99

Figure 3.3 t(8;21) oncofusion protein RUNX1-ETO downregulates *RASSF2* transcription 100

Figure 3.4 RASSF2 re-expression screen in a panel of AML cell lines 103

Figure 3.5 RASSF2 suppresses RUNX1-ETO leukemic transformation ability in a serial replating / colony formation assay 104

Figure 3.6 Re-expression of RASSF2 prolongs survival in a RUNX1-ETO9a (RE9a) primary murine leukemia model 105

Figure 3.7 Peripheral blood parameters in the RE9a / Rassf2 primary AML model 106

Figure 3.8 Representative Wright-Giemsa stained cytospins from moribund leukemic splenocytes of the indicated mice 107

Figure 3.9 RASSF2 is exclusively localized in the cytoplasmic fraction in leukemia cells 109

Figure 3.10 RASSF2 expression does not affect oncogenic Ras signaling in AML. 110

Figure 3.11 Schematic of RASSF2 proteins expressed in replating assays.....112

Figure 3.12 RASSF2 SARAH domain is required for suppression of RUNX1-ETO leukemic transformation ability 113

Figure 3.13 RASSF2-mediated suppression of RUNX1-ETO leukemic transformation is dependent on presence of Hippo kinases MST1/2 (*STK4/3*)..... 114

Figure 3.14 RASSF2 does not affect signaling through canonical Hippo pathway targets MOB1 and LATS1 117

Figure 3.15 MST1 functions as a tumor suppressor in t(8;21) AML independent of kinase activity..... 118

Figure 3.16 RASSF2 stability is dependent on the Hippo kinase SARAH domain.. 119

Figure 3.17 Destabilization of RASSF2 in Hippo kinase knockout hematopoietic stem/progenitor cells 120

Figure 3.18 Mapping the RASSF2-proximal proteome by proximity-based biotin labeling (BioID2)..... 125

Figure 3.19 Proximity-based biotin labeling identifies RASSF2 endogenous interactions with Rho-GTPase related proteins 126

Figure 3.20 RASSF2 interacts with DOCK2 and positively regulates GEF activity towards Rac-GTP..... 127

Figure 3.21 MST1 stabilizes RASSF2 interaction with DOCK2 and increases DOCK2-mediated Rac activation 128

Figure 3.22 *RASSF2* knockdown impairs basal Rac-GTPase activation in AML…. 131

Figure 3.23 *RASSF2* knockdown by four independent shRNAs in AML cells…….. 132

Figure 3.24 *RASSF2* knockdown impairs cell proliferation and causes G0/G1 cell cycle arrest in AML cells *in vitro* and *in vivo* 133

Figure 3.25 *RASSF2* knockdown profoundly alters the transcriptional signatures of AML cells 134

Figure 3.26 *RASSF2* knockdown-dependent cell cycle arrest is associated with an activated Rb signature and inhibited E2F transcription factor activity 135

Figure 3.27 CPYPP treatment in panel of AML cell lines with varied expression of RASSF2 139

Figure 3.28 RASSF2 expression is the best predictor for sensitivity to small molecule inhibition of DOCK2/Rac-GTP in AML cells 140

Figure 3.29 Therapeutic targeting of DOCK2 in primary AML patient cells with CPYPP 141

LIST OF TABLES

Table 1.1. Summary of del(20q) minimal common deleted region genomic mapping. 11

Table 1.2. Summary of functional studies characterizing del(20q) CDR genes in hematological context. 20

Table 3.1 RASSF2-proximal proteome as identified by BioID method..... 124

ACKNOWLEDGEMENTS

I would like to thank my mentor Dong-Er Zhang, for being a constant source of positive support and encouragement, both scientifically and personally, throughout the course of the PhD. I truly appreciate the time that I shared with all current and former members of the Zhang Lab throughout the course of this PhD, it would not have been possible without all of you. I thank all of my committee members, for providing meaningful scientific help and career guidance. I am truly grateful for the guidance each committee member and my advisor have provided towards my development as a scientist. Of course, none of this would be possible without the love and support of my family, especially my parents and sister; as well as many many friends that have always been there for me over the years.

Chapter 1, in part, is being prepared for submission for publication by: Stoner SA and Zhang DE. The dissertation author is the primary investigator and author of the manuscript.

Chapter 2, in full, has been submitted for publication. Stoner SA, Yan M, Liu K, Arimoto K, Shima T, Wang HY, Johnson DT, Bejar R, Jamieson C, Guan KL, and Zhang DE. “Hippo Kinase Loss Contributes to Del(20q) Hematologic Malignancies through Chronic Innate Immune Activation.” The dissertation author is the primary investigator and author of the manuscript.

Chapter 3, in part, is being prepared for submission for publication by: Stoner SA, Liu K, Andrews ET, Davis AG, Arimoto K, Yan M, and Zhang DE. The dissertation author is the primary investigator and author of the manuscript.

VITA

2011 Bachelor of Science, University of California San Diego

2019 Doctor of Philosophy, University of California San Diego

PUBLICATIONS

1. Arimoto KI, Miyauchi S, **Stoner SA**, Fan JB, and Zhang DE. Negative Regulation of Type I Interferon Signaling. *Journal of Leukocyte Biology*. 2018 Jan. Review.

2. Arimoto KI*, Lochte S*, **Stoner SA**, Burkart C, Zhang Y, Miyauchi S, Wilmes S, Fan JB, Heinisch JJ, Li Z, Yan M, Pellegrini S, Colland F, Piehler J, and Zhang DE. STAT2 is an Essential Adaptor in USP18-mediated Suppression of Type I Interferon Signaling. *Nat Struct Mol Biol*. 2017 Mar;24(3):279-289.

3. Weng S, Matsuura S, Mowery CT, **Stoner SA**, Lam K, Ran D, Davis AG, Lo MC, Zhang DE. Restoration of MYC-repressed Targets Mediates the Negative Effects of GM-CSF on RUNX1-ETO Leukemogenicity. *Leukemia*. 2017 Jan;31(1):159-169.

4. Weng S, **Stoner SA**, Zhang DE. Sex Chromosome Loss and the Pseudoautosomal Region Genes in Hematological Malignancies. *Oncotarget*. 2016 Nov 1;7(44):72356-72372. Review..

5. **Stoner SA***, Duggan E*, Condello D, Guerrero A, Turk JR, Narayanan PK, Nolan JP. High Sensitivity Flow Cytometry of Membrane Vesicles. *Cytometry A*. 2016 Feb;89(2):196-206..

6. Nolan JP, **Stoner SA.** A Trigger Channel Threshold Artifact in Nanoparticle Analysis. *Cytometry A.* 2013 Mar;83(3):301-5.

7. Nolan JP, Duggan E, Liu E, Condello D, Dave I, **Stoner SA**. Single Cell Analysis Using Surface Enhanced Raman Scattering (SERS) Tags. *Methods.* 2012 Jul;57(3):272-9.

* Denotes equal authorship

ABSTRACT OF THE DISSERTATION

Characterization of Chromosomal Abnormalities Reveals Non-Canonical Hippo Kinase Functions in Hematologic Malignancy

by

Samuel Alton Stoner

Doctor of Philosophy in Biomedical Sciences

University of California San Diego, 2019

Professor Dong-Er Zhang, Chair

Chromosomal abnormalities are frequent events in human cancer and are especially prevalent in hematological malignancies. Here, through the characterization of chromosomal abnormalities del(20q) and t(8;21) we reveal unexpected non-canonical functions of the mammalian Hippo kinase in hematologic cancer.

Somatic heterozygous deletions on chromosome 20q are detected in several hematopoietic malignancies, including myelodysplastic syndrome (MDS), classical

myeloproliferative neoplasm (MPN), MDS/MPN overlap disorders, and acute leukemias. To date, identification of genes in the del(20q) common deleted region that contribute to disease development have remained elusive. Through assessment of patient gene expression we have identified *STK4* (encoding Hippo kinase MST1) as a 20q gene that is downregulated below haploinsufficient amounts in MDS and MPN. Functional modeling of hematopoietic-specific gene inactivation in mice revealed Hippo kinase loss to cause phenotypes that closely resemble those observed in patients harboring del(20q), and to cooperate with JAK2-V617F mutation in promoting adverse MPN disease progression to myelofibrosis. Mechanistic studies revealed that myelofibrotic transformation in mice was associated with cooperative effects of JAK2-V617F and Hippo kinase inactivation on IRAK1-dependent innate immune-associated proinflammatory cytokine production, including IL-1β and IL-6. In summary, we find Hippo kinase MST1 (*STK4*) as having a central role in the biology of del(20q)-associated hematologic malignancies.

Through biochemical and functional studies based on the characterization of t(8;21) in acute myeloid leukemia, we also define a novel Hippo-RASSF2 signaling pathway that regulates basal Rac GTPase activity in hematological cancer and can be exploited for therapy in patients. This non-canonical signaling mechanism is independent of Hippo kinase activity, and is instead mediated by a SARAH domain-dependent interaction. Using proximity-based biotin labeling, we associate RASSF2 with Rho GTPase-related complexes and identify a direct interaction with the critical Rac guanine nucleotide exchange factor (GEF), DOCK2. RASSF2 promotes DOCK2 GEF activity *in vitro*; and *RASSF2* knockdown is sufficient to functionally abolish

GTP-bound Rac and promote growth-arrest in leukemia cells. Importantly, RASSF2 expression is broadly correlated with leukemia cell sensitivity to small-molecule inhibition of DOCK2 GEF activity, revealing novel mechanistic insight and providing a functional biomarker for sensitivity to perturbation of this pathway in hematological cancer.

Chapter 1. Introduction

1.1. Del(20q) chromosomal abnormality in hematological malignancy

Heterozygous somatic deletions within the q arm of chromosome 20, or del(20q), are among the most frequently detected chromosomal abnormalities in overt myeloid neoplasms such as myelodysplastic syndrome (MDS) and classical myeloproliferative neoplasm (MPN), as well as in clonal hematopoiesis associated with aging. Del(20q) is especially prevalent in MPN, where it is the most frequent cytogenetic abnormality found in primary myelofibrosis. When present as a sole chromosomal abnormality, del(20q) is typically associated with a favorable prognosis in patients. Thrombocytopenia, or a relatively reduced platelet count, is the most consistent hematological phenotype across both MDS and MPN patients harboring del(20q), suggesting that it is a defining clinical feature caused by this chromosomal abnormality. Genomic studies have mapped a minimal common deleted region shared among patient cohorts that is centered on chromosome 20q11.23 – 20q13.12. To date, functional analyses and modeling in mice have implicated several genes in this region that contribute to del(20q)-associated hematologic malignancies: *L3MBTL1*, *MYBL2*, *PTPN1*, and *STK4*. Although there is no evidence of homozygous inactivation of del(20q) genes through mutation, functional modeling suggests that haploinsufficiency of these genes may uniquely contribute to the specific hematologic phenotypes that together define the clinical presentation of the del(20q) mutation in patients.

Chromosomal abnormalities are frequent events in human cancer and are especially prevalent in hematological malignancies[1]. Hematologic-specific examples of these abnormalities include recurring chromosomal translocations that are functional driver mutations in acute myeloid leukemia (AML), as well as large-scale genomic copy number gain/loss events, such as recurring interstitial chromosomal deletions observed across myeloid neoplasms, among numerous other examples[2]. The incorporation of this genomic information is essential for the clinical evaluation of hematological malignancy patients, and is informative with regards to diagnosis, prognosis, and choice of therapy[3].

Heterozygous somatic deletions within the q arm of chromosome 20 (del(20q)) are among the most frequent of these chromosomal abnormalities detected across several hematological malignancies, including myelodysplastic syndrome (MDS), classical myeloproliferative neoplasm (MPN), MDS/MPN overlap disorders such as chronic myelomonocytic leukemia (CMML), and acute leukemias. The presence of this chromosomal deletion event (which has since been mapped to human chromosome 20q) in myeloid neoplasms was first identified over 50 years ago[4,5]. Since then, a substantial body of both basic laboratory research and clinical investigation has significantly improved our understanding of the involvement of this chromosomal abnormality in diverse hematological malignancies. Here we will seek to comprehensively review del(20q) in hematological malignancy. First, we will briefly summarize the clinical characteristics, including prevalence, prognostic information, and unique hematological phenotypes associated with del(20q) across numerous myeloid neoplasms and in clonal hematopoiesis associated with aging. Then we will

discuss genomic mapping efforts performed to identify a 20q minimal common deleted region (CDR), and the associated functional and mechanistic consequences of loss of this genomic region as determined by characterizing inactivation of 20q genes in mouse models and biochemical studies.

1.1.1. Del(20q) in Myelodysplastic Syndrome

Myelodysplastic Syndrome (MDS) is a heterogeneous hematologic malignancy that is defined by peripheral cytopenias, cellular morphological dysplasia, aberrant clonal hematopoietic output, and increased propensity for transformation to acute leukemia[6]. Recurring large-scale chromosomal abnormalities are frequently detected in MDS and provide meaningful diagnostic and prognostic information in patients[6]. Del(20q) is typically reported at overall frequencies ranging between 2 – 7% in MDS patient cohorts[7-9], making it less common than other recurring cytogenetic abnormalities, such as del(5q) and monosomy 7 / del(7q). In contrast to some other cytogenetic abnormalities, detection of del(20q) in a bone marrow karyotypic analysis is not considered to be MDS-defining in a cytopenic patient without additional evidence of diagnostic morphologic dysplasia, according to WHO classification[2]. Incidental detection of del(20q) in bone marrow specimens, but in absence of peripheral cytopenias, was reported to not confer increased risk for later development of MDS[10]. Cases of therapy-related MDS with del(20q) are also rarely detected relative to other recurring cytogenetic abnormalities[11,12]. Del(20q), without the presence of other complex genetic abnormalities, confers a favorable prognosis

in MDS. Long-term follow-up in a large cohort of MDS patients revealed del(20q) as a sole abnormality to confer overall median survival of ~5.9 years[8], however this rapidly declines if it is part of a more complex karyotype. The revised MDS International Prognostic Scoring System (IPSS-R)[13], which incorporates five cytogenetic prognostic subgroups, includes del(20q) as a single abnormality in the 'Good' subgroup. This is the second-most favorable prognostic group, and is associated with a median overall survival of ~4.1 years[14].

In the largest analyzed cohort of 217 patients with del(20q) MDS, 161 (~75%) had MDS without evidence of blast increase, the majority of which were classified as refractory anemia / refractory cytopenia with unilineage dysplasia (RA/RCUD)[11]. Among the remaining ~25% of patients with advanced MDS, the majority were classified as refractory anemia with excess blasts type 1 (RAEB-1). Assessment of MDS patients with del(20q) as a sole cytogenetic abnormality has revealed specific clinical characteristics and phenotypes that are associated with this molecular lesion[11,15,16]. MDS with del(20q) as a sole abnormality frequently presents as an indolent disease with isolated thrombocytopenia and minimal evidence of morphological dysplasia that is restricted to the erythroid and megakaryocytic lineages[15,16]. As such, reduced platelet count compared to non-del(20q) MDS (mean 144 versus 196 x 10^9/L) has been reported as a significant clinical phenotypic feature associated with this abnormality[15]. Importantly, this thrombocytopenia phenotype is consistently observed in del(20q) across additional hematologic malignancies (see further discussion of MPN below), suggesting that it is a defining feature of chromosome 20q deletions. Anemia is often observed, though less frequently than

thrombocytopenia, and if present is typically mild and normocytic in sole del(20q) MDS[15,16]. Lower bone marrow blast frequencies (mean 3.9% versus 5.6%) have also been reported for patients with sole del(20q) MDS relative to non-del(20q) MDS[15]. Despite the lower blast counts, the rate of progression to AML among sole del(20q) patients is similar to that observed in patients with non-del(20q) favorable karyotype MDS[11,15]. Within del(20q) MDS patients, co-mutation of *ASXL1* is associated with significantly inferior survival and accelerated transformation to AML[11], demonstrating that evaluation of *ASXL1* status is particularly important in MDS patients harboring del(20q).

1.1.2. Del(20q) in classical Myeloproliferative Neoplasm

The classical myeloproliferative neoplasms (MPNs), also known as *BCR-ABL*$^{-}$ MPNs, are classified into three distinct entities that are defined by the overproduction of terminally differentiated blood cells. Polycythemia Vera (PV) is characterized by excessive production of erythrocytes with variable megakaryocytic and granulocytic hyperplasia; Essential thrombocythemia (ET) is characterized by excessive platelet production and megakaryocytic hyperplasia; and Primary Myelofibrosis (PMF) presents with more heterogenenous phenotypes, but is characterized by bone marrow fibrosis, myeloproliferation in the spleen, and variable megakaryocytic hyperplasia[17]. Del(20q) is among the most frequently detected cytogenetic abnormality in MPN patients, where it is typically reported at frequencies between 7 – 25% in patient cohorts overall[18-21]. Furthermore, it is the most frequently detected

cytogenetic abnormality in PMF[18,21], making this mutation a high priority for further characterization in this disease context. Among MPNs, prognosis of PMF patients in particular remains dismal[22]. Incorporation of cytogenetics, in addition to other factors and hematological phenotypes, is informative with regards to prognosis and risk stratification in PMF[23]. A recently revised cytogenetic risk stratification in PMF identifies del(20q) as a sole chromosomal abnormality to be included in the 'favorable' risk category, for which median survival in patients is ~4.4 years[21]. In this cohort, the survival of patients with del(20q) as a sole abnormality is not significantly different from patients with normal karyotype[21]. Del(20q) does not appear to be associated with any change in risk for MPN transformation to AML[24].

Within MPNs, PMF has the highest frequency of cytogenetic abnormalities overall[19]. Interestingly, del(20q) mutation appears to be exclusively associated with PV, PMF, and post-PV myelofibrosis, but almost never detected in ET[19]. Similar as to in MDS, thrombocytopenia is a significant clinical phenotypic correlate in del(20q) PMF patients, (~50% of patients with platelet counts $<100 \times 10^9/L$)[20]. Together, these findings reinforce the idea that impaired platelet production is a defining feature of the del(20q) mutation, regardless of type of malignancy. Peripheral leukopenia has also been reported as a significant phenotypic correlate that appears to be unique among del(20q) PMF patients, and leukocytosis is less frequently observed in del(20q) PMF relative to non-del(20q) PMF[20].

1.1.3. Del(20q) in additional hematologic malignancies and clonal hematopoiesis

There are many documented cases of detection of del(20q) clones in patients initially diagnosed with immune thrombocytopenia (ITP, formerly designated as idiopathic thrombocytopenic purpura), an acquired autoimmune disorder resulting in immune-mediated destruction of platelets[25,26]. These diagnoses are typically made upon bone marrow examination of elderly patients that have not responded to standard ITP therapy[26]. Given the hypodysplastic nature and frequent isolated thrombocytopenic presentation of MDS with del(20q) as a sole abnormality[11,15,16], these likely represent misdiagnosis of an indolent MDS without clear evidence of cellular morphological dysplasia. Incorporation of cytogenetic analysis from bone marrow sampling is therefore critical for distinction between MDS with del(20q) and ITP[16].

Del(20q) is detected at appreciable frequency in the MDS/MPN overlap disorder CMML. Approximately 30% of CMML patients are detected with abnormal karyotype. Del(20q) is among the most frequent of these, being detected in ~8% of CMML patients overall[27,28]. In contrast to MDS, CMML-specific cytogenetic risk stratification incorporates del(20q) mutations in the intermediate risk group, demonstrating that it is not universally associated with a more favorable prognosis across all hematologic malignancies[29,30]. Based on one study of 38 patients, del(20q) appears to be especially prevalent in MPN with chronic eosinophila, where it was the most frequently detected large-scale genomic loss event (32%)[31].

In the absence of overt cancer, somatic mosaic chromosomal abnormalities are detectable in the peripheral blood at frequencies that increase with age and approach 1 - 2% of individuals by 75 years[32,33]. Detectable age-related clonal hematopoiesis is also associated with single nucleotide variants in genes that are commonly mutated in overt hematological malignancy, such as *DNMT3A*, *TET2*, and *ASXL1*[34,35]. Detection of these events is associated with significantly increased risk for later development of hematological cancer, demonstrating a biologically meaningful existence of 'pre-malignant' clonal hematopoiesis that coincides with aging[32-37]. Recently, it has become appreciated that somatic deletions within chromosome 20q are the most common large-scale chromosomal abnormality detected in the peripheral blood of the aging human population. Del(20q) has been detected in aging individuals without overt evidence of myeloid malignancy at prevalences of 0.11%[38] and 0.09%[39], or approximately one in 1000 individuals over the age of 55. Assessment of health outcomes (4 – 9 years post DNA sampling) in the largest cohort of individuals to date, found the presence of somatic heterozygous del(20q) mutations to confer significantly increased risk for development of any blood cancer, further demonstrating that this mutation is of functional consequence and not simply a passenger mutation[39]. The presence of multiple genes within the deleted region of chromosome 20q encoding transcriptional regulatory proteins that contribute to cell cycle progression and differentiation of hematopoietic stem cells (HSCs) likely underlies the association between del(20q) and clonal hematopoiesis (see further discussion below).

1.1.4. Genomic mapping of the minimal common deleted region

Genomic mapping of the minimal common deleted region (CDR) of large-scale genomic loss events has facilitated identification of the critical genes and underlying molecular mechanisms associated with myeloid malignancy. A variety of methods have been utilized to define the minimally common deleted region (CDR) shared amongst all individuals harboring del(20q) mutations (**Table 1.1, Figure 1.1**)[11,38,40-46]. Two early studies using Microsatellite PCR defined a highly similar CDR across MDS, MPN, and AML patients; which maps to an approximately 5 Mb region spanning chromosome 20q12 – 20q13.12[40,41]. Using fluorescence *in situ* hybridization (FISH), a follow-up study further narrowed the CDR to an approximately 1.7 Mb region that was common between MDS and MPN patients[42]. A nearly identical minimal 1.7 Mb CDR was recently recapitulated by SNP-array in a large cohort of individuals harboring clonal somatic del(20q) mutations in their peripheral blood without overt hematologic cancer[38]. The majority of mapping studies to date have defined a similar region, albeit slightly larger and extended at the telomeric side within 20q13.12[11,44,46]. As such, most of the initial del(20q) functional studies have focused on characterization of genes located within the minimally-defined 1.7 Mb CDR spanning chromosome 20q11.23– 20q13.12.

Interestingly, at least two studies did not identify a conclusive CDR shared amongst all individuals with del(20q) in their cohorts of 23 and 130 individuals, respectively[39,45]. The first of these studies proposed the idea for two distinct CDRs, one within band q11.23, and another within band q13.12, however these regions were primarily defined by the unique breakpoints of a single patient[45]. In the most

comprehensive analysis of clonal somatic chromosomal alterations to date, including SNP-array mapping for 130 individuals with chromosome 20q deletions[39], it is readily apparent that there is no definitive CDR shared amongst all of these individuals. Further complicating interpretation of critical genes in the del(20q) region, it is important to note that the minimal CDR does not reflect the typical size of the deleted region in individuals. In fact, the majority of individuals harbor significantly larger deletions that are greater than 10 Mb, with an average size of 15-20 Mb, and there is a large amount of variation in breakpoints between individuals. It is also important to note that individuals in this cohort[39] do not have overt hematologic malignancy, only age-related clonal hematopoiesis, and whether specific gene deletion events may skew the propensity for overt malignancy may warrant further investigation.

Table 1.1. Summary of del(20q) minimal common deleted region genomic mapping.

MDS, myelodysplastic syndrome; MPN, myeloproliferative neoplasm; AML, acute myeloid leukemia; CDR, common deleted region; PCR, polymerase chain reaction; FISH, fluorescence *in situ* hybridization; CGH, comparative genomic hybridization; SNP, single nucleotide polymorphism.

Study	Cohort	Method	Minimal CDR
Wang, *et al.* (1998)[40]	23 patients (MDS, MPN, AML)	Microsatellite PCR	5.8 Mb, 20q12-20q13.12 (hg38: chr20:39,662,385-45,267,845)
Bench, *et al.* (1998)[41]	31 patients (MDS and MPN)	Microsatellite PCR	MDS: 5.0 Mb, 20q12-20q13.12 (hg38: chr20:40,168,149-45,139,903) MPN: 6.0 Mb, 20q12-20q13.12 (hg38: chr20:39,096,517-45,139,903)
Bench, *et al.* (2000)[42]	42 patients (MDS, MPN, AML)	FISH	1.7 Mb, 20q12-20q13.12 (hg38: chr20:42,201,801-44,069,496)
Douet-Guilbert, *et al.* (2008)[43]	38 patients (MDS, MPN, MDS/MPN)	FISH	6.6 Mb, 20q11.23-20q13.12 (hg38: chr20:38,533,628-44,815,789)
Schaub, *et al.* (2009)[44]	8 patients (MPN)	Array-CGH	9.0 Mb, 20q11.23-20q13.12
Huh, *et al.* (2010)[45]	23 patients (MDS, MPN, AML)	SNP Array	CDR1: 2.5 Mb, 20q11.23-20q12 (hg18: chr20:34968,632-37,417,814) CDR2: 1.8 Mb, 20q13.12 (hg18: chr20:43,636,105-45,417,399)
Okada, *et al.* (2012)[46]	12 patients (MDS, MPN, AML)	Array-CGH	7.2 Mb, 20q12-20q13.13 (hg18: chr20:39,933,662-47,180,979)
Bacher, *et al.* (2014)[11]	30 patients (MDS)	Array-CGH	4.6 Mb, 20q12-20q13.12 (hg18: chr20:41,067,253-45,700,000)
Machiela, *et al.* (2017)[38]	107 individuals w/o hematologic malignancy (clonal hematopoiesis)	SNP Array	1.7 Mb, 20q12-20q13.12 (hg18: chr20:40,425,000-42,155,000)
Loh, *et al.* (2018)[39]	130 individuals w/o hematologic malignancy (clonal hematopoiesis)	SNP Array	None defined

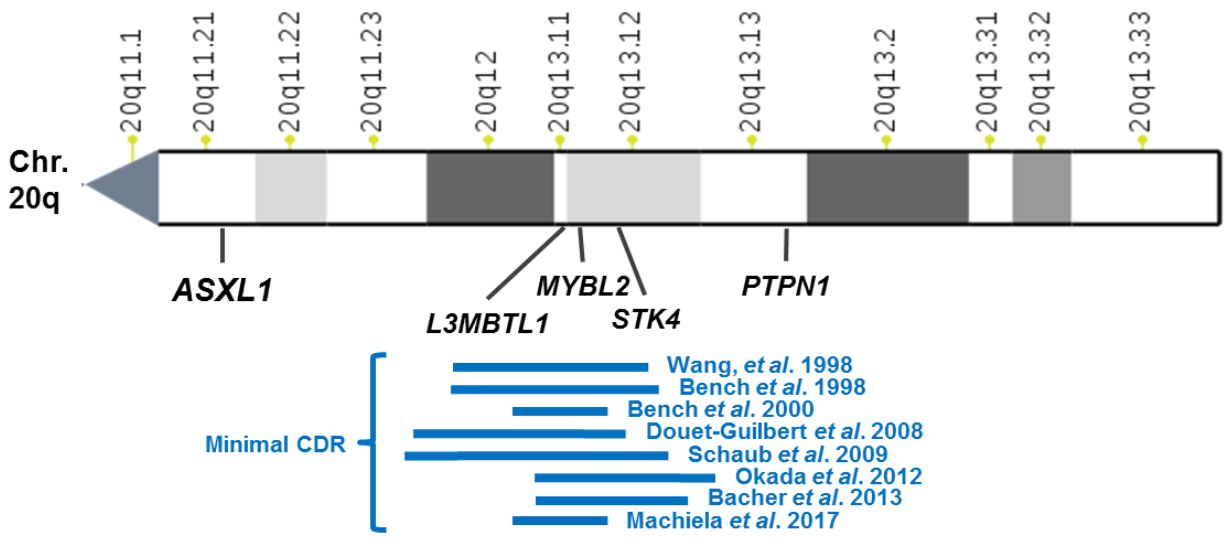

Figure 1.1. Summary of genomic mapping of the del(20q) minimal common deleted region (CDR) in hematological malignancy patients and individuals with clonal hematopoiesis associated with aging.

1.1.5. Functional characterization of del(20q)-relevant genes

Several attempts to identify loss of heterozygosity (LOH) of individual genes or regions on the intact chromosome 20 have been performed, with no success to date. These results suggest that combined haploinsufficiency of multiple 20q genes is likely more important for disease onset than complete inactivation of a single tumor suppressor. The absence of homozygous deletions may also indicate that inactivation of one or more genes within the 20q CDR is incompatible with normal adult hematopoiesis and/or detrimental to clonal hematopoietic stem cell (HSC) outgrowth. Importantly, a portion of the 20q CDR was found to be a maternally-imprinted locus in humans[47]. At least two genes, *L3MBTL1* and *SGK2*, show complete loss of transcript expression via imprinting in del(20q) patient-derived CD34+ hematopoietic cells and in two AML cell lines with heterozygous del(20q)[48]. These findings are suggestive that specific deletion of the paternally-derived chromosome 20q locus favors development of malignancy, however further studies would be needed to clarify this. Against this idea, at least two studies have found evidence of both paternally-derived and maternally-derived del(20q) clones in patient cohorts[44,49]. Studies performing the functional characterization of del(20q) CDR genes in a hematological context are summarized in **Table 1.2.**

L3MBTL1, the first-identified candidate tumor suppressor within the del(20q) CDR, encodes a chromatin reader that is a homolog of *Drosophila* Polycomb-group proteins. L3MBTL1 promotes chromatin compaction and transcriptional repression through direct interaction with mono- and di-methylated lysine residues on histones H4 and H1b, in a manner dependent on three *malignant brain tumor* (MBT)-repeat

domains[47,50-53]. Initial chromatin immunoprecipitation (ChIP) analysis revealed L3MBTL1-bound targets to be enriched for Rb/E2F-regulated genes, including *MYC* and *CCNE1*, suggesting a role in cell cycle regulation[52]. L3MBTL1 was also found to associate with, and promote repression of, p53-target genes through a direct interaction with mono-methylated p53 protein[54]. Knockdown of *L3MBTL1* in non-hematopoietic cancer cell lines results in increased DNA damage and G2/M-phase cell cycle arrest[55]. In the hematopoietic context, shRNA-mediated knockdown of *L3MBTL1* in primary human CD34+ cells results in enhanced differentiation towards the erythroid, but not the megakaryocytic or myeloid lineage; potentially contributing to the high frequency of del(20q)-associated Polycythemia Vera (PV)[48,56]. In addition to increasing erythroid differentiation of HSCs, shRNA knockdown of *L3MBTL1* primes human induced pluripotent stem cells (iPSCs) towards hematopoietic commitment via de-repression of a BMP/SMAD5-dependent transcriptional network[57]. Together, these data demonstrate a meaningful physiological role for genetic-depletion of L3MBTL1 affecting hematopoietic cell-fate specification via its function as a repressive chromatin reader. Surprisingly, and contrary to these findings, mice with germline genetic inactivation of *L3mbtl1* were born at normal ratios with no developmental defects, and possessed no detectable hematopoietic phenotypes or altered cell cycle regulation[58]. Although these findings may convolute our understanding of L3MBTL1 as a critical del(20q) tumor suppressor in malignancy, it remains possible that genetic background or genetic compensation by other MBT-domain proteins[59] can explain the difference between mouse and human. To the best of our knowledge, whether somatic hematopoietic inactivation in adult mice (such as

using interferon-inducible *Mx1*-Cre) may produce different phenotypes has not been investigated.

MYBL2 (B-MYB) is a MYB-related transcription factor that plays an important role in cell-cycle progression in a variety of proliferating cell types, including hematopoietic stem cells and megakaryocytes[60,61]. Two independent studies found *MYBL2* expression to be significantly downregulated not only in del(20q) MDS patients, but also more broadly across MDS patients regardless of mutation status, highlighting its important role as a tumor suppressor in this disease[62,63]. Genetic modeling in mice has further revealed the importance of MYBL2 as a tumor suppressor in hematological malignancy, especially MDS. Conditional heterozygous inactivation of *Mybl2* increased the propensity for development of myeloid disease in aged (>52-weeks) mice, including MDS, MPN, and AML[62]. Similarly, shRNA-mediated knockdown of *Mybl2* to sub-haploinsufficient amounts promotes a competitive clonal growth advantage in HSCs and recapitulates myelodysplastic phenotypes in mice [63]. From a mechanistic standpoint, MYBL2 was recently found to be an important regulator of DNA double-strand break (DSB) repair in HSCs[64]. Here it was shown that both low *MYBL2*-expressing MDS patient-derived CD34+ cells and *Mybl2*$^{+/-}$ murine HSCs have delayed DSB repair kinetics, suggesting that del(20q)-associated MYBL2 loss may contribute to malignancy through increasing genomic instability.

PTPN1 (PTP1B) is a non-transmembrane protein tyrosine phosphatase that dephosphorylates numerous cellular targets, including JAK2[65]. As such, PTPN1 is considered an important negative regulator of JAK/STAT pathway activation in a

variety of cellular contexts[66]. Somatic inactivating mutations affecting *PTPN1* that result in increased JAK/STAT activation have been reported at high frequency in both Hodgkin lymphoma and primary mediastinal B cell lymphoma, highlighting a tumor suppressor role in hematopoietic cancer[67,68]. Similarly, alternative splice products of *PTPN1* have been reported to encode dominant negative proteins that can further contribute to enhanced JAK/STAT activation in Hodgkin lymphoma cells[69]. Although located slightly telomeric relative to the defined CDR (see Figure 1), *PTPN1* was recently identified as being deleted in a majority of del(20q) malignancy patients, with especially high prevalence in MPN[70]. Remarkably, this study found that conditional homozygous inactivation of *Ptpn1* in mice was sufficient to induce MPN-associated phenotypes, including splenomegaly, peripheral neutrophilia, and reticulin fibrosis in the bone marrow and spleen; as well as increase the activation of JAK/STAT and MAPK signaling in hematopoietic bone marrow cells. These data highlight a role for del(20q)-associated *PTPN1* loss contributing to MPN development by further amplifying driver mutation-mediated hyperactivation of the JAK/STAT signaling pathway.

STK4 (MST1) encodes a serine/threonine kinase that is one of two mammalian orthologues of *Drosophila* Hippo, an upstream regulator of the tumor suppressive Hippo signaling pathway[71]. In contrast to most tissues and solid tumor types, however, STK4 functions through numerous non-canonical mechanisms, rather than the canonical Hippo pathway, in the hematopoietic context[72]. Notably, STK4 has recently been found to be an important negative regulator of innate immune activation of NF-kB through TLR/IRAK1-dependent signaling pathways in

macrophages[73,74]. The importance of *STK4* in normal hematopoietic / immune cell function has been further revealed by the identification of rare individuals harboring homozygous germline inactivating mutations, which present as a combined immunodeficiency with frequent autoimmune manifestations[75-77]. Through assessment of published gene expression in MDS and MPN patient cohorts, we recently identified *STK4* as being consistently downregulated to sub-haploinsufficient amounts in patients harboring the del(20q) mutation. Through modeling conditional gene inactivation in mice we found that sub-haploinsufficient Hippo kinase inactivation induces a robust thrombocytopenia phenotype that is associated with megakaryocytic dysplasia, demonstrating the presence of this gene within the 20q deleted region to contribute to the distinct platelet-related phenotypes associated with del(20q) in patients. Importantly, we also found that heterozygous gene inactivation cooperates with JAK2-V617F expression to accelerate MPN progression to lethal myelofibrosis, which was mediated by cooperative activation of innate-immune proinflammatory cytokine expression, including IL-1B and IL-6. This aberrantly elevated proinflammatory cytokine production was IRAK1-dependent, revealing a potential therapeutic strategy for mitigating chronic innate immune activation associated with del(20q) in PMF. In long-term competitive bone marrow transplant assays heterozygous Hippo kinase inactivation was not sufficient to promote a clonal advantage in HSCs, suggesting that it must cooperate with loss of additional 20q genes, such as those described above, to drive the full del(20q) hematopoietic phenotype.

ASXL1 warrants its own special consideration in the context of chromosome 20q mutations. *ASXL1* mutations are among the most frequent recurrent somatic mutations in myeloid neoplasms and clonal hematopoiesis[78]. *ASXL1* mutations are located towards the C-terminal end of the translated protein and are primarily thought to result in loss-of-function or exert dominant negative function through expression of a C-terminally truncated protein[78]. Inactivation of ASXL1 in the hematopoietic context results in accelerated development of myeloid malignancies, myelodysplasia, and clonal HSC expansion through loss of interactions with Polycomb Repressive Complex 2 (PRC2) components and reduced H3K27me3 at genes poised for transcription in hematopoietic stem cells, such as the *HOXA* cluster[78-80]. *ASXL1* is located on the q arm of chromosome 20; however it falls well outside the defined minimal CDR to the centromeric side (**see Figure 1**). As such, *ASXL1* deletion occurs in only ~30% of all cases of del(20q), in which the deletion extends towards the centromere. Interestingly, at least one study identified multiple individual patients containing both a 20q deletion incorporating *ASXL1* loss and an *ASXL1* gene mutation, suggesting that in some rare cases *ASXL1* may experience homozygous inactivation through loss of heterozygosity in del(20q) MDS[11]. It was not definitively determined whether del(20q) and *ASXL1* mutation occurred within the same clone in these cases, however. This suggests that del(20q) patients may have variable *ASXL1* status that can include intact wild-type alleles, heterozygous inactivation, or homozygous inactivation. Importantly, *ASXL1* mutation was the only gene mutation found to be significantly associated with reduced overall survival in a large cohort of del(20q) MDS patients[11], highlighting the relevance of this status to disease

characterization. However, given that *ASXL1* is not located within the CDR and is intact in the majority of del(20q) patients, it is difficult to consider as a true driver of the del(20q) hematopoietic phenotype.

Table 1.2. Summary of functional studies characterizing del(20q) CDR genes in hematological context.
MDS, myelodysplastic syndrome; MPN, myeloproliferative neoplasm; HSC, hematopoietic stem cell; DSB, double-strand break; iPSCs, induced pluripotent stem cells.

Gene(s) Analyzed	Study	Model(s)	20q-Relevant Phenotypes
L3MBTL1	Perna, *et al.* (2010)[56]	shRNA knockdown in human CD34+ cells	Biased erythroid differentiation, expansion of erythroid progenitors
L3MBTL1	Perna, *et al.* (2015)[57]	shRNA knockdown in human iPSCs	Enhanced hematopoietic lineage commitment, reduced neuronal lineage commitment
L3mbtl1	Qin, *et al.* (2010)[58]	Germline homozygous inactivation in mice	No observed phenotypes in hematopoietic system
Mybl2	Clarke, *et al.* (2013)[62]	Germline heterozygous inactivation in mice	Development of MPN and MDS upon aging, competitive clonal HSC advantage
Mybl2	Heinrichs, *et al.* (2013)[63]	shRNA knockdown to sub-haploinsufficiency (~30% of normal)	Competitive clonal HSC advantage, development of MDS, extramedullary hematopoiesis in spleen
MYBL2, Mybl2	Bayley, *et al.* (2018)[64]	Primary MDS CD34+ cells, germline heterozygous inactivation	Transcriptional downregulation of DNA repair genes, impaired DSB repair kinetics in HSCs
Ptpn1	Jobe, *et al.* (2017)[70]	Conditional (Mx1) homozygous inactivation in mice	Splenomegaly, competitive clonal HSC advantage, development of MPN, hyperactive JAK/STAT signaling
Stk4 (and homolog *Stk3*)	Stoner, *et al.* (this dissertation)	Conditional (Vav1, Mx1) heterozygous and homozygous inactivation in mice	Megakaryocytic dysplasia and thrombocytopenia, splenomegaly, cooperation with JAK2-V617F in accelerated myelofibrosis development

1.1.6. Cooperating mutations in del(20q) malignancies

With regards to cooperation between del(20q) and additional mutations in hematologic malignancy, several interesting trends have been reported to date. However, given the relatively small patient cohort sizes analyzed, and the lack of functional modeling of cooperating mutational studies, the potential significance of any cooperating effects remains unknown. Assessment of all mutated genes in a del(20q) MDS patient cohort revealed the most frequent co-occurring mutations to be in splicing factors *U2AF1* and *SRSF2*, as well as in *ASXL1*[11]. A similar trend towards co-mutation of del(20q) with *U2AF1* was reported in an additional cohort[81], however it remains to be determined whether this is a biologically meaningful co-association. In the absence of additional cytogenetic abnormalities, *ASXL1* mutation appears to be the only molecular lesion associated with adverse overall survival in del(20q) MDS patients[11]. Del(20q) frequently co-occurs with *JAK2* or *ASXL1* mutation in PMF, however given the high overall frequencies with which each of these mutations occur independently in this disease, the biological significance of this remains to be determined[19]. Interestingly, *SRSF2* and del(20q) mutations have been detected to co-occur in PMF patients, but never in PV patients, suggesting that these events may cooperatively accelerate myelofibrotic transformation in MPN, or perhaps that *SRSF2* mutation is incompatible with PV development[19,20].

1.2. t(8;21) chromosomal translocation in AML

Acute myeloid leukemia (AML) is the most common leukemia among adults, and the incidence is rising as the population ages[82]. AML is a heterogeneous disorder which is characterized by accumulation of abnormal hematopoietic progenitor cells, or blasts, in the marrow[83]. These malignant blasts have lost their ability to differentiate into mature blood cells and respond to normal regulatory signals[84,85]. Stable chromosomal translocations which result in abnormal fusion proteins are a frequent occurrence in AML. Among the most common of these is the t(8;21)(q22;q22) chromosomal translocation, which occurs in approximately 5-10% of de novo AML cases[86]. These cases are almost exclusively FAB-M2 subtype AML.

The t(8;21) translocation results in the stable fusion of the *RUNX1* (*AML1*) and *ETO* (*RUNX1T1*) genes[87]. RUNX1 is a member of the Runt-related family of DNA-binding transcription factors, and is essential for regulating definitive hematopoeisis[88,89]. *RUNX1* is disrupted through chromosomal translocation or mutation in numerous blood disorders including multiple leukemias, familial platelet disorder, and myelodisplastic syndrome[90]. ETO (which is not normally expressed in blood cells) is thought to be a transcriptional co-repressor and contains four Nervy homology regions (NHR) for facilitating protein interactions[91]. The RUNX1-ETO fusion protein is composed of the N-terminal portion of RUNX1, which includes the DNA-binding Runt-homology domain, and nearly the full-length ETO protein. The ETO portion directly interacts with the nuclear hormone co-repressors N-CoR and mSin3A through distinct sites, and these proteins all co-immunoprecipitate with type I

Histone deacetylase as part of large repressive complexes[92,93]. Therefore, the primary accepted mechanism by which RUNX1-ETO promotes leukemia is the aberrant recruitment of N-CoR/mSin3A/HDAC complexes to the promoter region of RUNX1 target genes to repress their transcription[94].

Chapter 1, in part, is being prepared for submission for publication by: Stoner SA and Zhang DE. The dissertation author is the primary investigator and author of the manuscript.

Chapter 2. Hippo Kinase Loss Contributes to Del(20q) Hematologic Malignancies through Chronic Innate Immune Activation

Heterozygous deletions within chromosome 20q, or del(20q), are frequent cytogenetic abnormalities detected in hematologic malignancies. To date, identification of genes in the del(20q) common deleted region that contribute to disease development have remained elusive. Through assessment of patient gene expression we have identified *STK4* (encoding Hippo kinase MST1) as a 20q gene that is downregulated below haploinsufficient amounts in myelodysplastic syndrome (MDS) and myeloproliferative neoplasm (MPN). Hematopoietic-specific gene inactivation in mice revealed Hippo kinase loss to induce splenomegaly, thrombocytopenia, megakaryocytic dysplasia, and a propensity for chronic granulocytosis; phenotypes that closely resemble those observed in patients harboring del(20q). In a JAK2-V617F model, heterozygous Hippo kinase inactivation led to accelerated development of lethal myelofibrosis, recapitulating adverse MPN disease progression and revealing a novel genetic interaction between these two molecular events. Quantitative serum protein profiling showed that myelofibrotic transformation in mice was associated with cooperative effects of JAK2-V617F and Hippo kinase inactivation on innate immune-associated proinflammatory cytokine production, including IL-1β and IL-6.. Mechanistically, MST1 interacted with IRAK1, and shRNA-mediated knockdown was sufficient to increase IRAK1-dependent innate immune activation of NF-κB in human myeloid cells. Consistent with this, treatment with a small molecule IRAK1/4 inhibitor rescued the aberrantly elevated IL-1β production in the JAK2-V617F MPN model. This study identifies Hippo kinase MST1

(*STK4*) as having a central role in the biology of del(20q)-associated hematologic malignancies and reveals a novel molecular basis of adverse MPN progression that may be therapeutically exploitable via IRAK1 inhibition.

2.1. Introduction

Recurring chromosome abnormalities, such as large-scale deletion mutations, are frequent events in cancer and are especially prevalent in hematologic neoplasms[1]. Modeling loss-of-function of critical genes affected by large deletions has significantly enhanced our understanding of the associated disease and revealed novel therapeutic approaches in myeloid malignancy[95-100]. Somatic heterozygous deletions on chromosome 20q are detected in several hematopoietic malignancies, including myelodysplastic syndrome (MDS), classical myeloproliferative neoplasm (MPN), MDS/MPN overlap disorders, and acute leukemias[7,27,101-103]. Del(20q) is especially prevalent in MPN patients (~10-15%), where it is the most commonly detected cytogenetic abnormality associated with primary myelofibrosis (PMF) and post-Polycythemia Vera myelofibrosis (MF)[18]. These findings suggest that there are unique tumor-suppressor genes located in this region that, upon loss, contribute to diverse del(20q)-associated hematopoietic phenotypes.

Several studies have mapped a ~3Mb minimal commonly deleted region (CDR) spanning chromosome 20q12-20q13.12 and encompassing more than 50 genes[11,42,43]. There is no current evidence for homozygous gene inactivation in this region through mutation[48]. To date, two transcriptional regulators, *L3MBTL1* and *MYBL2*, are primarily implicated in the pathogenesis of del(20q)-associated malignancies. Knockdown of L3MBTL1 causes an erythroid differentiation bias in human CD34+ cells[56]. MYBL2 is a MYB-related transcription factor that is found downregulated in MDS patients regardless of 20q status, and inactivation promotes

MDS development in aged mice[62,63]. Genetic inactivation of 20q gene *PTPN1*, a non-receptor tyrosine phosphatase that negatively regulates JAK/STAT signaling, was recently shown to promote MPN in mice[70]. There remains a significant need to identify genes within this region that mediate the specific clinical features associated with del(20q) malignancy.

Located within the del(20q) CDR is *STK4*, encoding MST1, one of two mammalian orthologues of the evolutionarily-conserved Hippo kinase. In the canonical signaling pathway, Hippo kinases MST1 and MST2 (encoded by *STK4* and *STK3*) phosphorylate and activate downstream kinases LATS1 and LATS2 in complex with their regulatory protein MOB1, which in turn phosphorylate the oncoproteins YAP and TAZ resulting in their cytoplasmic sequestration and degradation[104]. The role of the canonical Hippo pathway in hematopoietic cancers remains controversial[105]; and enforced expression of a constitutively active YAP mutant does not affect normal hematopoietic stem cell (HSC) biology or promote malignancy[106]. Instead, MST1 plays critical roles in the biology of hematopoietic cells via diverse non-canonical mechanisms[72]. In T-lymphocytes, MST1 has an essential role in the regulation of thymic egress, adhesion, and apoptosis[107-110]. MST1-deficient phagocytes show defects in migration and bactericidal activity[74,111], and MST1-deficient dendritic cells display altered cytokine secretion with detrimental effects on immune function[112,113]. These hematopoietic-specific functions have significant implications in human disease, as rare individuals harboring germline homozygous inactivating mutations in *STK4* have been identified with clinical presentation as a

primary immunodeficiency characterized by susceptibility to chronic infection and frequent autoimmune manifestations[75-77].

Here we have identified *STK4* as a sub-haploinsufficient tumor-suppressor gene in MDS and MPN. Our data demonstrate that Hippo kinase loss in hematopoietic cells induces several phenotypes in mice that resemble specific clinical features associated with del(20q) malignancy. Importantly, using a JAK2-V617F model of MPN, we identified a novel genetic interaction with heterozygous Hippo kinase inactivation leading to accelerated disease progression to myelofibrosis, which was caused by cooperative effects on chronic activation of innate immune signaling and NF-kB.

2.2. Results

2.2.1. Hippo kinase *STK4* is transcriptionally downregulated in del(20q) MDS and MPN patients

To identify 20q genes that play a role in the biology of del(20q)-associated malignancies we assessed gene expression data in bone-marrow derived CD34+ cells from MDS patients compared to those from healthy controls. We utilized a published dataset that contained six patients harboring the 20q deletion[81]. Given that not all 20q genes are expressed in hematopoietic cells, and that genetic haploinsufficiency does not necessarily alter transcriptional output, we rationalized that genes involved in disease pathogenesis could be identified through consistent downregulation in del(20q) patients. We found that nine (*STK4*, *SERINC3*, *DDX27, ARFGEF2*, *IFT52*, *ADA*, *ADNP*, *RBL1*, and *RNF114*) of the top-25 significantly downregulated genes in del(20q) MDS were located on chromosome 20q (**Figure 2.1**). The top hit located within the 20q CDR was *STK4*, which encodes Hippo kinase MST1. *STK4* was downregulated to sub-haploinsufficient amounts (mean 3.6-fold) in the six del(20q)-harboring patients compared to ten healthy controls. Given the high frequency of del(20q) in MPN, we further assessed the expression of these genes in independent cohorts of myelofibrosis (MF) patients[114,115]. This assessment revealed two of these genes to be significantly downregulated in patients with myelofibrosis (MF) regardless of 20q status, one of which was *STK4,* highlighting its potential importance in MPN progression regardless of 20q mutation (**Figure 2.2A and 2.2B**). Similar to MDS, *STK4* was downregulated to sub-haploinsufficient amounts in three

del(20q) MF patients (**Figure 2.2C**). Given the position within the defined 20q CDR (**Figure 2.3**), its stark downregulation in multiple patient cohorts, and its emerging roles in regulation of normal hematopoietic cell function and inflammatory signaling, *STK4* was a high-priority candidate to functionally characterize in the context of hematological malignancy.

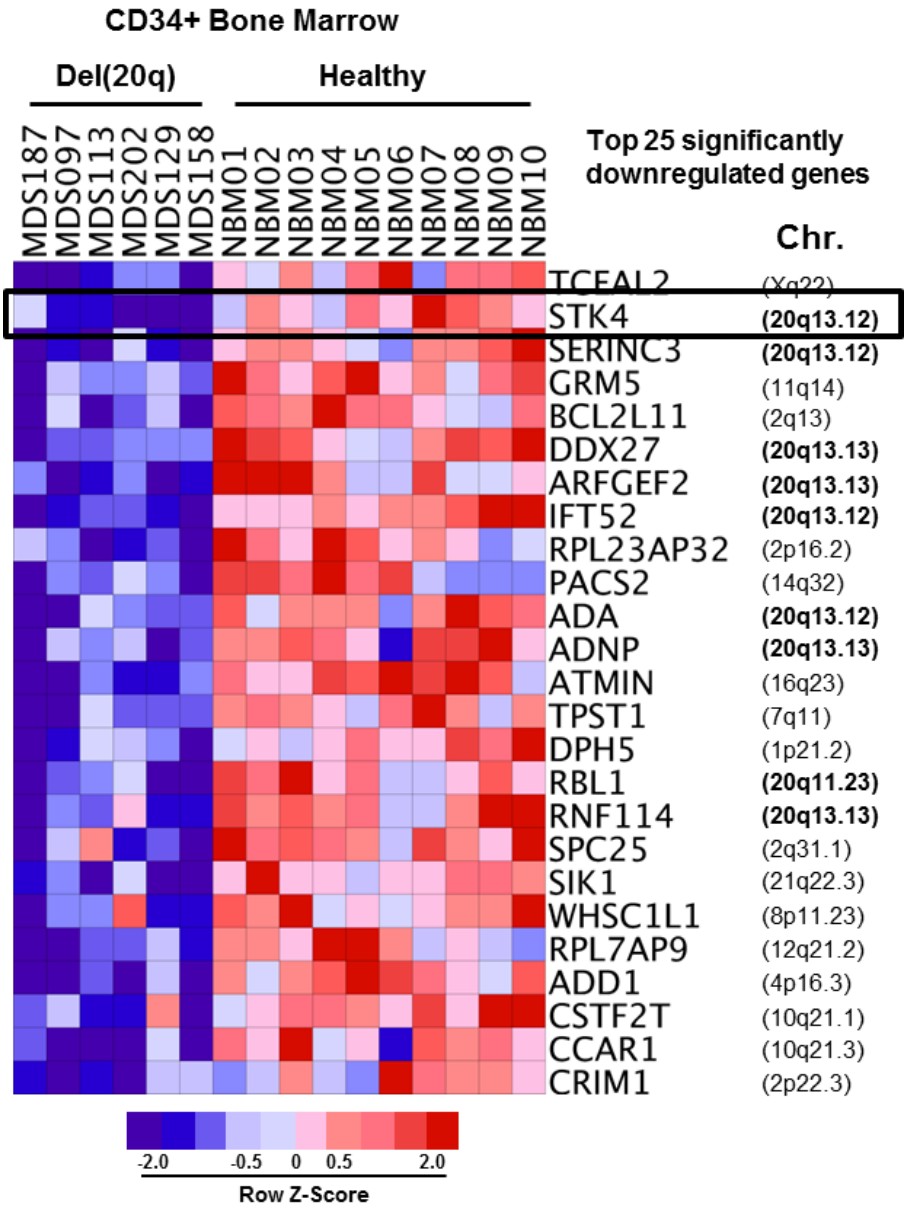

Figure 2.1 Hippo kinase *STK4* is located in the 20q CDR and downregulated in MDS and MPN patients with del(20q).

Row-normalized heatmap of gene expression in CD34+ bone marrow cells from 6 del(20q) MDS patients (left) compared to CD34+ bone marrow cells from 10 healthy controls (right). The top 25 significantly downregulated genes in del(20q) patients, along with their chromosomal position in the genome are depicted. Data are from GSE58831.

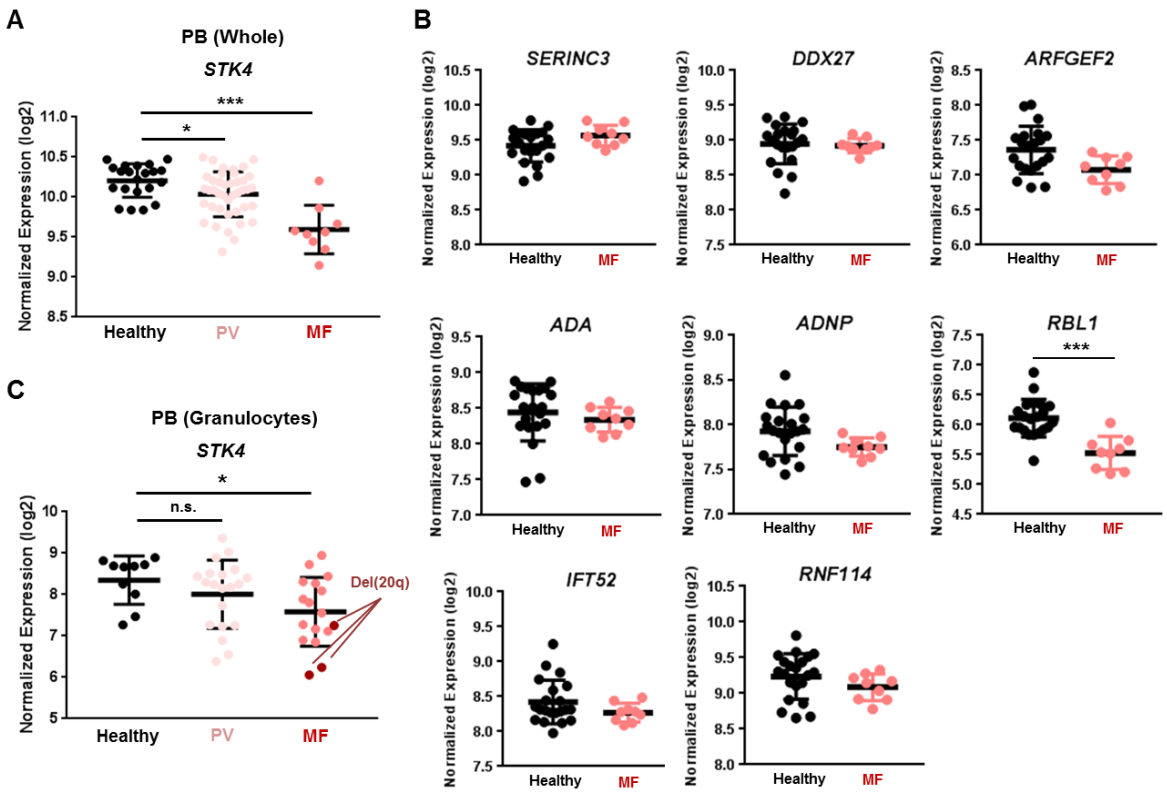

Figure 2.2. Assessment of 20q gene expression in myelofibrosis patients.
(A) *STK4* gene expression measured by microarray in total peripheral blood from healthy controls (black) and MPN patients with Polycythemia Vera (PV, pink) or Primary Myelofibrosis (MF, red). Data are from GSE26049. **(B)** 20q gene expression measured by microarray in total peripheral blood from healthy controls (black) and MPN patients with Primary Myelofibrosis (MF, red). Data are from GSE26049. Statistical significance is determined by two-tailed student's t-test, * $p < 0.001$. **(C)** *STK4* gene expression measured by microarray in peripheral blood granulocytes from healthy controls (black) and MPN patients with Polycythemia Vera (PV, pink) or Myelofibrosis (MF, red). Samples identified as del(20q) are indicated. Data are from GSE54646.

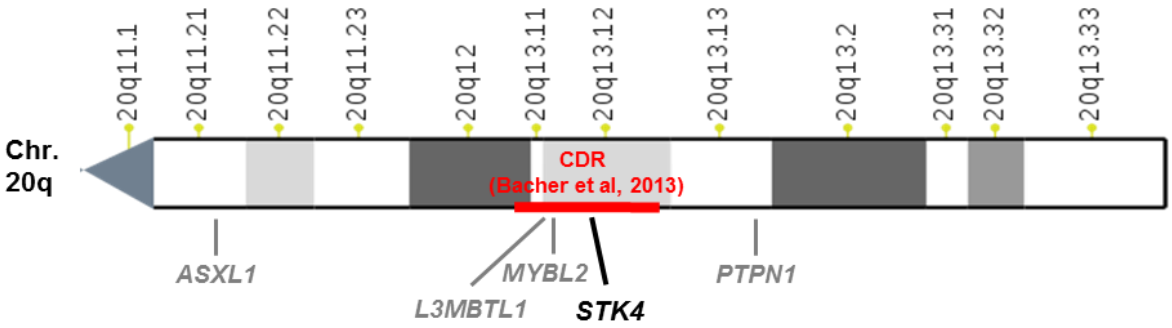

Figure 2.3 Position of *STK4* within the del(20q) common deleted region.
NCBI chromosome ideogram showing the q arm of chromosome 20. Minimal common deleted region (CDR) measured by array comparative genomic hybridization in a cohort of 30 MDS patients[11] is indicated in red. Positions of genes previously implicated in the pathogenesis of myeloid malignancies are indicated in gray. The position of *STK4* is indicated in black.

2.2.2. Hematopoietic-specific Hippo kinase inactivation results in lethal bone marrow failure with clinical features of del(20q) MDS

We examined hematopoietic-specific Hippo kinase loss by intercrossing Stk4/Stk3-floxed mice with Vav1-iCre transgenic mice. Assessment of protein expression for MST1 (Stk4) and MST2 (Stk3), as well as their physiological phosphorylation target MOB1[116,117], confirmed Cre-mediated inactivation in hematopoietic cells (**Figure 2.4**). Homozygous deletion within the hematopoietic system (Stk4-/-Stk3-/-) resulted in fully-penetrant, post-embryonic lethality due to bone marrow failure (**Figure 2.5A**). This lethality was associated with progressive weight loss post-weaning (**Figures 2.5B and 2.5C**), frequent splenomegaly (**Figures 2.5D, 2.5E and 2.5F**), and a dramatic reduction in bone marrow cellularity (**Figure 2.6A**). Enlarged spleens showed evidence of extramedullary erythropoiesis and accumulation of CD71hi/Ter119+ (stage II) erythroblasts (**Figure 2.5F**). Pancytopenia was readily apparent in the peripheral blood of Stk4-/-Stk3-/- mice (**Figures 2.6B, 2.6C, 2.6D, and 2.6E**).

To represent hematopoietic-specific Hippo kinase 'sub-haploinsufficient' conditions, we also characterized Stk4+/-Stk3-/- littermates, which demonstrated slightly less than 50% of normal Hippo kinase function using phosphorylated MOB1 as a readout (**Figure 2.4**). Although in most tissues MST1 and MST2 are functionally redundant, MST1 is the dominant homolog in hematopoietic cells, owing to its vastly increased mRNA expression[72]. Based on our observations above showing greater than two-fold downregulation of STK4 expression in del(20q) MDS and MPN patients,

these mice may represent the physiological conditions observed in patients. A single copy of Stk4 was sufficient to rescue the weight loss, splenomegaly, and early lethality (**Figures 2.5A, 2.5B, 2.5C, 2.5D, and 2.5E**). Stk4+/-Stk3-/- mice had more heterogeneous phenotypes in the peripheral blood, but typically showed thrombocytopenia with a trend towards mild anemia (**Figures 2.6B, 2.6C, 2.6D, and 2.6E**). These findings are similar to the clinical presentation of MDS patients with isolated deletion of chromosome 20q[15,16]. Peripheral leukopenia observed in Stk4-/-Stk3-/- mice was due to the reported absence of T-lymphocytes from circulation and secondary lymphoid organs[107,108] (**Figures 2.7A and 2.7B**). B-lymphocytes were also drastically reduced in the bone marrow, but not peripheral blood (**Figures 2.7A and 2.7B**). Relative frequencies of granulocytes were increased in the bone marrow and spleen (**Figures 2.7A, 2.7B, and 2.7C**). Assessment of immature cell populations revealed accumulation of cells at the Lin-Sca1+cKIT+ (LSK) progenitor stage in the bone marrow of Stk4-/-Stk3-/- mice, while phenotypic long-term hematopoietic stem cells (LSK+CD48-CD150+, LT-HSC) were depleted (**Figure 2.8A**). Consistent with peripheral thrombocytopenia, the number of mature megakaryocytes in histological sections of Stk4-/-Stk3-/- bone marrow was significantly reduced compared to littermate controls (**Figure 2.8B**). We also frequently detected the presence of dysplastic megakaryocytes with highly irregular nuclear morphology in the bone marrow of Stk4-/-Stk3-/- mice (**Figures 2.8C and 2.8D**). Together, Hippo kinase loss results in megakaryocytic abnormalities that likely contribute to thrombocytopenia that is a defining feature of del(20q) MDS.

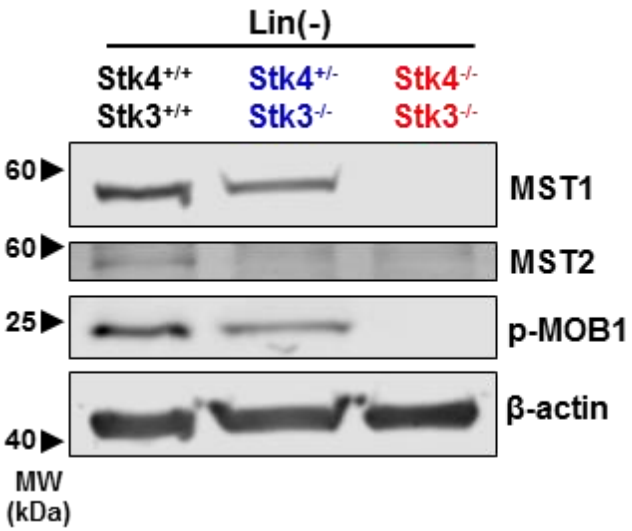

Figure 2.4. Conditional Hippo kinase inactivation in hematopoietic cells. Genotypes analyzed for this figure include: *Stk4*$^{f/f}$*Stk3*$^{f/f}$;Vav1-Cre^{+} (Stk4$^{-/-}$Stk3$^{-/-}$), *Stk4*$^{f/+}$*Stk3*$^{f/f}$; Vav1-Cre^{+} (Stk4$^{+/-}$Stk3$^{-/-}$), *Stk4*$^{f/f}$*Stk3*$^{f/f}$;Vav1-Cre^{-} or *Stk4*$^{f/+}$*Stk3*$^{f/f}$;Vav1-Cre^{-} (Stk4$^{+/+}$Stk3$^{+/+}$). All mice were analyzed in groups with littermates. Unless otherwise indicated, data are derived from mice of 6 - 9 weeks in age. Western blot showing MST1 (*Stk4*), MST2 (*Stk3*), phosphorylated MOB1, and β-actin (loading control) proteins in Lin^{-} hematopoietic cells. Bone-marrow and spleen-derived mononuclear hematopoietic cells from two mice per genotype were pooled prior to Lin^{-} isolation and protein lysate generation.

Figure 2.5. Hematopoietic-specific inactivation of Hippo kinases results in lethal bone marrow failure with frequent extramedullary erythropoiesis in the spleen.

Genotypes analyzed for this figure include: *Stk4*$^{f/f}$*Stk3*$^{f/f}$;Vav1-Cre^{+} (Stk4$^{-/-}$Stk3$^{-/-}$), *Stk4*$^{f/+}$*Stk3*$^{f/f}$; Vav1-Cre^{+} (Stk4$^{+/-}$Stk3$^{-/-}$), *Stk4*$^{f/f}$*Stk3*$^{f/f}$;Vav1-Cre^{-} or *Stk4*$^{f/+}$*Stk3*$^{f/f}$;Vav1-Cre^{-} (Stk4$^{+/+}$Stk3$^{+/+}$). All mice were analyzed in groups with littermates. Unless otherwise indicated, data are derived from mice of 6 - 9 weeks in age. Data are presented as mean values with error bars representing S.E.M. and individual data points for mice. * = $p < 0.05$, ** = $p < 0.01$, *** = $p < 0.001$. **(A)** Kaplan-Meier survival plots for mice of indicated genotypes. **(B)** Representative image of 7 week-old, sex-matched littermates of mice of the indicated genotypes. **(C)** Weekly weight measurement (grams) for multiple cohorts of mice between 3 and 7 weeks of age. N = 6-10 mice per genotype. Statistical significance was determined at week 7 by One-way ANOVA followed by comparison against Stk4$^{+/+}$Stk3$^{+/+}$ values using post-hoc Tukey test. **(D)** Representative spleen images for 6-8 week-old mice of the indicated genetic backgrounds. **(E)** Measurement of spleen weight (grams) divided by total body weight (grams) for mice of indicated genotypes. Line indicates mean and individual data points represent individual mice. **(F)** Representative erythroid progenitor (CD71/Ter-119) flow cytometry staining within total splenocytes from mice of the indicated genotypes. The four stages of erythroblast development (I-IV) are indicated.

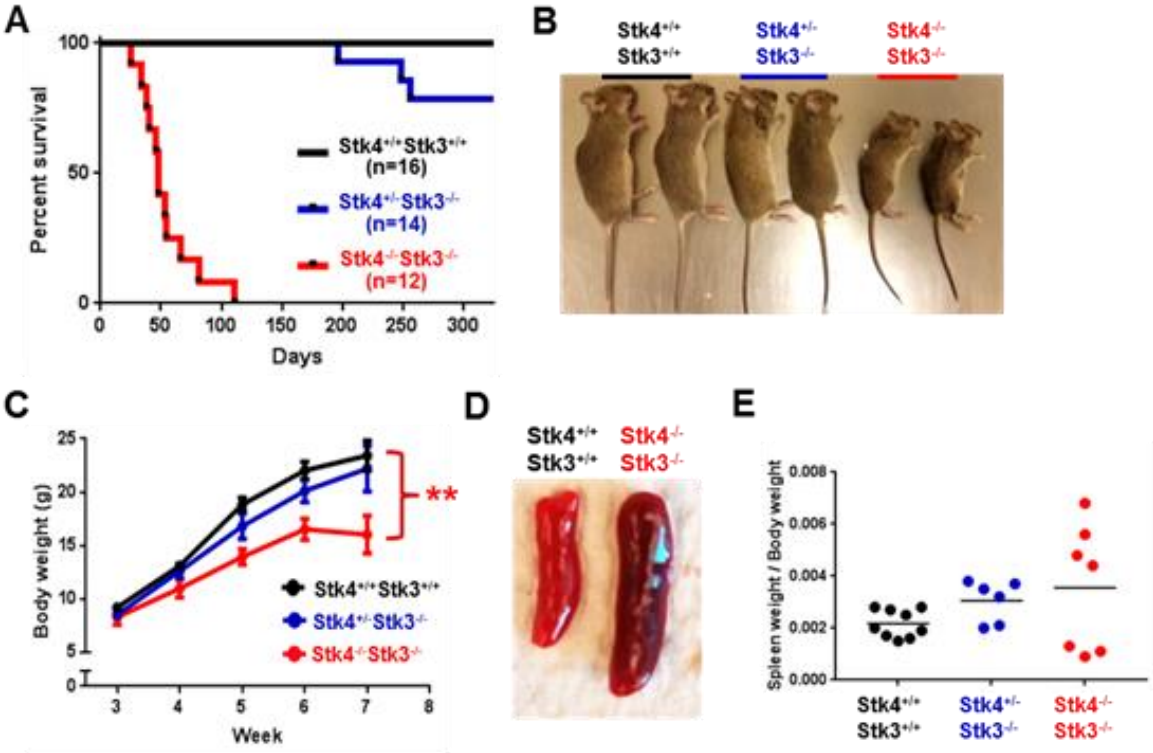
A
Percent survival
Days
Stk4+/+Stk3+/+ (n=16)
Stk4+/-Stk3-/- (n=14)
Stk4-/-Stk3-/- (n=12)
B
Stk4+/+ Stk3+/+
Stk4+/- Stk3-/-
Stk4-/- Stk3-/-
C
Body weight (g)
Week
**
D
E
Spleen weight / Body weight
F
Spleen
CD71-PE
Ter119-FITC
I 0.2
II 4.1
III 0.5
IV 11.8
I 0.5
II 19.0
III 0.9
IV 9.0
I 0.9
II 45.2
III 1.8
IV 23.1

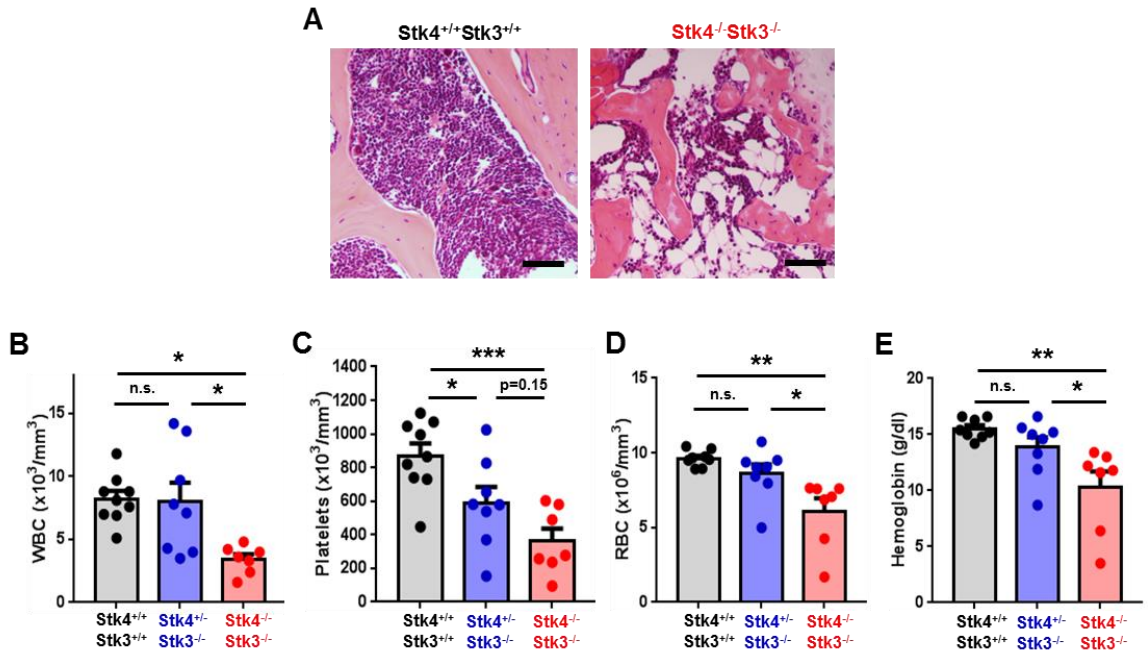

Figure 2.6. Hypocellular bone marrow and pancytopenia in Hippo kinase knockout mice.

Genotypes analyzed for this figure include: *Stk4*$^{f/f}$*Stk3*$^{f/f}$;Vav1-Cre^{+} (Stk4$^{-/-}$Stk3$^{-/-}$), *Stk4*$^{f/+}$*Stk3*$^{f/f}$; Vav1-Cre^{+} (Stk4$^{+/-}$Stk3$^{-/-}$), *Stk4*$^{f/f}$*Stk3*$^{f/f}$;Vav1-Cre^{-} or *Stk4*$^{f/+}$*Stk3*$^{f/f}$;Vav1-Cre^{-} (Stk4$^{+/+}$Stk3$^{+/+}$). All mice were analyzed in groups with littermates. Unless otherwise indicated, data are derived from mice of 6 - 9 weeks in age. Data are presented as mean values with error bars representing S.E.M. and individual data points for mice. * = $p < 0.05$, ** = $p < 0.01$, *** = $p < 0.001$. **(A)** Representative Hematoxylin & Eosin (H&E) stained bone marrow sections for 6-8 week-old mice. Scale bar = 200 μm. **(B)-(E)** Peripheral blood measurements for: **B)** White blood cell (WBC) number, **C)** Platelet number, **D)** Red blood cell (RBC) number, and **E)** Hemoglobin. Statistical significance was determined by One-way ANOVA followed by post-hoc Tukey test for multiple comparisons.

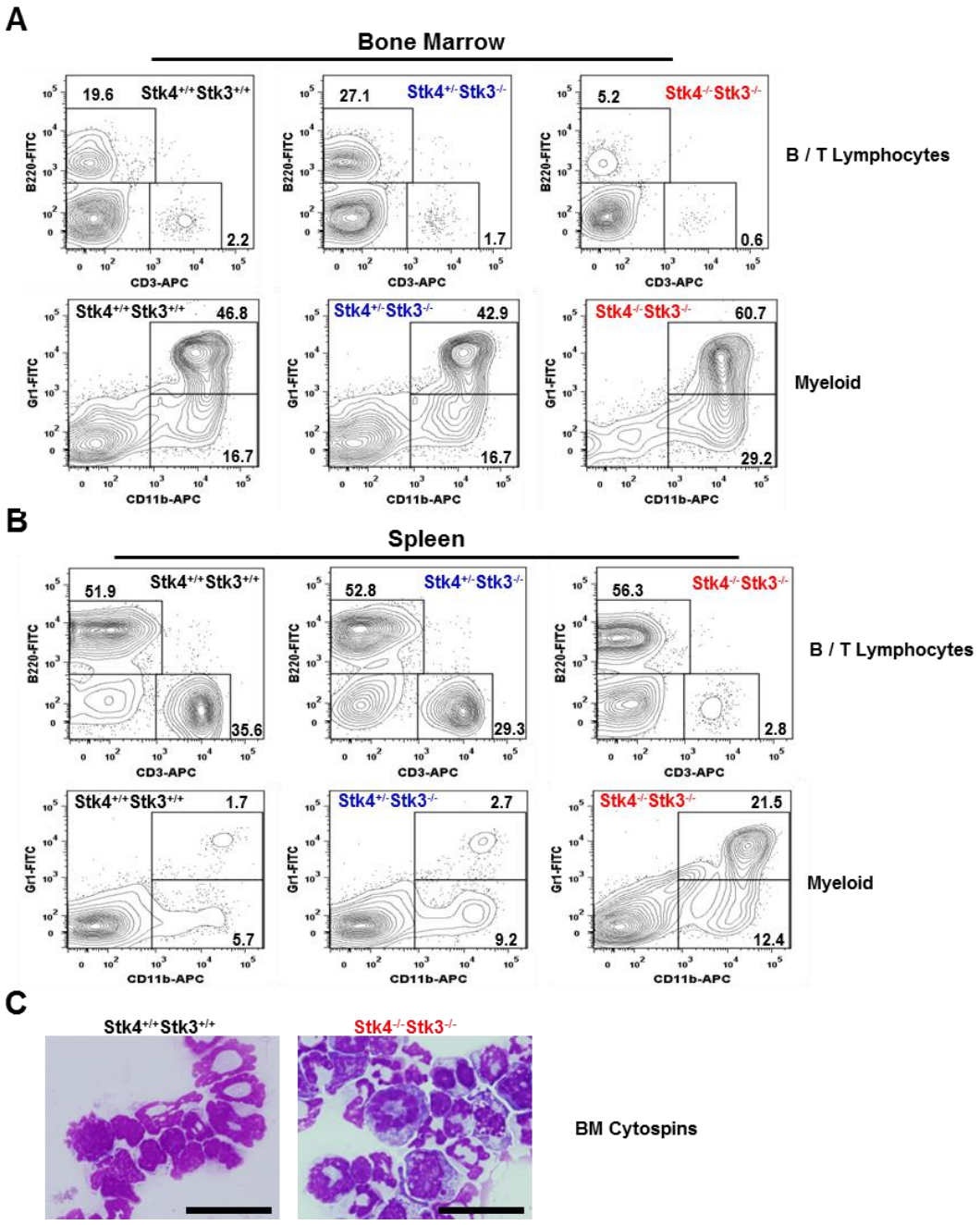

Figure 2.7. Granulocytic skewing in bone marrow and spleen of Hippo kinase knockout mice.

(A) Representative lymphoid (CD3/B220, top) and myeloid (CD11b/Gr-1, bottom) flow cytometry plots of mononuclear bone marrow cell populations for mice of indicated genotypes. **(B)** As (A) but for spleens. **(C)** Representative bone marrow cytospins of mice of the indicated genotypes. Scale bar = 50 μM.

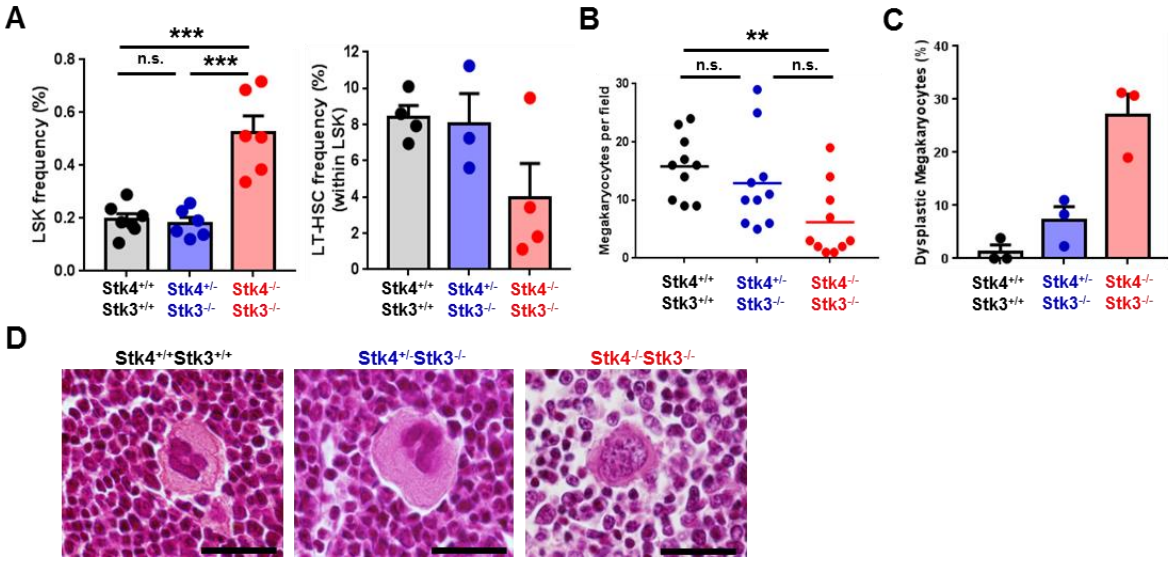

Figure 2.8. Frequent megakaryocytic abnormalities in Hippo kinase knockout mice.

Genotypes analyzed for this figure include: *Stk4*$^{f/f}$*Stk3*$^{f/f}$;Vav1-Cre^{+} (Stk4$^{-/-}$Stk3$^{-/-}$), *Stk4*$^{f/+}$*Stk3*$^{f/f}$; Vav1-Cre^{+} (Stk4$^{+/-}$Stk3$^{-/-}$), *Stk4*$^{f/f}$*Stk3*$^{f/f}$;Vav1-Cre^{-} or *Stk4*$^{f/+}$*Stk3*$^{f/f}$;Vav1-Cre^{-} (Stk4$^{+/+}$Stk3$^{+/+}$). All mice were analyzed in groups with littermates. Unless otherwise indicated, data are derived from mice of 6 - 9 weeks in age. Data are presented as mean values with error bars representing S.E.M. and individual data points for mice. * = $p < 0.05$, ** = $p < 0.01$, *** = $p < 0.001$. **(A)** Bone marrow frequencies of hematopoietic stem/progenitor populations as measured by flow cytometry in mice of the indicated genotypes. LSK, Lin^{-}Sca1^{+}cKIT^{+}. LT-HSC, LSK^{+}CD48^{-}CD150^{+}. **(B)** The number of mature morphological megakaryocytes per 20x magnification field in H&E-stained bone marrow sections. Data are derived from five representative sections each of two mice per genotype. Statistical significance was determined by One-way ANOVA followed by post-hoc Tukey test for multiple comparisons. **(C)** Frequencies (%) of dysplastic megakaryocytes detected in representative H&E-stained bone marrow sections from three independent mice of the indicated genotypes. **(D)** Representative images of megakaryocytes observed in H&E-stained bone marrow sections in mice of the indicated genotypes. A representative dysplastic megakaryocyte with irregular nuclear morphology is indicated (rightmost panel). Scale bar = 60 µm.

2.2.3. Inducible Hippo kinase inactivation recapitulates features of MDS and MPN in adult mice

We also assessed the consequences of inducible Hippo kinase inactivation in adult mice by using the interferon-inducible Mx1-Cre system. To ensure hematopoietic-intrinsic specificity of observed phenotypes we generated bone marrow chimeric mice prior to treatment with polyinosinic:polycytidylic acid (pIpC) to induce gene deletion (**Figure 2.9A**). We assessed both homozygous ($Stk4^{\Delta/\Delta}Stk3^{\Delta/\Delta}$) and heterozygous ($Stk4^{\Delta/+}Stk3^{\Delta/+}$) bone marrow inactivation compared to bone marrow from Mx1-Cre^{-} littermate controls ($Stk4^{+/+}Stk3^{+/+}$). Inducible gene inactivation was confirmed by RT-qPCR in sorted $Lin^{-}cKIT^{+}$ (LK) bone marrow cells (**Figure 2.9B**). Peripheral leukopenia, peripheral thrombocytopenia, and splenomegaly were readily apparent following inducible homozygous Hippo kinase deletion (**Figures 2.10A, 2.10B, and 2.10C**). Surprisingly, heterozygous inactivation in the adult hematopoietic system led to a chronic increase in peripheral leukocyte counts (**Figure 2.10A**), which was due to elevated numbers of granulocytes and granulocytic skewing in the peripheral blood (**Figures 2.10D and 2.10E**). Thrombocytopenia in mice was accompanied by a pronounced increase in mean platelet volume, further highlighting defects in the megakaryocytic lineage (**Figures 2.10F and 2.10G**). In contrast to Vav1-Cre, only two out of fourteen (~15%) $Stk4^{\Delta/\Delta}Stk3^{\Delta/\Delta}$ mice in total experienced lethal bone marrow failure during the course of long-term observations (up to one year post-pIpC), and there were no indications of anemia (**Figure 2.10H**). This is most likely due to selection pressure towards non-excised alleles in the Mx1-

Cre model, as Hippo kinase protein and mRNA expression were more abundant in Lin- bone marrow cells of mice one year following pIpC-induced gene inactivation (**Figure 2.11A and 2.11B**). Regardless, we found consistent evidence supporting both heterozygous and homozygous Hippo kinase inactivation contributing to specific clinical features associated with del(20q) MDS and MPN.

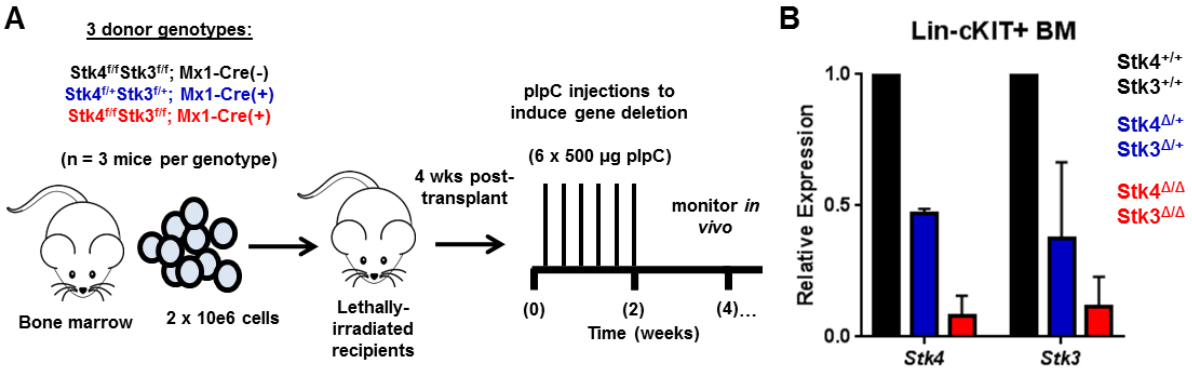

Figure 2.9. Experimental strategy for inducible somatic inactivation of Hippo kianses Stk4 and Stk3.
(A) Experimental schematic depicting generation of bone marrow chimeras and pIpC treatment to induce hematopoietic-specific gene deletion for indicated genotypes. **(B)** Gene expression for *Stk4* and *Stk3* measured by RT-qPCR in flow-sorted $Lin^{-}cKIT^{+}$ hematopoietic progenitor cells derived from two representative mice of the indicated genotypes, two weeks following completion of pIpC treatment.

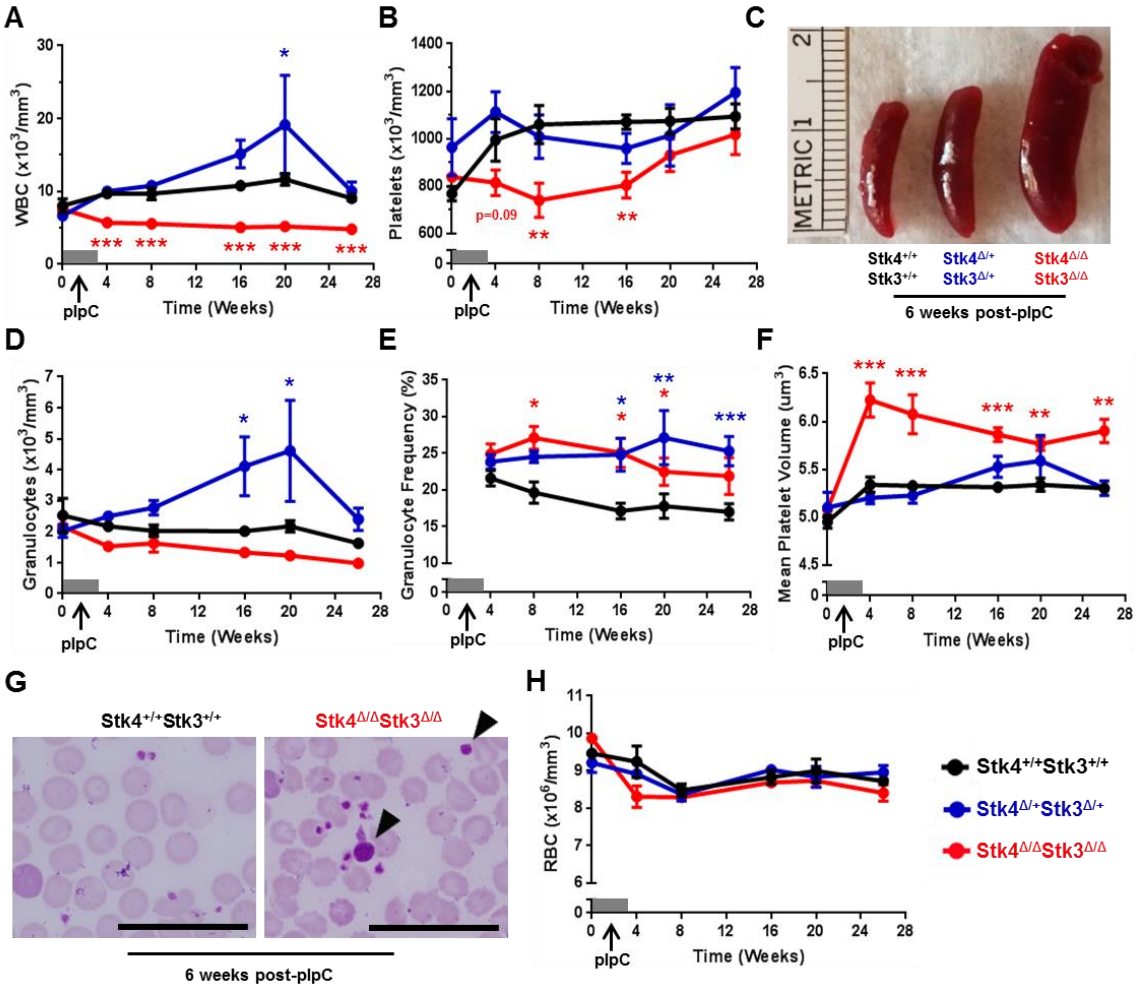

Figure 2.10. Inducible somatic Hippo kinase inactivation recapitulates clinical features of del(20q) MDS and MPN.
Recipient mice analyzed in this figure are derived from genotypes: *Stk4*$^{f/f}$*Stk3*$^{f/f}$;Mx1-Cre^{+} (Stk4$^{\Delta/\Delta}$Stk3$^{\Delta/\Delta}$, red), *Stk4*$^{f/+}$*Stk3*f$^{/+}$;Mx1-Cre^{+} (Stk4$^{\Delta/+}$Stk3$^{\Delta/+}$, blue), and *Stk4*$^{f/f}$*Stk3*$^{f/f}$;Mx1-Cre^{-} (Stk4$^{+/+}$Stk3$^{+/+}$, black). N = 9 mice per genotype. Data are representative of two independent experiments. Homozygous and heterozygous groups were independently tested for statistical significance against controls by multiple t-testing with Holm-Sidak correction. * = $p < 0.05$, ** = $p < 0.01$, *** = $p < 0.001$. **(A)** Peripheral blood white blood cell (WBC) counts. **(B)** Peripheral blood platelet counts. **(C)** Representative spleens from mice of the indicated genotypes, six weeks post-pIpC treatment. **(D)** Peripheral blood granulocyte counts. **(E)** Peripheral blood granulocyte (CD11b+Gr1+) frequencies measured via flow cytometry. **(F)** Peripheral blood mean platelet volume (MPV). **(G)** Representative Wright-Giemsa stained peripheral blood smears from mice of the indicated genotypes, six weeks post-pIpC treatment. Black arrows indicate abnormally large platelets. Scale bar = 50 μm. **(H)** Peripheral blood red blood cell (RBC) counts.

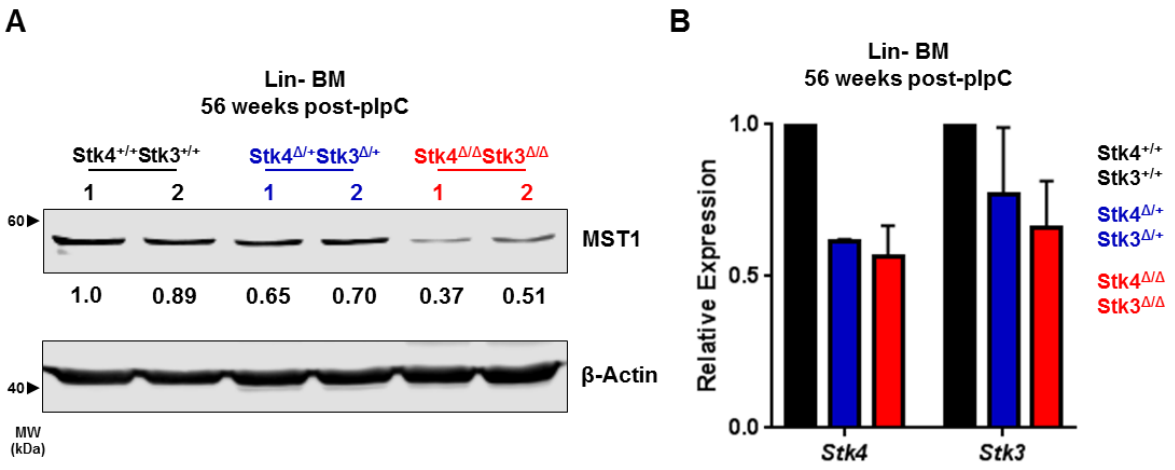

Figure 2.11. Selection pressure towards non-excised alleles upon aging in Mx1-Cre model.

Mice used in this Figure are of the following genotypes: *Stk4*$^{f/f}$*Stk3*$^{f/f}$;Mx1-Cre^{+} (Stk4$^{\Delta/\Delta}$Stk3$^{\Delta/\Delta}$), *Stk4*$^{f/+}$*Stk3*f$^{/+}$;Mx1-Cre^{+} (Stk4$^{\Delta/+}$Stk3$^{\Delta/+}$), and *Stk4*$^{f/f}$*Stk3*$^{f/f}$;Mx1-Cre^{-} (Stk4$^{+/+}$Stk3$^{+/+}$) **(A)** Western blot (from two mice per genotype) depicting indicated proteins in murine hematopoietic progenitor (Lin-) bone marrow cells, 56 weeks post-treatment with pIpC to induce gene deletion. **(B)** RT-qPCR analysis showing relative expression for indicated genes (from two mice per genotype) in murine hematopoietic progenitor (Lin-) bone marrow cells, 56 weeks post-treatment with pIpC to induce gene deletion.

2.2.4. Hippo kinase inactivation promotes macrothrombocytopenia upon aging even in absence of malignant clonal HSC expansion

In addition to malignancy, somatic deletions of chromosome 20q are detected at low frequency in otherwise healthy individuals that experience clonal hematopoiesis during aging[118,119], suggesting that loss of 20q genes promotes clonal/pre-malignant expansion of HSCs. We therefore asked whether Hippo kinase inactivation contributes to HSC clonal expansion by performing serial competitive bone marrow transplantation assays. Hippo kinase deletion resulted in a gene dosage-dependent defect in initial engraftment in the bone marrow of recipient mice. This was indicated by a near complete lack of $Stk4^{-/-}Stk3^{-/-}$ CD45.2 cells in the peripheral blood at 4 weeks post-transplantation **(Figures 2.12A, 2.12B, 2.12C, and 2.12D).** We attempted to transplant cells in a non-competitive manner and confirmed a defect in engraftment potential (**Figure 2.13**). Following initial engraftment, heterozygous inactivation resulted in no detectable competitive advantage over 48 weeks in primary and secondary transplantations (**Figures 2.12A, 2.12B, 2.12C, and 2.12D**). $Stk4^{+/-}Stk3^{+/-}$ HSCs maintained relatively normal output to all mature lineages except for the T-cell (CD3+) lineage, which displayed consistently reduced donor-derived contribution (**Figure 2.12D**). We also assessed the CD45.2 donor-derived frequencies in stem/progenitor populations in the bone marrow at 48 weeks (**Figure 2.14**). $Stk4^{+/-}Stk3^{+/-}$ donor cells showed a comparable distribution to control donor cells within the total bone marrow and LSK populations. No mice developed any overt malignancy, however upon aging (40-48 weeks), assessment of peripheral blood

revealed several mice receiving Stk4$^{+/-}$Stk3$^{+/-}$ donor cells to have developed macrothrombocytopenia (**Figure 2.15**). This observation demonstrates that the presence of Stk4$^{+/-}$Stk3$^{+/-}$ hematopoietic cells, even as a minor clone within the bone marrow, exerts a dominant negative effect on platelet production upon aging.

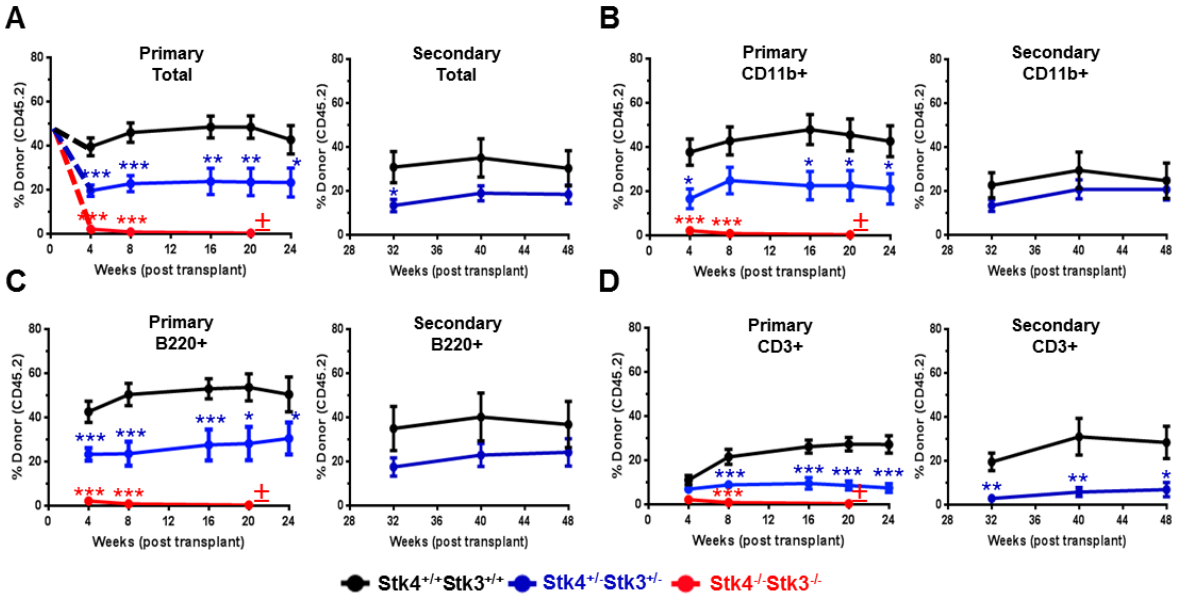

Figure 2.12. Hippo kinase inactivation does not provide a competitive HSC advantage.
Genotypes analyzed for this figure include: *Stk4*$^{f/f}$*Stk3*$^{f/f}$;Vav1-Cre^{+} (Stk4$^{-/-}$Stk3$^{-/-}$, red), *Stk4*$^{f/+}$*Stk3*$^{f/+}$; Vav1-Cre^{+} (Stk4$^{+/-}$Stk3$^{+/-}$, blue), and *Stk4*$^{f/f}$*Stk3*$^{f/f}$;Vav1-Cre^{-} (Stk4$^{+/+}$Stk3$^{+/+}$, black). Primary transplantations: N = 10 (Stk4$^{+/+}$Stk3$^{+/+}$), N = 10 (Stk4$^{+/-}$Stk3$^{+/-}$), N = 9 (Stk4$^{-/-}$Stk3$^{-/-}$). Secondary transplantations: N = 8 (Stk4$^{+/+}$Stk3$^{+/+}$), N = 8 (Stk4$^{+/-}$Stk3$^{+/-}$). Data are presented as mean +/- S.E.M. * = $p < 0.05$, ** = $p < 0.01$, *** = $p < 0.001$. Donor-derived frequencies (CD45.2%) in the peripheral blood over the course of primary and secondary bone marrow transplants are shown for: **(A)** total mononuclear cells, **(B)** myeloid-lineage cells (CD11b+), **(C)** B-lineage cells (B220+), and **(D)** T-lineage cells (CD3+).

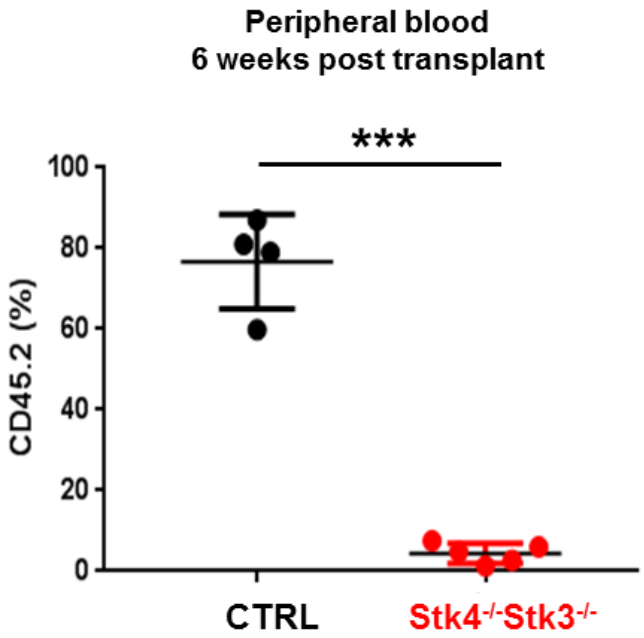

Figure 2.13. Hippo kinase-deficient hematopoietic cells fail to properly engraft in bone marrow.

Genotypes analyzed for this figure include: *Stk4*$^{f/f}$*Stk3*$^{f/f}$;Vav1-Cre^{+} (Stk4$^{-/-}$Stk3$^{-/-}$) and *Stk4*$^{f/f}$*Stk3*$^{f/f}$;Vav1-Cre^{-} or *Stk4*$^{f/+}$*Stk3*$^{f/f}$;Vav1-Cre^{-} (Stk4$^{+/+}$Stk3$^{+/+}$). CD45.2 donor-derived frequencies in the peripheral blood of lethally irradiated CD45.1 recipient mice, 6 weeks following non-competitive transplantation of bone marrow-derived cells. Statistical significance is determined using student's t-test, *** = $p < 0.001$.

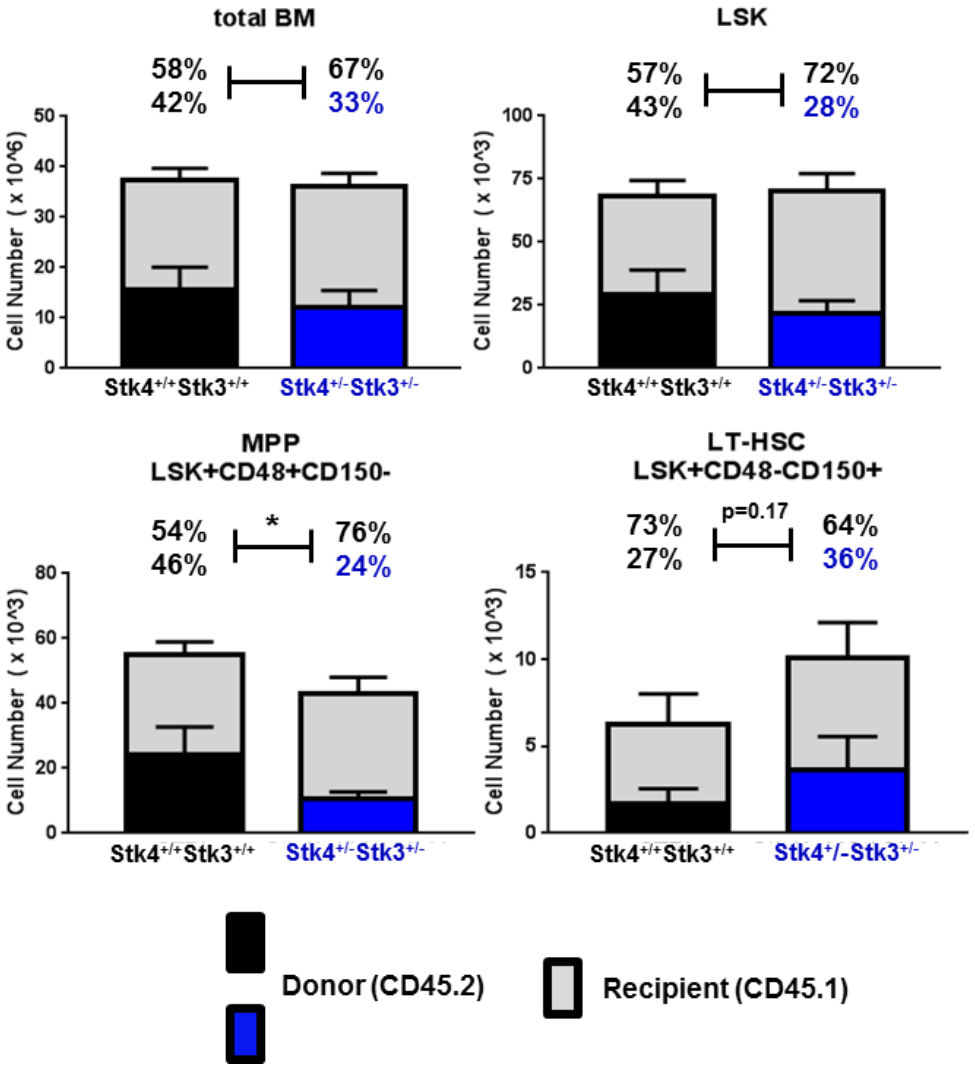

Figure 2.14. Heterozygous Hippo kinase inactivation does not promote malignant HSC expansion in the bone marrow.
Analysis of hematopoietic stem/progenitor cell donor-derived frequencies (CD45.2%) in total bone marrow at the experimental endpoint (48 weeks). Total cell number for the indicated populations are shown (left axis). Mean donor-derived and recipient-derived frequencies are indicated as percentage. Statistical significance is determined by two-tailed student's t-test.

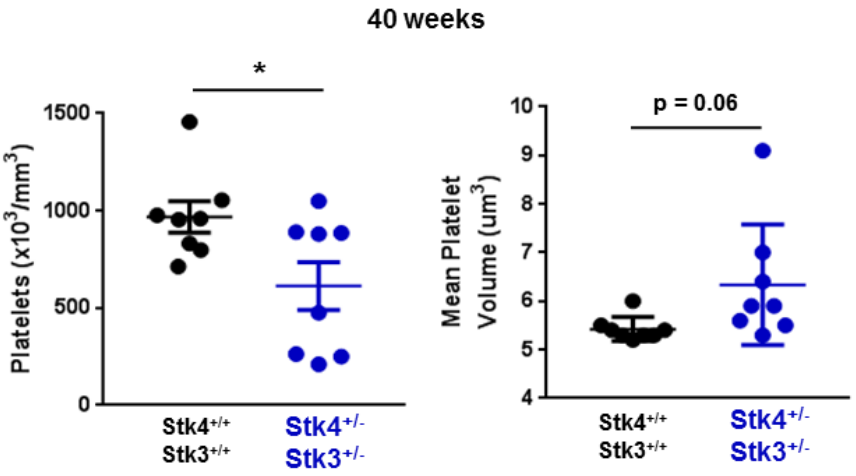

Figure 2.15. Heterozygous Hippo kinase inactivation promotes macrocytic thrombocytopenia upon aging.
Platelet count and mean platelet volume in peripheral blood of mice receiving indicated donor genotypes at 40 weeks post-transplant. Statistical significance is determined by two-tailed student's t-test.

2.2.5. Heterozygous Hippo kinase inactivation cooperates with JAK2-V617F to promote lethal myelofibrosis

Given the high frequency of del(20q) in MPN, especially in JAK2-mutant Polycythemia Vera and PMF[19,20], we hypothesized that heterozygous Hippo kinase inactivation may cooperate with this driver mutation to modify disease phenotypes and progression. We utilized a human JAK2-V617F retroviral transduction/transplantation model of MPN that presents as Polycythemia Vera with a low rate of progression to MF in C57BL/6 recipient mice[120]. HSC-enriched bone marrow cells from $Stk4^{+/-}Stk3^{+/-}$ and littermate control ($Vav1\text{-}Cre^{-}$) mice were transduced at equal efficiencies (**Figure 2.16A**) with JAK2-V617F (V617F) or empty vector control (Vector), and transplants were monitored by peripheral blood sampling for 36 weeks (**Figure 2.16B**). Engraftment efficiencies of V617F-expressing (GFP+) cells were similar between genotypes at four weeks post-transplantation, and GFP+ cell frequency gradually increased with mean frequencies of approximately 15% at 20 weeks (**Figure 2.16C**). Both V617F-expressing genotypes showed a similar degree of Polycythemia (**Figure 2.17A**). Platelet counts were variable with no significant differences between groups (**Figure 2.17B**). The most pronounced difference detected was elevated granulocyte number in the V617F-$Stk4^{+/-}Stk3^{+/-}$ group compared to V617F-$Stk4^{+/+}Stk3^{+/+}$ (**Figure 2.17C**). Importantly, mice receiving V617F-$Stk4^{+/-}Stk3^{+/-}$ cells were significantly more likely to experience adverse MPN progression and succumb to a lethal MF within the course of the 36-week analysis (**Figure 2.17D**). Upon necessary euthanasia of moribund mice, massive splenomegaly was apparent (**Figure 2.19A**) and mice had experienced a sharp

decline in peripheral cell numbers and were both thrombocytopenic and anemic (**Figure 2.19B**). High-grade reticulin fibrosis was readily apparent in bone marrow sections from moribund mice (**Figure 2.19C**). Enlarged spleens showed increased vascularity with greater reticulin fiber deposition outside of vasculature (**Figure 2.19D**). None of the moribund mice showed detectable myeloid blasts or further evidence of transformation to AML (not shown). Together, these phenotypes were consistent with a diagnosis of post-Polycythemia Vera MF. We terminated the experiment at an endpoint of 36 weeks and euthanized remaining mice in order to assess the relative degree of MPN progression. Higher-grade bone marrow reticulin fibrosis, relative bone marrow hypocellularity, and a trend towards enhanced splenomegaly were apparent within the total population of V617F-Stk4$^{+/-}$Stk3$^{+/-}$ compared to V617F-Stk4$^{+/+}$Stk3$^{+/+}$ (**Figures 2.17E, 2.17F, 2.18, and 2.19E**). These results demonstrate that heterozygous Hippo kinase inactivation contributed to accelerated MPN progression towards myelofibrotic transformation.

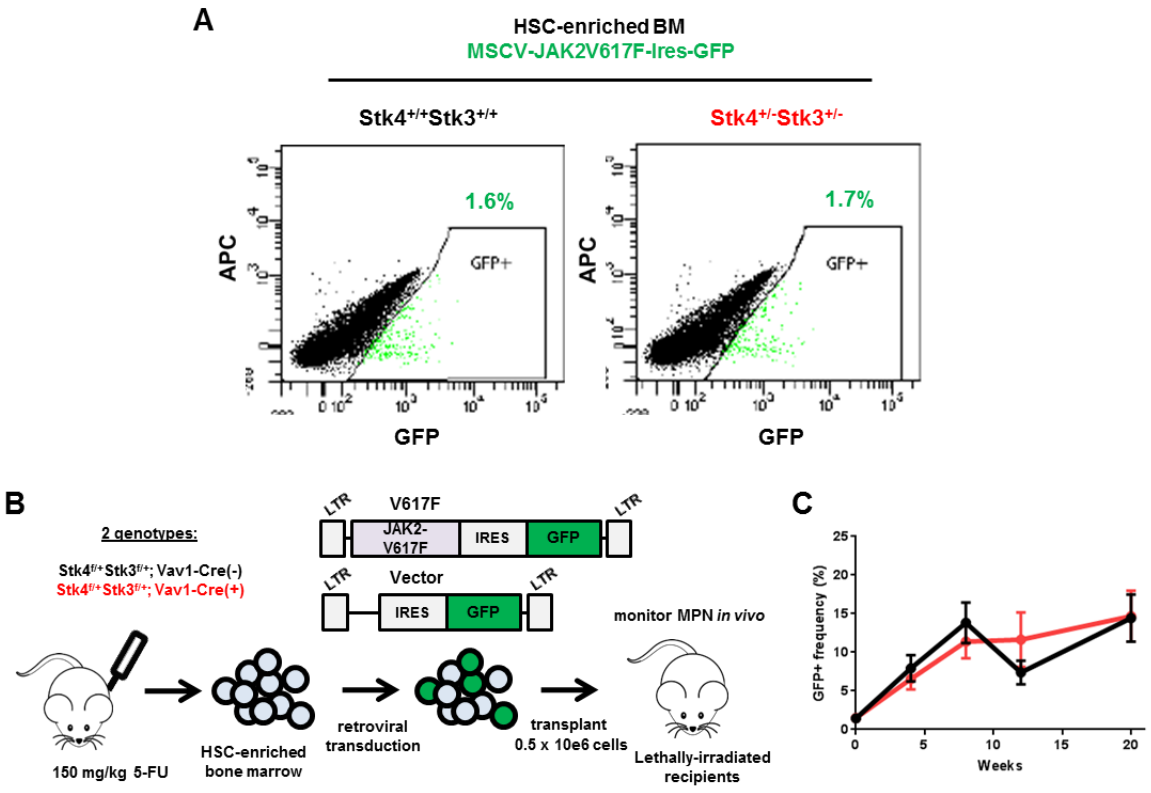

Figure 2.16. Modeling heterozygous Hippo kinase inactivation in a JAK2-V617F MPN model.

(A) Flow cytometry plot, gated on viable cells (PI-), measuring GFP+ percentages in transduced HSC-enriched bone marrow cells approximately 24 hours post-transduction. **(B)** Experimental schematic demonstrating strategy for JAK2-V617F retroviral transduction/transplantation murine model of MPN. Mice were monitored up 36 weeks post-transplant. 5-FU treated bone marrow was pooled from nine mice per genotype per transduction/transplantation experiment. Total numbers of mice analyzed in this model are as follows: N = 11 (Vector-Stk4$^{+/+}$Stk3$^{+/+}$), N = 10 (Vector-Stk4$^{+/-}$Stk3$^{+/-}$), N = 14 (V617F-Stk4$^{+/+}$Stk3$^{+/+}$), and N = 15 (V617F-Stk4$^{+/-}$Stk3$^{+/-}$). **(C)** Peripheral blood GFP+ (JAK2-V617F expressing) cell frequencies at indicated time points measured via flow cytometry. N = 14 (V617F-Stk4$^{+/+}$Stk3$^{+/+}$), N = 15 (V617F-Stk4$^{+/-}$Stk3$^{+/-}$). Data are mean +/- S.E.M.

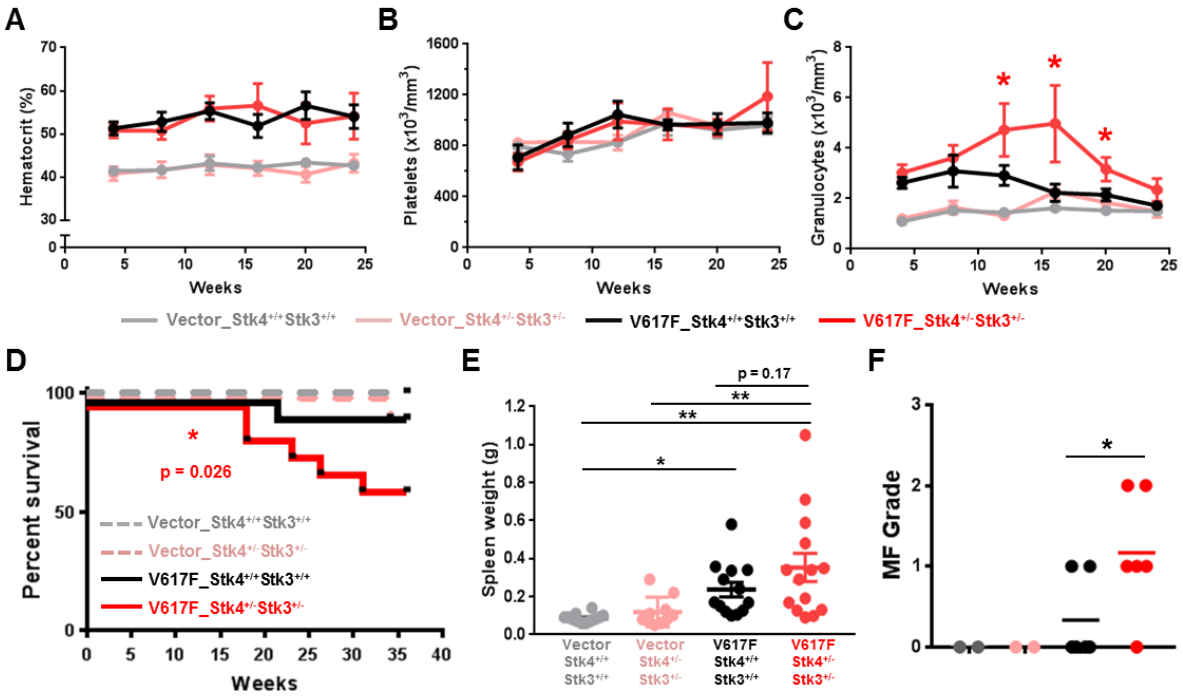

Figure 2.17. Heterozygous Hippo kinase inactivation cooperates with JAK2-V617F to promote lethal myelofibrosis.

(A) Peripheral blood hematocrit (%) measurements at indicated time points. N = 11 (Vector-Stk4$^{+/+}$Stk3$^{+/+}$), N = 10 (Vector-Stk4$^{+/-}$Stk3$^{+/-}$), N = 7 (V617F-Stk4$^{+/+}$Stk3$^{+/+}$), and N = 8 (V617F-Stk4$^{+/-}$Stk3$^{+/-}$). Data are mean +/- S.E.M. * = $p < 0.05$. **(B)** As (A), but for platelet counts. **(C)** As (A), but for granulocyte counts. **(D)** Kaplan-Meier survival plot indicating overall survival for the indicated groups over the course of 36 weeks. Statistical significance is determined by Log rank (Mantel-Cox) test. N = 11 (Vector-Stk4$^{+/+}$Stk3$^{+/+}$), N = 10 (Vector-Stk4$^{+/-}$Stk3$^{+/-}$), N = 14 (V617F-Stk4$^{+/+}$Stk3$^{+/+}$), and N = 15 (V617F-Stk4$^{+/-}$Stk3$^{+/-}$). * = $p < 0.05$. **(E)** Spleen weights for mice of the indicated groups analyzed at the 36 week endpoint or upon necessary euthanasia due to disease progression. N = 11 (Vector-Stk4$^{+/+}$Stk3$^{+/+}$), N = 10 (Vector-Stk4$^{+/-}$Stk3$^{+/-}$), N = 13 (V617F-Stk4$^{+/+}$Stk3$^{+/+}$), and N = 14 (V617F-Stk4$^{+/-}$Stk3$^{+/-}$). Statistical significance is determined by one-way ANOVA followed by post-hoc Tukey test for multiple comparisons. Data are mean +/- S.E.M. * = $p < 0.05$, ** = $p < 0.01$. **(F)** Quantification of MF grade (0 – 3) in murine bone marrow sections, 36 weeks post-transplant, based on an established fibrosis grading scale (see methods). Statistical significance between V617F groups was determined by two-tailed student's t-test. * = $p < 0.05$.

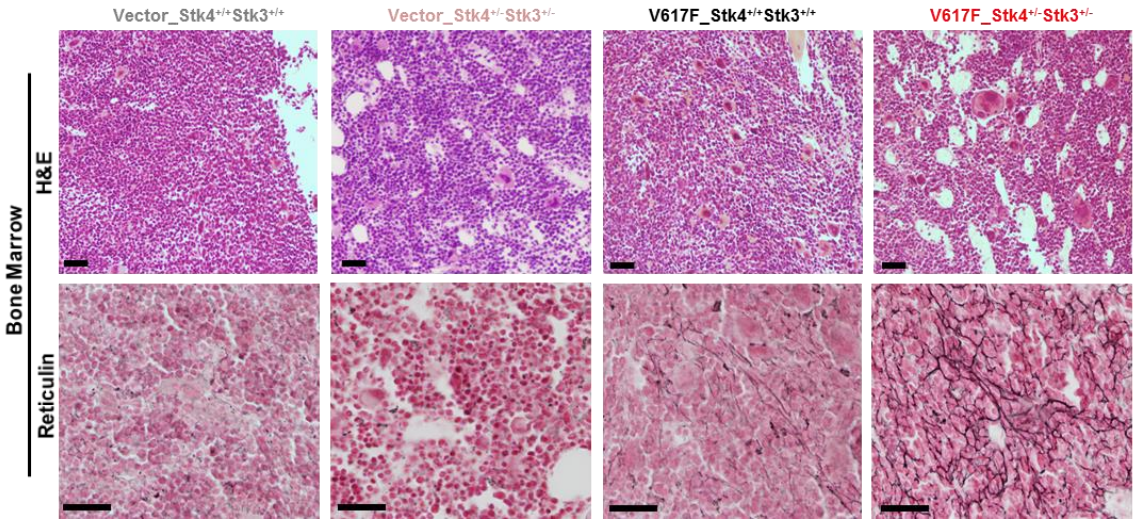

Figure. 2.18. Enhanced reticulin bone marrow fibrosis in JAK2-V617F;Stk4$^{+/-}$ Stk3$^{+/-}$ mice.

Representative H&E-stained (top) and Reticulin-stained (bottom) images from the three groups indicated. Vector are representative of grade 0 MF, V617F-Stk4$^{+/+}$Stk3$^{+/+}$ is representative of grade 0 - 1 MF, and V617F-Stk4$^{+/-}$Stk3$^{+/-}$ is representative of grade 1 - 2 MF. Scale bar = 100 µM.

Figure 2.19. Additional characterization of bone marrow and splenic fibrosis in moribund JAK2-V617F;Stk4$^{+/-}$Stk3$^{+/-}$ mice.
Genotypes used in this model are: Stk4$^{f/+}$Stk3$^{f/+}$;Vav1-Cre^{+} (Stk4$^{+/-}$Stk3$^{+/-}$) and Stk4$^{f/+}$Stk3$^{f/+}$; Vav1-Cre^{-} (Stk4$^{+/+}$Stk3$^{+/+}$), with or without transduction with JAK2-V617F (V617F) **(A)** Representative splenomegaly from mice that were euthanized due to progression to MF (right side) are compared to a representative wild-type control spleen (left side). Ruler is shown for scale. **(B)** Image shows representative femur (inside Eppendorf tube) from a wild-type control (left) and moribund V617F-Stk4$^{+/-}$Stk3$^{+/-}$ (right) mouse demonstrating visible anemia in the bone marrow. **(C)** Reticulin-stained bone marrow section from wild-type (left) or moribund V617F-Stk4$^{+/-}$ Stk3$^{+/-}$ mouse (right) with post-Polycythemia vera myelofibrosis. Scale bar = 100 μM. **(D)** Reticulin-stained spleen section from wild-type (left) or moribund V617F-Stk4$^{+/-}$ Stk3$^{+/-}$ mouse (right) with post-Polycythemia vera myelofibrosis. Scale bar = 500 μM. **(E)** Representative spleens from mice of the indicated groups and genotypes at the experimental endpoint of 36 weeks. Ruler is shown for scale.

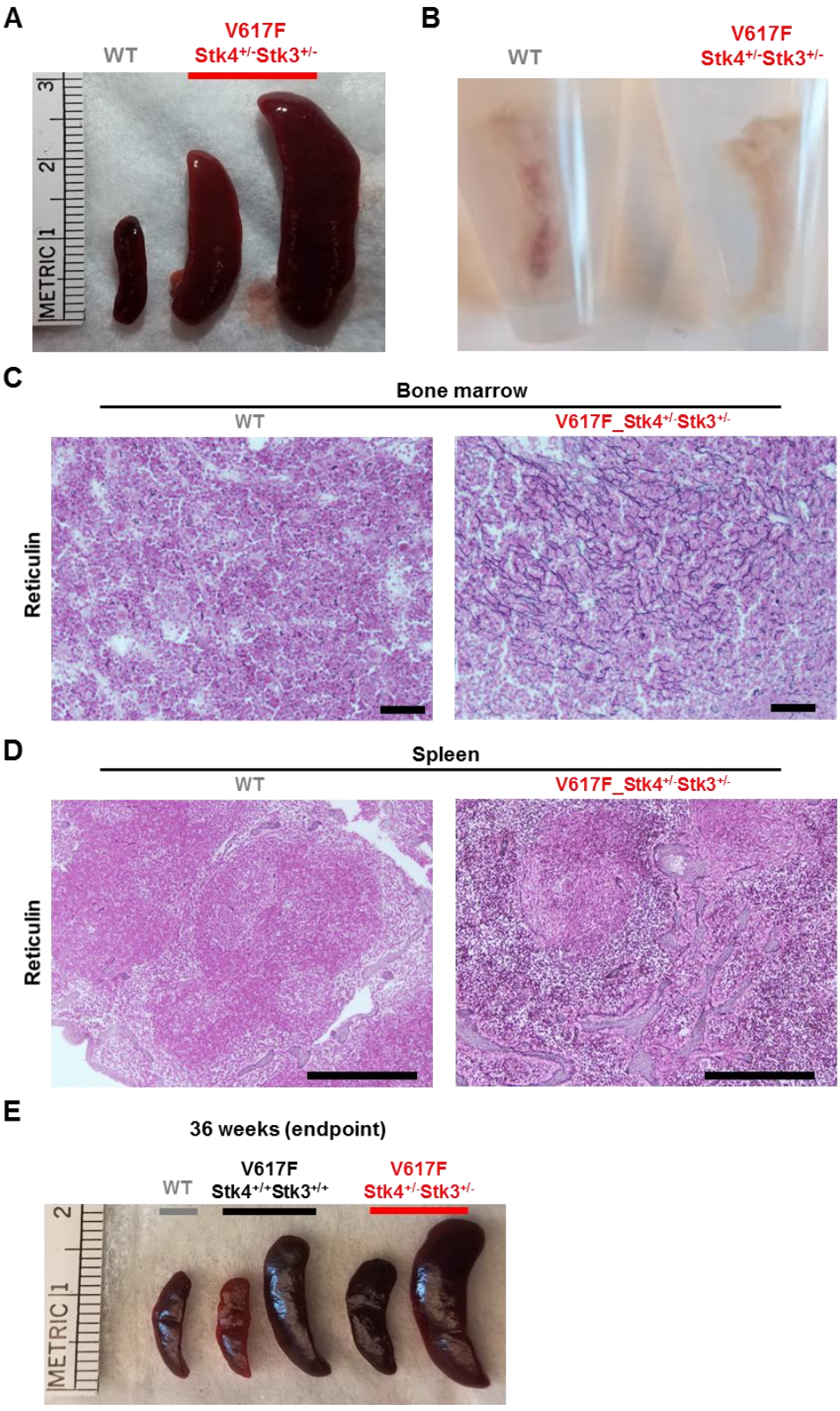
A
WT
V617F
Stk4+/-Stk3+/-
METRIC
B
WT
V617F
Stk4+/-Stk3+/-
C
Bone marrow
WT
V617F_Stk4+/-Stk3+/-
Reticulin
D
Spleen
WT
V617F_Stk4+/-Stk3+/-
Reticulin
E
36 weeks (endpoint)
WT
V617F
Stk4+/+Stk3+/+
V617F
Stk4+/-Stk3+/-
METRIC

2.2.6. *Stk4* loss cooperates with JAK2-V617F to activate innate immune responses and proinflammatory cytokine production

Altered cytokine production is important for MPN pathogenesis in both human patients and mouse models[121-123]. To identify the biological basis through which loss of Hippo kinase signaling contributes to MPN progression, we performed *in vivo* quantitative cytokine profiling using a multiplex Quantibody array[124] (**Figure 2.20A**). We reliably measured the abundance of 153 unique proteins in three mice each of the four experimental groups in our MPN model (**Figure 2.20A**). Principal component analysis and hierarchical clustering indicated that JAK2-V617F expression had a greater overall effect on variance in cytokine abundance than did genotype (**Figure 2.21A and 2.21B**). This analysis identified a core subset of proteins that were uniquely more or less abundant (**Figure 2.20B**) in serum from the V617F-Stk4$^{+/-}$ Stk3$^{+/-}$ group. To further explore the unique differences in our MPN model, we compared significantly elevated proteins in each of the V617F-expressing groups against vector-transduced control mice from both genotypes (**Figure 2.20C**). A total of 18 proteins were significantly elevated in V617F-expressing mice relative to vector controls. Among these, seven were common between genotypes, including CXCL1, CXCL9 (MIG), and TGF-β1; while another seven were unique to V617F-Stk4$^{+/-}$Stk3$^{+/-}$, including IL-6, IL-1β, IL-15, and MMP-3. We also performed Ingenuity Pathway Analysis, using a ranked list based on z-score against a background reference of the entire set of measured proteins, to predict upstream regulators in hematopoietic cells that define the unique cytokine profile associated with the V617F-Stk4$^{+/-}$Stk3$^{+/-}$ group (**Figure 2.20D**). This analysis predicted several activated upstream regulators

associated with innate immune signaling, including TLR4, TLR2, MYD88, and IKKα, consistent with the most significantly elevated cytokines in the double mutant context being canonical proinflammatory mediators associated with NF-κB activation.

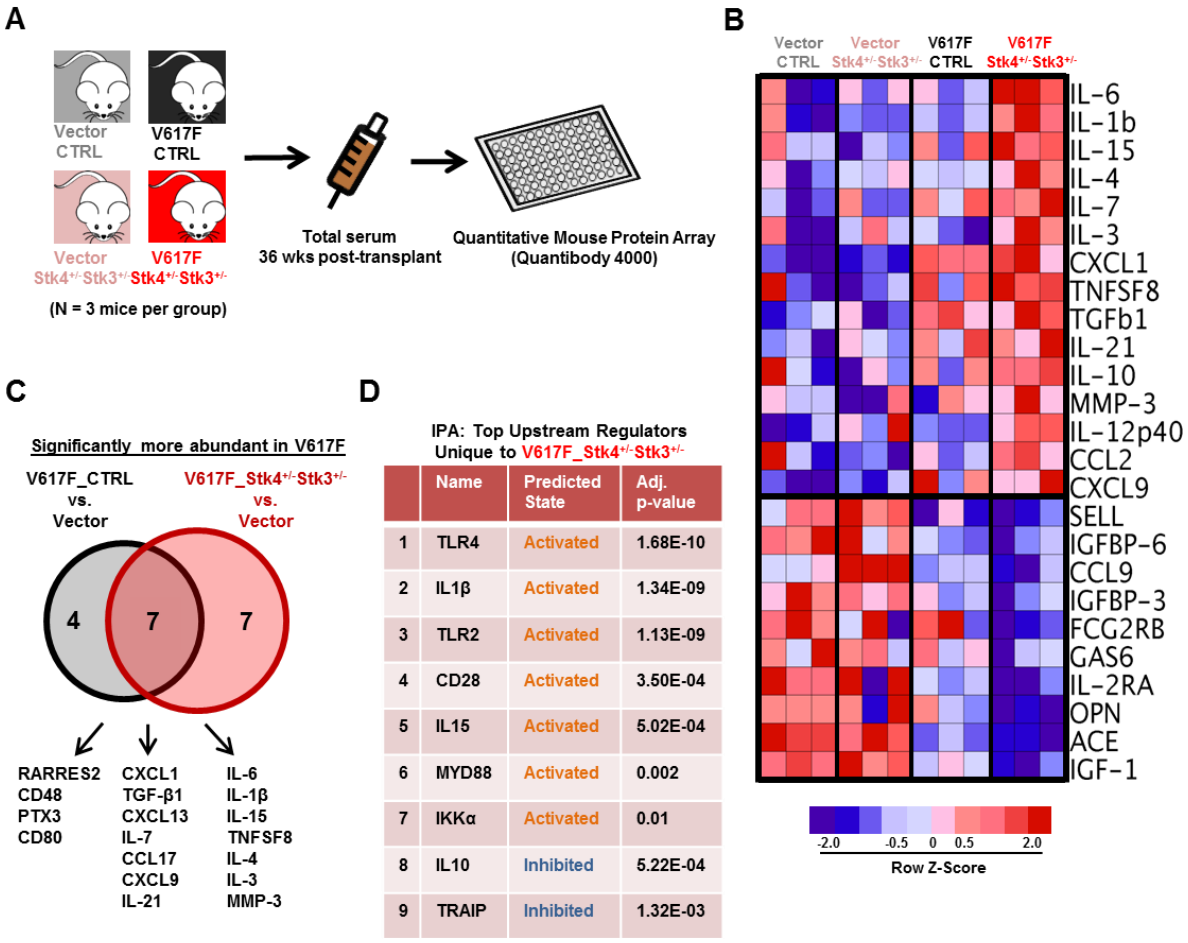

	Name	Predicted State	Adj. p-value
1	TLR4	Activated	1.68E-10
2	IL1β	Activated	1.34E-09
3	TLR2	Activated	1.13E-09
4	CD28	Activated	3.50E-04
5	IL15	Activated	5.02E-04
6	MYD88	Activated	0.002
7	IKKα	Activated	0.01
8	IL10	Inhibited	5.22E-04
9	TRAIP	Inhibited	1.32E-03

Figure 2.20. Hippo kinase deletion cooperates with JAK2-V617F to activate innate immune response and proinflammatory cytokine production.
(A) Experimental schematic for array-based serum cytokine profiling in JAK2-V617F MPN model *in vivo*. **(B)** Heatmap displaying the relative abundance of the most uniquely enriched (top) or depleted (bottom) cytokines in V617F-Stk4$^{+/-}$Stk3$^{+/-}$ mice (based on mean z-scores of three independent mice). **(C)** Venn diagram comparing the significantly more abundant (FDR < 0.1) cytokines in either V617F-Stk4$^{+/+}$Stk3$^{+/+}$ group (left circle) or V617F-Stk4$^{+/-}$Stk3$^{+/-}$ group (right circle) when compared against six Vector-transduced mice. **(D)** List depicting the results of Ingenuity Pathway Analysis (IPA) top predicted upstream regulators analysis, based on submission of a ranked-list of relative cytokine abundance z-scores in V617F-Stk4$^{+/-}$Stk3$^{+/-}$ against a reference background of the entire set of measured cytokines in the array. Upstream regulator name, predicted activation state (activated or inhibited), and adjusted p-values are indicated.

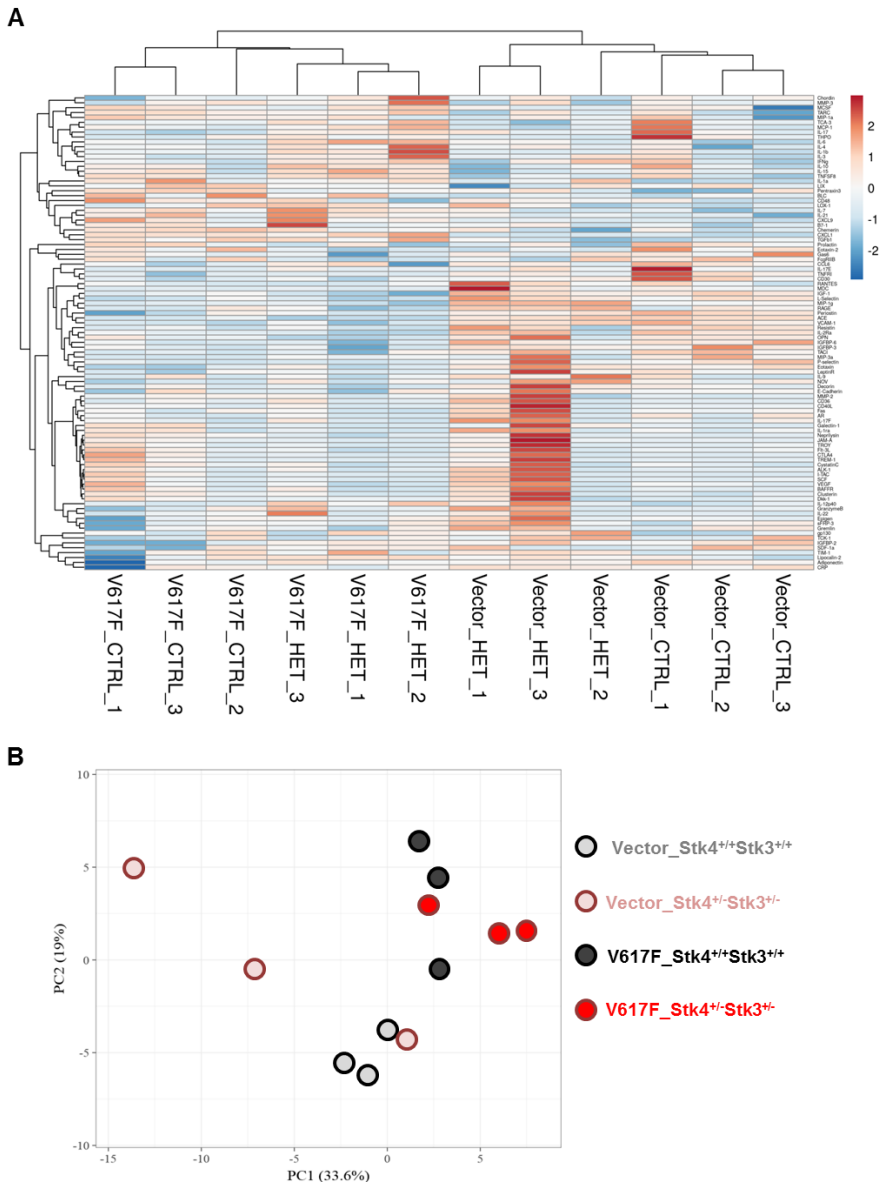

Figure 2.21. JAK2-V617F expression has a greater effect on serum cytokine variance than does genotype.
(A) Hierarchical clustering analysis of serum protein abundance in three mice per experimental group is performed for both columns (individual mice) and rows (individual serum proteins) by using correlation distance and average linkage. Unit variance scaling is applied for row normalization. **(B)** Principal component analysis (PCA) of serum protein abundance in three mice per experimental group is performed by singular value decomposition (SVD) with imputation method. Unit variance scaling is applied for row normalization. Principal component 1 (PC1) and principal component 2 (PC2) explain 33.6% and 19% of total variance, respectively. Both panels are generated using ClustVis (https://biit.cs.ut.ee/clustvis/).

2.2.7 MST1 negatively regulates IRAK1/TRAF6-mediated innate immune activation of NF-κB

The *in vivo* analysis of cytokine profiles in our JAK2-V617F model led us to hypothesize that del(20q)-associated loss of *STK4* may contribute to hematologic malignancy through chronic innate immune activation. To explore the relevance of MST1-mediated negative regulation of innate immune signaling through TLR/IL-1R signaling pathways we confirmed a recently reported interaction between MST1 and IRAK1[73] (**Figure 2.22A**). To test whether MST1 may negatively regulate NF-κB activation in myeloid malignancy we performed *STK4* knockdown in human myeloid THP-1 cells. Even in the absence of an external inflammatory stimulus, *STK4* knockdown was sufficient to induce an NF-κB transcriptional response including upregulation of proinflammatory cytokine genes *IL6*, *IL1B*, and *IL15* that were enriched in the mouse model, and are elevated in myelofibrosis patients (**Figure 2.22B**)[125]. Consistent with a negative regulatory role at the level of IRAK1, *STK4* knockdown resulted in enhanced phosphorylation of innate immune signaling components IκBα, NF-κB p65, and IRAK1, following LPS stimulation (**Figure 2.22C**).

Increased activation of innate immune signaling through IRAK1/TRAF6 is well-established to induce MDS phenotypes and bone marrow failure in mice[96,126,127]. We therefore performed co-immunoprecipitation experiments with HA-tagged ubiquitin (HA-Ub) to measure TRAF6 E3 ubiquitin ligase activity and self-ubiquitin chain formation, which facilitate downstream assembly and activation of the TAK1-TAB and IκB kinase complexes in innate immune signaling[128]. Co-expression of MST1, but not a kinase-dead mutant MST1-K59R, was sufficient to reduce ubiquitin chain formation

on TRAF6 (**Figure 2.23A**).Co-expression of MST1 also significantly reduced TRAF6-mediated activation of a NF-κB luciferase reporter construct to approximately 60% of levels observed in controls, confirming its negative effect on downstream activation of NF-κB (**Figure 2.23B**). Together, these data demonstrate that MST1 has a biological role in suppression of NF-κB activation in innate immune signaling through IRAK1/TRAF6.

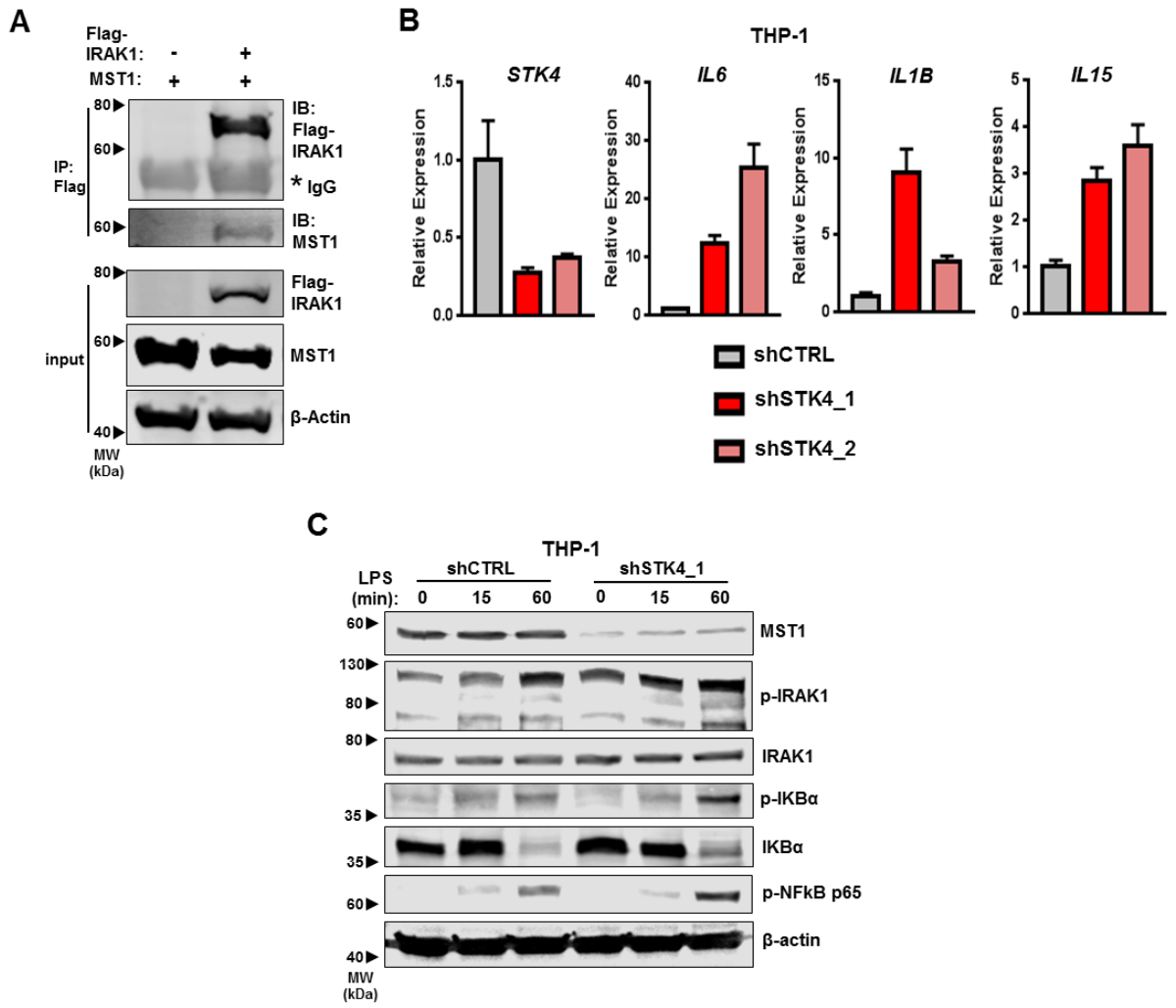

Figure 2.22. MST1 negatively regulates NF-κB activation through IRAK1.
(A) Interaction between IRAK1 and MST1 is assessed in HEK293T cell lysates by immunoblotting for MST1 and Flag-IRAK1 following Flag-IP. Input is shown below by immunoblotting for Flag-IRAK1, MST1, and β-Actin as a loading control. **(B)** Gene expression measured by RT-qPCR in THP-1 cells 72 hours post-transduction with control shRNA (shCTRL, grey) or two independent *STK4*-targeting shRNAs (shSTK4_1/2, red/pink). Data are mean +/- S.E.M. for three independent biological replicates. **(C)** Western blot showing indicated protein and phospho-protein abundance in THP-1 cells 72 hours post-transduction with shCTRL or shSTK4_1 vectors and stimulated with LPS (100 ng/mL) for the times indicated.

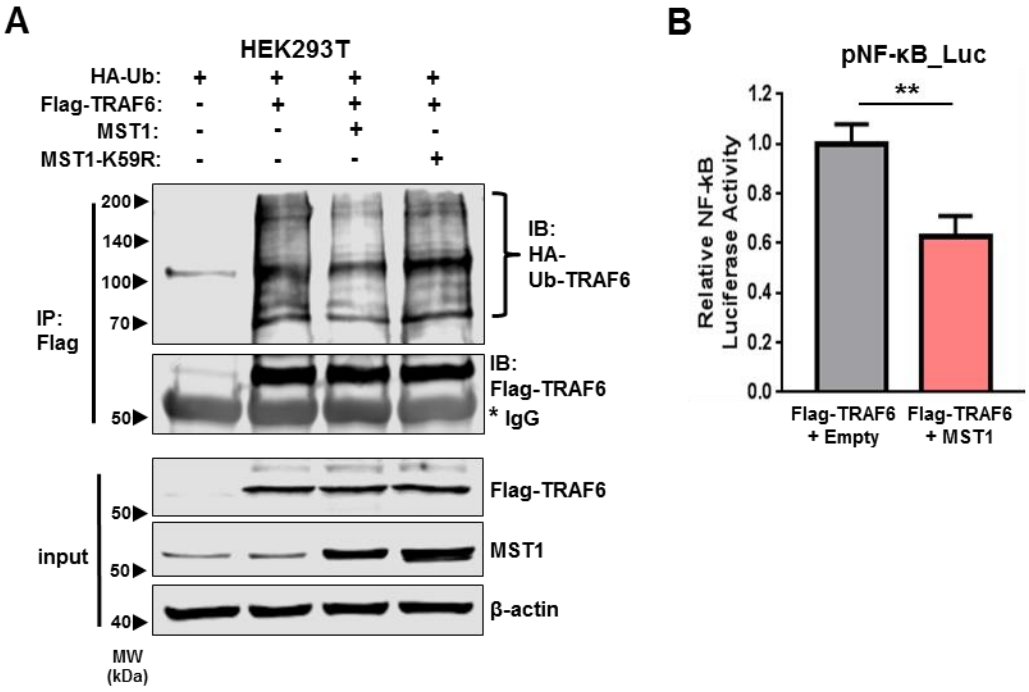

Figure 2.23. MST1 negatively regulates innate immune activation through IRAK1/TRAF6.

(A) Relative ubiquitination of TRAF6 in HEK293T cells transfected to express HA-Ubiquitin (HA-Ub), Flag-TRAF6 and either empty vector (-), MST1, or kinase dead mutant MST1-K59R, assessed by immunoblotting for HA-Ub following Flag-IP (HA-Ub-TRAF6). Input is shown below by immunoblotting for Flag, MST1, and β-Actin as a loading control. **(B)** Relative luficerase activity of a pNF-κB_Luciferase reporter construct (4X NF-κB responsive elements upstream of minimal promoter and firefly luciferase) co-transfected in HEK293T cells with Flag-TRAF6 and either empty vector or MST1 expression vector. pRL-TK (Renilla luciferase reporter) is co-transfected as loading control, and firefly luciferase signal is normalized relative to renilla. Data are mean +/- S.E.M. for three independent biological replicates. Statistical significance is determined by two-tailed student's t-test, ** $p < 0.01$.

2.2.8 IRAK1 inhibition rescues the aberrant inflammatory cytokine production associated with Hippo kinase loss in MPN

Given our identification of *STK4* loss resulting in increased activation of innate immune signaling through IRAK1 and increased proinflammatory cytokine production in the JAK2-V617F MPN model, we wondered whether these phenotypes may be amenable to therapeutic targeting. IRAK1 has been reported as a promising therapeutic target in several hematologic malignancies. To test whether IRAK1 inhibition may be effective in reducing the aberrantly elevated proinflammatory cytokine production associated with accelerated MPN progression to myelofibrosis, we established JAK2-V617F expressing MPNs in both mouse genotypes ($Stk4^{+/+}Stk3^{+/+}$ and $Stk4^{+/-}Stk3^{+/-}$) with similar JAK2-V617F (GFP+) cell engraftment at six weeks post-transplantation, and monitored *in vivo* IL-1β abundance in serum by ELISA (**Figure 2.24A and 2.24B**). Consistent with our previous observations, serum IL-1β was significantly increased in a Hippo kinase loss-dependent manner (**Figure 2.24C**). At this point we administered a course of inhibitor treatment using the small molecule IRAK1/4-inhibitor. Four weeks of IRAK1/4 inhibitor treatment was sufficient to reduce serum IL-1β abundance in V617F-$Stk4^{+/-}Stk3^{+/-}$ mice to comparable amounts as observed in healthy wild-type control mice (**Figure 2.24C**). IRAK1/4-inhibitor treatment similarly reduced the excessive innate immune signaling activation in LPS-stimulated THP-1 cells with *STK4* knockdown (**Figure 2.25**). Together, these results demonstrate the importance of IRAK1 signaling in mediating the aberrant proinflammatory phenotypes associated with Hippo kinase inactivation. We also asked whether a similar course of IRAK1/4-inhibitor administration could rescue

additional hematopoietic phenotypes associated with somatic homozygous Hippo kinase inactivation (**Figure 2.26A**). IRAK1 inhibition was not sufficient to rescue these hematopoietic defects, including the peripheral leukopenia and macrocytic thrombocytopenia (**Figures 2.26B, 2.26C, and 2.26D**), suggesting that there are additional mechanisms and/or signaling pathways involved in the complex hematopoietic phenotypes associated with Hippo kinase loss in these models.

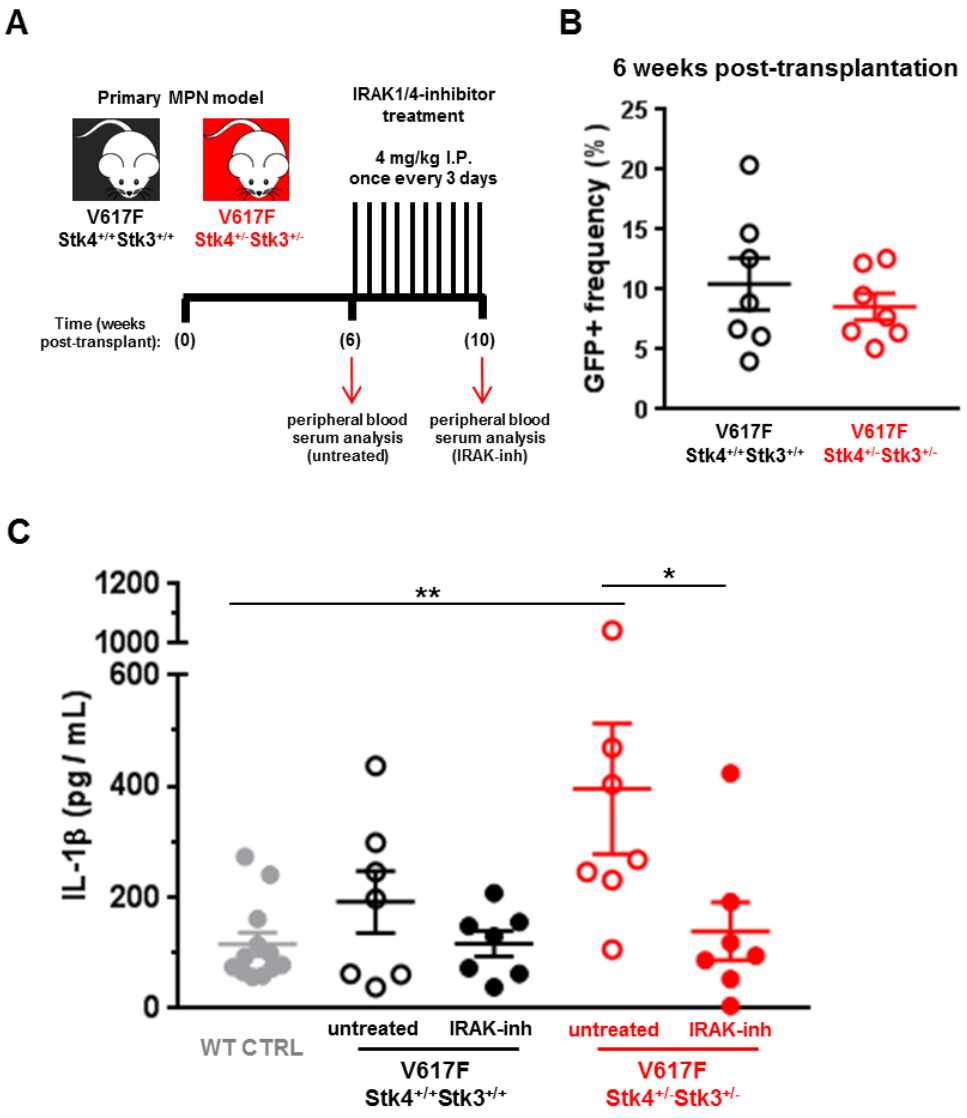

Figure 2.24. IRAK1 inhibition rescues the aberrant proinflammatory cytokine production associated with Hippo kinase loss in MPN.

(A) Experimental schematic depicting strategy for generation of JAK2-V617F MPN model in two genotypes ($Stk4^{+/+}Stk3^{+/+}$ and $Stk4^{+/-}Stk3^{+/-}$) followed by IRAK1/4-inhibitor treatment, 4 mg/kg by intraperitoneal (I.P.) injection once every three days for four weeks. N = 12 (wild type controls), N = 7 (V617F-$Stk4^{+/+}Stk3^{+/+}$), N = 7 (V617F-$Stk4^{+/-}Stk3^{+/-}$). **(B)** GFP+ cell frequencies in peripheral blood measured by flow cytometry at six weeks following transplantation with JAK2-V617F expressing cells of indicated genotypes. **(C)** IL-1β abundance measured by ELISA in peripheral blood serum from mice of the indicated genotypes, pre- (untreated) or post- (IRAK-inh) IRAK1/4-inhibitor treatment as described in (A). Statistical significance is determined by one-way ANOVA followed by post-hoc Tukey test for multiple comparisons, * = $p < 0.05$, ** = $p < 0.01$.

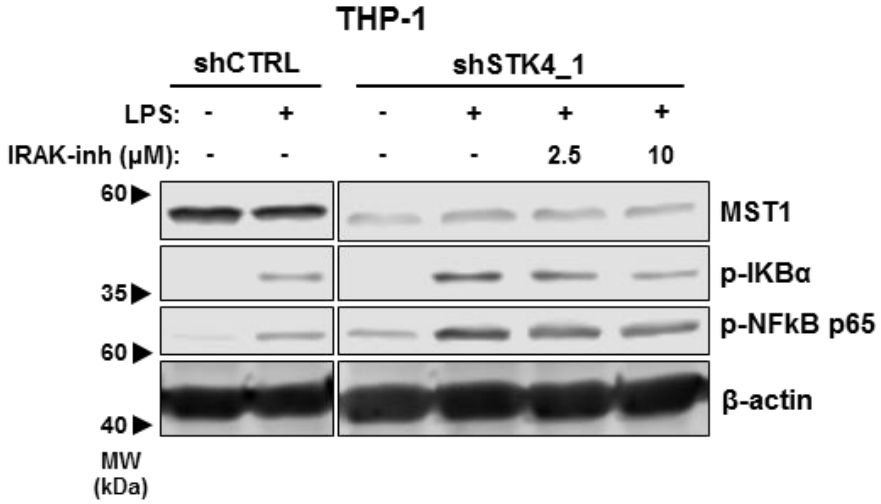

Figure 2.25. IRAK1 inhibition reduces aberrant NF-κB activation associated with *STK4* knockdown.

Western blot showing indicated protein and phospho-protein abundance in THP-1 cells 72 hours post-transduction with shCTRL or shSTK4_1 vectors and stimulated with LPS (100 ng/mL) for two hours. Cells are pre-treated with IRAK1/4-inhibitor (IRAK-inh) overnight at the indicated concentrations and this concentration is maintained during the LPS stimulation period.

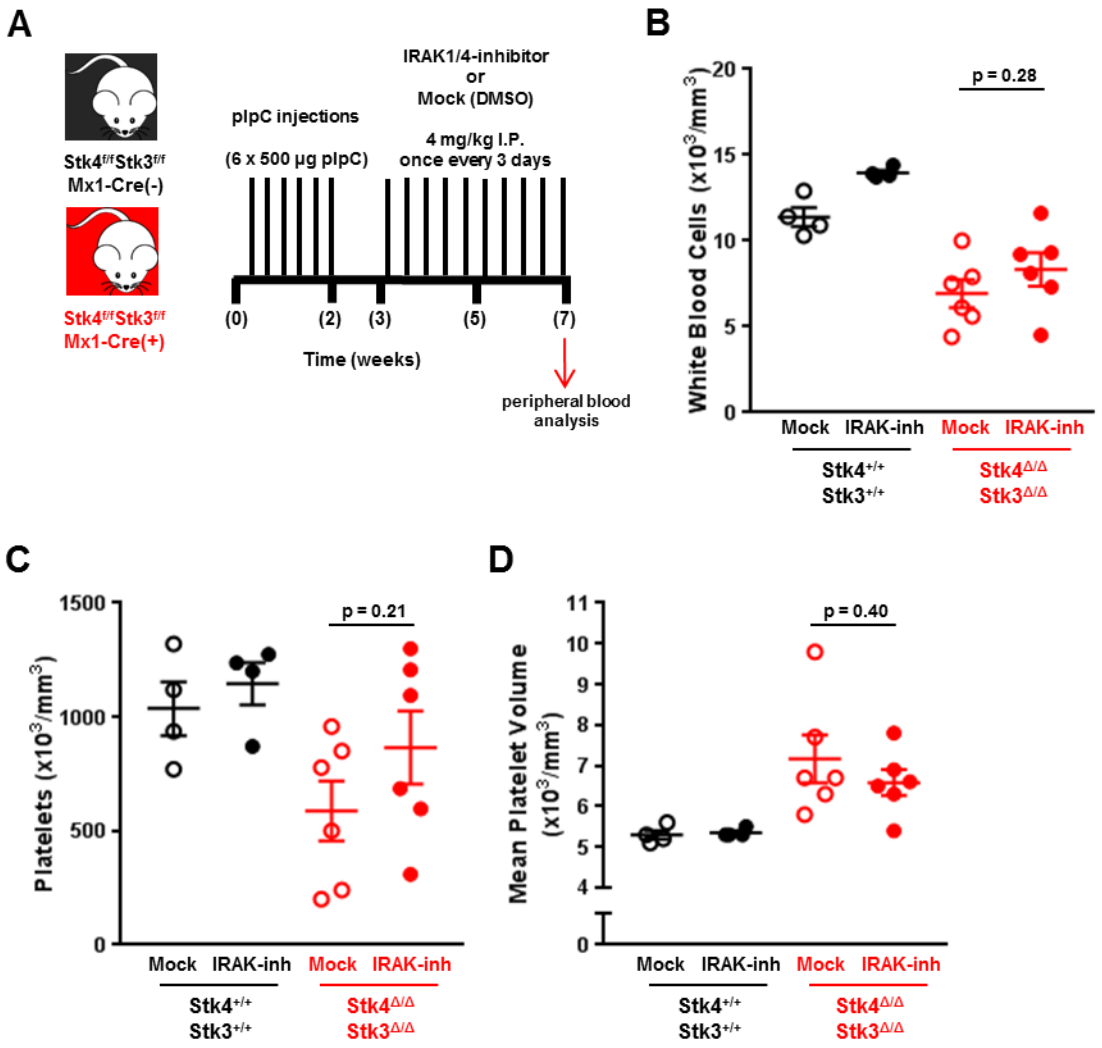

Figure 2.26. IRAK1 inhibition does not rescue additional hematopoietic phenotypes associated with homozygous somatic Hippo kinase inactivation.
(A) Experimental schematic depicting strategy for generation inducible gene inactivation with pIpC followed by IRAK1/4-inhibitor treatment, 4 mg/kg by intraperitoneal (I.P.) injection once every three days for four weeks. N = 4 ($Stk4^{+/+}Stk3^{+/+}$, mock treated), 4 ($Stk4^{+/+}Stk3^{+/+}$, IRAK1/4-inhibitor treated), N = 6 ($Stk4^{\Delta/\Delta}Stk3^{\Delta/\Delta}$, mock treated), N = 6 ($Stk4^{\Delta/\Delta}Stk3^{\Delta/\Delta}$, IRAK1/4-inhibitor treated). **(B)** Peripheral white blood cell counts for mice of the indicated genotypes, following four weeks of mock (5% DMSO) or IRAK1/4-inhibitor treatment, as described in (A). Statistical significance between mock and IRAK-inh treated groups in $Stk4^{\Delta/\Delta}Stk3^{\Delta/\Delta}$ genotype is determined by two-tailed student's t-test. **(C)** As (B), but for platelet counts. **(D)** As (B), but for mean platelet volume (MPV).

2.3. Discussion

Chronic innate immune activation and dysregulated inflammatory signaling has become appreciated as a driver of myelodysplastic syndrome (MDS) pathogenesis[129,130]. Immune activation in MDS can be derived from both cell-extrinsic and cell-intrinsic mechanisms[129-131]. Recent evidence shows that mutations affecting genes involved in seemingly disparate pathways have a common underlying mechanism of activated inflammatory signaling in MDS[132-135]. Chronic NF-κB activation has also been strongly implicated in myeloproliferative neoplasm (MPN) pathogenesis; however the exact mechanisms causing this remain less well-defined[123]. Here we identified a novel mechanistic connection between the non-canonical functions of MST1 in chronic innate immune activation and NF-κB signaling in disease. These data link the recurring del(20q) chromosome abnormality with a commonly disrupted signaling pathway in myeloid malignancy.

The specific molecular events that cooperate with activated JAK2 to promote MPN disease progression to myelofibrosis (MF) are still incompletely understood, and myelofibrotic transformation remains a significant health burden in patients[17,136]. Here we observed clear evidence of accelerated progression from Polycythemia Vera to lethal MF upon heterozygous inactivation of the Hippo kinases in a JAK2-V617F MPN model. Furthermore, a significant portion of double-mutant mice analyzed in our cohorts experienced disease progression that closely resembles what is typically observed in patients, including a pre-fibrotic phase dominated by peripheral granulocytosis followed by progressive anemia and thrombocytopenia with

extramedullary myeloproliferation in the spleen[17]. The genetic interaction between *STK4* inactivation and JAK2-V617F mutation is one of the most clinically significant findings as it indicates cooperation between these lesions could lead to accelerated myelofibrotic transformation in human disease.

This is the first study to implicate the non-canonical functions of Hippo kinase MST1 in MDS and MPN, laying the groundwork for future studies in these disease contexts. Our data demonstrate that MST1 is a negative regulator of innate immune signaling through IRAK1, including the ability to suppress TRAF6 auto-ubiquitination and dampen downstream NF-κB activation in myeloid cells. Development of PMF, or post-Polycythemia Vera MF, is a complex process involving an important role for cytokine secretion and crosstalk between hematopoietic cell populations and bone marrow stromal cells[137]. Our data suggest an important role for hematopoietic-intrinsic activation of innate immune signaling as contributing to this process. Through quantitative serum protein profiling in our mouse model of MPN, we identified significantly elevated proinflammatory cytokines that contributed to remodeling of the bone marrow microenvironment and myelofibrotic progression. Several of the same cytokines identified in our model, including IL-6, IL-1β, and IL-15 are elevated in serum of myelofibrosis patients[125], highlighting the clinical relevance of our study. We further confirmed that the aberrantly elevated IL-1β production in JAK2-V617F and $Stk4^{+/-}Stk3^{+/-}$ double mutant mice was apparent at a relatively early time point in MPN progression. Importantly, we found that IRAK1/4-inhibitor treatment was sufficient to inhibit this chronic innate immune activation and reduce IL-1β abundance in serum in MPN. These findings demonstrate the importance of IRAK1

activation in mediating the proinflammatory phenotypes associated with Hippo kinase inactivation, and are consistent with another study that found *STK4* downregulation in macrophages could accelerate hepatocellular carcinoma development through increased IRAK1-mediated inflammatory signaling[73].

Although Hippo kinase deficiency alone was not sufficient to promote clonal pre-malignant expansion of hematopoietic stem/progenitor populations, we found that it was sufficient to cause specific myelodysplastic features and phenotypes associated with del(20q) in patients. In MDS, del(20q) as a sole abnormality frequently presents as isolated thrombocytopenia[15,16] and, consistent with this, we reproducibly observed megakaryocytic/platelet abnormalities in our conditional knockout mice. There is strong evidence that abnormal megakaryocyte biology leading to reduced platelet production is an inherent feature of del(20q)-associated malignancy. Del(20q) is amongst the most frequent cooperating mutations in MPN overall, yet it is exceedingly rare in essential thrombocythemia patients[19]; and thrombocytopenia (a consistent phenotype in our models) is a significant phenotypic correlation in PMF patients with del(20q)[20]. In contrast to the proinflammatory signaling in the JAK2-V617F model, however, IRAK1 inhibition was not sufficient to rescue the abnormal platelet phenotypes associated with somatic Hippo kinase inactivation, at least in the course of our observations. There are likely additional signaling pathways that may be affected upon Hippo kinase loss and further studies characterizing megakaryocyte-specific inactivation may be interesting to pursue.

In our genetic models we have characterized the consequences of loss of both homologous Hippo kinases *Stk4* (MST1) and *Stk3* (MST2). At the time of performing

this study, mice with floxed alleles for individual Hippo kinase genes were not commercially available. *STK3* is located on chromosome 8 and we did not detect it to be downregulated in MDS or MPN patient cohorts. In most normal tissues MST1 and MST2 are able to functionally compensate for one another, however in the hematopoietic system MST1 is functionally dominant owing to its drastically higher (10-20 fold) mRNA and protein expression. Consistent with this, homozygous germline *Stk4* inactivation results in severe hematopoietic defects in mice, while homozygous germline *Stk3* inactivation has no hematopoietic phenotypes[72]. Therefore, the contribution of *Stk3*/MST2 loss in our described phenotypes is minimal; and where applicable, we utilized *Stk3* allele inactivation to additionally provide a very modest further reduction in total Hippo kinase abundance in an attempt to more closely resemble the total activity that would be observed in patients with sub-haploinsufficient *STK4* expression as was observed in del(20q) MDS and MPN patients.

In summary, our data suggest that loss of Hippo kinase signaling contributes to pathogenesis of myeloid malignancies with chromosome 20q deletions. Heterozygous Hippo kinase inactivation significantly accelerated myelofibrotic transformation in a JAK2-V617F MPN model through effects on innate immune signaling and proinflammatory cytokine production. Further efforts towards therapies aimed at mitigating chronic innate immune activation through IRAK1 may be beneficial in del(20q)-associated myelofibrosis.

2.4. Materials and Methods

ANIMALS

All animal protocols were approved by the UCSD Institutional Animal Care and Use Committee (IACUC). Mice were housed in standard conditions with up to 5 mice per cage, fed standard chow, and monitored in accordance with IACUC guidelines. C57BL/6J (stock # 000664) mice were obtained from The Jackson Lab and maintained in our animal facility for more than 10 generations. Vav1-Cre (stock # 008610)[138] and Mx1-Cre (stock # 003556)[139] transgenic mice were obtained from The Jackson Lab and maintained as hemizygotes in our animal facility for more than 10 generations. *Stk4*- and *Stk3*- floxed mice (stock # 017635)[140] were obtained from The Jackson Lab and maintained as homozygotes for floxed alleles in our animal facility. *Stk4*- and *Stk3*-floxed mice were crossed into the various Cre strains as described in main text. To control for any potential genetic background effects, all mice (or mouse-derived hematopoietic cells used for transplantations) were analyzed in groups with littermates of the same generation of backcross into respective Cre strains. For use in all described competitive bone marrow transplant assays, the C57BL/6 congenic strain carrying the differential CD45.1 leukocyte receptor, B6.SJL-*Ptprc*^{a} *Pepc*^{b}/BoyJ (stock # 002014) were obtained from The Jackson Lab and maintained in our animal facility for more than 10 generations. Genotyping for floxed alleles and Cre transgenes was conducted as described on The Jackson Lab website for each respective strain.

ANTIBODIES

Western blotting: MST1 (Cell Signaling, #3682); MST2 (Cell Signaling, #3952); Phospho-MOB1 (Thr35) (Cell Signaling, #8699); Phospho-IκBα (Ser 32) (Cell Signaling, #2859); IκBα (L35A5) (Cell Signaling, #4814); Phospho-NF-kB p65 (Ser536) (93H1) (Cell Signaling, #3033); Phospho-IRAK1 (T209) (Abcam, #ab218130); IRAK1 (D51G7) (Cell Signaling, #4505); Monoclonal Anti-Flag M2 (Sigma, #F3165); Monoclonal Anti-HA (HA-7) (Sigma, #H9658); β-Actin clone AC-15 (Millipore Sigma, #A1978); IRDye 800CW anti-mouse IgG (Li-Cor, #925-32210); IRDye 680LT anti-rabbit IgG (Li-Cor, #925-68021)

Flow cytometry: FITC anti-mouse CD45.1 (eBioscience, #11-0453-85); FITC anti-mouse CD45.2 (Biolegend, #109806); FITC anti-mouse Ter-119 (eBioscience, #11-5921-81); FITC anti-mouse Ly-6G (Biolegend, #127606); FITC anti-mouse B220 (Biolegend, #103206); PE anti-mouse CD71 (eBioscience, #12-071-82); PE anti-mouse CD48 (Biolegend, #103406); PerCP/Cy5.5 anti-mouse CD3ε (Biolegend, #100328) [Lineage cocktail]; PerCP/Cy5.5 anti-mouse CD4 (Biolegend, #100540) [Lineage cocktail]; PerCP/Cy5.5 anti-mouse CD8α (eBioscience, #45-0081-82) [Lineage cocktail]; PerCP/Cy5.5 anti-mouse CD11b (Biolegend, #101228) [Lineage cocktail]; PerCP/Cy5.5 anti-mouse Gr-1 (Biolegend, #108428) [Lineage cocktail]; PerCP/Cy5.5 anti-mouse Ter-119 (Biolegend, #116228) [Lineage cocktail]; PerCP/Cy5.5 anti-mouse B220 (Biolegend, #103236) [Lineage cocktail]; PerCP/Cy5.5 anti-mouse CD19 (eBioscience, #45-0193-82) [Lineage cocktail]; PerCP/Cy5.5 anti-mouse CD127 (eBioscience, #45-1271-82) [Lineage cocktail]; PE/Cy7 anti-mouse CD117 (Biolegend, #105814); APC anti-mouse CD3ε

(eBioscience, #17-0031-82); APC anti-mouse CD11b (Biolegend, #101212); APC anti-mouse B220 (Biolegend, #103212); APC anti-mouse Sca-1 (Biolegend, #108112); Biotin anti-mouse CD150 (eBioscience, #13-1501-82); APC/AlexaFlour750 Streptavidin (Molecular Probes, #SA1027).

BONE MARROW TRANSPLANTATION

C57BL/6J (stock # 000664) transplant recipient mice were obtained from The Jackson Lab and maintained in our animal facility for more than 10 generations. For use in all described competitive bone marrow transplant assays, the C57BL/6 congenic strain carrying the differential CD45.1 leukocyte receptor, B6.SJL-*Ptprc*^{a} *Pepc*^{b}/BoyJ (stock # 002014) were used as recipients. These were obtained from The Jackson Lab and maintained in our animal facility for more than 10 generations. Recipient mice were between 8-12 weeks of age at time of transplantation and contained equal distributions of males and females. Recipient mice were randomly allocated amongst experimental groups while maintaining a matched distribution based on both age and sex. All lethal irradiations were performed as a single administration of a dosage of 9.5 Gy approximately 6-8 hours prior to transplantation of cells.

For non-competitive transplantation experiments, total bone marrow from three mice each of indicated genotypes was harvested as described in the ‘Hematopoietic cell isolation and collection’ section and pooled together based on genotype. These total bone marrow cells were then immediately used for transplantations via resuspension in PBS at a density of 2 x 10^{7} cells/mL and 100 µl of cell suspension

was administered per mouse (i.e. 2 x 10^6 cells per recipient mouse) via intravenous tail-vein injection. No additional helper cells were used during the transplantation experiments, and therefore the post-irradiation bone marrow of recipient mice is derived from the transplant donor cell genotype.

For competitive bone marrow transplantation experiments, total bone marrow from three mice each of indicated genotypes (in CD45.2 leukocyte receptor background) was harvested as described in the 'Hematopoietic cell isolation and collection' section and pooled together based on genotype. Total bone marrow was harvested in parallel from three mice of C57BL/6 congenic strain carrying the differential CD45.1 leukocyte receptor and pooled. CD45.2 ('donor') bone marrow cells were mixed at a 1:1 ratio with CD45.1 ('recipient') cells, and these cells were then immediately used for transplantations via resuspension in PBS at a density of 2 x 10^7 cells/mL and 100 µl of cell suspension was administered per mouse (i.e. 2 x 10^6 cells per recipient mouse) via intravenous tail-vein injection in B6.SJL-*Ptprc*^{a} *Pepc*^{b}/BoyJ (CD45.1) recipient mice. For analysis, donor-derived (CD45.2) frequencies were then measured in the peripheral blood beginning four weeks post-transplantation.

For the JAK2-V617F MPN model, hematopoietic stem cell-enriched (via 5-FU administration) bone marrow cells were harvested as described in the 'Hematopoietic cell isolation and collection' section and transduced as described in the 'Viral Transduction' section. The total population of cells (of which ~2% are transduced with JAK2-V617F) were resuspended in PBS at a density of 0.5 x 10^7 cells/mL and 100 µl of cell suspension was administered per mouse (i.e. 0.5 x 10^6 total cells per recipient

mouse) via intraveneous tail-vein injection. No additional helper cells were used during the transplantation experiments, only the untransduced bone marrow cell population of the indicated genotype, and therefore the post-irradiation bone marrow of recipient mice is derived from the transplant donor cell genotype (i.e. $Stk4^{+/+}Stk3^{+/+}$ or $Stk4^{+/-}Stk3^{+/-}$), of which ~2% are transduced with JAK2-V617F (GFP+) at initial time of transplantation. Successful engraftment of transduced donor bone marrow cells were confirmed via measuring GFP+ cell frequency in the peripheral blood four weeks post-transplantation, and any mice showing undetectable GFP+ cell frequency are excluded from further analysis in the model.

CELL LINES

HEK293T cells were acquired from ATCC. Cells were cultured in DMEM (HyClone, #SH30022.01) supplemented with 10% bovine calf serum and 1% penicillin/streptomycin at standard conditions of 5% CO_2 at 37°C. THP-1 cells were acquired from ATCC. Cells were cultured in RPMI supplemented with 10% fetal bovine serum and 1% penicillin/streptomycin at standard conditions of 5% CO_2 at 37°C.

CHEMICAL AND INHIBITOR TREATMENTS

IRAK1/4 inhibitior was purchased from Tocris Bioscience (#5665-50). IRAK1/4 inhibitor was resuspended in DMSO at a concentration of 10 mM and aliquoted prior to use. For injection into mice working solutions were prepared by dilution of stock inhibitor solution 1:20 into 0.22 μM filtered PBS. Working solutions were then heated

to 55 °C for approximately 15 minutes and subjected to rocking at room temperature for 4 – 6 hours to aid in resuspension. Where applicable, an equal volume of 5% DMSO solutions were injected as controls (Mock treatment). For *in vivo* IRAK1/4 inhibitor experiments, 4 mg/kg intraperitoneal (I.P.) injections were performed once every three days throughout the total course of treatment (4 weeks). For cell culture experiments working solutions were prepared via dilution in cell culture media (supplemented RPMI), heated to 37 °C, and similarly rocked at room temperature to aid in resuspension, prior to administering to cells. THP-1 cells were cultured overnight in media containing the indicated concentrations of inhibitor, or mock control media (0.1% DMSO), prior to, and during, stimulation with LPS (100 ng/mL) for two hours the next morning.

LPS (List Biological Laboratories, #201) stock solutions were prepared by resuspension in sterile H_20 at a concentration of 5 mg/mL. Working solutions were prepared by subsequent serial dilution in cell culture media, and administration to cells was performed at a final concentration of 100 ng/mL for the times indicated in the manuscript.

Polyinosinic-polycytidylic acid (pIpC) (Sigma, #P0913) was resuspended in sterile H_2O at a concentration of 1 mg/mL. Prior to injection, pIpC was temporarily heated to 65°C, and then cooled to room temperature. To induce gene inactivation *in vivo* using the Mx1-Cre system, 500 µg per mouse was injected intraperitoneally (I.P.) every other day for a total of 6 doses.

5-Fluorouracil (5-FU) (Sigma, #F6627) was resuspended in sterile H_2O at a concentration of 15 mg/mL. Prior to injection, 5-FU was temporarily heated to 70°C to

assist with resuspension, and then cooled to room temperature. 5-FU was administered to mice as a single dose of 150 mg/kg by intraperitoneal (I.P.) injection. Bone marrow from 5-FU treated mice for use in transplantation experiments was harvested 5 days following injections. Any mice that did not show myeloablation in the bone marrow at time of cell harvest were excluded from use for any downstream experiments.

FLOW CYTOMETRY AND CELL SORTING

Flow cytometric analysis was conducted using a BD FACSCanto instrument equipped with standard lasers (488 nm, 640 nm) and filters. Data collection was performed using BD FACSDiva software. Compensation was set up using appropriate single-stained controls and positive-staining gates were established using appropriate FMO controls. Post-acquisition data analysis was performed using FlowJo software (FlowJo, LLC). Flow sorting of bone-marrow mononuclear cells was performed on a FACSAriaII equipped with standard lasers (405 nm, 488 nm, 640 nm) and filters, and using a nozzle size of 85 μm. Stainings were conducted in PBS supplemented with 0.1% bovine serum albumin. Antibody validation and optimal antibody concentrations for stainings were pre-determined via titration.

GENE EXPRESSION ANALYSIS

For gene expression analysis in CD34+ bone marrow cells comparing del(20q) MDS patients with healthy normal individuals, we utilized a previously published MDS patient gene expression dataset (GSE58831). Individual Affymetrix CEL files from 6

del(20q) MDS patients (MDS097, MDS113, MDS129, MDS158, MDS187, MDS202) and 10 normal controls (NBM01-NBM10) were downloaded from NCBI GEO repository. Array normalization using the RMA method and differential gene expression file creation were performed using the 'ExpressionFileCreator' (V 12.0) module on the Gene Pattern public server. P-values were calculated by a standard Benjamini & Hochberg (False Discovery Rate) method. For display purposes, a gene expression heatmap was generated using the 'HeatMapImage' (V 6.0) module on the Gene Pattern public server. Color scheme for gene expression values are normalized by row. Data from the top 25 significantly downregulated genes (by adjusted p-value) were used for generation of heatmap. For more information, see the specific module descriptions on the Gene Pattern webpage (https://genepattern.broadinstitute.org).

HEMATOPOIETIC CELL COLLECTION AND ISOLATION

Bone marrow cells were harvested by flushing two femurs and two tibias per mouse with ice cold PBS using disposable syringes with 21-gauge needles. Splenocytes were harvested by physical tissue disruption and repeated pipetting in ice cold PBS. Red cell lysis was performed by resuspending cell mixture in ice cold ACK buffer (0.1 mM Na_2EDTA, 10 mM $KHCO_3$, 150 mM NH_4Cl) for 5 minutes, followed by washing with ice cold PBS and passage through a 40 μM cell strainer to eliminate large tissue/cell clumps and debris. For short-term culture and retroviral transduction/transplantation experiments, hematopoietic cells were resuspended in IMDM supplemented with 10% fetal bovine serum, 1% penicillin/streptomycin, recombinant mIL-3 (10 ng/mL), hIL-6 (10 ng/mL), and mSCF (20 ng/mL). Where

applicable, mouse lineage-negative (Lin^-) cells were isolated according to manufacturer's instructions using mouse Lineage Cell Depletion Kit (Miltenyi Biotec, #130-090-858), and enrichment efficiency was verified via flow cytometry.

LUCIFERASE ASSAY

HEK293T cells seeded in 24-well plates were transfected with a pNFκB_Luciferase reporter vector (100 ng) containing 4X NF-κB responsive elements upstream of a minimal TATA promoter, pRL-TK *Renilla* luciferase control vector (25 ng), MIP-empty or MIP-MST1 (80 ng), and pcDNA3-Flag-TRAF6 (10 ng). 48 hours following transfections, luciferase activity was measured on a BD Monolight 3010 luminometer using the Dual-Luciferase Reporter Assay System (Promega) according to manufacturer's instructions. pcDNA3-Flag-TRAF6 was first confirmed to activate pNFκB_Luciferase activity relative to an empty vector control.

PERIPHERAL BLOOD ANALYSIS

Peripheral blood samples (approximately 100 µl per mouse) were collected in EDTA-coated microvettes (Fisher Scientific, # NC9299309) by submandibular venipuncture using 5 mm animal lancets (Braintree Scientific, #GR5MM). Analysis of differential blood cell counts and parameters was performed using a Scil Vet abc Plus+ instrument (Henry Schein Animal Health). Instrument was regularly calibrated and maintained according to manufacturer's instructions. GFP+ cell frequencies in peripheral blood samples were measured by flow cytometry via dilution of peripheral blood samples in ACK buffer for 5 minutes, followed by washing once in 1 mL PBS,

and resuspension in 350 µl of PBS prior to flow cytometric analysis. Non-viable cells were excluded from analysis via addition of propidium iodide (PI). Differential blood cell frequencies were secondarily verified by flow cytometry (for example, CD11b+/Gr-1+ staining for measuring granulocyte frequencies).

PRINCIPAL COMPONENT ANALYSIS AND HIERARCHICHAL CLUSTERING

Principal component analysis (PCA) and hierarchical clustering of differentially abundant serum proteins were performed using ClustVis.[141] PCA is performed by singular value decomposition (SVD) method with unit variance scaling for row (individual serum proteins) normalization. Hierarchical clustering is performed using correlation distance and average linkage with unit variance scaling for row (individual serum proteins) normalization.

qPCR ANALYSIS

Cell lysis and RNA isolation were performed using Trizol reagent (ThermoFisher Scientific, #15596026) according to manufacturer's instructions. cDNA was prepared from 0.5 – 1 µg RNA using qScript cDNA Supermix (Quanta, #95048) according to manufacturer's protocol. Quantitative PCR was performed using KAPA SYBR Fast 2X Master Mix (KAPA Biosystems, #KK4618) according to manufacturer's protocol, in 20 µl reactions, each performed in technical duplicates. qPCR reactions were performed using a BioRad CFX Connect instrument. Data analysis was performed using a standard delta-delta Ct method relative to the

geometric-mean of two reference genes, *GAPDH* and *POLR2A* (human cell experiments), or relative to the mean of *Gapdh* (murine experiments).

SERUM PROTEIN PROFILING AND IL-1β ELISA

For Quantibody array based serum protein profiling aproximately 0.5 - 1 mL peripheral blood was collected in non-EDTA coated vacutainer tubes by submandibular venipuncture during terminal analysis of mice at 36 weeks post-transplantation from three mice per experimental group. Whole blood was incubated at room temperature for 20 minutes followed by centrifugation at 1,800 xg for 10 minutes at 4 °C. Serum was then collected, aliquoted, and stored at -80°C prior to shipping samples. Abundance of 200 mouse serum proteins/cytokines were analyzed by multiplexed sandwich ELISA-based quantitative array platform (Mouse Quantibody 4000 Array, Ray Biotech). Serum protein analysis and quantification was performed by Ray Biotech (https://www.raybiotech.com/). Post-quality controls, a total of 153 serum proteins were effectively quantified by this analysis.

For non-terminal serum assessment of cytokine abundance, 200 µl of peripheral blood was collected in non-EDTA coated vacutainer tubes by submandibular venipuncture. Whole blood was incubated at room temperature for 20 minutes followed by centrifugation at 1,800 xg for 10 minutes at 4 °C. Serum was then collected, diluted 1:4 in reagent diluent solution (1% BSA in 0.22 µm filtered PBS), and stored at -80 °C. Mouse IL-1 beta / IL-1F2 Duoset ELISA was purchased from R & D Systems (DY401-05). ELISA-based measurement of serum IL-1β in the JAK2-V617F model was performed according to manufacturer's instructions. For

IRAK1/4 inhibitor-related experiment, serum was analyzed from a total of 12 age-matched wild-type control mice, seven JAK2-V617F;$Stk4^{+/+}Stk3^{+/+}$ (measured pre- and post-IRAK1/4 inhibitor treatment), and seven JAK2-V617F;$Stk4^{+/-}Stk3^{+/-}$ (measured pre- and post-IRAK1/4 inhibitor treatment). Recombinant IL-1β standards used for establishment of standard curve quantification (working range: 15.6 pg/mL – 1000 pg/mL) were measured in technical triplicate, and experimental serum samples were measured in technical duplicates. Absorbance measurements were performed using a microplate reader at 450 nm wavelength with background correction for individual wells performed by subtraction of absorbance measured at 570 nm.

STATISTICAL ANALYSIS

Statistical analyses were conducted using GraphPad Prism (V 7.0) software. Individual statistical tests used for data analysis are indicated in figure legends. All data are displayed as mean (bar graph, horizontal line, or point) with error bars always representing S.E.M. All student's t-tests are conducted as two-tailed tests. Statistical significance in figures is displayed as follows: * = $p < 0.05$, ** = $p < 0.01$, *** = $p < 0.001$. In some cases, where p values are close to reaching a statistical significance threshold, exact values are displayed in figure panels. Where applicable, mouse sample sizes for measurement of various blood parameters were determined based on a minimal meaningful effect size of one standard deviation from a distribution of healthy wild-type control mice, assuming power = 0.9 and $\alpha = 0.05$.

TISSUE FIXATION AND HISTOLOGY

Femurs and tibias were decalcified and fixed for 72 hours at room temperature in Cal-Ex II (Fisher Scientific, #CS511-1D). Spleens were fixed for 72 hours at room temperature in 4% formaldehyde (Fisher Scientific, #BP531-500). All tissue processing and staining was performed by the UCSD Moores Cancer Center Tissue Technology Shared Resource. Multiple sections per paraffin block were stained with hematoxylin and eosin (H&E), reticulin silver stain for reticulin fiber deposition, and trichrome stain for collagen deposition. For grading myelofibrosis in mouse bone marrow sections a scale was established based on both criteria established in human MPN patients and in previous mouse models of JAK2(V617F)-driven MPN, using experimentally unrelated wild-type mice as negative controls:

0 – near absence of reticulin fibers, no more reticulin fibers than non-experimental wild-type C57BL/6 mice

1 – low/medium density of reticulin fibers throughout sections without a high-degree of interconnectedness between fibers or only showing intense staining and interconnectedness in focal areas

2 – high density and staining intensity of reticulin fibers throughout sections with consistently high degree of interconnectedness

3 – high density and staining intensity of reticulin fibers throughout sections with

consistently high degree of interconnectedness and significant collagen deposition as detected by trichome stain.

VECTORS

JAK2 (V617F)-pcw107-v5 was a gift from David Sabatini and Kris Wood (Addgene plasmid # 64610). To generate the MSCV-JAK2(V617F)-IRES-GFP vector used in the current study a JAK2(V617F) PCR fragment with added SalI sites was digested and subsequently ligated into XhoI-digested MSCV-IRES-GFP vector. pcDNA3-Flag-TRAF6 was a gift from Michael Karin (Addgene Plasmid # 66929). pJ3M-MST1 (Addgene Plasmid # 12203) and pJ3M-MST1-K59R (Addgene Plasmid # 12204) were gifts from Jonathan Chernoff. MST1 and MST1-K59R were subcloned into MSCV-Ires-Puro$_R$ (MIP) vector backbones for use in experiments described here. pcDNA3-HA-Ubiquitin (HA-Ub) was generated by sub-cloning processed wild-type ubiquitin cDNA into the pCDNA3.1-HA vector backbone. pNF-κB_Luc plasmid (Agilent Technologies) consists of 4X NF-κB responsive elements upstream of a minimal TATA promoter and firefly luciferase. pRL-TK *Renilla* luciferase control reporter vector was purchased from Promega. Vector cDNA sequences were confirmed by Sanger sequencing (Eton Bioscience, San Diego, CA).

VIRAL TRANSDUCTION

For retroviral transduction of JAK2-V617F: Transfections of HEK293T cells were conducted by combining 5 μg of MSCV-IRES-GFP or MSCV-JAK2(V617F)-IRES-GFP retroviral expression vector, 5 μg of ecotropic packaging vector (pIK6.1-

MCV.ecopac.UTd), and 40 µl of polyethylenimine (PEI) in 1 mL of Opti-MEM reduced serum medium (Gibco, #31985-070). Approximately 16 hours post-transfection, media was aspirated, cells were washed once in PBS, and 6 mL fresh IMDM (Gibco, #12440-053) supplemented with 10% fetal bovine serum was added to each plate. 24 hours following media change, IMDM media containing retroviral particles was collected, passed through a 0.45 µm syringe filter, pooled, and supplemented with recombinant cytokines mIL-3 (10 ng/mL), hIL-6 (10 ng/mL), and mSCF (20 ng/mL), and polybrene (4 µg/mL). For retroviral transduction, HSC-enriched bone-marrow mononuclear cells harvested from mice were resuspended in this supplemented retroviral supernatant at densities of 2-3 x 10^6 cells/mL and centrifuged (2,000 xg) in 6-well plates at 32°C for 3 hours (Allegra X-12R centrifuge, Beckman Coulter); followed by overnight culture at 37°C. Two consecutive retroviral transductions were performed in this manner on subsequent days. Transduction efficiency was measured (GFP+ frequency) by flow cytometry the morning following the second centrifugation (immediately prior to transplantation into recipient mice). Low retroviral titers were utilized, which were typically measured at ~1.5-2% GFP+ following two rounds of transduction.

For lentiviral transduction of shRNA constructs: Transfections of HEK293T cells were conducted by combining 5 µg of psPAX2, 2.5 µg of pMD2.G, and 3 µg of respective pLKO.1-based shRNA vector, and 44 µl of polyethylenimine (PEI) in 1 mL of Opti-MEM reduced serum medium (Gibco, #31985-070). Approximately 16 hours post-transfection, media was aspirated, cells were washed once in PBS, and 10 mL fresh RPMI supplemented with 10% fetal bovine serum was added to each plate. 24

hours following media change, RPMI media containing lentiviral particles was collected, passed through a 0.45 µm syringe filter, pooled, and supplemented with polybrene (final working concentration: 4 µg/mL). For lentiviral transduction, THP-1 cells were resuspended in this supplemented retroviral supernatant at densities of ~0.5 x 10^6 cells/mL and centrifuged (2,000 xg) in 6-well plates at 32°C for 3 hours (Allegra X-12R centrifuge, Beckman Coulter); followed by overnight culture at 37°C. Two consecutive transductions were performed in this manner on subsequent days. 24 hours following second transduction cells were resuspended in 1.0 µg/mL puromycin, and selected for 72 hours, at which point viable drug-resistant cells were enriched via FICOLL gradient. Post-selection cells were maintained in growth media supplemented with 0.5 µg/mL puromycin.

WESTERN BLOTTING and CO-IMMUNOPRECIPITATION

Samples were lysed in ice-cold NP-40 lysis buffer (50 mM Tris pH 8.0, 150 mM NaCl, 1% NP-40) supplemented with protease inhibitor (Roche, #11873580001) and phosphatase inhibitor (Roche, #4906845001). Lysates were cleared by centrifugation at 11,000 xg for 10 minutes at 4°C, and denatured in 2X loading buffer (0.125 M Tris-HCl pH 6.8, 4% SDS, 10% B-mercaptoethanol, 20% glycerol, 0.004% bromophenol blue). For co-immunoprecipitation experiments approximately 500 µg lysate was combined with 40 µl of anti-Flag M2 agarose beads (Sigma, #M8823) and incubated at 4°C with rotating overnight. The following morning beads were washed 4X with ice-cold NP-40 lysis buffer via centrifugation at 11,000 xg. Washed beads were then resuspended in 60 µl 2X loading buffer and denatured prior to loading.

Immunoblotting was performed using the Li-Cor Odyssey infrared imaging instrument. Post-acquisition image analysis and cropping was performed using Li-Cor Image Studio Lite (V 5.2.5) software.

For TRAF6 auto-ubiqutin chain formation co-immunoprecipitation experiments, transfections of HEK293T cells are performed in 10 cm plates using pcDNA3-empty or pcDNA3-Flag-TRAF6 (2.5 μg), MIP-empty or MIP-MST1 or MIP-MST1-K59R (5 μg), pcDNA3-HA-Ub (6 μg), and 55 μl polyethylenimine (PEI). Approximately 16 hours post-transfection, media was aspirated, cells were washed once in PBS, and 10 mL fresh media was added. 48 hours following initial transfection cells are harvested and lysed for subsequent western blotting and co-immunoprecipitation experiments as described above.

Chapter 2, in full, has been submitted for publication. Stoner SA, Yan M, Liu K, Arimoto K, Shima T, Wang HY, Johnson DT, Bejar R, Jamieson C, Guan KL, and Zhang DE. “Hippo Kinase Loss Contributes to Del(20q) Hematologic Malignancies through Chronic Innate Immune Activation.” The dissertation author is the primary investigator and author of the manuscript.

Chapter 3. A non-canonical Hippo-RASSF2 signaling pathway controls Rac-GTPase activation and is therapeutically exploitable in hematologic cancer

Ras-association domain family members (*RASSF1-10*), which encode peripheral Hippo pathway components with small GTPase binding ability, are among the most frequent transcriptionally-altered genes in cancer, yet remarkably little is known of their functions. Through biochemical and functional studies, we herein define a novel Hippo-RASSF2 pathway that regulates basal Rac GTPase activity in hematological cancer and can be exploited for therapy in patients. This non-canonical signaling mechanism is independent of Hippo kinase activity, and is instead mediated by a SARAH domain-dependent interaction. Using proximity-based biotin labeling, we associate RASSF2 with Rho GTPase-related complexes and identify a direct interaction with the critical Rac guanine nucleotide exchange factor (GEF), DOCK2. RASSF2 promotes DOCK2 GEF activity *in vitro*; and *RASSF2* knockdown is sufficient to functionally abolish GTP-bound Rac and promote growth-arrest in leukemia cells. Importantly, RASSF2 expression is broadly correlated with leukemia cell sensitivity to small-molecule inhibition of DOCK2 GEF activity, revealing novel mechanistic insight and providing a functional biomarker for sensitivity to perturbation of this pathway in hematological cancer.

3.1. Introduction

Hematologic cancer is dominated by mutations and large-scale chromosome abnormalities affecting transcription factors, splicing factors, and epigenetic regulators, which promote malignancy through alteration of gene expression[142-146]. These altered gene expression events effectively 're-program' signaling pathways in cancer cells to promote transformation; but also cause the acquisition of novel dependencies that can be therapeutically-exploited to inhibit malignant cell growth and survival[147]. Despite knowledge of the recurring somatic mutations affecting transcriptional regulators across cancer, the specific gene expression changes that contribute to development of individual malignancies, such as acute myeloid leukemia (AML), remain incompletely understood.

By performing gene expression analysis using a murine AML model driven by the t(8;21)-associated oncofusion protein, RUNX1-ETO (RUNX1-RUNX1T1, AML1-ETO)[90], we previously identified Ras-association domain family member 2 (*Rassf2*) as a gene that is significantly downregulated in murine leukemia blasts[148], and set out to characterize the significance of this in hematologic cancer. The 'classical' *RASSFs* (*RASSF1-6*) are among the most frequent transcriptionally-altered genes in human cancer[149]. RASSF proteins are non-enzymatic adaptors defined by the presence of both a small GTPase-binding (Ras-association) domain and a C-terminal Salvador-Rassf-Hippo (SARAH) domain[150]. Family member RASSF1A, in particular, functions as a ubiquitous tumor suppressor that experiences transcriptional silencing through promoter hypermethylation at high frequencies in cancer[151,152], which

contributes to tumorigenesis via several mechanisms[153-155]. Other individual RASSFs display more nuanced cell-type specific expression patterns and functions[107,108,156]. Although linked with both oncogenic Ras signaling[157] and the Hippo tumor suppressor pathway[158], the functions of RASSF2 remain largely unknown. In pursuing these functions, we herein identify an unexpected role for RASSF2 as a critical regulator of the Rac subfamily of Rho GTPases.

Rho-family small (~21kDa) GTPases are essential for regulation of numerous cellular functions. There are 20 members of the Rho family in mammals, of which four (Rac1, Rac2, Rac3, RhoG) belong to the Rac subfamily[159]. Each Rac GTPase functions as a molecular switch by cycling between an active GTP-bound form and an inactive GDP-bound form[160]. Activation of these proteins is tightly controlled in a tissue- and context-specific manner by guanine-nucleotide exchange factors (GEFs), GTPase activating proteins (GAPs), and guanine-nucleotide dissociation inhibitors (GDIs)[160-162]. In addition to their normal cellular functions, Rac GTPases contribute to cancer development as downstream effectors of growth factor receptor signaling and oncogenic mutations in the Ras pathway[163-165]. Activating point mutations in Rac1 and Rac2 have been detected in solid tumors and hematologic malignancies[166,167]. Furthermore, Rac1 and Rac2 are essential for sustained cell proliferation and survival in murine leukemia models[168,169]. Rac GTPases represent attractive targets for therapy in hematologic cancer, however direct targeting of small GTPases has proved difficult and largely ineffective[163,170,171]. A thorough understanding of the diverse mechanisms controlling Rac activation in cancer will therefore be essential towards identifying novel therapeutic avenues and improving outcomes in patients.

Here, through biochemical and functional characterization of RASSF2 in leukemia models, we have identified a novel signaling mechanism linking non-canonical functions of mammalian Hippo kinases with control of Rac GTPase activation in hematologic cancer. We find targeting this pathway via shRNA-mediated perturbation or through the use of a small molecule inhibitor of the atypical Rac-specific GEF, DOCK2, to be therapeutically effective in leukemia. Furthermore, we demonstrate that RASSF2 expression serves as a functional biomarker for determining sensitivity to these inhibition strategies in leukemia patients, opening the door for novel approaches to therapy.

3.2. Results

3.2.1. *RASSF2* transcription is differentially-regulated across specific AML subtypes

Using a mouse model of t(8;21) AML, we previously identified *Rassf2* as a gene that is transcriptionally-downregulated greater than 20-fold in leukemic blasts compared to normal murine hematopoietic progenitors[148]. We therefore set out to study RASSF2 in the context of myeloid leukemia development. Consistent with an initial report[157], we found *RASSF2* transcript expression to be most abundant in normal human peripheral blood tissue (**Figure 3.1A**). During normal human hematopoiesis *RASSF2* is highly expressed across the majority of lineages and differentiation stages, with further elevated transcription in mature monocyte, neutrophil, and myeloid dendritic-cell populations (**Figure 3.1B**); suggestive of important functions in the myelo-granulocytic lineage. To follow-up on our murine leukemia study we assessed *RASSF2* transcript expression in two cohorts of AML patients (TCGA[142] and GSE13159[172], **Figure 3.2A**). Consistent with the mouse model, *RASSF2* is uniquely downregulated in t(8;21) AML patients relative to other AML subtypes and healthy-donor CD34+ hematopoietic cells. We also found both RASSF2 mRNA (**Figure 3.2B**) and protein (**Figure 3.2C**) expression to be drastically downregulated (~10-50 fold) specifically in t(8;21) AML cell lines relative to non-t(8;21) AML cell lines and human CD34+ cells.

We next sought to determine whether this transcriptional repression was directly mediated by the RUNX1-ETO oncofusion protein in t(8;21) AML[90]. Supporting

this hypothesis, both the canonical *RASSF2* promoter CpG island[173] and a downstream alternative transcription start site demonstrated chromatin co-occupancy of RUNX1-ETO, repressive histone deacetylases (HDAC1/2), and RUNX1-ETO transcription factor complex component LYL1[174], in t(8;21) AML cells (**Figure 3.3A**). These genomic regions are bound by the major hematopoietic transcription factors RUNX1, ERG, and FLI1 in healthy human CD34+ cells[175], demonstrating that they are the major regulatory elements for controlling *RASSF2* expression during hematopoiesis (**Figure 3.1C**). Retroviral transduction of cord-blood derived human CD34+ cells with a RUNX1-ETO expression vector was sufficient to reduce *RASSF2* transcript (**Figure 3.3B**). Similarly, *RUNX1-ETO* knockdown using siRNA targeted to the fusion site[176] was sufficient to increase *RASSF2* mRNA expression in a t(8;21) AML cell line (**Figure 3.3C**). These findings are consistent with published studies in which *RASSF2* is frequently one of the most dynamically upregulated genes following *RUNX1-ETO* knockdown[174,177,178]. Together, these results demonstrate that *RASSF2* is differentially expressed across AML subtypes and is a transcriptional target of the RUNX1-ETO oncofusion protein.

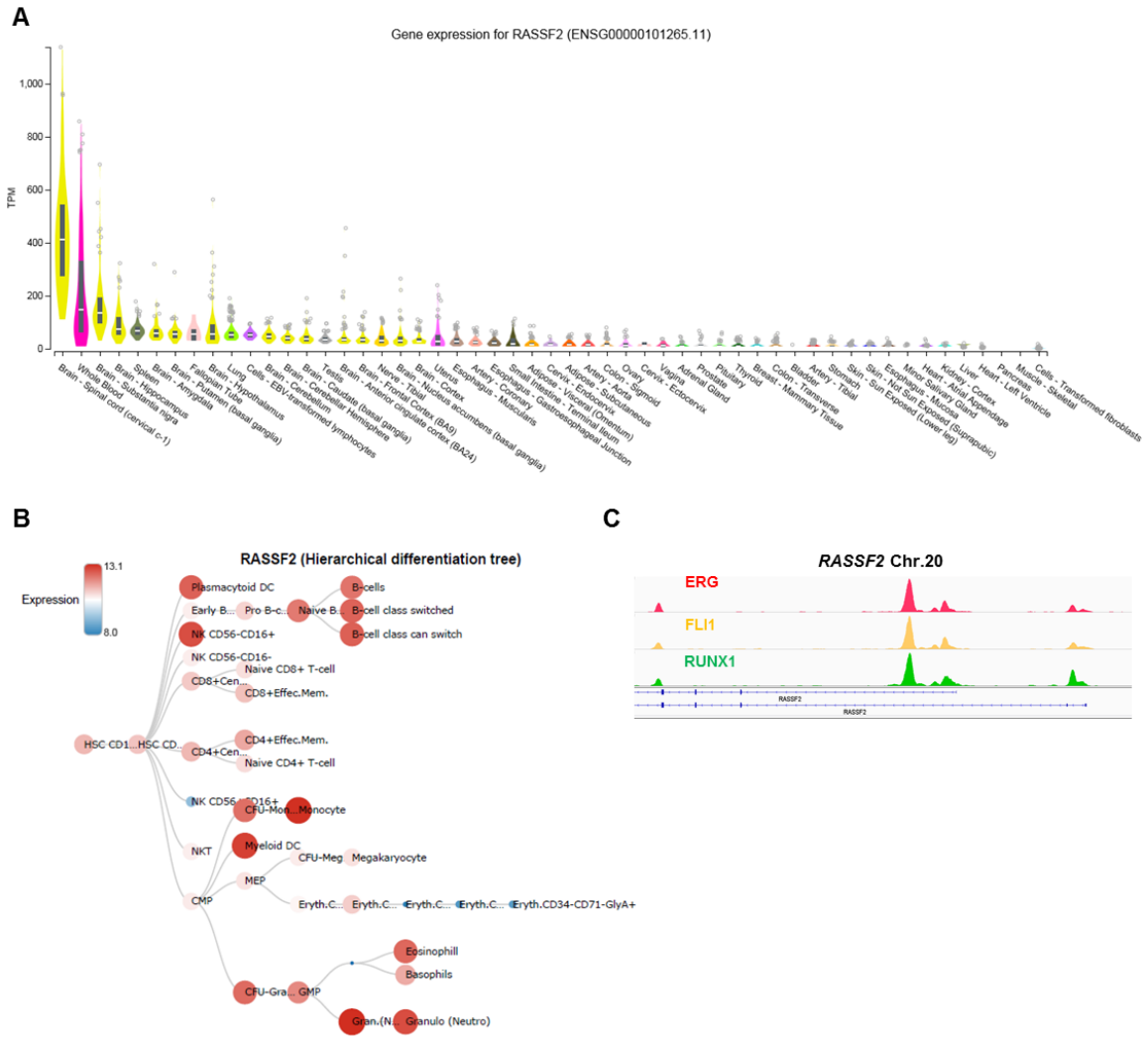

Figure 3.1. Expression and transcriptional regulation of *RASSF2* in normal human hematopoiesis.

(A) *RASSF2* transcript expression across healthy primary human tissue, ranked by abundance. Displayed data are from the human genotype-tissue expression (GTEX) portal[179]. TPM, transcripts per million. **(B)** *RASSF2* transcript expression across normal human hematopoiesis. Data are from [180] and visualized using BloodSpot[181] (www.bloodspot.eu). **(C)** ChIP-seq tracks showing binding of indicated transcription factors within the *RASSF2* genomic locus in normal human CD34+ cells. Data are from [175].

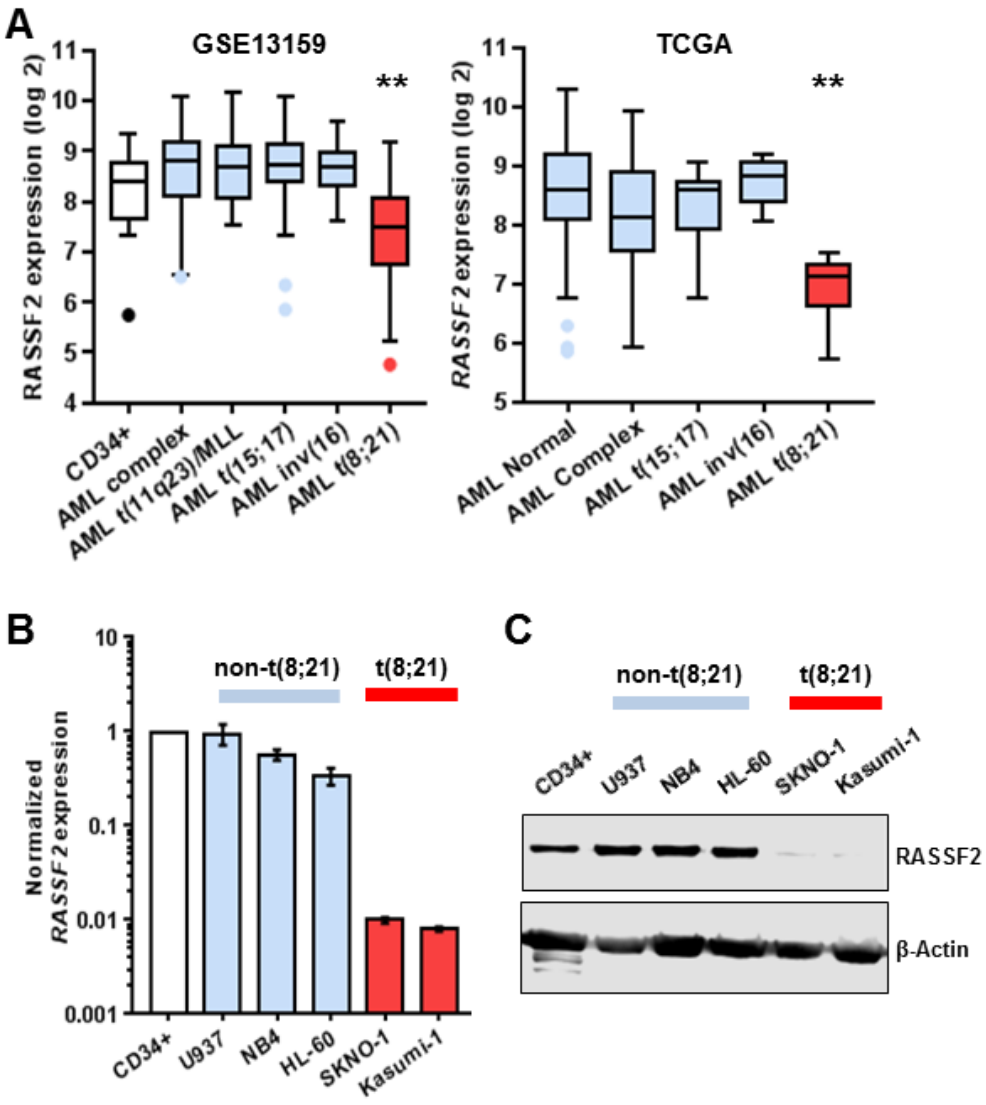

Figure 3.2. Transcriptional repression of *RASSF2* specifically in t(8;21) AML patients.
(A) Normalized *RASSF2* expression from two independent cohorts of AML patients (GSE13159[172], left and TCGA[142], right). For GSE13159, CD34+ cells from healthy donors (n = 18) are indicated in white, non-t(8;21) AML patients (n = 192) are indicated in blue, and t(8;21) AML patients (n = 60) are indicated in red. For TCGA, non-t(8;21) AML patients (n = 164) are indicated in blue, and t(8;21) AML patients (n = 7) are indicated in red. Data are presented as Tukey boxplots with outliers indicated by individual points. ** $p < 0.01$, ANOVA followed by post-hoc Tukey test. **(B)** RT-qPCR data showing *RASSF2* expression in non-t(8;21) (blue) and t(8;21) (red) AML cell lines. Data are normalized relative to healthy CD34+ cord-blood cells and presented as mean +/- s.e.m. of three experiments. **(C)** Western blot showing protein from whole cell lysates as indicated, data are representative of 3 experiments.

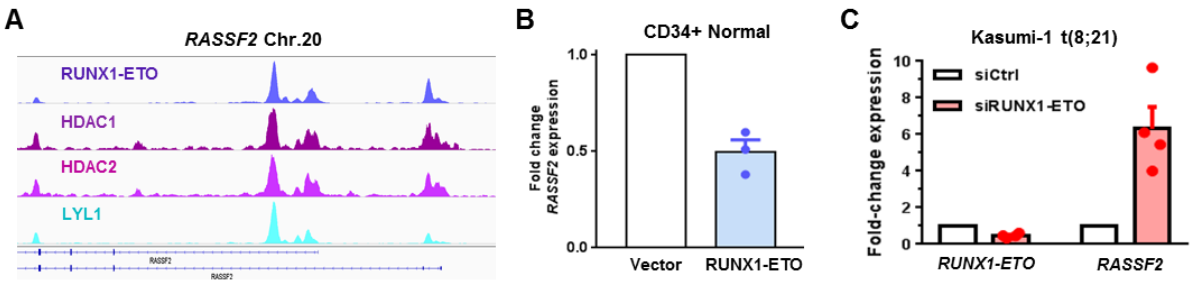

Figure 3.3. t(8;21) oncofusion protein RUNX1-ETO downregulates *RASSF2* transcription.

(A) ChIP-seq tracks showing binding of indicated transcription/epigenetic factors within the *RASSF2* genomic locus in the Kasumi-1 t(8;21) AML cell line. **(B)** Normalized RT-qPCR data showing fold-change *RASSF2* expression in cord-blood CD34+ cells 72 hours post-transduction with empty or RUNX1-ETO expression vectors. Data are mean +/- s.e.m. of three experiments (indicated by points). **(C)** Normalized RT-qPCR data showing fold-change *RASSF2* expression in Kasumi-1 cells 72 hours post-nucleofection with control or RUNX1-ETO targeting siRNA. Data are mean +/- s.e.m. of four experiments (indicated by points).

3.2.2. Re-expression of RASSF2 is tumor-suppressive specifically in t(8;21) AML

We next explored the functional consequences of this transcriptional repression to leukemogenesis *in vitro* and *in vivo*. Using retroviral GFP-based reporter vectors, we screened the effect of RASSF2 expression on cell proliferation across a panel of AML cell lines. Only upon expression in the t(8;21) AML cell lines, Kasumi-1 and SKNO-1, did RASSF2 impart a competitive growth disadvantage relative to control-transduced (GFP only) populations (**Figure 3.4A**). Importantly, assessment of protein expression in sorted GFP+ RASSF2-transduced cell populations showed that RASSF2 re-expression occurred in a physiologically-relevant manner and was not overexpressed compared to endogenous amounts observed in non-t(8;21) AML cell lines (**Figure 3.4B**). These results suggest that RASSF2 is a context-specific, rather than general, tumor suppressor protein in myeloid leukemia. We next assessed the ability of RASSF2 to suppress RUNX1-ETO-mediated leukemic transformation of primary murine hematopoietic progenitors using a serial replating / colony formation assay (**Figure 3.5A**). Re-expression of RASSF2 was sufficient to block RUNX1-ETO-mediated long-term clonogenic self-renewal after 3 – 4 weeks (**Figures 3.5B and 3.5C**). We also assessed RASSF2-mediated tumor suppression *in vivo* using a murine retroviral transduction and transplantation model of t(8;21) AML with the alternatively-spliced luekomogenic protein variant, RUNX1-ETO9a (RE9a, **Figure 3.6A**)[182]. Co-expression of *Rassf2* significantly delayed RE9a leukemia onset (median survival 214 vs 150 days) compared to an empty-vector control (**Figure 3.6B**). The delay in leukemia onset was

associated with reduced leukemic burden indicated by the frequency of circulating GFP+ blasts in the peripheral blood (**Figures 3.7A, 3.7B, 3.7C, and 3.7D**), and less severe anemia (**Figures 3.7E and 3.7F**) at an intermediate time point. Terminal assessment of myeloid leukemia cells in moribund mice revealed no significant morphological differences between cohorts (**Figure 3.8**). Interestingly, several terminal AMLs in the *Rassf2* cohort had lost detectable expression of the tdTomato reporter, demonstrating clonal selective pressure against *Rassf2*-expressing cells in t(8;21) AML. These data reveal RASSF2 to be a physiologically-relevant tumor suppressor, but only within the context of a specific AML subtype in which it is transcriptionally repressed.

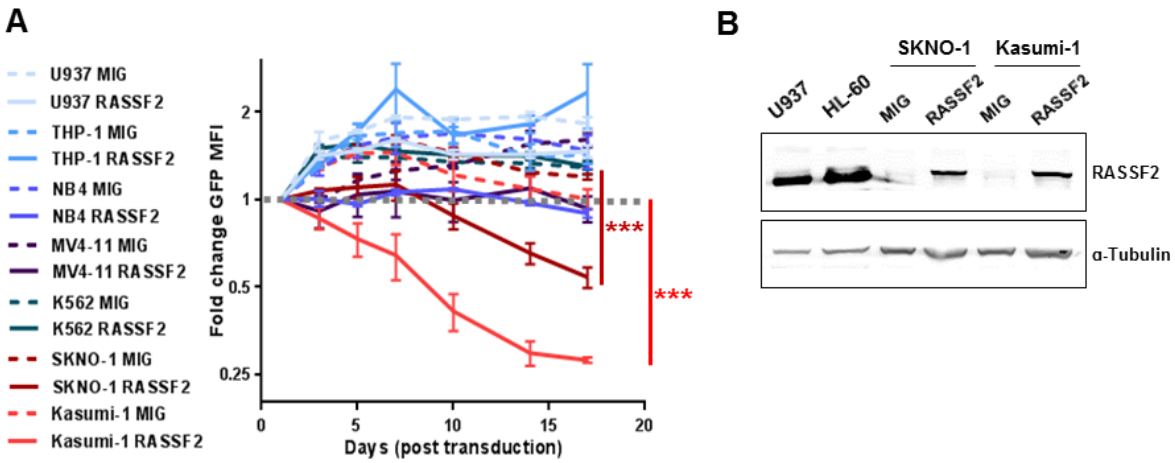

Figure 3.4. RASSF2 re-expression screen in a panel of AML cell lines.
(A) Fold-change in population mean GFP fluorescence intensity (MFI) over time was measured by flow cytometry in the indicated cell lines following transduction (efficiencies ~50-60%) with retroviral MSCV-IRES-GFP (MIG), or MSCV-RASSF2-IRES-GFP (RASSF2) vectors. Data are mean +/- s.e.m. of four experiments. *** $p < 0.001$, two-tailed student's t-test performed at day 17 for cell lines in which GFP MFI of one vector-transduced population dropped below initial measurement value (day 1 post-transduction), which is indicated by dashed grey line. **(B)** Western blot for indicated proteins. For SKNO-1 and Kasumi-1 cell lines, GFP+ cells are sorted three days post transduction with retroviral expression vectors, MSCV-IRES-GFP (MIG) or MSCV-RASSF2-IRES-GFP (RASSF2).

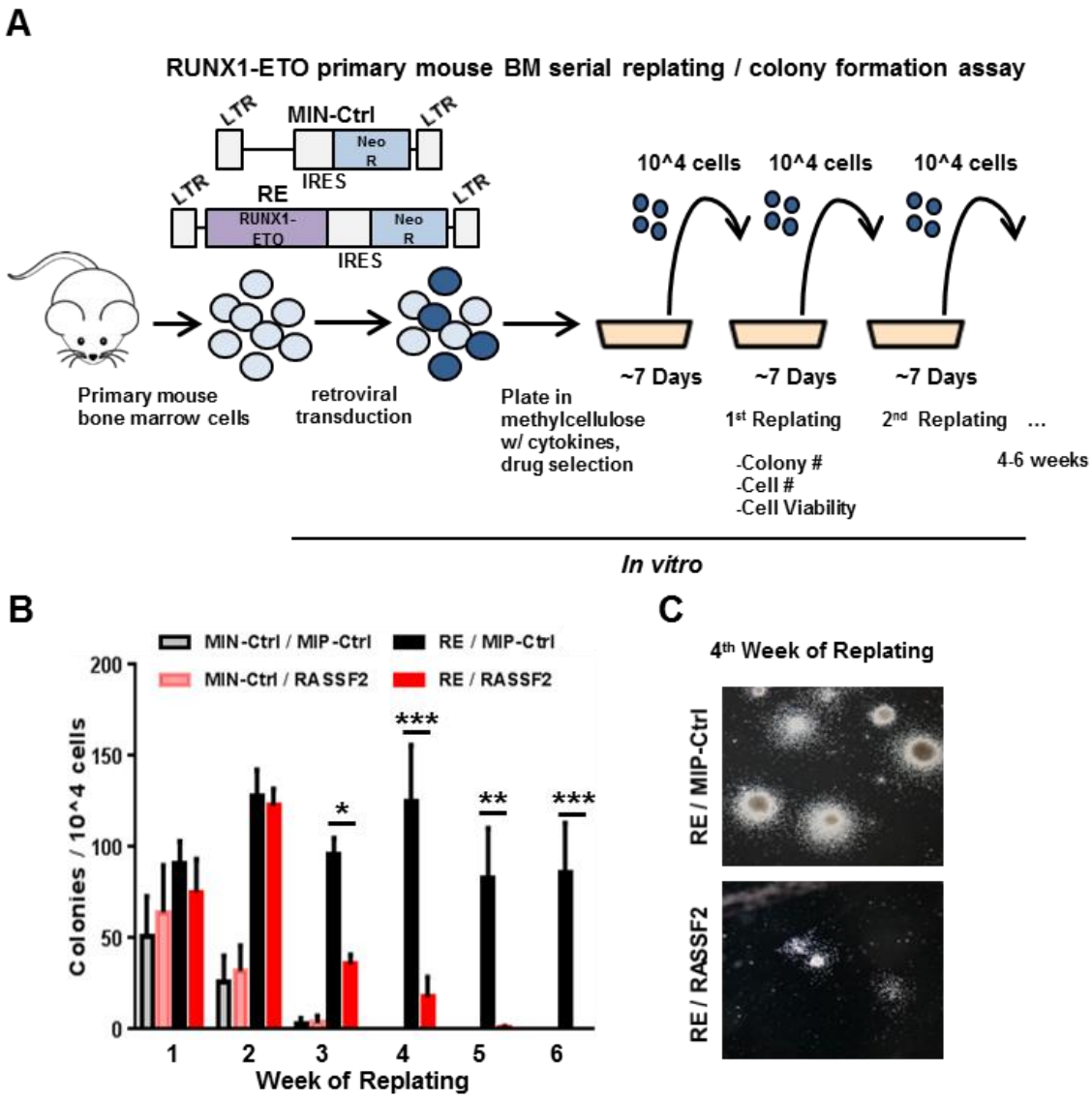

Figure 3.5. RASSF2 suppresses RUNX1-ETO leukemic transformation ability in a serial replating / colony formation assay.

(**A**) Experimental schematic of the colony formation / serial replating in vitro assay of RUNX1-ETO mediated leukemic transformation. (**B**) Number of colonies (per 10,000 plated cells) for each week of serial replating of primary murine bone marrow cells transduced with vectors as indicated. Data are mean +/- s.e.m. of five experiments. * $p < 0.05$, ** $p < 0.01$, *** $p < 0.001$, two-tailed student's t-test. (**C**) Representative images of colonies from fourth week of replating for indicated populations.

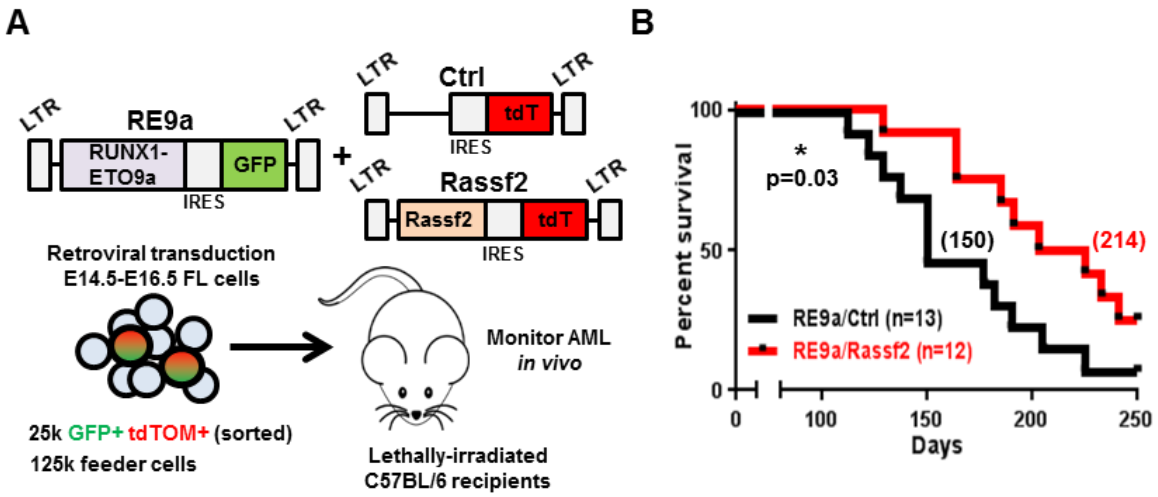

Figure 3.6. Re-expression of RASSF2 prolongs survival in a RUNX1-ETO9a (RE9a) primary murine leukemia model.
(A) Schematic for primary RUNX1-ETO9a retroviral transduction/transplantation murine model of t(8;21) AML with re-expression of *Rassf2* (RE9a/Rassf2) or vector control (RE9a/Ctrl). **(B)** Survival analysis for experiment described in **(j),** significance determined by log-rank (Mantel-Cox) test.

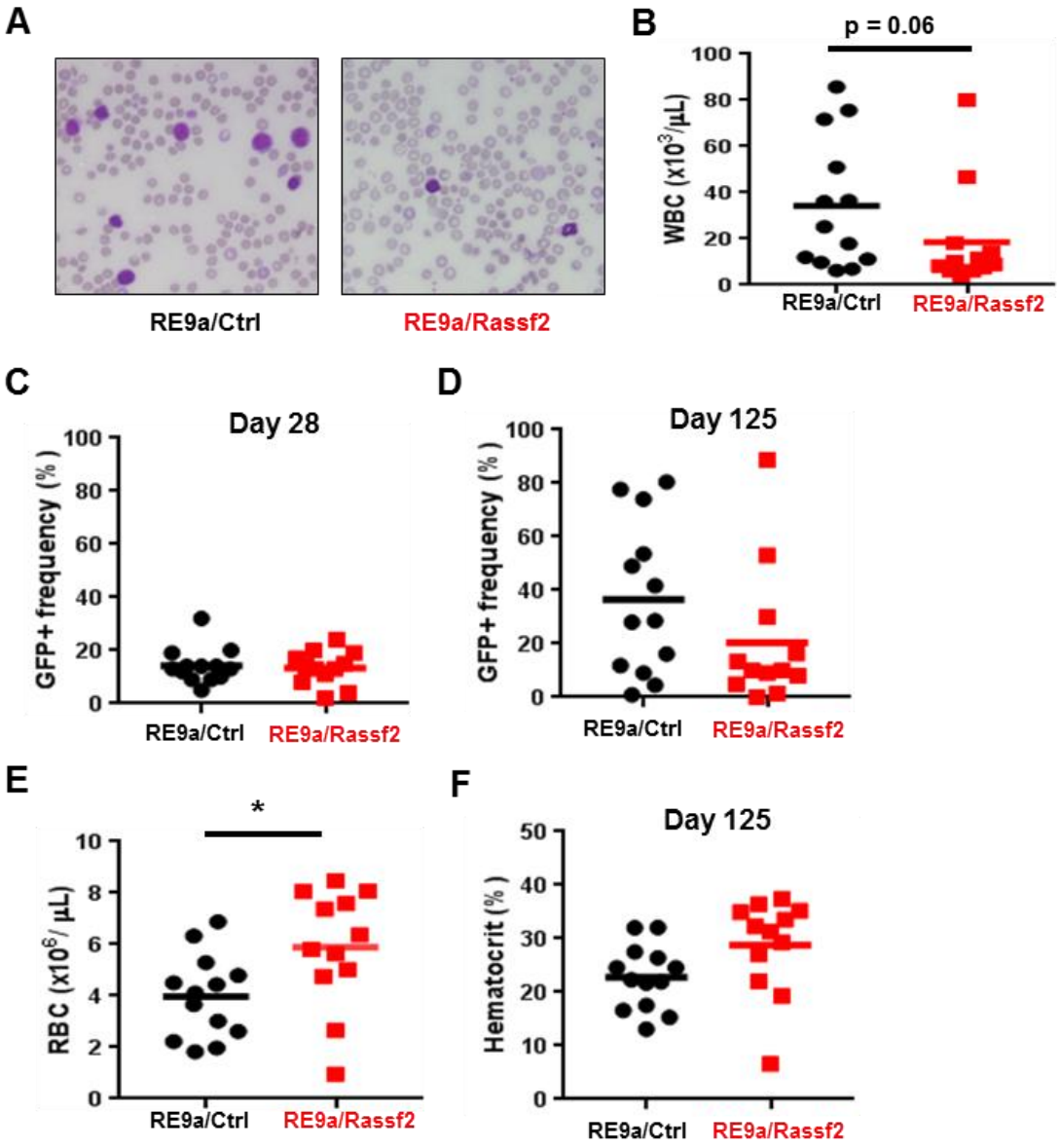

Figure 3.7. Peripheral blood parameters in the RE9a / Rassf2 primary AML model.

(A) Representative peripheral blood smears of indicated mice at 125 days post-transplantation. **(B)** Peripheral white blood cell (WBC) counts of indicated mice at 125 days post-transplantation, solid lines indicate population mean. * $p < 0.05$, two-tailed student's t-test. **(C)** As (B) but for GFP+ cell frequency at 28 days post-transplantation. **(D)** As (C) but at 125 days post-transplantation. **(E)** As (B) but for red blood cell counts (RBC). **(F)** As (B) but for Hematocrit (HCT%).

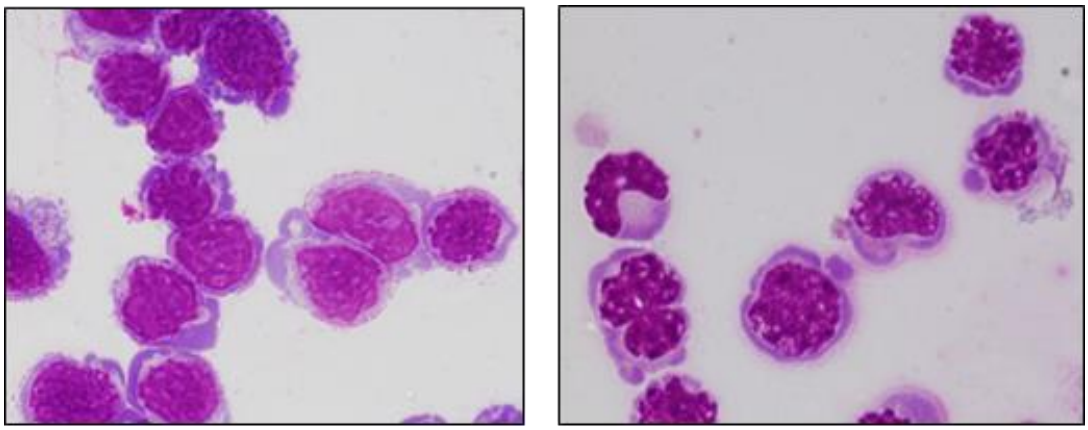

Figure 3.8. Representative Wright-Giemsa stained cytospins from moribund leukemic splenocytes of the indicated mice.

3.2.3. RASSF2 function is unrelated to oncogenic Ras signaling or nucleo-cytoplasmic shuttling in hematologic cancer

We next explored the mechanism of RASSF2 function in myeloid leukemogenesis. RASSF proteins possess no enzymatic activity and are primarily thought to function as scaffolds through their protein-protein interaction domains[150]. RASSF2 is reported to exert tumor-suppressive functions as a nucleo-cytoplasmic shuttling protein[183]. We could not, however, detect any evidence for nuclear localization of endogenous or exogenous RASSF2 in myeloid leukemia cell lines; while still replicating nucleo-cytoplasmic shuttling upon expression in HEK293T cells (**Figures 3.9A, 3.9B, and 3.9C**). These results are consistent with data from the Human Protein Atlas[184], in which RASSF2 is exclusively localized to the cytoplasmic / membranous compartments in hematopoietic cells (www.proteinatlas.org). Several RASSFs have been implicated in negative regulation of oncogenic Ras function through the Ras-association (RA) domain[149,150,157]. Activating point mutations in *NRAS* and *KRAS* are frequent in AML and often co-occur with t(8;21)[185]. Despite this, upon re-expression of RASSF2 in t(8;21) AML cells we could not detect any negative effects on canonical Ras signaling through the MAPK/ERK or AKT pathways following stimulation with cytokines or serum (**Figure 3.10A**). Furthermore, we found no evidence of correlation between *RASSF2* expression and the presence of oncogenic *RAS* mutations more broadly across myeloid leukemia patients (**Figure 3.10B**). These data are consistent with Ras-centric proteomic studies that have not identified RASSF proteins as bona-fide endogenous interactors of either wild-type or

mutant Ras proteins[186], and thus warranted investigation of RASSF2 function through additional mechanisms.

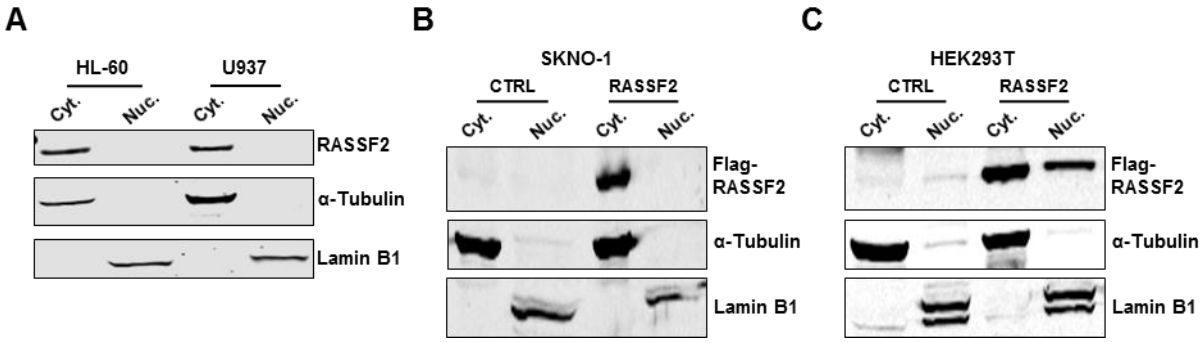

Figure 3.9. RASSF2 is exclusively localized in the cytoplasmic fraction in leukemia cells.
(A) Western blots from cellular fractionation lysates for endogenous proteins in cell lines as indicated. Cyt, cytoplasmic fraction, Nuc, nuclear fraction. Data are representative of three experiments. **(B)** as (A), but with stable transduction of MSCV-IRES- Puro^R (CTRL) or MSCV-Flag-RASSF2-IRES-Puro^R (RASSF2) in SKNO-1 cells. **(C)** as (B), but with stable transfection of indicated vectors in HEK293T cells.

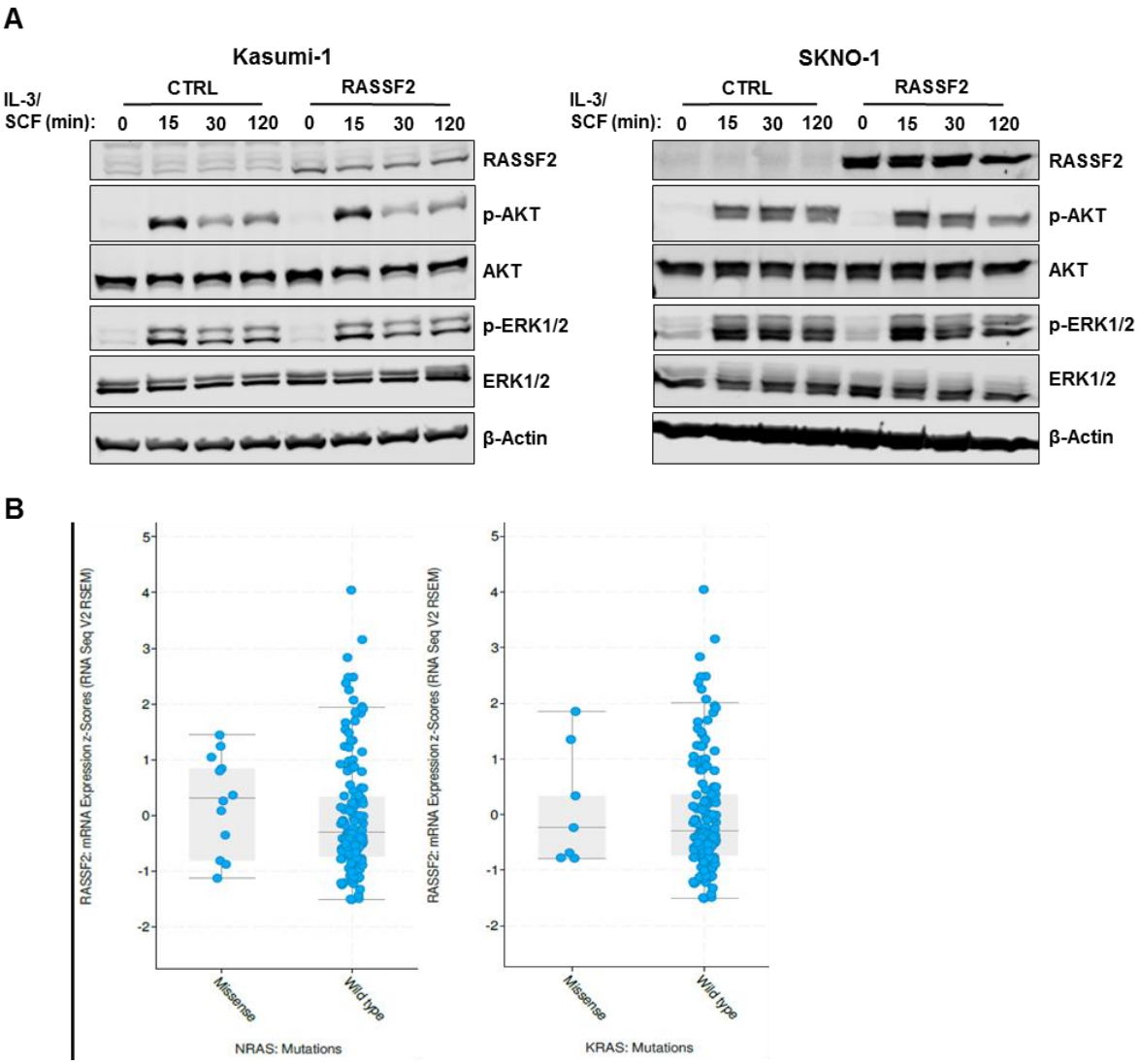

Figure 3.10. RASSF2 expression does not affect oncogenic Ras signaling in AML.

(A) Western blots for indicated proteins and phospho-proteins in Kasumi-1 (left) and SKNO-1 (right) AML cell lines with stable transduction of MSCV-IRES- Puro^R (CTRL) or MSCV-Flag-RASSF2-IRES-Puro^R (RASSF2). Cells are serum starved overnight, and then stimulated with recombinant human IL-3 (20 ng/mL) and SCF (50 ng/mL) for times indicated. Data are representative of three experiments. **(B)** *RASSF2* mRNA expression from TCGA AML patient cohort, stratified based on presence or absence of activating mutation in *NRAS* (left) or *KRAS* (right). Data are visualized from cBioPortal (www.cbioportal.org).

3.2.4. RASSF2-mediated functions are dependent on interaction with Hippo kinases MST1/2

All six classical RASSFs contain a highly-conserved C-terminal Salvador-Rassf-Hippo (SARAH) domain that is unique to protein components of the Hippo signaling pathway and mediates homo- or hetero-dimerization between SARAH domain-containing proteins[150]. Structural and biochemical analyses suggest that the mammalian Hippo kinases, MST1 and MST2, primarily exist as SARAH-mediated heterodimers with RASSF proteins under basal cellular conditions[187]. To determine whether interaction with MST1/2 was required for RASSF2 function, we generated a RASSF2 deletion mutant lacking the SARAH domain (RASSF2ΔSARAH) for use in the serial replating / colony formation assay (**Figure 3.11**). RASSF2ΔSARAH completely lost the ability to suppress RUNX1-ETO leukemic transformation and induce apoptosis in RUNX1-ETO expressing cells (**Figures 3.12A, 3.12B, 3.12C, 3.12D**). To further confirm the requirement of Hippo kinases for RASSF2-mediated tumor suppression we generated mice with conditional gene inactivation of both MST1 (*Stk4*) and MST2 (*Stk3*) in hematopoietic cells (Vav1-Cre). By co-expression of RUNX1-ETO and RASSF2 in the background of control (Vav1-Cre^{-}), heterozygous ($Stk4^{f/+}Stk3^{f/+}$;Vav1-Cre^{+}), and homozygous ($Stk4^{f/f}Stk3^{f/f}$;Vav1-Cre^{+}) knockout mice, we found that the presence of MST1/2 was essential for the ability of RASSF2 to inhibit RUNX1-ETO leukemic transformation (**Figure 3.13**). These data revealed the importance of the Hippo-RASSF2 interaction and we set out to further characterize this in myeloid leukemia.

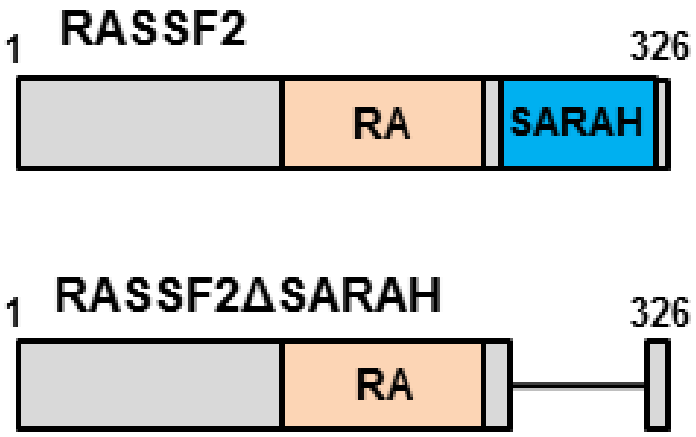

Figure 3.11. **Schematic of RASSF2 proteins expressed in replating assays.** RA, Ras-association domain, SARAH, Salvador-Rassf-Hippo domain.

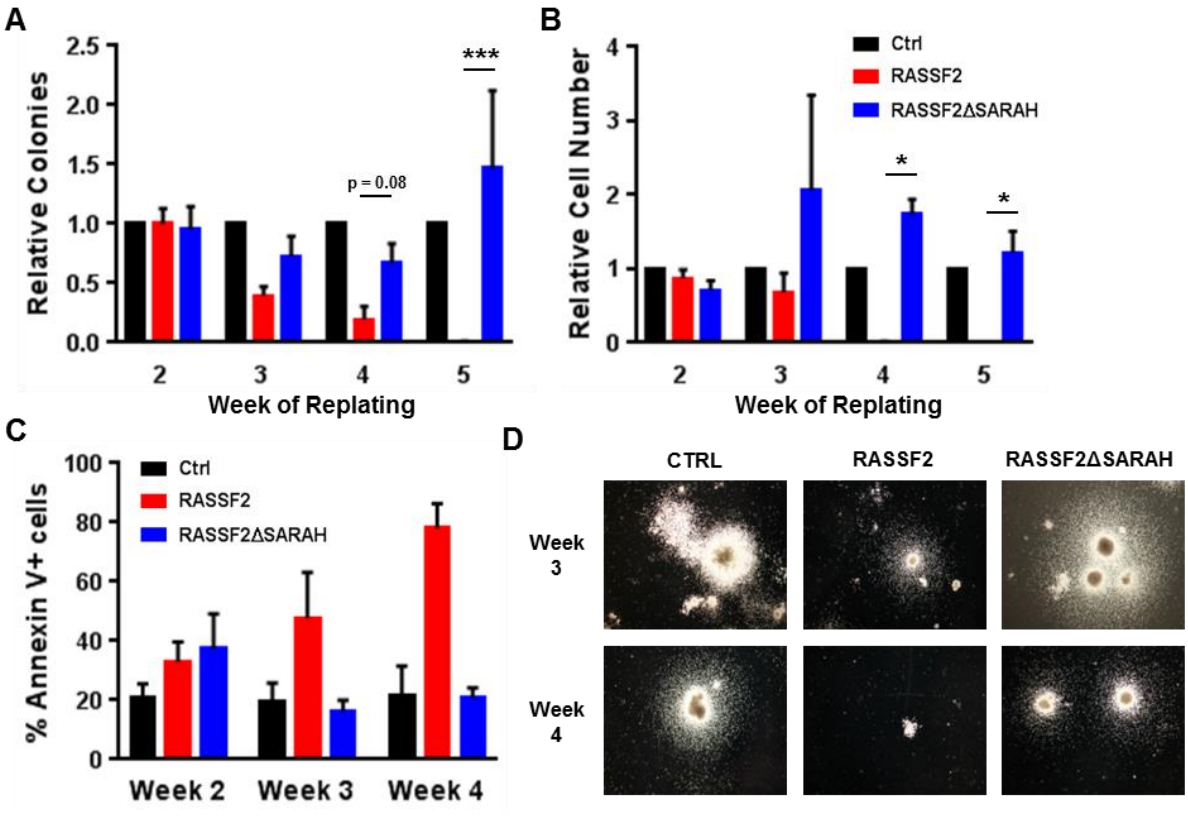

Figure 3.12. RASSF2 SARAH domain is required for suppression of RUNX1-ETO leukemic transformation ability.
(A) Colony number (per 10,000 cells plated). **(B)** Total viable cell number (per 10,000 cells plated). **(C)** Frequency of Annexin-V+ apoptotic cells. **(D)** Representative images of colonies; for RUNX1-ETO serial replating / colony formation assay with co-transduction of indicated vectors. Data are normalized relative to empty vector control-transduced populations and presented as mean +/- s.e.m. of four independent experiments. * $p < 0.05$, ** $p < 0.01$, *** $p < 0.001$, two-tailed student's t-test.

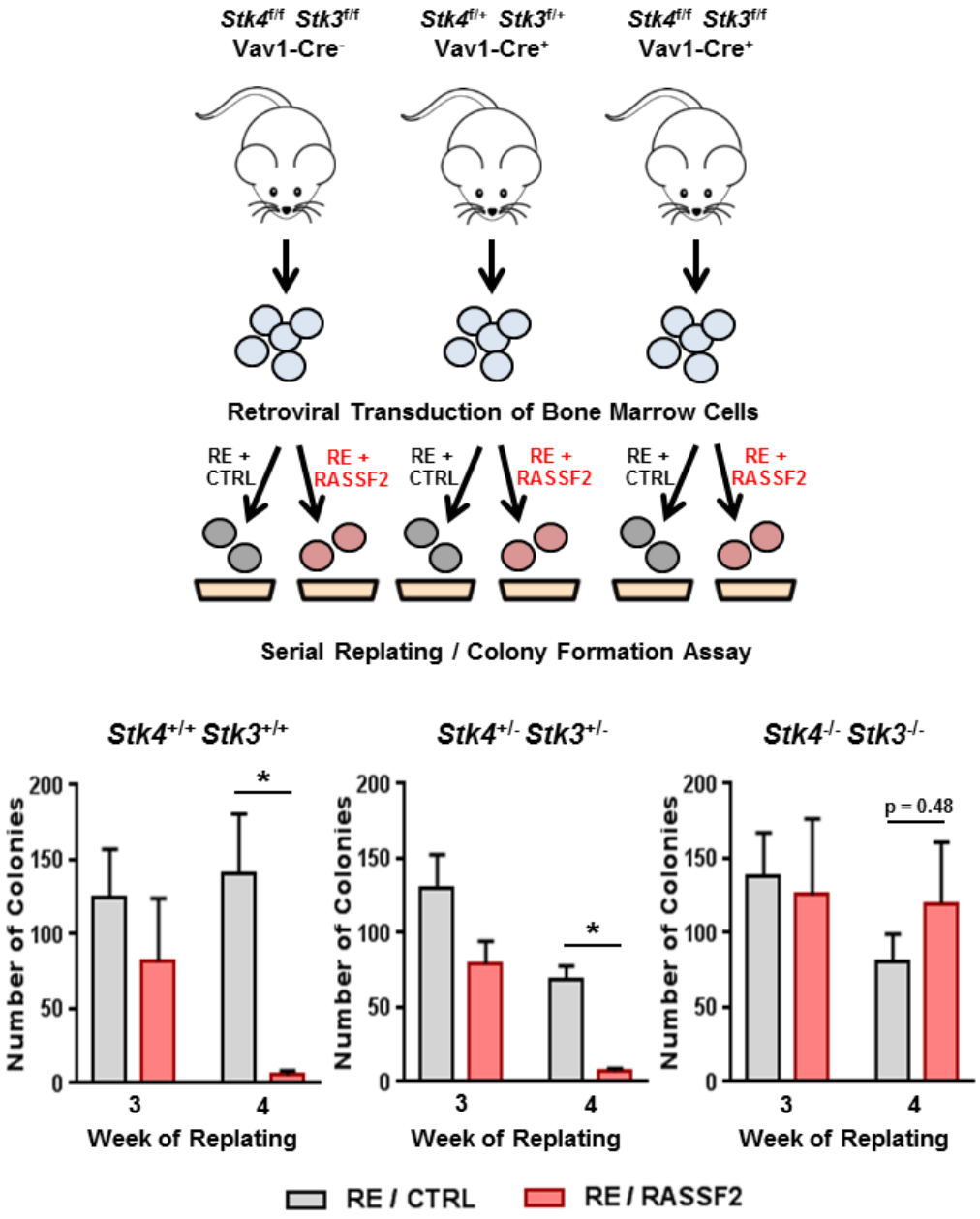

Figure 3.13. RASSF2-mediated suppression of RUNX1-ETO leukemic transformation is dependent on presence of Hippo kinases MST1/2 (*STK4/3*). RUNX1-ETO primary murine serial replating / colony formation assay was performed in mice of three indicated genotypes, with expression of RASSF2 or empty vector control, as shown at left. Colony numbers (per 10,000 cells plated) are shown for third and fourth week of replating for each genotype. Data are mean +/- s.e.m. of three experiments. * $p < 0.05$, two-tailed student's t-test.

3.2.5. SARAH domain-mediated stabilization of RASSF2 is a non-canonical MST1 signaling mechanism with functional consequences in leukemia

Despite a modest stabilizing effect on MST1 and MST2, RASSF2 expression did not alter signaling through canonical Hippo pathway targets MOB1 and LATS1[158] in t(8;21) AML cells (**Figures 3.14A and 3.14B**). These findings are consistent with another report in which RASSF2 expression did not affect canonical MST1/2 phosphorylation targets[188]. We therefore asked whether MST1 kinase activity was at all required for the RASSF2 tumor-suppressive function against t(8;21) AML cells through expression of a kinase-dead point-mutant protein, MST1-K59R (**Figure 3.15A**). We also included a biologically-relevant C-terminal truncation mutant of MST1 that mimics caspase-cleavage at amino acid 326 (MST1Δ326), which is widely-accepted to exert increased proapoptotic kinase activity through removal of an auto-inhibitory domain (AID), while also losing its ability to dimerize with RASSF proteins through the SARAH domain (**Figure 3.15A**)[189]. We confirmed MST1-K59R to act as a dominant negative kinase towards MOB1 phosphorylation upon expression in t(8;21) AML cells (**Figure 3.15B**). Remarkably, expression of either full-length MST1 or dominant-negative MST1-K59R, but not C-terminally truncated MST1Δ326, was sufficient to induce apoptosis and suppress growth of t(8;21) AML cells (**Figures 3.15C and 3.15D**). This revealed that the ability of MST1 to interact with RASSF2 through the SARAH domain, rather than its kinase activity, contributes to its function in myeloid leukemia cells. Based on this, we further explored the kinetics of RASSF2 protein stability and its relationship with Hippo kinase MST1.

Using a cyclohexamide chase assay to measure protein stability we found RASSF2 to have a relatively short half-life of 2 – 3 hours in HEK293T cells (**Figure 3.16A**). This degradation was proteasome-dependent as treatment with the selective proteasome inhibitor lactacystin rescued RASSF2 protein amount (**Figure 3.16B**). We then assessed the ability of MST1 and its protein variants to protect RASSF2 from proteasomal degradation. Consistent with being independent of kinase activity, both MST1 and MST1-K59R, but not MST1Δ326, effectively protected RASSF2 from degradation following cyclohexamide treatment (**Figures 3.16C and 3.16D**). To confirm the relevance of this non-canonical Hippo kinase function *in vivo* we assessed protein expression in murine hematopoietic progenitor cells from the conditional knockout mice described above, and found endogenous RASSF2 protein to be completely dependent on the presence of MST1/2 for stabilization (**Figure 3.17**). These data demonstrate that a previously unappreciated kinase-independent function of the Hippo kinases MST1/2 can contribute to regulation of cancer cell growth through SARAH domain-dependent stabilization of RASSFs.

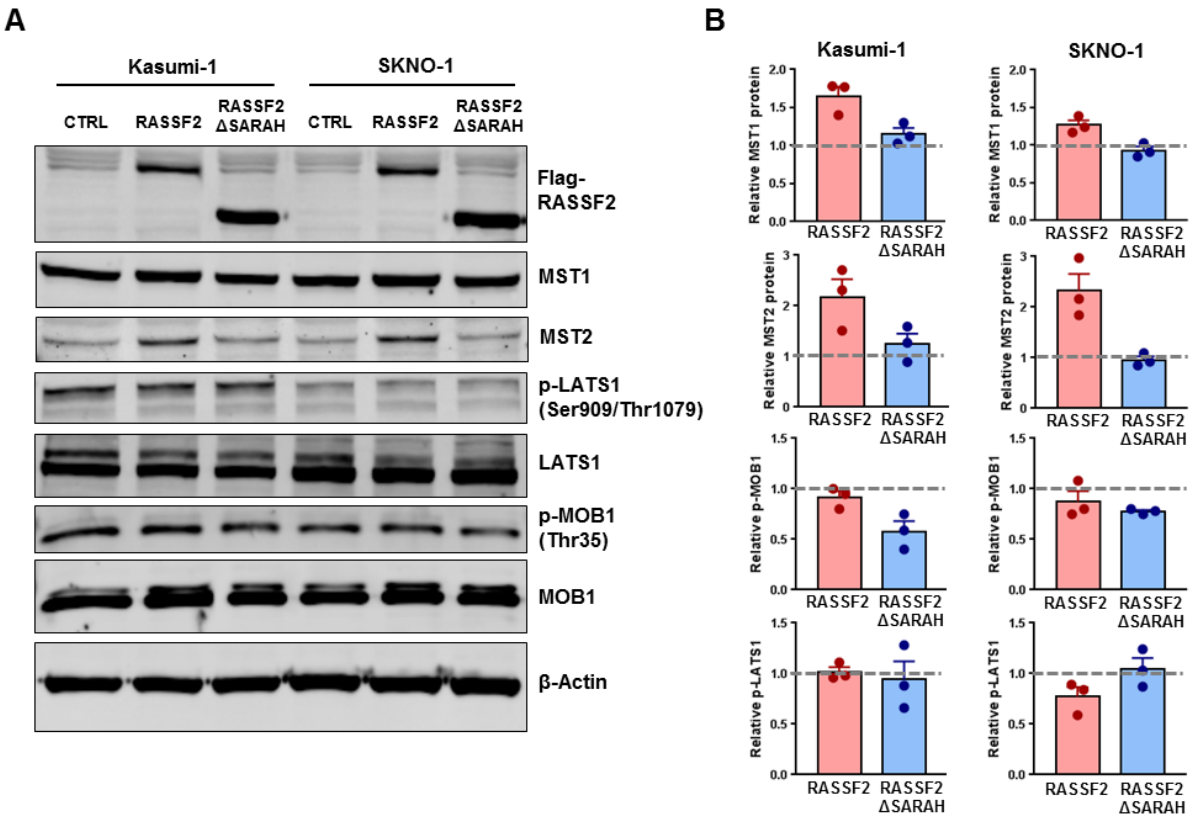

Figure 3.14. RASSF2 does not affect signaling through canonical Hippo pathway targets MOB1 and LATS1.
(A) Western blots for indicated proteins and phospho-proteins in Kasumi-1 and SKNO-1 AML cell lines with stable transduction of MSCV-IRES- Puro^R (CTRL), MSCV-Flag-RASSF2-IRES-Puro^R (RASSF2), or MSCV-Flag-RASSF2ΔSARAH-IRES-Puro^R (RASSF2ΔSARAH). Data are representative of three experiments. **(B)** Quantification of multiple experiments described in (A). Signal intensities are normalized to β-Actin loading and plotted relative to MSCV-IRES- Puro^R (CTRL) cells, which are indicated with dashed gray lines.

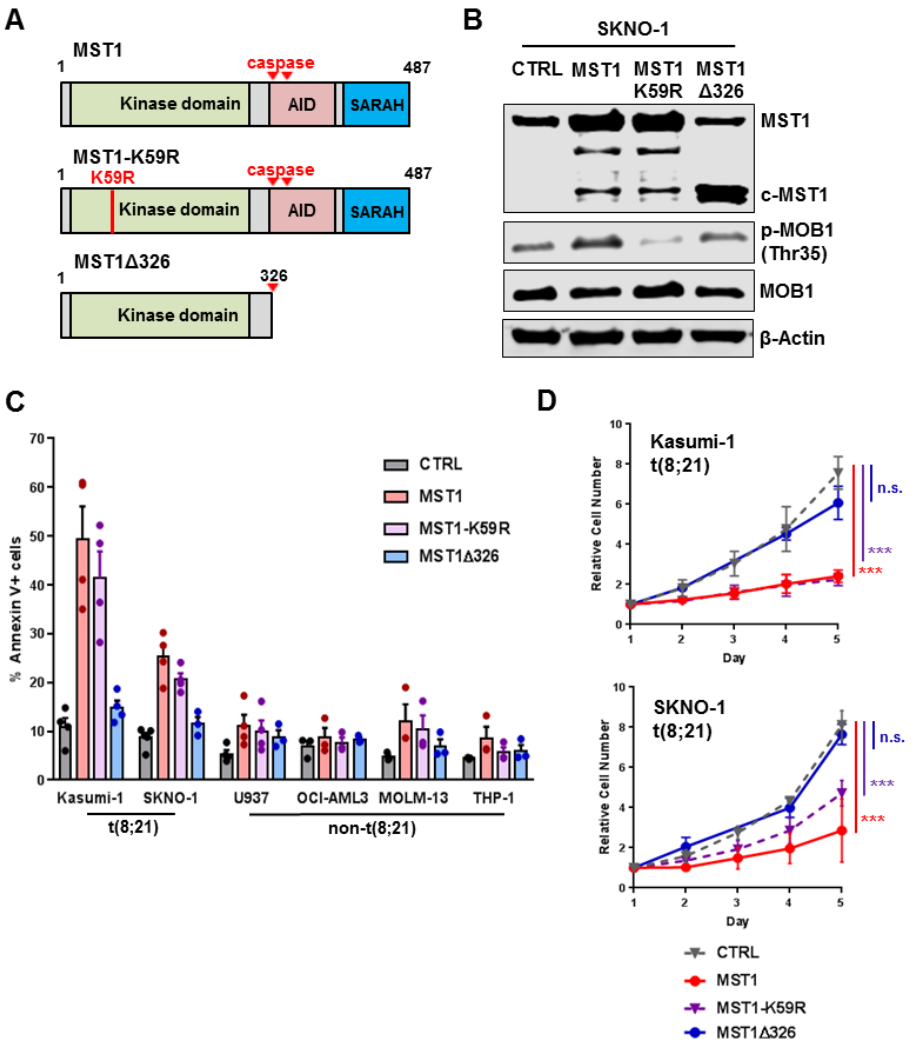

Figure 3.15. MST1 functions as a tumor suppressor in t(8;21) AML independent of kinase activity.

(A) Schematic of MST1 protein variants. K59R, substitution of arginine for lysine at amino acid residue 59 results in kinase-dead protein that functions as dominant negative, AID, auto-inhibitory domain, SARAH, Salvador-Rassf-Hippo domain, red arrows represent endogenous caspase-cleavage sites. **(B)** Western blot showing protein from whole cell lysates in the SKNO-1 t(8;21) cell line transduced with MST1-variant retroviral expression vectors as indicated. c-MST1, caspase-cleaved MST1. **(C)** Apoptotic cell (Annexin-V+) frequencies in six indicated AML cell lines four days post-transduction with MST1-variant retroviral expression vectors as indicated. Data are mean +/- s.e.m. of four experiments (indicated by points). **(D)** Relative cell proliferation of indicated AML cell lines transduced with MST1-variant retroviral expression vectors as indicated, cells were seeded at equal density at day 1, which represents four days post-transduction. Data are mean +/- s.e.m. of four experiments. *** $p < 0.001$, two-tailed student's t-test with Holm-Sidak correction for multiple comparisons.

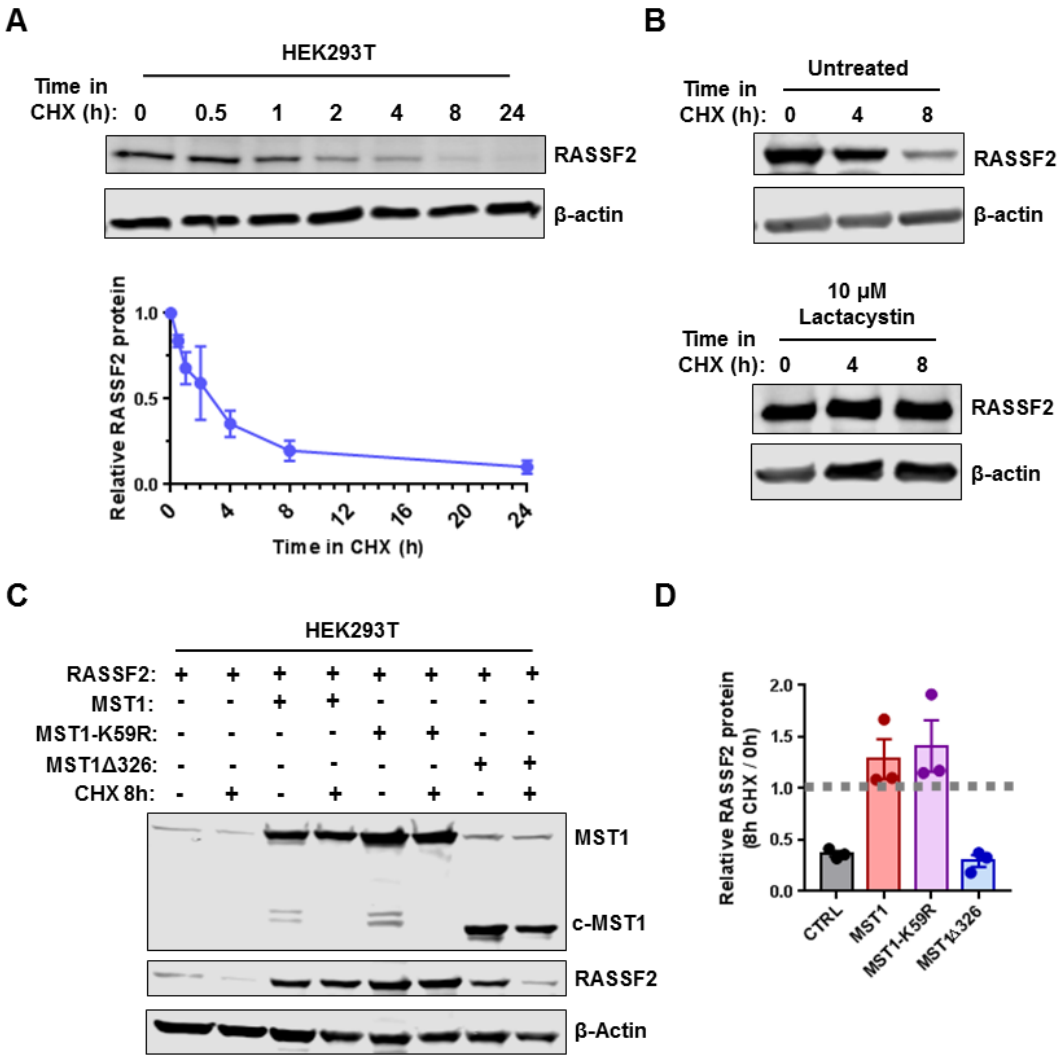

Figure 3.16. RASSF2 stability is dependent on the Hippo kinase SARAH domain.

(A) Western blot showing time-course of protein expression following addition of 25 μM cyclohexamide (CHX) from HEK293T whole cell lysates beginning 48 hours post-transfection with RASSF2 expression vector. Quantification of three experiments is shown below. **(B)** Western blot showing time-course of protein expression following addition of 25 μM cyclohexamide (CHX) from HEK293T whole cell lysates beginning 48 hours post-transfection with RASSF2 expression vector, with (bottom) or without (top) the addition of 10 μM Lactacystin. Data are representative of three experiments. **(C)** Western blot showing protein from HEK293T whole cell lysates 72 hours post-transfection with indicated expression vectors, with or without the addition of 25 μM cyclohexamide (CHX) for the final 8 hours as indicated. Data are representative of three experiments. **(D)** Quantification of relative change in RASSF2 protein abundance with or without cyclohexamide treatment from three experiments described in (C).

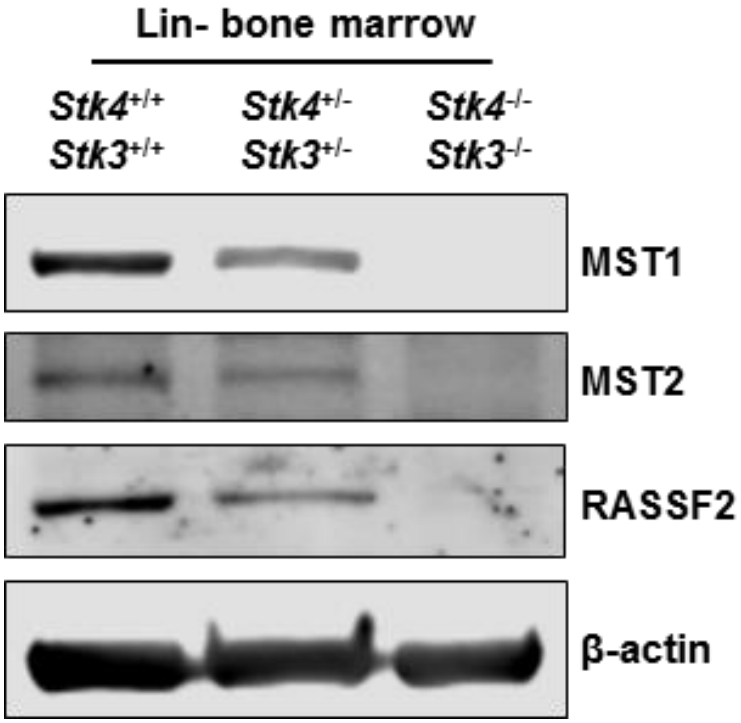

Figure 3.17. Destabilization of RASSF2 in Hippo kinase knockout hematopoietic stem/progenitor cells.
Western blot showing protein from whole cell lysates of Lineage-marker negative (Lin-) primary murine hematopoietic cells derived from bone marrow of mice of indicated genotypes. Data are representative of two experiments.

3.2.6. Proximity-dependent biotin labeling defines the endogenous RASSF2-proximal proteome and reveals a novel role in regulation of Rac GTPase activation via DOCK2

Given our data suggesting RASSF2 functions downstream of MST1-mediated stabilization, rather than upstream of MST1 kinase activity, we set out to identify novel proteins/complexes associated with RASSF2 in leukemia cells. To do this, we employed a proximity-dependent biotin labeling (BioID) approach[190] to identify physiologically-relevant proximal proteins upon re-expression of RASSF2 in t(8;21) AML cells. We tested three different orientations for expression of the RASSF2-BioID2[191] fusion cassette, and ultimately chose a C-terminal fusion separated with a linker peptide based on its retained ability to interact with and biotinylate MST1 as a positive control (**Figures 3.18A, 3.18B, 3.18C, and 3.19A**). Affinity purification of biotinylated proteins was performed using steptavidin-conjugated beads and samples were submitted for mass spectromety analysis following stringent washing conditions (**Figures 3.18D and 3.19B**). After strict filtering based on the CRAPome[192] we identified 60 unique RASSF2-specific proximal proteins across three independent replicates in Kasumi-1 cells (**Table 3.1**). Hippo kinases MST1 and MST2 were the first- and sixth-ranked significant hits, respectively, highlighting the accuracy and reproducibility of this approach. Gene ontology analysis of the full list revealed RASSF2 to be associated with several pathways and cellular functions that are enriched for proteins related to signaling by Rho-family GTPases (**Figure 3.19C**). This proximal proteome includes proteins that are general downstream Rho-effectors

related to regulation of microtubule polymerization, including PPP1CC, NUDC, SEH1L, STMN1, STMN2, FKBP4, and MAP4; as well as proteins involved in specific-regulation of the localization and activation of Rac-family GTPases, DVL2, ANXA2, and DOCK2. Interestingly, no additional canonical Hippo pathway components or SARAH domain-containing proteins were identified, demonstrating the discrete nature of the Hippo-RASSF2 non-canonical signaling complex in leukemia cells.

One specific protein identified was the critical hematopoietic Rac1/2-specific guanine exchange factor (GEF), DOCK2. DOCK2 functions as a Rac1/2-specific GEF via catalyzing the nucleotide exchange reaction through the DHR2 domain. We validated this novel RASSF2-DOCK2 interaction via co-immunoprecipitation in HEK293T cells (**Figure 3.20A**). Given this novel interaction between RASSF2 and DOCK2, we examined whether RASSF2 may have an effect on DOCK2 enzyme activity towards Rac-GTPases. We co-expressed HA-tagged RAC1 with RASSF2 and DOCK2, either individually or together, and measured the abundance of active (GTP-bound) RAC1 in HEK293T cells using the well-descibed PAK1-binding domain based pull-down assay. In this context, RASSF2 expression alone had no effect on RAC1-GTP abundance; however RASSF2 significantly enhanced DOCK2-mediated RAC1 activation upon co-expression (**Figures 3.20B and 3.20C**). These data demonstrate that RASSF2 functions as a DOCK2-specific co-factor for promotion of quinine nucleotide exchange and Rac-GTPase activation. To determine whether MST1 may play a role in this process we performed co-immunopreciptation and Rac-GTPase assays in HEK293T cells at a longer time course, in which RASSF2 would experience significant proteasomal degradation in the absence of MST1-mediated

stabilization. Indeed, co-expression of MST1 or MST1-K59R, but not MST1Δ326, increased the ability of RASSF2 to interact with DOCK2, and promoted prolongued activation of Rac-GTP through DOCK2 GEF activity (**Figures 3.21A and 3.21B**).

Table 3.1. RASSF2-proximal proteome as identified by BioID method.

Protein IDs	Mapped Gene Symbol	Intensity Ctl	Intensity RASSf2	log2 FC	MS/MS count Ctl	MS/MS count RASSf2	CRAPome Num of Expt. Found
Q13043	STK4	-	76,929,400.00	26.20	0	52	9
P50749	**RASSF2**	**-**	**44,222,000.00**	25.40	0	48	**0**
P62266	RPS23	-	17,772,400.00	24.08	2	3	160
Q9UNZ2	NSFL1C	-	15,709,900.00	23.91	0	11	32
O00151	PDLIM1	-	7,850,640.00	22.90	0	7	32
Q13188	STK3	-	7,197,310.00	22.78	0	12	8
Q93045	STMN2	-	6,595,200.00	22.65	0	9	56
Q5SW79	CEP170	-	6,127,600.00	22.55	1	6	46
P16949	STMN1	-	5,284,100.00	22.33	0	12	78
Q13765;E9PAV3	NACA	-	4,843,400.00	22.21	1	4	125
Q15154	PCM1	-	4,257,400.00	22.02	0	14	31
O43432	EIF4G3	-	4,182,390.00	22.00	0	4	42
O95391	SLU7	-	3,819,000.00	21.86	1	3	45
Q13263	TRIM28	-	3,333,100.00	21.67	0	3	177
Q9BYG3	NIFK	-	3,216,560.00	21.62	2	4	-
Q69YH5	CDCA2	-	3,194,800.00	21.61	2	3	25
Q9BXS5	AP1M1	-	3,149,800.00	21.59	0	2	12
Q5T3I0	GPATCH4	-	2,592,830.00	21.31	1	4	37
Q9Y266	NUDC	-	2,453,940.00	21.23	1	6	99
P37802	TAGLN2	-	2,399,300.00	21.19	0	2	156
Q15050	RRS1	-	2,378,760.00	21.18	1	3	38
P55197	MLLT10	-	2,128,100.00	21.02	2	4	2
Q12830	BPTF	-	1,851,910.00	20.82	4	5	32
Q9BRP8	WIBG	-	1,831,400.00	20.80	0	6	39
Q99733	NAP1L4	-	1,826,850.00	20.80	0	4	90
P35658	NUP214	-	1,601,470.00	20.61	0	13	49
Q14444	CAPRIN1	-	1,529,920.00	20.55	1	8	120
Q02790	FKBP4	-	1,414,810.00	20.43	1	3	95
Q6P1Q9	METTL2B	-	1,390,800.00	20.41	2	3	1
Q96CS3	FAF2	-	1,077,120.00	20.04	1	5	25
Q7Z4S6;O75037	KIF21A	-	896,840.00	19.77	1	2	1
P62633	CNBP	-	858,850.00	19.71	0	3	16
P49790	NUP153	-	439,370.00	18.75	0	2	48
O14641;Q92997	DVL2	-	431,640.00	18.72	0	4	22
Q96EE3	SEH1L	-	399,920.00	18.61	2	5	38
Q96L96	ALPK3	-	384,382.00	18.55	0	3	1
Q9H6Z4	RANBP3	-	349,480.00	18.41	2	4	28
P30740	SERPINB1	-	344,850.00	18.40	3	5	1
Q6Y7W6	GIGYF2	-	333,730.00	18.35	2	3	45
Q5UIP0	RIF1	-	317,186.00	18.27	1	5	61
P63241;Q9GZV4	EIF5A	191,710.00	8,002,568.00	5.38	2	4	125
O43491	EPB41L2	187,190.00	3,432,910.00	4.20	4	10	51
P27816	MAP4	4,087,500.00	71,442,000.00	4.13	5	30	86
P06454	PTMA	125,080.00	1,735,230.00	3.79	4	6	68
P61981	YWHAG	464,690.00	5,316,400.00	3.52	4	3	131
Q8NDI1	EHBP1	694,710.00	7,773,080.00	3.48	6	15	19
Q92608	DOCK2	609,870.00	6,619,100.00	3.44	2	5	2
Q9UPN4	CEP131	1,345,300.00	11,757,600.00	3.13	4	22	-
Q86UE4	MTDH	725,410.00	5,838,500.00	3.01	3	14	50
O15355	PPM1G	939,920.00	7,098,600.00	2.92	8	15	42
P60468	SEC61B	378,580.00	2,694,300.00	2.83	5	5	35
Q9H6T3	RPAP3	2,000,200.00	12,962,200.00	2.70	4	13	36
P27348	YWHAQ	814,290.00	4,258,520.00	2.39	2	5	153
Q3ZCQ8	TIMM50	373,240.00	1,822,390.00	2.29	5	7	124
Q92522	H1FX	3,011,500.00	13,836,300.00	2.20	3	8	121
P36873	PPP1CC	882,760.00	4,030,100.00	2.19	1	3	123
Q76FK4	NOL8	181,660.00	801,750.00	2.14	3	2	24
P23588	EIF4B	3,451,870.00	14,753,100.00	2.10	10	15	167
P07355;A6NMY6	ANXA2	11,479,660.00	46,496,100.00	2.02	18	26	150
P54577	YARS	104,940.00	424,070.00	2.01	1	3	71

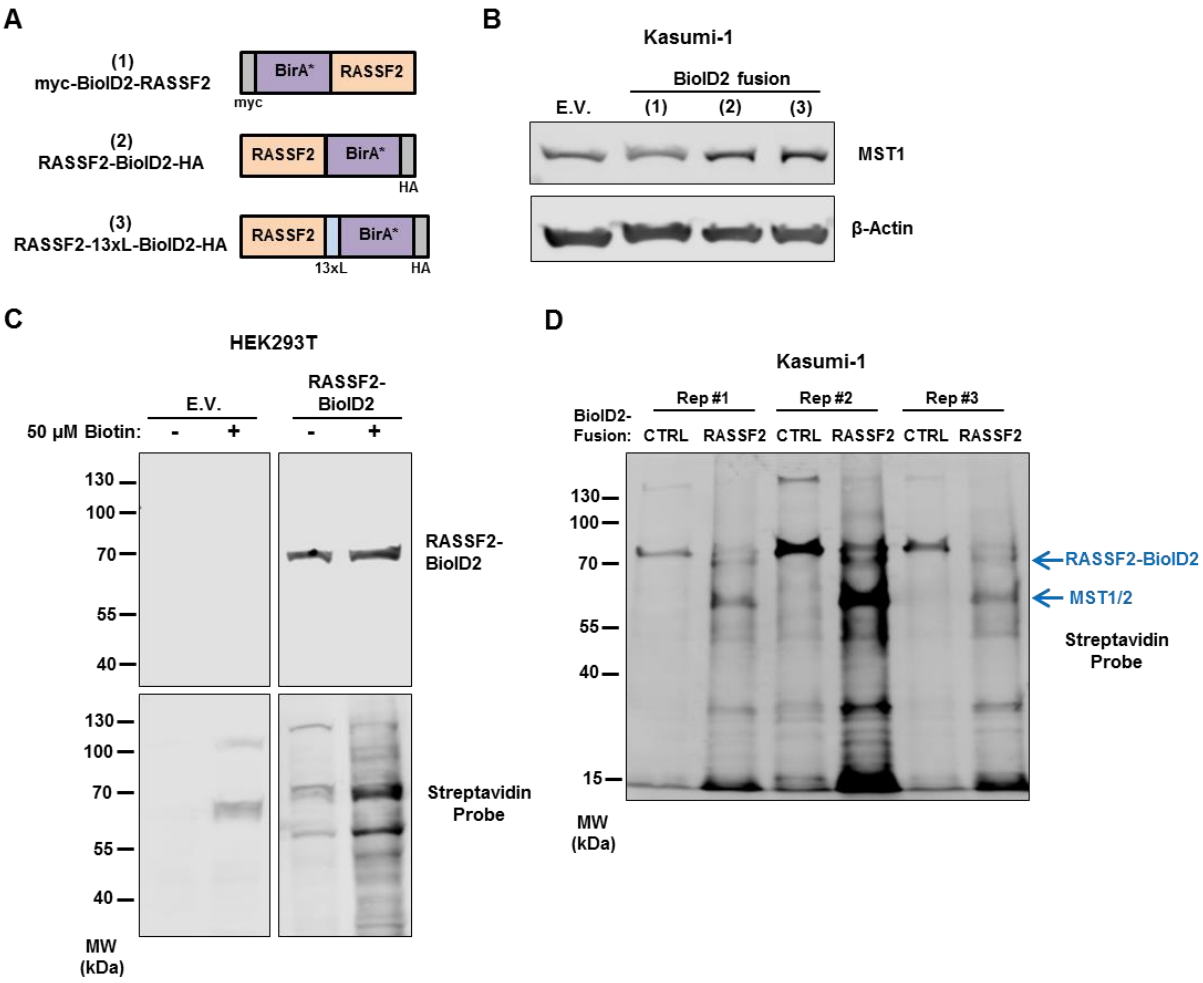

Figure 3.18. Mapping the RASSF2-proximal proteome by proximity-based biotin labeling (BioID2).

(A) Schematic for RASSF2-BioID2 fusion protein inserts tested for use in proximity-based biotin labeling assay. All three inserts were cloned into MSCV-based retroviral expression vectors for expression of AML cell lines. **(B)** Western blot showing indicated protein amounts following stable transduction of Kasumi-1 AML cell line with vectors indicated. Data are representative of two experiments. **(C)** Western blot showing detection of RASSF2-13xL-BioID2 fusion protein and total biotinylated proteins (probed with Streptavidin) following transfection and supplementation with 50 μM biotin in the culture media for 24 hours. Data are representative of two experiments. **(D)** Western blot showing detection of total biotinylated proteins (probed with Streptavidin) following stable transduction and supplementation with 50 μM biotin in the culture media for 48 hours. The three independent replicates that were submitted for mass spectometry are included. Biotinylated RASSF2-BioID2 fusion and MST1/2 bands are indicated.

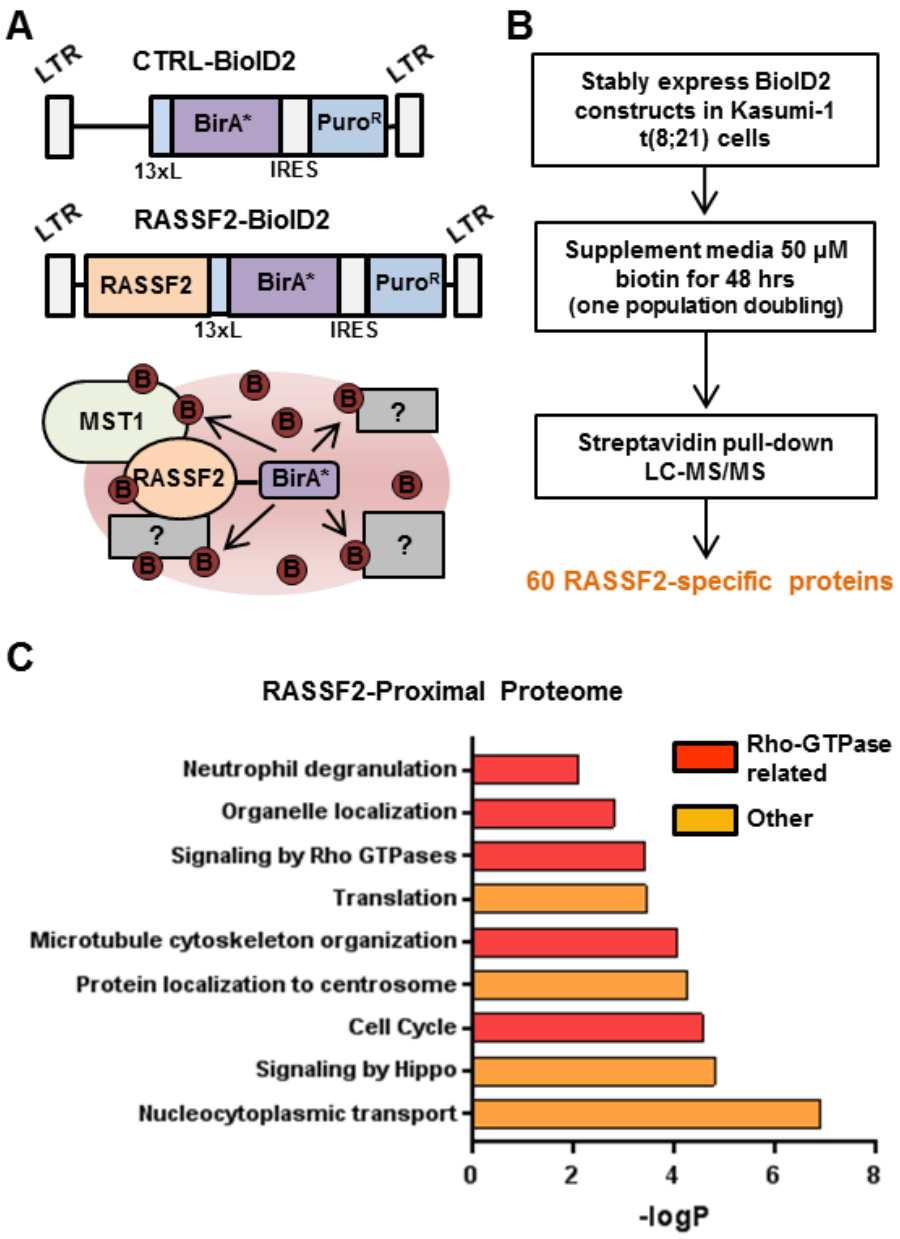

Figure 3.19. Proximity-based biotin labeling identifies RASSF2 endogenous interactions with Rho-GTPase related proteins.
(A) Schematic showing retroviral expression vectors and general assay principle for performing proximity-based biotin labeling and identification using an improved biotin ligase (BioID2, see Methods). **(B)** Strategy for performing proximity-based biotin labeling in Kasumi-1 t(8;21) cell line. Experiment was performed in three independent replicates that were submitted for mass-spectrometric analysis, and 60 unique high-confidence RASSF2-proximal proteins were identified across three replicates. **(C)** Bar graph showing significantly enriched Gene Ontology (GO) terms associated with the RASSF2-specific protein hits identified by proximity-based biotin labeling.

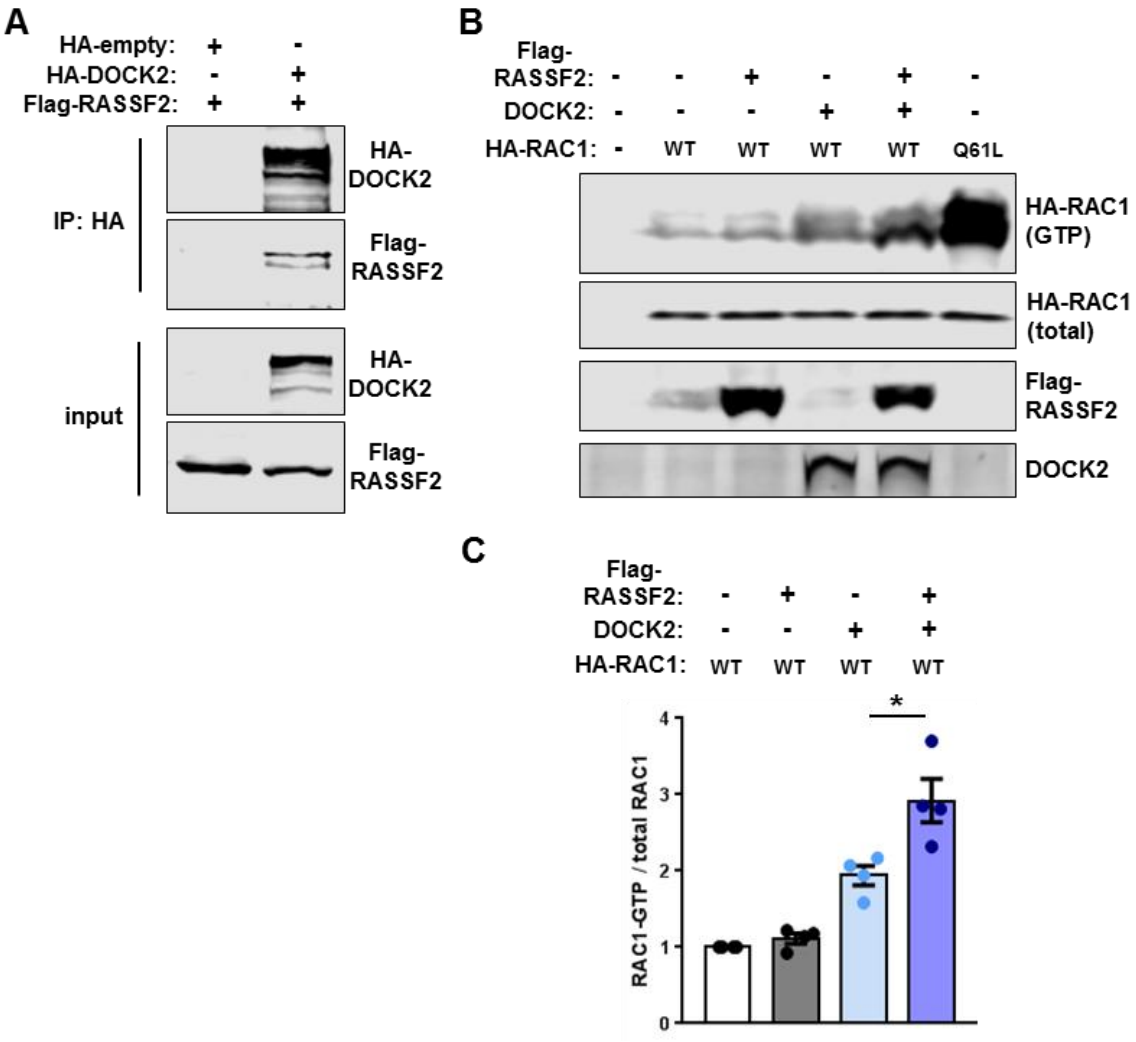

Figure 3.20. RASSF2 interacts with DOCK2 and positively regulates GEF activity towards Rac-GTP.

(A) Western blot showing interaction between HA-DOCK2 and Flag-RASSF2 as assessed in HEK293T cell lysates by immunoblotting for HA and Flag following HA-immunoprecipitation (IP), 36 hours post-transfection with indicated constructs. Inputs are shown below. Data are representative of three experiments. **(B)** Immunoblotting for active (GTP-bound) Rac by PAK1 pull-down assay performed in HEK293T cells 36 hours post-transfection with indicated constructs. Constitutively active RAC1-Q61L mutant is used as a positive control. Data are representative of four experiments. **(C)** Quantification of experiments described (above) for indicated samples. Data are mean +/- s.e.m. of four experiments (individual points). * $p < 0.05$, two-tailed student's t-test.

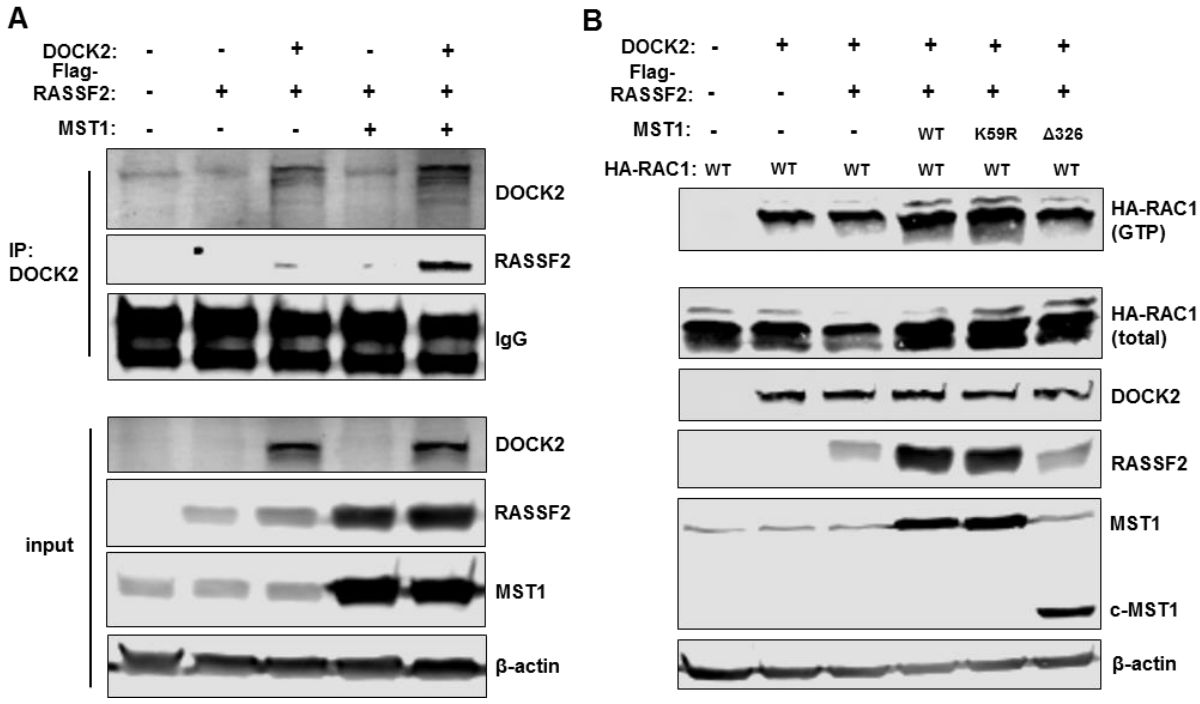

Figure 3.21. MST1 stabilizes RASSF2 interaction with DOCK2 and increases DOCK2-mediated Rac activation.

(A) Western blot showing interaction between DOCK2 and Flag-RASSF2 as assessed in HEK293T cell lysates by immunoblotting for DOCK2 and Flag following DOCK2-immunoprecipitation (IP), 72 hours post-transfection with indicated constructs. Inputs are shown below. Data are representative of two experiments. **(B)** Immunoblotting for active (GTP-bound) Rac by PAK1 pull-down assay performed in HEK293T cells 72 hours post-transfection with indicated constructs. Data are representative of two experiments.

3.2.7. RASSF2 is a critical regulator of Rac GTPase activation in acute myeloid leukemia

We found RASSF2 to be a positive regulator of DOCK2-mediated RAC1 activation in transient transfection-based biochemical assays. We therefore asked what effect RASSF2 perturbation would have on endogenous Rac-GTP abundance in myeloid leukemia cells. Strikingly, lentiviral shRNA-mediated knockdown of *RASSF2* in myeloid leukemia cells was sufficient to profoundly reduce endogenous Rac-GTP to ~30% of basal amounts (**Figures 3.22A and 3.22B**). These results were surprising given the critical importance of sustained Rac GTPase activity for leukemia cell survival and cell cycle progression[165,168], and suggested that non-canonical MST1-RASSF2-DOCK2 signaling could play an oncogenic role in the context of some AML subtypes. Consistent with this, *RASSF2* knockdown using four independent shRNAs induced a profound growth defect across several AML cell lines with a variety of driver mutations, including *MLL*/*MLLT* rearrangements, *PML-RARA*, *NPM1*, *RAS,* and *FLT3*-ITD (**Figures 3.23 and 3.24A**). *RASSF2* knockdown also significantly delayed leukemia onset *in vivo* upon transplantation of human AML cells into NSG mice (**Figure 3.24B**). The *RASSF2* knockdown-associated growth defect and delay in leukemia onset was the result of impaired cell cycle progression due to increased G0/G1 arrest (**Figure 3.24C**). We also performed transcriptional profiling in Rac-dependent THP-1 AML cells following *RASSF2* knockdown with two independent shRNAs (**Figure 3.25A**). *RASSF2* knockdown profoundly altered the global transcriptional signature (**Figure 3.25B**). Interestingly, gene set enrichment

analysis (GSEA)[193] revealed *RASSF2* knockdown to cause loss of a gene expression signature specifically associated with AML patients harboring *MLL* rearrangements[194], and gain a gene expression signature defined by expression of the t(8;21) oncofusion protein RUNX1-ETO[195] (**Figure 3.25C**). This observation further highlights the clinical relevance of a single gene transcriptional repression event, as well as signaling through the Rac pathway, to overall AML subtype-specific downstream transcriptional output. The most striking enrichments by GSEA analysis were for downregulation of numerous cell-cycle associated gene expression signatures. These included several E2F-family target gene signatures, quiescent hematopoietic stem cell-associated signatures, as well as a strong inverse correlation with an Rb loss-of-function signature (**Figures 3.26A and 3.26B**). Enrichr[196] analysis further confirmed significant enrichment for E2F transcription factor binding, along with binding of other cell cycle regulators (MYC, MAX) and several components of the AP-1 transcription factor complex (JUN, JUND, FOS, ATF1), in proximity to the genomic loci of the 978 downregulated genes. These results suggest that *RASSF2* knockdown-mediated inhibition of Rac signaling results in growth arrest through an Rb/E2F-dependent pathway in AML[197,198].

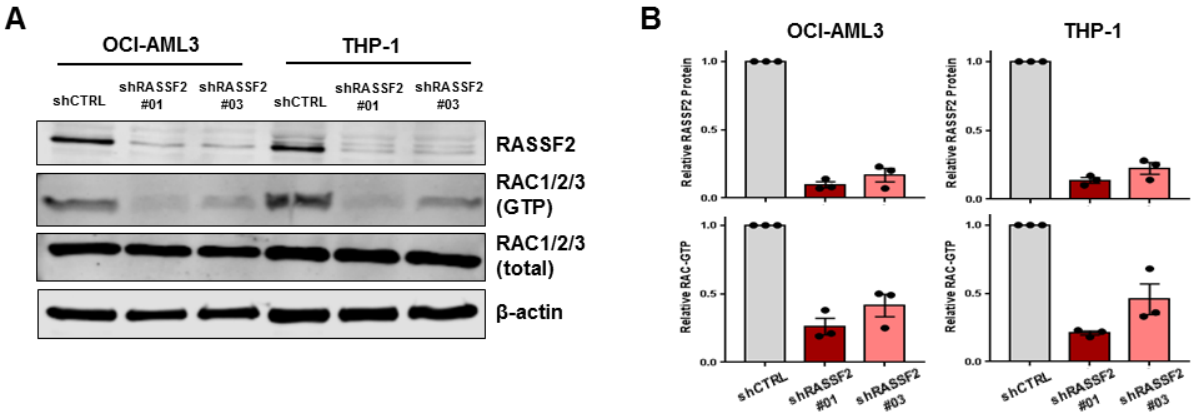

Figure 3.22. *RASSF2* knockdown impairs basal Rac-GTPase activation in AML. **(A)** Immunoblotting for active (GTP-bound) Rac by PAK1 pull-down assay performed in two representative AML cell lines four days post-transduction with lentiviral shRNAs targeting control sequence (shCTRL) or *RASSF2* (shR2#1, shR2#3) as indicated. Data are representative of three experiments. **(B)** Quantification of experiments performed in (A). Data are normalized relative to β-Actin protein abundance and presented as mean +/- s.e.m. of three experiments.

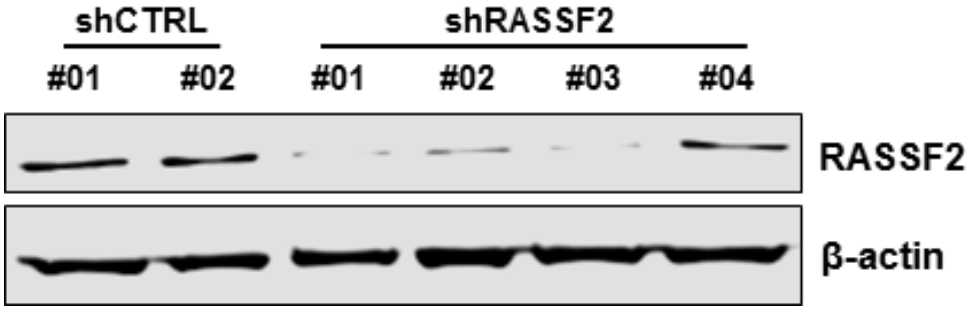

Figure. 3.23. *RASSF2* knockdown by four independent shRNAs in AML cells. Western blot showing RASSF2 protein following lentiviral shRNA-mediated knockdown with two control (shCTRL) and four RASSF2-targeting (shRASSF2) sequences in OCI-AML3 cells. Data are representative of two experiments performed across multiple AML cell lines as indicated.

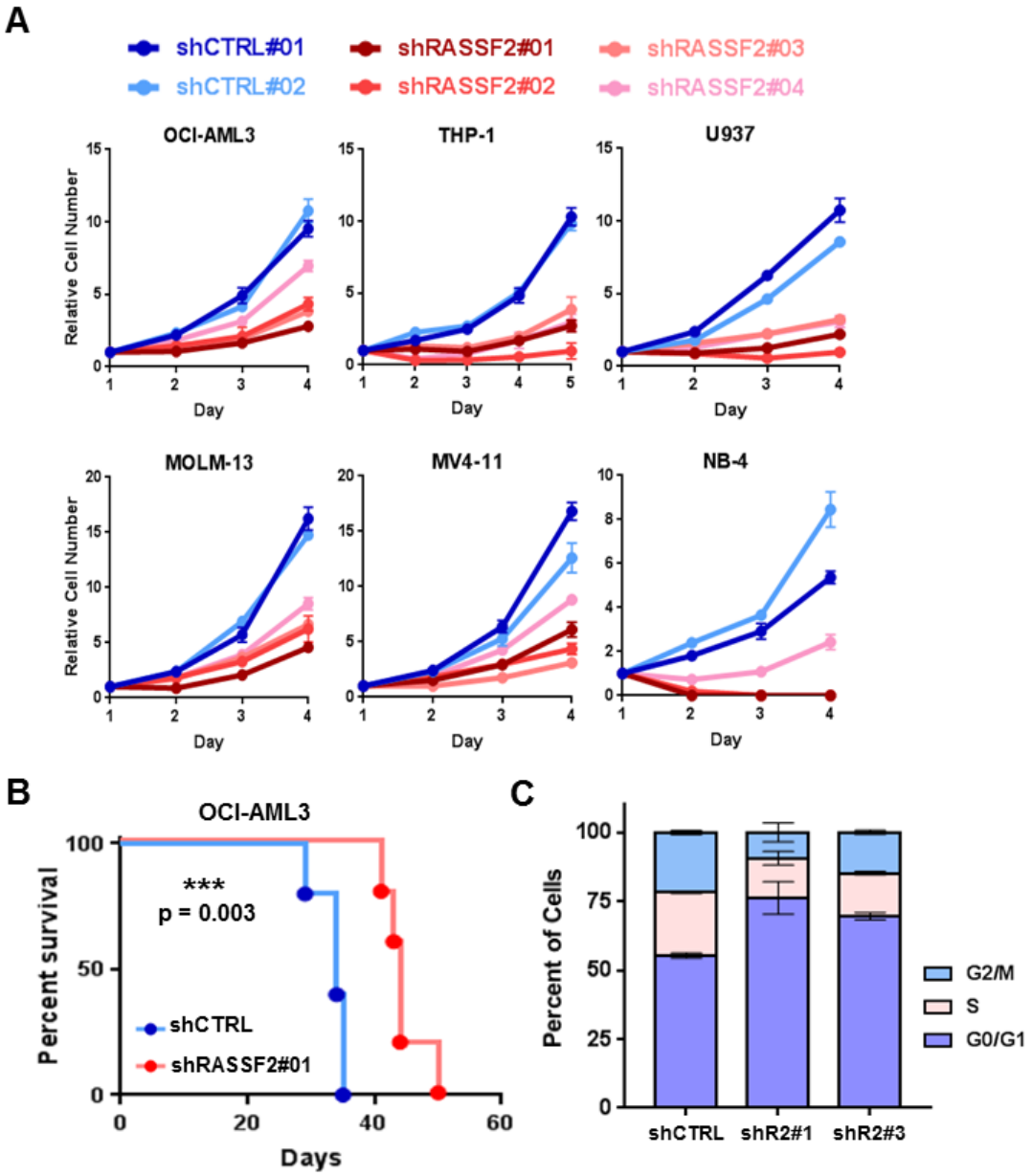

Figure 3.24. *RASSF2* knockdown impairs cell proliferation and causes G0/G1 cell cycle arrest in AML cells *in vitro* and *in vivo*.
(A) Relative cell proliferation of indicated AML cell lines transduced with lentiviral shRNAs targeting two independent control sequences (shCTRL) or four independent *RASSF2* sequences (shRASSF2) as indicated. Cells were seeded at equal density at day 1, which represents four days post-transduction. Data are mean +/- s.e.m. of four experiments. **(B)** Survival analysis of NSG mice transplanted with 1.0 x 10^6 AML cells (OCI-AML3) stably transduced to express lentiviral shRNA vectors as indicated. Significance is determined by log-rank (Mantel-Cox) test. **(C)** Cell cycle analysis in human THP-1 cells stably transduced to express lentiviral shRNA vectors as indicated.

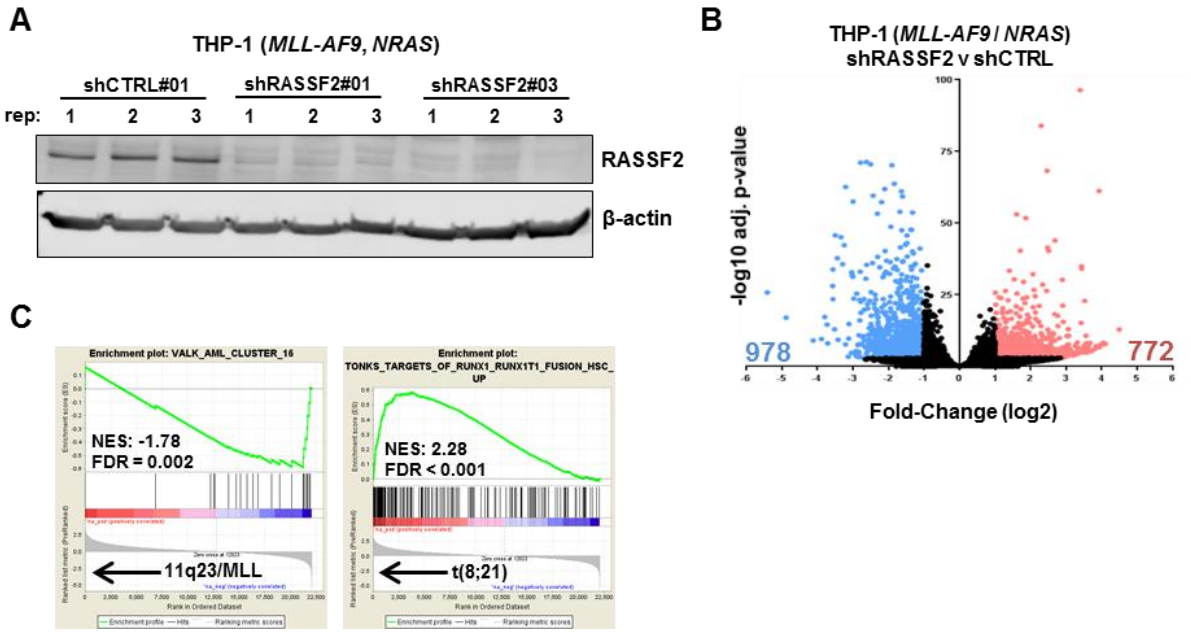

Figure 3.25. *RASSF2* knockdown profoundly alters the transcriptional signatures of AML cells.
(A) Western blot showing RASSF2 protein in THP-1 cells following lentiviral transduction with indicated shRNAs. Data for nine independent replicates (three shCTRL, six shRASSF2) that were submitted for RNA-sequencing analysis are included. **(B)** Volcano plot of RNA-sequencing analysis depicting fold-change expression and significance for all detected genes in human THP-1 cells with stable transduction of two independent RASSF2-targeting shRNAs (shRASSF2, three replicates each) compared to control-targeting shRNA (shCTRL, three replicates). Significantly changed genes are highlighted (downregulated, blue; upregulated, red). **(C)** Gene-set enrichment plots as indicated derived from gene expression analysis. NES, normalized enrichment score, FDR, false discovery rate.

Figure 3.26. *RASSF2* knockdown-dependent cell cycle arrest is associated with an activated Rb signature and inhibited E2F transcription factor activity.
(A) Gene-set enrichment plots as indicated derived from gene expression analysis. NES, normalized enrichment score, FDR, false discovery rate. **(B)** Heatmap depicting row z-scores for THP-1 RNA-sequencing normalized count values for all E2F-target genes derived from Gene Set Enrichment Analysis depicted in (A) (ISHIDA_E2F_TARGETS).

A

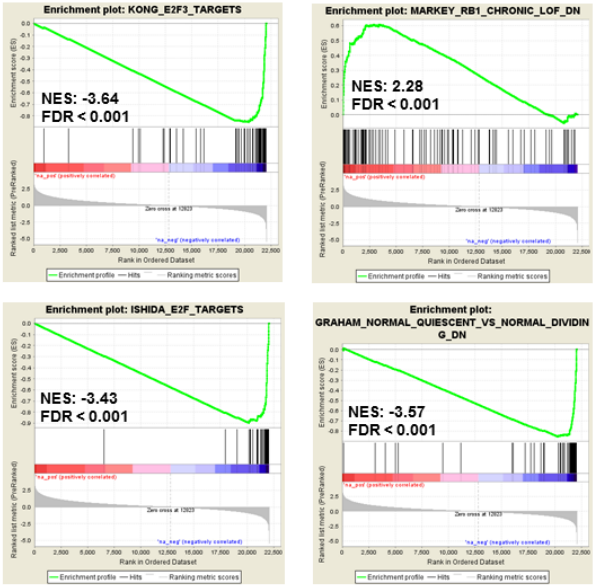
Enrichment plot: KONG_E2F3_TARGETS
NES: -3.64
FDR < 0.001
Enrichment plot: MARKEY_RB1_CHRONIC_LOF_DN
NES: 2.28
FDR < 0.001
Enrichment plot: ISHIDA_E2F_TARGETS
NES: -3.43
FDR < 0.001
Enrichment plot: GRAHAM_NORMAL_QUIESCENT_VS_NORMAL_DIVIDING_DN
NES: -3.57
FDR < 0.001

B

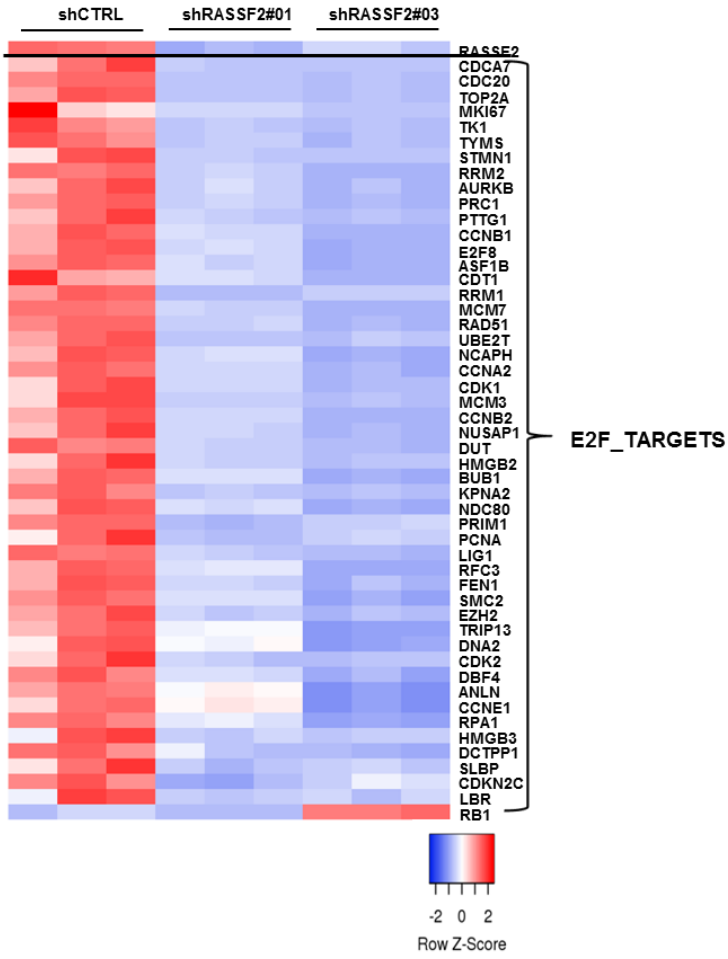
shCTRL
shRASSF2#01
shRASSF2#03
RASSF2
CDCA7
CDC20
TOP2A
MKI67
TK1
TYMS
STMN1
RRM2
AURKB
PRC1
PTTG1
CCNB1
E2F8
ASF1B
CDT1
RRM1
MCM7
RAD51
UBE2T
NCAPH
CCNA2
CDK1
MCM3
CCNB2
NUSAP1
DUT
HMGB2
BUB1
KPNA2
NDC80
PRIM1
PCNA
LIG1
RFC3
FEN1
SMC2
EZH2
TRIP13
DNA2
CDK2
DBF4
ANLN
CCNE1
RPA1
HMGB3
DCTPP1
SLBP
CDKN2C
LBR
RB1
E2F_TARGETS
-2 0 2
Row Z-Score

3.2.8. RASSF2 expression predicts sensitivity to small-molecule inhibition of DOCK2 GEF activity as a therapeutic strategy in myeloid leukemia

Given the importance of sustained Rac activation in numerous leukemia subtypes, we hypothesized that this pathway may be amenable to therapeutic targeting. To test this, we took advantage of the recently discovered small molecule, CPYPP, which binds the catalytic DHR2 domain of DOCK2 and inhibits GEF activity towards Rac1 and Rac2[199]. CPYPP treatment potently reduced Rac-GTP abundance in human AML cells (**Figure 3.27A**). We then assessed dose-response curves measuring relative leukemia cell growth with increasing concentrations of CPYPP in a panel of 10 human AML cell lines (**Figure 3.27B**). This panel included seven lines with 'high' *RASSF2* transcription (defined by >16 TPM) and three with 'low' *RASSF2* transcription (defined by <8 TPM), a demarcation that was even more clearly defined at the protein level (**Figure 3.27B and 3.27C**). Remarkably, there was a sharp distinction in sensitivity to CPYPP treatment that was defined by the presence or absence of RASSF2 (RASSF2-high mean IC_{50}: 5.5 μM, RASSF2-low mean IC_{50}: 24.5 μM) (**Figure 3.27B**). *RASSF2* expression was a far better predictor of human AML cell sensitivity to inhibition of DOCK2 GEF activity than was expression of *RAC1, RAC2,* or *DOCK2* (**Figure 3.28**). We further confirmed the relevance to therapy in CD34+ cells isolated from two primary patient AML samples (**Figure 3.29A**). Both AML patients expressed RASSF2 protein and were sensitive to dose-dependent growth inhibition by CPYPP treatment (**Figure 3.29B**). Importantly, the sample expressing approximately 50% reduced RASSF2 protein (AML patient 1) was less

sensitive to the 15 μM dose of CPYPP treatment, confirming the observations observed across AML cell lines.

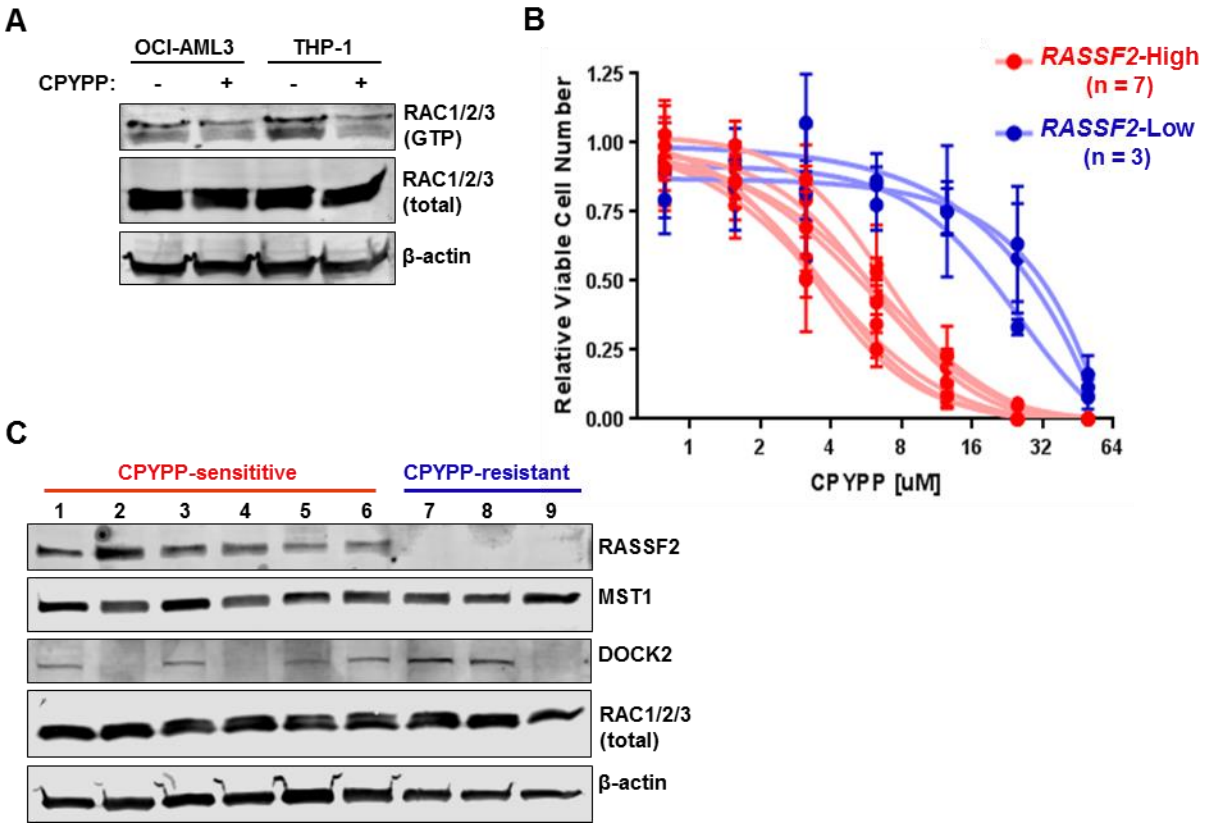

Figure 3.27. CPYPP treatment in panel of AML cell lines with varied expression of RASSF2.

(A) Immunoblotting for active (GTP-bound) Rac by PAK1 pull-down assay in human AML cell lines indicated with or without treatment with 12.5 μM CPYPP. Data are representative of two experiments. **(B)** Dose-response curves depicting relative cell proliferation (normalized to mock treatment- 0.1% DMSO) with increasing concentrations of the small molecule DOCK2 GEF inhibitor, CPYPP. Cells are seeded at equal density and proliferation is measured 72 hours following addition of inhibitor. Data for a panel of 10 human AML cell lines are shown. *RASSF2*-High (TPM > 16, red), and *RASSF2*-Low (TPM < 8, blue) expressing cell lines are indicated. Data are mean +/- S.D. of three experiments. TPM, transcripts per million. **(C)** Western blot showing endogenous amounts of indicated proteins across a panel of nine human AML cell lines. AML cell lines included are: EOL-1 (1), U937 (2), OCI-AML3 (3), NB-4 (4), THP-1 (5), HEL (6), Kasumi-1 (7), SKNO-1 (8), and K562 (9). Data are representative of two experiments.

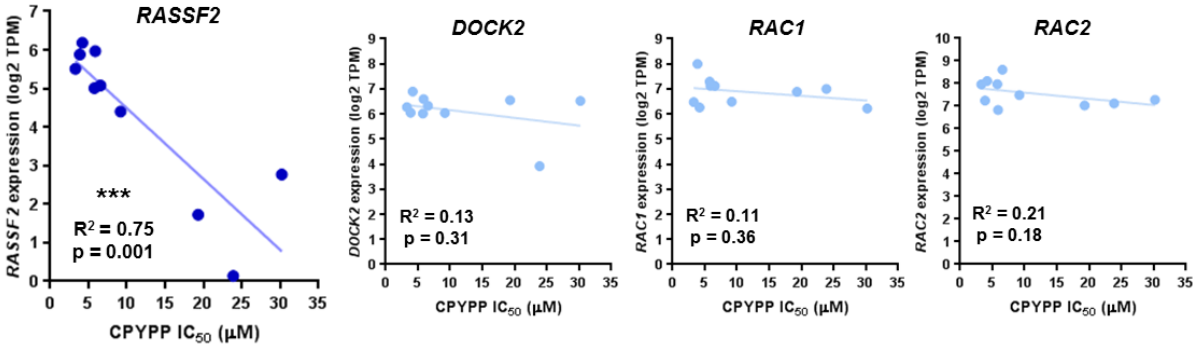

Figure 3.28. RASSF2 expression is the best predictor for sensitivity to small molecule inhibition of DOCK2/Rac-GTP in AML cells.
Correlation plots comparing transcript expression for indicated genes with sensitivity to growth inhibition by CPYPP (IC_{50} values) as measured for the panel of 10 AML cell lines. Goodness of fit (R^2) values and statistical significance of linear regression models are indicated for each gene. TPM, transcripts per million.

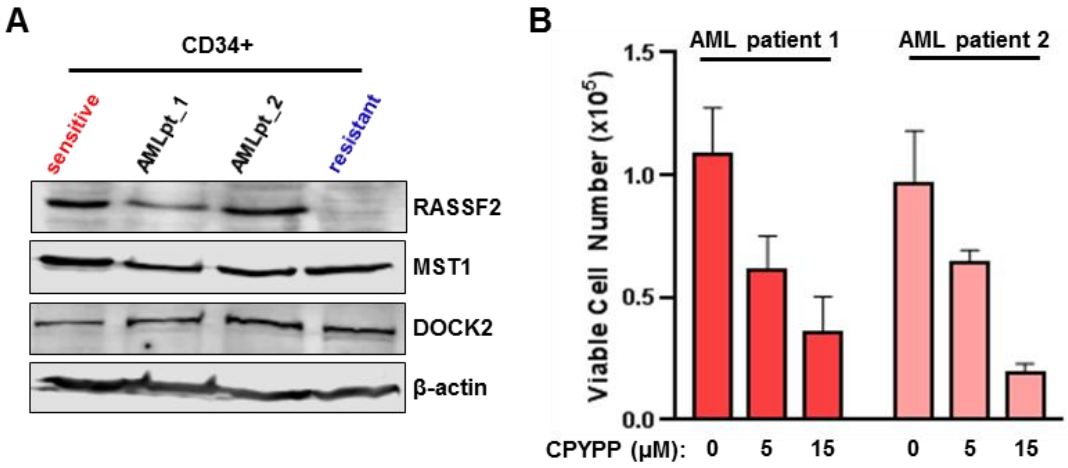

Figure 3.29. Therapeutic targeting of DOCK2 in primary AML patient cells with CPYPP.

(A) Western blot showing endogenous amounts of indicated proteins from two patient-derived AML samples (AMLpt_1 and AMLpt_2) following CD34+ blast enrichment. Lysates from CPYPP-sensitive (OCI-AML3), and CPYPP-resistant (SKNO-1) cell lines are included for comparison. For AML patient samples, lysates from three experiments are pooled. **(B)** Viable cell number of CD34+ blast-enriched AML patient samples. Cells are seeded at equal density and cell number is measured 48 hours following addition of indicated concentrations of CPYPP. Data are mean +/- s.e.m. of three experiments.

3.3. Discussion

In summary, we provide compelling evidence as to the significance of a single gene transcriptional event, *RASSF2*, in controlling leukemia cell fate and revealing dependence on sustained activation of Rac1/2 GTPases by DOCK2. We found RASSF2 to function as a tumor suppressor in only one specific subtype of AML with t(8;21), while in the majority of AML subtypes RASSF2 knockdown induced profound growth defects and cell cycle arrest. These findings highlight the importance of transcriptional regulation of *RASSF2*, and presumably other poorly characterized *RASSF* genes, in human cancer; and demonstrate the ability of this family of non-enzymatic adaptor proteins to exert control over critical oncogenic signaling pathways.

In performing this characterization we identify a non-canonical Hippo pathway that functions independently of Hippo kinase activity and instead relies on SARAH domain-dependent stabilization of RASSF2. Recently, rare families harboring homozygous germline inactivating mutations in *STK4* (MST1) have been identified with clinical presentation of a lethal combined immunodeficiency syndrome[75,76]. Remarkably, there is striking phenotypic overlap between individuals with *STK4* deficiency, and individuals with immunodeficiencies caused by homozygous inactivation of the atypical Rac-GEFs, *DOCK2* and *DOCK8*[200,201]. This is compelling functional evidence in humans, which is further supported by modeling in mice[74,110,202], demonstrating the existence of a non-canonical Hippo pathway in hematopoietic cell types. Our data provide the underlying mechanistic basis for this

phenomenon, in the form of Hippo-RASSF signaling that converges on regulation of GEF activity towards Rac GTPases.

Despite longstanding observations that Rac GTPases are critical mediators of oncogenic transformation and signaling[164,165], therapeutics designed for their inhibition have not been effective. Small GTPases, such as Ras and Rac, are generally considered to be 'undruggable' in cancer, due to the general lack of stable binding pockets within the proteins and the extremely high binding affinity of the nucleotide-binding pocket for GDP/GTP[171]. Perturbation of GEF activity represents a more attractive approach for inhibition of oncogenic small GTPases. Consistent with this, another Rac-specific GEF, PREX1, was recently identified by genome-wide CRISPR screening as a promising target in AML cells harboring oncogenic Ras mutations[203]. Our data, including that from primary patient cells, demonstrates DOCK2 as an important target in leukemia, but only in the context of RASSF2 expression. Given the recent identification of DOCK2 as a mediator of Rac activation and signaling downstream of activating *FLT3* mutations[204] (~30% AML patients harbor *FLT3* mutations), DOCK2 likely represents the broadest and most attractive therapeutic GEF target in myeloid leukemia patients. The IC50 values measuring human AML cell sensitivity to CPYPP treatment here are lower than those previously reported to inhibit DOCK2-mediated Rac activation at the T-cell receptor in normal murine T-cell populations[199], suggesting a viable therapeutic window for DOCK2 inhibition in human AML.

A major difference between the Ras-association (RA) domain of RASSFs and other Ras-binding domain (RBD)-containing proteins is that RASSFs contain a

unique binding site for the switch II region of small GTPases, leading to a longer-lived interaction than traditional effectors[205]. Although this unique binding site may lend itself to the nature of RASSFs as non-catalytic 'adaptor' proteins, rather than traditional catalytic effector proteins, the biological significance of switch II binding remains unknown. The vast majority of Rho-family GEFs catalyze guanine nucleotide exchange via a Dbl homology (DH) region; while the smaller Dedicator of Cytokinesis (DOCK)-family of atypical Rho GEFs catalyze guanine nucleotide exchange via an alternate DOCK homology region (DHR2). Interestingly, structural analysis has revealed that a fundamental difference in the mechanism of GDP exchange between these two families lies within the specific contacts made in the switch II region; in that DOCK-family GEFs fail to displace the conserved Alanine-59 residue of small-GTPases and sterically inhibit Mg^{2+} binding[206,207]. Therefore, we speculate that a RASSF-mediated conformational change within this switch II region of Rho-GTPases may be an essential cooperating step for maximal exchange factor activity of DOCK proteins. Transcriptional regulation of *RASSF2* therefore reflects the overall cellular rate of, and preference for, DOCK2-mediated Rac-GTPase activation. Future studies will seek to investigate this mechanism further.

3.4. Materials and Methods

Generation of Viral Supernatant and Transduction

For retroviral transduction experiments: Transfections of HEK293T cells were conducted by combining 5 µg of MSCV-IRES-GFP/Puro vectors 5 µg of packaging vector (pCL-10A1), and 40 µl of polyethylenimine (PEI) in 1 mL of Opti-MEM reduced serum medium (Gibco, #31985-070). Approximately 16 hours post-transfection, media was aspirated, cells were washed once in PBS, and 6 mL fresh IMDM (Gibco, #12440-053) supplemented with 10% fetal bovine serum was added to each plate. 24 hours following media change, IMDM media containing retroviral particles was collected, passed through a 0.45 µm syringe filter, pooled, and supplemented with recombinant cytokines mIL-3 (10 ng/mL), hIL-6 (10 ng/mL), and mSCF (20 ng/mL), and polybrene (4 µg/mL). For retroviral transduction, HSC-enriched bone-marrow mononuclear cells harvested from mice were resuspended in this supplemented retroviral supernatant at densities of 2-3 x 10^6 cells/mL and centrifuged (2,000x *g*) in 6-well plates at 32°C for 3 hours (Allegra X-12R centrifuge, Beckman Coulter); followed by overnight culture at 37°C. Two consecutive retroviral transductions were performed in this manner on subsequent days. Transduction efficiency was measured (GFP+ frequency) by flow cytometry the morning following the second centrifugation (immediately prior to transplantation into recipient mice). Low retroviral titers were utilized, which were typically measured at ~1.5-2% GFP+ following two rounds of transduction.

For lentiviral transduction of shRNA constructs: Transfections of HEK293T cells were conducted by combining 5 µg of psPAX2, 2.5 µg of pMD2.G, and 3 µg of respective pLKO.1-based shRNA vector, and 44 µl of polyethylenimine (PEI) in 1 mL of Opti-MEM reduced serum medium (Gibco, #31985-070). Approximately 16 hours post-transfection, media was aspirated, cells were washed once in PBS, and 10 mL fresh RPMI supplemented with 10% fetal bovine serum was added to each plate. 24 hours following media change, RPMI media containing lentiviral particles was collected, passed through a 0.45 µm syringe filter, pooled, and supplemented with polybrene (final working concentration: 4 µg/mL). For lentiviral transduction, THP-1 cells were resuspended in this supplemented retroviral supernatant at densities of ~ 0.5 x 10^6 cells/mL and centrifuged (2,000x *g*) in 6-well plates at 32°C for 3 hours (Allegra X-12R centrifuge, Beckman Coulter); followed by overnight culture at 37°C. Two consecutive transductions were performed in this manner on subsequent days. 24 hours following second transduction cells were resuspended in 1.0 µg/mL puromycin, and selected for 72 hours, at which point viable drug-resistant cells were enriched via FICOLL gradient. Post-selection cells were maintained in growth media supplemented with 0.5 µg/mL puromycin.

siRNA Nucleofection

RUNX1-ETO and control-targeting double stranded siRNAs were synthesized and purchased from GE Dharmacon (Lafayette, CO). Lyophilized siRNAs were resuspended in siRNA buffer (20 mM KCl, 6 mM HEPES pH 7.5, 0.02 mM MgCl). Nucleofections were performed by addition of 2 µL siRNA to 100 µL cells (1.5 x

10^7/mL) in Amaxa buffer V using program P-019 in an Amaxa nucleofector according to manufacturer's protocols (Lonza, Cologne, Germany).

siRUNX1-ETO (sense strand):

5'-CCUCGAAAUCGUACUGAGAAG-3'

Non-targeting siCTRL (sense strand):

5'-CGUACGCGGAAUACUUCGATT-3'

Serial Replating / Colony Formation Assay

Transfections of HEK293T cells were conducted by combining 2.5 µg of MSCV-PGK-Neo_R or MSCV-RUNX1-ETO-PGK-Neo_R retroviral expression vector, 2.5 µg of MSCV-IRES-$Puro_R$ or MSCV-Rassf2-IRES- $Puro_R$ (and variants), 5 µg of ecotropic packaging vector (plK6.1-MCV.ecopac.UTd), and 40 µl of polyethylenimine (PEI) in 1 mL of Opti-MEM reduced serum medium (Gibco, #31985-070). Approximately 16 hours post-transfection, media was aspirated, cells were washed once in PBS, and 6 mL fresh IMDM (Gibco, #12440-053) supplemented with 10% fetal bovine serum was added to each plate. 24 hours following media change, IMDM media containing retroviral particles was collected, passed through a 0.45 µm syringe filter, pooled, and supplemented with recombinant cytokines mIL-3 (10 ng/mL), hIL-6 (10 ng/mL), and mSCF (20 ng/mL), and polybrene (4 µg/mL). For retroviral transduction, total murine bone marrow mononuclear cells were resuspended in this supplemented retroviral supernatant at densities of ~4 x 10^6 cells/mL and centrifuged (2,000x *g*) in 6-well plates at 32°C for 3 hours (Allegra X-12R centrifuge, Beckman Coulter); followed by overnight culture at 37°C. Two consecutive retroviral

transductions were performed in this manner on subsequent days. For initial drug selection, 5 x 10^5 cells were plated per 2 mL of murine cytokine-supplemented methylcellulose culture media (MethoCult GF M3534, Stem Cell Technologies, Vancouver, Canada) containing 0.5 µg / mL puromycin and 0.25 mg/mL G418. After one week of selection, replating is performed by resuspension of methylcellulose-embedded colonies in IMDM, followed by plating of 10,000 cells per 2 mL of murine cytokine-supplemented methylcellulose (MethoCult GF M3534) plate. Colony counts therefore represent number of colonies per 10,000 cells plated. Only colonies containing at least 50 cells were scored as colonies. Colonies were counted and replated in this manner weekly for up to six weeks.

RUNX1-ETO9a / Rassf2 Primary Leukemia Model

Transfections of HEK293T cells were conducted by combining 2.5 µg of MSCV-IRES-GFP or MSCV-RUNX1-ETO9a-IRES-GFP retroviral expression vector, 2.5 µg of MSCV-IRES-tdTomato or MSCV-Rassf2-IRES-tdTomato, 5 µg of ecotropic packaging vector (plK6.1-MCV.ecopac.UTd), and 40 µl of polyethylenimine (PEI) in 1 mL of Opti-MEM reduced serum medium (Gibco, #31985-070). Approximately 16 hours post-transfection, media was aspirated, cells were washed once in PBS, and 6 mL fresh IMDM (Gibco, #12440-053) supplemented with 10% fetal bovine serum was added to each plate. 24 hours following media change, IMDM media containing retroviral particles was collected, passed through a 0.45 µm syringe filter, pooled, and supplemented with recombinant cytokines mIL-3 (10 ng/mL), hIL-6 (10 ng/mL), and mSCF (20 ng/mL), and polybrene (4 µg/mL). For retroviral transduction, primary

murine fetal liver cells were resuspended in this supplemented retroviral supernatant at densities of 2-3 x 10^6 cells/mL and centrifuged (2,000x *g*) in 6-well plates at 32°C for 3 hours (Allegra X-12R centrifuge, Beckman Coulter); followed by overnight culture at 37°C. Two consecutive retroviral transductions were performed in this manner on subsequent days. Transduction efficiencies were measured (GFP+ and tdTomato+ frequencies) by flow cytometry the morning following the second centrifugation. Transduced cell populations were flow sorted and then pooled with untransduced 'helper' fetal liver cells at a ratio of 1:6. For the primary leukemia model, approximately 150,000 total cells per mouse were then transplanted into lethally-irradiated (9.5 Gy) recipients and leukemia was monitored over time in recipients.

Peripheral Blood Collection and Analysis

Peripheral blood samples (approximately 100 µl per mouse) were collected in EDTA-coated microvettes (Fisher Scientific, # NC9299309) by submandibular venipuncture using 5 mm animal lancets (Braintree Scientific, #GR5MM). Analysis of differential blood cell counts and parameters was performed using a Scil Vet abc Plus+ instrument (Henry Schein Animal Health). Instrument was regularly calibrated and maintained according to manufacturer's instructions. Fluorescent cell frequencies in peripheral blood samples were measured by flow cytometry via dilution of peripheral blood samples in ACK buffer for 5 minutes, followed by washing once in 1 mL PBS, and resuspension in 350 µl of PBS prior to flow cytometric analysis. Non-viable cells were excluded from analysis via addition of propidium iodide (PI).

qPCR Analysis

Cell lysis and RNA isolation were performed using Trizol reagent (ThermoFisher Scientific, #15596026) according to manufacturer's instructions. cDNA was prepared from 0.5 – 1 µg RNA using qScript cDNA Supermix (Quanta, #95048) according to manufacturer's protocol. Quantitative PCR was performed using KAPA SYBR Fast 2X Master Mix (KAPA Biosystems, #KK4618) according to manufacturer's protocol, in 20 µl reactions, each performed in technical duplicates. qPCR reactions were performed using a BioRad CFX Connect instrument. Data analysis was performed using a standard delta-delta Ct method relative to the geometric-mean of two reference genes, *GAPDH* and *POLR2A.*

Apoptosis Measurement

Apoptotic cell death was monitored by flow cytometry using the APC Annexin V apoptosis kit with 7-AAD (BioLegend, San Diego, CA) as described by manufacturer's protocol.

Cell Proliferation Measurement

Relative cell proliferation was measured by daily manual counting using a hemocytometer, with trypan-blue (Sigma, St. Louis, MO) staining to exclude dead cells.

Western Blotting and Co-Immunoprecipitation

Samples were lysed in ice-cold NP-40 lysis buffer (50 mM Tris pH 8.0, 150 mM NaCl, 1% NP-40) supplemented with protease inhibitor (Roche, #11873580001) and phosphatase inhibitor (Roche, #4906845001). Lysates were cleared by centrifugation at 11,000 xg for 10 minutes at 4°C, and denatured in 2x loading buffer (0.125 M Tris-HCl pH 6.8, 4% SDS, 10% β-mercaptoethanol, 20% glycerol, 0.004% bromophenol blue). For co-immunoprecipitation experiments approximately 500 µg lysate was combined with 40 µl of anti-Flag M2 agarose beads (Sigma #M8823, St. Louis, MO), anti-HA beads (Fisher Scientific # 22-037-959, Waltham, MA) and incubated at 4°C with rotating overnight. For DOCK2 protein pull-down experiments without using tag, lysates were first pre-cleared by incubation with 40 µl protein G-sepharose bead slurry (Invitrogen, Carlsbad, CA) for one hour with rotating at 4°C, followed by washing and then combining 500 µg cell lysates with protein G-sepharose bead slurry and 2 µg monoclonal DOCK2 (E-7) antibody (Santa Cruz Biotechnology, Dallas, TX). The following morning beads were washed 4x with ice-cold NP-40 lysis buffer via centrifugation at 11,000 xg. Washed beads were then resuspended in 60 µl 2x loading buffer and denatured prior to loading. Immunoblotting was performed using the Li-Cor Odyssey infrared imaging instrument. Post-acquisition image analysis and cropping was performed using Li-Cor Image Studio Lite (V 5.2.5) software.

PAK1-based Pull-down Assay for Active Rac-GTP Measurement

Rac1 GTPase Activation Assay (Cell Biolabs # STA-401-1, San Diego, CA) was performed essentially as described by manufacturer's instructions. Briefly,

lysates from approximately 6 x 10^6 cells were prepared as described above but with 1X GTPase assay/lysis buffer (25 mM HEPES, pH 7.5, 150 mM NaCl, 1% NP-40, 10 mM $MgCl_2$, 1 mM EDTA, 2% Glycerol). After clearing, 5% of cell lysates were separated and denatured in 2X loading buffer for use as input protein measurements. For pull-down, remaining cell lysates were combined with 36 µL PAK1 PBD agarose beads (#STA-411) and incubated at 4°C with rotating either for 3 hours (human AML cell lines) or overnight (HEK293T cells). Following this, beads were washed 3x with ice-cold 1X Assay/Lysis buffer via centrifugation at 11,000 xg. Washed beads were then resuspended in 50 µl 2x loading buffer and denatured prior to loading. Immunoblotting was performed using the Li-Cor Odyssey infrared imaging instrument. Post-acquisition image analysis and cropping was performed using Li-Cor Image Studio Lite (V 5.2.5) software. For measuring Rac-GTP in cells, pan-Rac antibody (see Antibody section), rather than anti-Rac1 monoclonal antibody provided by kit was used. Positive and negative assay controls using 100X GTPγS and 100X GDP were performed in parallel using excess cell lysates.

Proximity-based Biotin Labeling and Protein Identification

Proximity-based biotin labeling for identification of proximal proteins using the BioID2-based methods and vectors was performed essentially as described in Roux, *et al.*[190]

RNA-seq Analysis

Cell lysis and RNA isolation were performed using Trizol reagent (ThermoFisher Scientific, #15596026) according to manufacturer's instructions, isolated RNA was aliquoted and stored at -80 °C. Library preparation and sequencing were performed by Novogene (Sacramento, CA). Post-QC, mRNA from eukaryotic organisms is enriched using oligo(dT) beads. For prokaryotic samples, rRNA is removed using the Ribo-Zero kit that leaves the mRNA. First, the mRNA is fragmented randomly by adding fragmentation buffer, then the cDNA is synthesized by using mRNA template and random hexamers primer, after which a custom second-strand synthesis buffer (Illumina) , dNTPs, RNase H and DNA polymerase I are added to initiate the second-strand synthesis. Second, after a series of terminal repair, ligation and sequencing adaptor ligation, the double-stranded cDNA library is completed through size selection and PCR enrichment. The qualified libraries are fed into HiSeq/MiSeq sequencers after pooling according to its effective concentration and expected data volume. Differential expression analysis was conducted by established methods using HISAT2 for human genome alignment (hg38), followed by featureCounts and DESeq2 for differential gene expression analysis.

AML Xenografts

NSG mice were sub-lethally irradiated with a dose of 2.5 Gy approximately 6 hours prior to transplantation with indicated human AML cell lines. AML cells stably transduced with indicated lentiviral shRNA vectors were pelleted, washed once in cold PBS and resuspended at a density of 0.5×10^7 cells / mL in PBS. 1.0×10^6 cells (200 µL) were transplanted per mouse (n = 4 or 5 mice each group, per experiment).

Mice were regularly monitored and were euthanized upon signs of AML burden, including hind-leg paralysis, lethargy, and hunched posture. AML development in cell line xenograft models was independently verified by flow cytometric assessment of human CD45 cell frequencies in bone marrow and spleen at time of euthanasia in an independent cohort of mice.

Cell Cycle Analysis

Cell cycle in cultured AML cell lines was first synchronized via serum starvation for 24 hours (culture media supplemented with 0.2% FBS), followed by re-stimulation with serum (normal culture media supplemented with 10% FBS) for 24 hours. Cycling cells were pelleted, washed once in cold PBS, and resuspended in ice-cold 70% ethanol / 30% PBS, and stored at -20 °C until staining. Fixed cells were then washed twice in PBS, and resuspended in PBS with 0.5 mg/mL RNaseA (Fisher Scientific, Waltham, MA) and 0.05 mg/mL propidium iodide (PI). DNA content was then assessed via flow cytometry detection of PI fluorescent intensity using a linear fluorescent axis. Cell cycle stage quantification was performed using FlowJo (FlowJo, LLC) software.

Gene Ontology Analysis

Gene ontology analysis was performed using Metascape. Gene list of RASSF2-specific protein hits was uploaded and compared against full human genome list.

CPYPP Inhibitor Treatment

4-[3-(2-Chlorophenyl)-2-propen-1-ylidene]-1-phenyl-3,5-pyrazolidinedione (CPYPP) was purchased from Tocris Biosciences (#4568, Bristol, UK). Stock solution was prepared via resuspension in DMSO at a concentration of 10 mM. Stock solution was subsequently diluted in RPMI culture media for experiments involving treatment against AML cells.

Human CD34+ Cell Isolation

Human CD34+ cell isolation was performed using human CD34 Microbead Kit (Miltenyi Biotec, Gladbach, Germany) according to manufacturer's protocol. Frozen primary patient samples were briefly thawed in PBS supplemented with DNase I (1 mg/mL) prior to performing FICOLL gradient separation to obtain a suspension of viable mononuclear cells. Live mononuclear cells were washed in cold PBS, then resuspended in MACS buffer (Miltenyi Biotec) before proceeding with CD34 isolation procedure.

Bone Marrow Mononuclear Cell Collection

Bone marrow cells were harvested by flushing two femurs and two tibias per mouse with ice cold PBS using disposable syringes with 21-gauge needles. Splenocytes were harvested by physical tissue disruption and repeated pipetting in ice cold PBS. Red cell lysis was performed by resuspending cell mixture in ice cold ACK buffer (0.1 mM Na_2EDTA, 10 mM $KHCO_3$, 150 mM NH_4Cl) for 5 minutes, followed by washing with ice cold PBS and passage through a 40 μM cell strainer to

eliminate large tissue/cell clumps and debris. For short-term culture and retroviral transduction/transplantation experiments, hematopoietic cells were resuspended in IMDM supplemented with 10% fetal bovine serum, 1% penicillin/streptomycin, recombinant mIL-3 (10 ng/mL), hIL-6 (10 ng/mL), and mSCF (20 ng/mL). Where applicable, mouse lineage-negative (Lin^-) cells were isolated according to manufacturer's instructions using mouse Lineage Cell Depletion Kit (Miltenyi Biotec, #130-090-858), and enrichment efficiency was verified via flow cytometry.

Flow Cytometry and Cell Sorting

Flow cytometric analysis was conducted using a BD FACSCanto instrument equipped with standard lasers (488 nm, 640 nm) and filters. Data collection was performed using BD FACSDiva software. Compensation was set up using appropriate single-stained controls and positive-staining gates were established using appropriate FMO controls. Post-acquisition data analysis was performed using FlowJo software (FlowJo, LLC). Flow sorting of bone-marrow mononuclear cells was performed on a FACSAriaII equipped with standard lasers (405 nm, 488 nm, 640 nm) and filters, and using a nozzle size of 85 µm. Stainings were conducted in PBS supplemented with 0.1% bovine serum albumin. Antibody validation and optimal antibody concentrations for stainings were pre-determined via titration.

Cell Lines

Human AML cell lines Kasumi-1, SKNO-1, THP-1, EoL-1, MV4-11, U937, NB-4, K562, HEL, and HEK293T cells were purchased from ATCC and maintained as

low passage stocks in the lab. MOLM-13 AML cell line was kindly provided by Leighton H. Grimes (Cincinnati Children's Hospital, Cincinnati, OH). OCI-AML3 AML cell line was kindly provided by Suming Huang (University of Florida, Gainesville, FL).

Mice

All animal protocols were approved by the UCSD Institutional Animal Care and Use Committee (IACUC). Mice were housed in standard conditions with up to 5 mice per cage, fed standard chow, and monitored in accordance with IACUC guidelines. C57BL/6J (stock # 000664) mice were obtained from The Jackson Lab and maintained in our animal facility for more than 10 generations. Vav1-Cre (stock # 008610)[138] transgenic mice were obtained from The Jackson Lab and maintained as hemizygotes in our animal facility for more than 10 generations. NOD.Cg-*Prkdc*^{scid}*Il2rg*^{tm1Wjl}/SzJ ('NSG') mice were obtained from The Jackson Lab (stock # 005557) and maintained in our animal facility for short-term experiments. *Stk4*- and *Stk3*- floxed mice (stock # 017635)[140] were obtained from The Jackson Lab and maintained as homozygotes for floxed alleles in our animal facility. *Stk4*- and *Stk3*- floxed mice were crossed into Cre strains as described. To control for any potential genetic background effects, all mice (or mouse-derived hematopoietic cells used for transplantations) were analyzed in groups with littermates of the same generation of backcross into respective Cre strains. Genotyping for floxed alleles and Cre transgenes was conducted as described on The Jackson Lab website for each respective strain.

Antibodies

Antibodies used in this study are indicated as follows: Human/Mouse RASSF2 (R&D Systems, #AF5639), MST1 (Cell Signaling, #3682), MST2 (Cell Signaling, #3952), Phospho-MOB1 (Thr35) (Cell Signaling, #8699), MOB1 (E1N9D) (Cell Signaling, #13730), Phospho-LATS1 (Thr1079) (Cell Signaling, #8654), Phospho-LATS1 (Ser909) (Cell Signaling, #9157), LATS1 (C66B5) (Cell Signaling, #3477), DOCK2 (E-7) (Santa Cruz, #sc-365242), Rac1/2/3 (Cell Signaling, #2465), Phospho-p44/42 (ERK1/2) (Thr202/Tyr204) (D13.14.4E) (Cell Signaling, #4370), p44/42 MAPK (ERK1/2) (Cell Signaling, #9102), Phospho-AKT (Ser473) (Cell Signaling, #4060), AKT (Cell Signaling, #9272), Monoclonal Anti-Flag M2 (Sigma, #F3165), Monoclonal Anti-HA (HA-7) (Sigma, #H9658), β-Actin clone AC-15 (Millipore Sigma, #A1978), Alpha-Tubulin (DSHB, #12G10), Lamin B1 (B-10) (Santa Cruz, #sc-374015), IRDye 800CW anti-mouse IgG, IRDye 800CW anti-rabbit IgG, IRDye 800CW anti-goat IgG, IRDye 680LT anti-mouse IgG, IRDye 680LT anti-rabbit IgG, IRDye 680LT anti-goat IgG (Li-Cor).

Statistical Analysis

Statistical analyses were conducted using GraphPad Prism (V 7.0) software. Individual statistical tests used for data analysis are indicated in figure legends. All data are displayed as mean (bar graph, horizontal line, or point) with error bars always representing S.E.M. All student's t-tests are conducted as two-tailed tests. Statistical significance in figures is displayed as follows: * = $p < 0.05$, ** = $p < 0.01$, *** = $p < 0.001$. In some cases, where p values are close to reaching a statistical

significance threshold, exact values are displayed in figure panels. Where applicable, mouse sample sizes for measurement of various blood parameters were determined based on a minimal meaningful effect size of one standard deviation from a distribution of healthy wild-type control mice, assuming power = 0.9 and $\alpha = 0.05$.

Chapter 3, in part, is being prepared for submission for publication by: Stoner SA, Liu K, Andrews ET, Davis AG, Arimoto K, Yan M, and Zhang DE. The dissertation author is the primary investigator and author of the manuscript.

References

1 Frohling, S. & Dohner, H. Chromosomal abnormalities in cancer. *N Engl J Med* **359**, 722-734 (2008).

2 Arber, D. A., Orazi, A., Hasserjian, R., Thiele, J., Borowitz, M. J., Le Beau, M. M., Bloomfield, C. D., Cazzola, M. & Vardiman, J. W. The 2016 revision to the World Health Organization classification of myeloid neoplasms and acute leukemia. *Blood* **127**, 2391-2405 (2016).

3 Taylor, J., Xiao, W. & Abdel-Wahab, O. Diagnosis and classification of hematologic malignancies on the basis of genetics. *Blood* **130**, 410-423, doi:10.1182/blood-2017-02-734541 (2017).

4 Kay, H. E., Lawler, S. D. & Millard, R. E. The chromosomes in polycythaemia vera. *Br. J. Haematol.* **12**, 507-528, doi:10.1111/j.1365-2141.1966.tb00134.x (1966).

5 Testa, J. R., Kinnealey, A., Rowley, J. D., Golde, D. W. & Potter, D. Deletion of the long arm of chromosome 20 [del(20)(q11)] in myeloid disorders. *Blood* **52**, 868-877 (1978).

6 Sperling, A. S., Gibson, C. J. & Ebert, B. L. The genetics of myelodysplastic syndrome: from clonal haematopoiesis to secondary leukaemia. *Nat Rev Cancer* **17**, 5-19 (2017).

7 Bacher, U., Schnittger, S., Kern, W., Weiss, T., Haferlach, T. & Haferlach, C. Distribution of cytogenetic abnormalities in myelodysplastic syndromes, Philadelphia negative myeloproliferative neoplasms, and the overlap MDS/MPN category. *Ann Hematol* **88**, 1207-1213 (2009).

8 Haase, D., Germing, U., Schanz, J., Pfeilstöcker, M., Nösslinger, T., Hildebrandt, B., Kundgen, A., Lübbert, M., Kunzmann, R., Giagounidis, A. A. N., Aul, C., Trümper, L., Krieger, O., Stauder, R., Müller, T. H., Wimazal, F., Valent, P., Fonatsch, C. & Steidl, C. New insights into the prognostic impact of the karyotype in MDS and correlation with subtypes: evidence from a core dataset of 2124 patients. *Blood* **110**, 4385-4395, doi:10.1182/blood-2007-03-082404 (2007).

9 Papaemmanuil, E., Gerstung, M., Malcovati, L., Tauro, S., Gundem, G., Van Loo, P., Yoon, C. J., Ellis, P., Wedge, D. C., Pellagatti, A., Shlien, A., Groves, M. J., Forbes, S. A., Raine, K., Hinton, J., Mudie, L. J., McLaren, S., Hardy, C., Latimer, C., Della Porta, M. G., O'Meara, S., Ambaglio, I., Galli, A., Butler, A. P., Walldin, G., Teague, J. W., Quek, L., Sternberg, A., Gambacorti-Passerini,

C., Cross, N. C. P., Green, A. R., Boultwood, J., Vyas, P., Hellstrom-Lindberg, E., Bowen, D., Cazzola, M., Stratton, M. R., Campbell, P. J. & Chronic Myeloid Disorders Working Group of the International Cancer Genome, C. Clinical and biological implications of driver mutations in myelodysplastic syndromes. *Blood* **122**, 3616-3627; quiz 3699, doi:10.1182/blood-2013-08-518886 (2013).

10 Jawad, M. D., Shi, M., Oliveira, J. L., Hoyer, J. D., Christopher Hook, C. & Go, R. S. Clinical course of patients with incidental finding of 20q- in the bone marrow without a morphologic evidence of myeloid neoplasm. *Am. J. Hematol.* **91**, 556-559, doi:10.1002/ajh.24347 (2016).

11 Bacher, U., Haferlach, T., Schnittger, S., Zenger, M., Meggendorfer, M., Jeromin, S., Roller, A., Grossmann, V., Krauth, M. T., Alpermann, T., Kern, W. & Haferlach, C. Investigation of 305 patients with myelodysplastic syndromes and 20q deletion for associated cytogenetic and molecular genetic lesions and their prognostic impact. *Br J Haematol* **164**, 822-833 (2014).

12 Kanagal-Shamanna, R., Yin, C. C., Miranda, R. N., Bueso-Ramos, C. E., Wang, X. I., Muddasani, R., Medeiros, L. J. & Lu, G. Therapy-related myeloid neoplasms with isolated del(20q): comparison with cases of de novo myelodysplastic syndrome with del(20q). *Cancer Genetics* **206**, 42-46, doi:10.1016/j.cancergen.2012.12.005 (2013).

13 Greenberg, P. L., Tuechler, H., Schanz, J., Sanz, G., Garcia-Manero, G., Solé, F., Bennett, J. M., Bowen, D., Fenaux, P., Dreyfus, F., Kantarjian, H., Kuendgen, A., Levis, A., Malcovati, L., Cazzola, M., Cermak, J., Fonatsch, C., Le Beau, M. M., Slovak, M. L., Krieger, O., Luebbert, M., Maciejewski, J., Magalhaes, S. M. M., Miyazaki, Y., Pfeilstöcker, M., Sekeres, M., Sperr, W. R., Stauder, R., Tauro, S., Valent, P., Vallespi, T., van de Loosdrecht, A. A., Germing, U. & Haase, D. Revised international prognostic scoring system for myelodysplastic syndromes. *Blood* **120**, 2454-2465, doi:10.1182/blood-2012-03-420489 (2012).

14 Montalban-Bravo, G. & Garcia-Manero, G. Myelodysplastic syndromes: 2018 update on diagnosis, risk-stratification and management. *Am. J. Hematol.* **93**, 129-147, doi:10.1002/ajh.24930 (2018).

15 Braun, T., de Botton, S., Taksin, A. L., Park, S., Beyne-Rauzy, O., Coiteux, V., Sapena, R., Lazareth, A., Leroux, G., Guenda, K., Cassinat, B., Fontenay, M., Vey, N., Guerci, A., Dreyfus, F., Bordessoule, D., Stamatoullas, A., Castaigne, S., Terre, C., Eclache, V., Fenaux, P. & Ades, L. Characteristics and outcome of myelodysplastic syndromes (MDS) with isolated 20q deletion: a report on 62 cases. *Leuk Res* **35**, 863-867 (2011).

16 Gupta, R., Soupir, C. P., Johari, V. & Hasserjian, R. P. Myelodysplastic syndrome with isolated deletion of chromosome 20q: an indolent disease with

minimal morphological dysplasia and frequent thrombocytopenic presentation. *Br J Haematol* **139**, 265-268 (2007).

17 Vainchenker, W. & Kralovics, R. Genetic basis and molecular pathophysiology of classical myeloproliferative neoplasms. *Blood* **129**, 667-679 (2017).

18 Hussein, K., Van Dyke, D. L. & Tefferi, A. Conventional cytogenetics in myelofibrosis: literature review and discussion. *Eur J Haematol* **82**, 329-338 (2009).

19 Song, J., Hussaini, M., Zhang, H., Shao, H., Qin, D., Zhang, X., Ma, Z., Hussnain Naqvi, S. M., Zhang, L. & Moscinski, L. C. Comparison of the Mutational Profiles of Primary Myelofibrosis, Polycythemia Vera, and Essential Thrombocytosis. *Am J Clin Pathol* **147**, 444-452 (2017).

20 Wassie, E., Finke, C., Gangat, N., Lasho, T. L., Pardanani, A., Hanson, C. A., Ketterling, R. P. & Tefferi, A. A compendium of cytogenetic abnormalities in myelofibrosis: molecular and phenotypic correlates in 826 patients. *Br J Haematol* **169**, 71-76 (2015).

21 Tefferi, A., Nicolosi, M., Mudireddy, M., Lasho, T. L., Gangat, N., Begna, K. H., Hanson, C. A., Ketterling, R. P. & Pardanani, A. Revised cytogenetic risk stratification in primary myelofibrosis: analysis based on 1002 informative patients. *Leukemia* **32**, 1189-1199, doi:10.1038/s41375-018-0018-z (2018).

22 Rumi, E. & Cazzola, M. Diagnosis, risk stratification, and response evaluation in classical myeloproliferative neoplasms. *Blood* **129**, 680-692 (2017).

23 Gangat, N., Caramazza, D., Vaidya, R., George, G., Begna, K., Schwager, S., Van Dyke, D., Hanson, C., Wu, W., Pardanani, A., Cervantes, F., Passamonti, F. & Tefferi, A. DIPSS plus: a refined Dynamic International Prognostic Scoring System for primary myelofibrosis that incorporates prognostic information from karyotype, platelet count, and transfusion status. *J. Clin. Oncol.* **29**, 392-397, doi:10.1200/jco.2010.32.2446 (2011).

24 Nguyen-Khac, F., Lesty, C., Eclache, V., Couronné, L., Kosmider, O., Andrieux, J., Collonge-Rame, M.-A., Penther, D., Lafage, M., Bilhou-Nabera, C., Chapiro, E., Mozziconacci, M.-J., Mugneret, F., Gachard, N., Nadal, N., Lippert, E., Struski, S., Dastugue, N., Cabrol, C., Bernard, O. A. & Groupe Francophone de Cytogénétique, H. Chromosomal abnormalities in transformed Ph-negative myeloproliferative neoplasms are associated to the transformation subtype and independent of JAK2 and the TET2 mutations. *Genes, Chromosomes & Cancer* **49**, 919-927, doi:10.1002/gcc.20802 (2010).

25 Lambert, M. P. & Gernsheimer, T. B. Clinical updates in adult immune thrombocytopenia. *Blood* **129**, 2829-2835, doi:10.1182/blood-2017-03-754119 (2017).

26 Soupir, C. P., Vergilio, J. A., Kelly, E., Dal Cin, P., Kuter, D. & Hasserjian, R. P. Identification of del(20q) in a subset of patients diagnosed with idiopathic thrombocytopenic purpura. *Br J Haematol* **144**, 800-802 (2009).

27 Patnaik, M. M. & Tefferi, A. Cytogenetic and molecular abnormalities in chronic myelomonocytic leukemia. *Blood Cancer J* **5**, 5 (2016).

28 Wassie, E. A., Itzykson, R., Lasho, T. L., Kosmider, O., Finke, C. M., Hanson, C. A., Ketterling, R. P., Solary, E., Tefferi, A. & Patnaik, M. M. Molecular and prognostic correlates of cytogenetic abnormalities in chronic myelomonocytic leukemia: a Mayo Clinic-French Consortium Study. *Am. J. Hematol.* **89**, 1111-1115, doi:10.1002/ajh.23846 (2014).

29 Patnaik, M. M. & Tefferi, A. Chronic myelomonocytic leukemia: 2018 update on diagnosis, risk stratification and management. *Am. J. Hematol.* **93**, 824-840, doi:10.1002/ajh.25104 (2018).

30 Such, E., Cervera, J., Costa, D., Solé, F., Vallespí, T., Luño, E., Collado, R., Calasanz, M. J., Hernández-Rivas, J. M., Cigudosa, J. C., Nomdedeu, B., Mallo, M., Carbonell, F., Bueno, J., Ardanaz, M. T., Ramos, F., Tormo, M., Sancho-Tello, R., del Cañizo, C., Gómez, V., Marco, V., Xicoy, B., Bonanad, S., Pedro, C., Bernal, T. & Sanz, G. F. Cytogenetic risk stratification in chronic myelomonocytic leukemia. *Haematologica* **96**, 375-383, doi:10.3324/haematol.2010.030957 (2011).

31 Arefi, M., Robledo, C., Peñarrubia, M. J., García de Coca, A., Cordero, M., Hernández-Rivas, J. M. & García, J. L. Genomic analysis of clonal eosinophils by CGH arrays reveals new genetic regions involved in chronic eosinophilia. *Eur. J. Haematol.* **93**, 422-428, doi:10.1111/ejh.12379 (2014).

32 Laurie, C. C., Laurie, C. A., Rice, K., Doheny, K. F., Zelnick, L. R., McHugh, C. P., Ling, H., Hetrick, K. N., Pugh, E. W., Amos, C., Wei, Q., Wang, L. E., Lee, J. E., Barnes, K. C., Hansel, N. N., Mathias, R., Daley, D., Beaty, T. H., Scott, A. F., Ruczinski, I., Scharpf, R. B., Bierut, L. J., Hartz, S. M., Landi, M. T., Freedman, N. D., Goldin, L. R., Ginsburg, D., Li, J., Desch, K. C., Strom, S. S., Blot, W. J., Signorello, L. B., Ingles, S. A., Chanock, S. J., Berndt, S. I., Le Marchand, L., Henderson, B. E., Monroe, K. R., Heit, J. A., de Andrade, M., Armasu, S. M., Regnier, C., Lowe, W. L., Hayes, M. G., Marazita, M. L., Feingold, E., Murray, J. C., Melbye, M., Feenstra, B., Kang, J. H., Wiggs, J. L., Jarvik, G. P., McDavid, A. N., Seshan, V. E., Mirel, D. B., Crenshaw, A., Sharopova, N., Wise, A., Shen, J., Crosslin, D. R., Levine, D. M., Zheng, X., Udren, J. I., Bennett, S., Nelson, S. C., Gogarten, S. M., Conomos, M. P., Heagerty, P., Manolio, T., Pasquale, L. R., Haiman, C. A., Caporaso, N. & Weir, B. S. Detectable clonal mosaicism from birth to old age and its relationship to cancer. *Nat Genet* **44**, 642-650 (2012).

33 Jacobs, K. B., Yeager, M., Zhou, W., Wacholder, S., Wang, Z., Rodriguez-Santiago, B., Hutchinson, A., Deng, X., Liu, C., Horner, M. J., Cullen, M., Epstein, C. G., Burdett, L., Dean, M. C., Chatterjee, N., Sampson, J., Chung, C. C., Kovaks, J., Gapstur, S. M., Stevens, V. L., Teras, L. T., Gaudet, M. M., Albanes, D., Weinstein, S. J., Virtamo, J., Taylor, P. R., Freedman, N. D., Abnet, C. C., Goldstein, A. M., Hu, N., Yu, K., Yuan, J. M., Liao, L., Ding, T., Qiao, Y. L., Gao, Y. T., Koh, W. P., Xiang, Y. B., Tang, Z. Z., Fan, J. H., Aldrich, M. C., Amos, C., Blot, W. J., Bock, C. H., Gillanders, E. M., Harris, C. C., Haiman, C. A., Henderson, B. E., Kolonel, L. N., Le Marchand, L., McNeill, L. H., Rybicki, B. A., Schwartz, A. G., Signorello, L. B., Spitz, M. R., Wiencke, J. K., Wrensch, M., Wu, X., Zanetti, K. A., Ziegler, R. G., Figueroa, J. D., Garcia-Closas, M., Malats, N., Marenne, G., Prokunina-Olsson, L., Baris, D., Schwenn, M., Johnson, A., Landi, M. T., Goldin, L., Consonni, D., Bertazzi, P. A., Rotunno, M., Rajaraman, P., Andersson, U., Beane Freeman, L. E., Berg, C. D., Buring, J. E., Butler, M. A., Carreon, T., Feychting, M., Ahlbom, A., Gaziano, J. M., Giles, G. G., Hallmans, G., Hankinson, S. E., Hartge, P., Henriksson, R., Inskip, P. D., Johansen, C., Landgren, A., McKean-Cowdin, R., Michaud, D. S., Melin, B. S., Peters, U., Ruder, A. M., Sesso, H. D., Severi, G., Shu, X. O., Visvanathan, K., White, E., Wolk, A., Zeleniuch-Jacquotte, A., Zheng, W., Silverman, D. T., Kogevinas, M., Gonzalez, J. R., Villa, O., Li, D., Duell, E. J., Risch, H. A., Olson, S. H., Kooperberg, C., Wolpin, B. M., Jiao, L., Hassan, M., Wheeler, W., Arslan, A. A., Bueno-de-Mesquita, H. B., Fuchs, C. S., Gallinger, S., Gross, M. D., Holly, E. A., Klein, A. P., LaCroix, A., Mandelson, M. T., Petersen, G., Boutron-Ruault, M. C., Bracci, P. M., Canzian, F., Chang, K., Cotterchio, M., Giovannucci, E. L., Goggins, M., Hoffman Bolton, J. A., Jenab, M., Khaw, K. T., Krogh, V., Kurtz, R. C., McWilliams, R. R., Mendelsohn, J. B., Rabe, K. G., Riboli, E., Tjonneland, A., Tobias, G. S., Trichopoulos, D., Elena, J. W., Yu, H., Amundadottir, L., Stolzenberg-Solomon, R. Z., Kraft, P., Schumacher, F., Stram, D., Savage, S. A., Mirabello, L., Andrulis, I. L., Wunder, J. S., Patino Garcia, A., Sierrasesumaga, L., Barkauskas, D. A., Gorlick, R. G., Purdue, M., Chow, W. H., Moore, L. E., Schwartz, K. L., Davis, F. G., Hsing, A. W., Berndt, S. I., Black, A., Wentzensen, N., Brinton, L. A., Lissowska, J., Peplonska, B., McGlynn, K. A., Cook, M. B., Graubard, B. I., Kratz, C. P., Greene, M. H., Erickson, R. L., Hunter, D. J., Thomas, G., Hoover, R. N., Real, F. X., Fraumeni, J. F., Jr., Caporaso, N. E., Tucker, M., Rothman, N., Perez-Jurado, L. A. & Chanock, S. J. Detectable clonal mosaicism and its relationship to aging and cancer. *Nat Genet* **44**, 651-658 (2012).

34 Jaiswal, S., Fontanillas, P., Flannick, J., Manning, A., Grauman, P. V., Mar, B. G., Lindsley, R. C., Mermel, C. H., Burtt, N., Chavez, A., Higgins, J. M., Moltchanov, V., Kuo, F. C., Kluk, M. J., Henderson, B., Kinnunen, L., Koistinen, H. A., Ladenvall, C., Getz, G., Correa, A., Banahan, B. F., Gabriel, S., Kathiresan, S., Stringham, H. M., McCarthy, M. I., Boehnke, M., Tuomilehto, J., Haiman, C., Groop, L., Atzmon, G., Wilson, J. G., Neuberg, D., Altshuler, D. & Ebert, B. L. Age-related clonal hematopoiesis associated with

adverse outcomes. *N. Engl. J. Med.* **371**, 2488-2498, doi:10.1056/NEJMoa1408617 (2014).

35 Genovese, G., Kähler, A. K., Handsaker, R. E., Lindberg, J., Rose, S. A., Bakhoum, S. F., Chambert, K., Mick, E., Neale, B. M., Fromer, M., Purcell, S. M., Svantesson, O., Landén, M., Höglund, M., Lehmann, S., Gabriel, S. B., Moran, J. L., Lander, E. S., Sullivan, P. F., Sklar, P., Grönberg, H., Hultman, C. M. & McCarroll, S. A. Clonal hematopoiesis and blood-cancer risk inferred from blood DNA sequence. *N. Engl. J. Med.* **371**, 2477-2487, doi:10.1056/NEJMoa1409405 (2014).

36 Shlush, L. I., Zandi, S., Mitchell, A., Chen, W. C., Brandwein, J. M., Gupta, V., Kennedy, J. A., Schimmer, A. D., Schuh, A. C., Yee, K. W., McLeod, J. L., Doedens, M., Medeiros, J. J. F., Marke, R., Kim, H. J., Lee, K., McPherson, J. D., Hudson, T. J., Consortium, H. P.-L. G. P., Brown, A. M. K., Yousif, F., Trinh, Q. M., Stein, L. D., Minden, M. D., Wang, J. C. Y. & Dick, J. E. Identification of pre-leukaemic haematopoietic stem cells in acute leukaemia. *Nature* **506**, 328-333, doi:10.1038/nature13038 (2014).

37 Steensma, D. P. Clinical consequences of clonal hematopoiesis of indeterminate potential. *Blood Advances* **2**, 3404-3410, doi:10.1182/bloodadvances.2018020222 (2018).

38 Machiela, M. J., Zhou, W., Caporaso, N., Dean, M., Gapstur, S. M., Goldin, L., Rothman, N., Stevens, V. L., Yeager, M. & Chanock, S. J. Mosaic chromosome 20q deletions are more frequent in the aging population. *Blood Adv* **1**, 380-385 (2017).

39 Loh, P. R., Genovese, G., Handsaker, R. E., Finucane, H. K., Reshef, Y. A., Palamara, P. F., Birmann, B. M., Talkowski, M. E., Bakhoum, S. F., McCarroll, S. A. & Price, A. L. Insights into clonal haematopoiesis from 8,342 mosaic chromosomal alterations. *Nature* **559**, 350-355 (2018).

40 Wang, P. W., Iannantuoni, K., Davis, E. M., Espinosa, R., Stoffel, M. & Le Beau, M. M. Refinement of the commonly deleted segment in myeloid leukemias with a del(20q). *Genes, Chromosomes & Cancer* **21**, 75-81 (1998).

41 Bench, A. J., Aldred, M. A., Humphray, S. J., Champion, K. M., Gilbert, J. G., Asimakopoulos, F. A., Deloukas, P., Gwilliam, R., Bentley, D. R. & Green, A. R. A detailed physical and transcriptional map of the region of chromosome 20 that is deleted in myeloproliferative disorders and refinement of the common deleted region. *Genomics* **49**, 351-362, doi:10.1006/geno.1998.5231 (1998).

42 Bench, A. J., Nacheva, E. P., Hood, T. L., Holden, J. L., French, L., Swanton, S., Champion, K. M., Li, J., Whittaker, P., Stavrides, G., Hunt, A. R., Huntly, B. J., Campbell, L. J., Bentley, D. R., Deloukas, P. & Green, A. R. Chromosome

20 deletions in myeloid malignancies: reduction of the common deleted region, generation of a PAC/BAC contig and identification of candidate genes. UK Cancer Cytogenetics Group (UKCCG). *Oncogene* **19**, 3902-3913 (2000).

43 Douet-Guilbert, N., Basinko, A., Morel, F., Le Bris, M. J., Ugo, V., Morice, P., Berthou, C. & De Braekeleer, M. Chromosome 20 deletions in myelodysplastic syndromes and Philadelphia-chromosome-negative myeloproliferative disorders: characterization by molecular cytogenetics of commonly deleted and retained regions. *Ann Hematol* **87**, 537-544 (2008).

44 Schaub, F. X., Jäger, R., Looser, R., Hao-Shen, H., Hermouet, S., Girodon, F., Tichelli, A., Gisslinger, H., Kralovics, R. & Skoda, R. C. Clonal analysis of deletions on chromosome 20q and JAK2-V617F in MPD suggests that del20q acts independently and is not one of the predisposing mutations for JAK2-V617F. *Blood* **113**, 2022-2027, doi:10.1182/blood-2008-07-167056 (2009).

45 Huh, J., Tiu, R. V., Gondek, L. P., O'Keefe, C. L., Jasek, M., Makishima, H., Jankowska, A. M., Jiang, Y., Verma, A., Theil, K. S., McDevitt, M. A. & Maciejewski, J. P. Characterization of chromosome arm 20q abnormalities in myeloid malignancies using genome-wide single nucleotide polymorphism array analysis. *Genes Chromosomes Cancer* **49**, 390-399 (2010).

46 Okada, M., Suto, Y., Hirai, M., Shiseki, M., Usami, A., Okajima, K., Teramura, M., Mori, N. & Motoji, T. Microarray CGH analyses of chromosomal 20q deletions in patients with hematopoietic malignancies. *Cancer Genet* **205**, 18-24 (2012).

47 Bench, A. J., Li, J., Huntly, B. J. P., Delabesse, E., Fourouclas, N., Hunt, A. R., Deloukas, P. & Green, A. R. Characterization of the imprinted polycomb gene L3MBTL, a candidate 20q tumour suppressor gene, in patients with myeloid malignancies. *Br. J. Haematol.* **127**, 509-518, doi:10.1111/j.1365-2141.2004.05278.x (2004).

48 Aziz, A., Baxter, E. J., Edwards, C., Cheong, C. Y., Ito, M., Bench, A., Kelley, R., Silber, Y., Beer, P. A., Chng, K., Renfree, M. B., McEwen, K., Gray, D., Nangalia, J., Mufti, G. J., Hellstrom-Lindberg, E., Kiladjian, J. J., McMullin, M. F., Campbell, P. J., Ferguson-Smith, A. C. & Green, A. R. Cooperativity of imprinted genes inactivated by acquired chromosome 20q deletions. *J Clin Invest* **123**, 2169-2182 (2013).

49 Nacci, L., Valli, R., Maria Pinto, R., Zecca, M., Cipolli, M., Morini, J., Cesaro, S., Boveri, E., Rosti, V., Corti, P., Ambroni, M., Pasquali, F., Danesino, C., Maserati, E. & Minelli, A. Parental origin of the deletion del(20q) in Shwachman-Diamond patients and loss of the paternally derived allele of the imprinted L3MBTL1 gene. *Genes, Chromosomes & Cancer* **56**, 51-58, doi:10.1002/gcc.22401 (2017).

50 Koga, H., Matsui, S., Hirota, T., Takebayashi, S., Okumura, K. & Saya, H. A human homolog of Drosophila lethal(3)malignant brain tumor (l(3)mbt) protein associates with condensed mitotic chromosomes. *Oncogene* **18**, 3799-3809, doi:10.1038/sj.onc.1202732 (1999).

51 Boccuni, P., MacGrogan, D., Scandura, J. M. & Nimer, S. D. The human L(3)MBT polycomb group protein is a transcriptional repressor and interacts physically and functionally with TEL (ETV6). *J. Biol. Chem.* **278**, 15412-15420, doi:10.1074/jbc.M300592200 (2003).

52 Trojer, P., Li, G., Sims, R. J., Vaquero, A., Kalakonda, N., Boccuni, P., Lee, D., Erdjument-Bromage, H., Tempst, P., Nimer, S. D., Wang, Y.-H. & Reinberg, D. L3MBTL1, a histone-methylation-dependent chromatin lock. *Cell* **129**, 915-928, doi:10.1016/j.cell.2007.03.048 (2007).

53 Kalakonda, N., Fischle, W., Boccuni, P., Gurvich, N., Hoya-Arias, R., Zhao, X., Miyata, Y., Macgrogan, D., Zhang, J., Sims, J. K., Rice, J. C. & Nimer, S. D. Histone H4 lysine 20 monomethylation promotes transcriptional repression by L3MBTL1. *Oncogene* **27**, 4293-4304, doi:10.1038/onc.2008.67 (2008).

54 West, L. E., Roy, S., Lachmi-Weiner, K., Hayashi, R., Shi, X., Appella, E., Kutateladze, T. G. & Gozani, O. The MBT repeats of L3MBTL1 link SET8-mediated p53 methylation at lysine 382 to target gene repression. *J. Biol. Chem.* **285**, 37725-37732, doi:10.1074/jbc.M110.139527 (2010).

55 Gurvich, N., Perna, F., Farina, A., Voza, F., Menendez, S., Hurwitz, J. & Nimer, S. D. L3MBTL1 polycomb protein, a candidate tumor suppressor in del(20q12) myeloid disorders, is essential for genome stability. *Proc Natl Acad Sci U S A* **107**, 22552-22557 (2010).

56 Perna, F., Gurvich, N., Hoya-Arias, R., Abdel-Wahab, O., Levine, R. L., Asai, T., Voza, F., Menendez, S., Wang, L., Liu, F., Zhao, X. & Nimer, S. D. Depletion of L3MBTL1 promotes the erythroid differentiation of human hematopoietic progenitor cells: possible role in 20q- polycythemia vera. *Blood* **116**, 2812-2821 (2010).

57 Perna, F., Vu, L. P., Themeli, M., Kriks, S., Hoya-Arias, R., Khanin, R., Hricik, T., Mansilla-Soto, J., Papapetrou, E. P., Levine, R. L., Studer, L., Sadelain, M. & Nimer, S. D. The polycomb group protein L3MBTL1 represses a SMAD5-mediated hematopoietic transcriptional program in human pluripotent stem cells. *Stem Cell Reports* **4**, 658-669, doi:10.1016/j.stemcr.2015.02.003 (2015).

58 Qin, J., Van Buren, D., Huang, H.-S., Zhong, L., Mostoslavsky, R., Akbarian, S. & Hock, H. Chromatin protein L3MBTL1 is dispensable for development and tumor suppression in mice. *J. Biol. Chem.* **285**, 27767-27775, doi:10.1074/jbc.M110.115410 (2010).

59 Bonasio, R., Lecona, E. & Reinberg, D. MBT domain proteins in development and disease. *Semin. Cell Dev. Biol.* **21**, 221-230, doi:10.1016/j.semcdb.2009.09.010 (2010).

60 Musa, J., Aynaud, M.-M., Mirabeau, O., Delattre, O. & Grünewald, T. G. MYBL2 (B-Myb): a central regulator of cell proliferation, cell survival and differentiation involved in tumorigenesis. *Cell Death Dis* **8**, e2895, doi:10.1038/cddis.2017.244 (2017).

61 García, P. & Frampton, J. The transcription factor B-Myb is essential for S-phase progression and genomic stability in diploid and polyploid megakaryocytes. *J. Cell. Sci.* **119**, 1483-1493, doi:10.1242/jcs.02870 (2006).

62 Clarke, M., Dumon, S., Ward, C., Jager, R., Freeman, S., Dawood, B., Sheriff, L., Lorvellec, M., Kralovics, R., Frampton, J. & Garcia, P. MYBL2 haploinsufficiency increases susceptibility to age-related haematopoietic neoplasia. *Leukemia* **27**, 661-670 (2013).

63 Heinrichs, S., Conover, L. F., Bueso-Ramos, C. E., Kilpivaara, O., Stevenson, K., Neuberg, D., Loh, M. L., Wu, W. S., Rodig, S. J., Garcia-Manero, G., Kantarjian, H. M. & Look, A. T. MYBL2 is a sub-haploinsufficient tumor suppressor gene in myeloid malignancy. *Elife* **16**, 00825 (2013).

64 Bayley, R., Blakemore, D., Cancian, L., Dumon, S., Volpe, G., Ward, C., Almaghrabi, R., Gujar, J., Reeve, N., Raghavan, M., Higgs, M. R., Stewart, G. S., Petermann, E. & García, P. MYBL2 Supports DNA Double Strand Break Repair in Hematopoietic Stem Cells. *Cancer Res.* **78**, 5767-5779, doi:10.1158/0008-5472.can-18-0273 (2018).

65 Myers, M. P., Andersen, J. N., Cheng, A., Tremblay, M. L., Horvath, C. M., Parisien, J. P., Salmeen, A., Barford, D. & Tonks, N. K. TYK2 and JAK2 are substrates of protein-tyrosine phosphatase 1B. *J. Biol. Chem.* **276**, 47771-47774, doi:10.1074/jbc.C100583200 (2001).

66 Babon, J. J., Lucet, I. S., Murphy, J. M., Nicola, N. A. & Varghese, L. N. The molecular regulation of Janus kinase (JAK) activation. *Biochem. J.* **462**, 1-13, doi:10.1042/bj20140712 (2014).

67 Tiacci, E., Ladewig, E., Schiavoni, G., Penson, A., Fortini, E., Pettirossi, V., Wang, Y., Rosseto, A., Venanzi, A., Vlasevska, S., Pacini, R., Piattoni, S., Tabarrini, A., Pucciarini, A., Bigerna, B., Santi, A., Gianni, A. M., Viviani, S., Cabras, A., Ascani, S., Crescenzi, B., Mecucci, C., Pasqualucci, L., Rabadan, R. & Falini, B. Pervasive mutations of JAK-STAT pathway genes in classical Hodgkin lymphoma. *Blood* **131**, 2454-2465, doi:10.1182/blood-2017-11-814913 (2018).

68 Gunawardana, J., Chan, F. C., Telenius, A., Woolcock, B., Kridel, R., Tan, K. L., Ben-Neriah, S., Mottok, A., Lim, R. S., Boyle, M., Rogic, S., Rimsza, L. M., Guiter, C., Leroy, K., Gaulard, P., Haioun, C., Marra, M. A., Savage, K. J., Connors, J. M., Shah, S. P., Gascoyne, R. D. & Steidl, C. Recurrent somatic mutations of PTPN1 in primary mediastinal B cell lymphoma and Hodgkin lymphoma. *Nat. Genet.* **46**, 329-335, doi:10.1038/ng.2900 (2014).

69 Zahn, M., Marienfeld, R., Melzner, I., Heinrich, J., Renner, B., Wegener, S., Mießner, A., Barth, T. F. E., Dorsch, K., Brüderlein, S. & Möller, P. A novel PTPN1 splice variant upregulates JAK/STAT activity in classical Hodgkin lymphoma cells. *Blood* **129**, 1480-1490, doi:10.1182/blood-2016-06-720516 (2017).

70 Jobe, F., Patel, B., Kuzmanovic, T., Makishima, H., Yang, Y., Przychodzen, B., Hutchison, R. E., Bence, K. K., Maciejewski, J. P. & Mohi, G. Deletion of Ptpn1 induces myeloproliferative neoplasm. *Leukemia* **31**, 1229-1234 (2017).

71 Ma, S., Meng, Z., Chen, R. & Guan, K.-L. The Hippo Pathway: Biology and Pathophysiology. *Annu. Rev. Biochem.* **88**, 577-604, doi:10.1146/annurev-biochem-013118-111829 (2019).

72 Kurz, A. R. M., Catz, S. D. & Sperandio, M. Noncanonical Hippo Signalling in the Regulation of Leukocyte Function. *Trends Immunol* **25**, 30106-30106 (2018).

73 Li, W., Xiao, J., Zhou, X., Xu, M., Hu, C., Xu, X., Lu, Y., Liu, C., Xue, S., Nie, L., Zhang, H., Li, Z., Zhang, Y., Ji, F., Hui, L., Tao, W., Wei, B. & Wang, H. STK4 regulates TLR pathways and protects against chronic inflammation-related hepatocellular carcinoma. *J Clin Invest* **125**, 4239-4254 (2015).

74 Geng, J., Sun, X., Wang, P., Zhang, S., Wang, X., Wu, H., Hong, L., Xie, C., Li, X., Zhao, H., Liu, Q., Jiang, M., Chen, Q., Zhang, J., Li, Y., Song, S., Wang, H. R., Zhou, R., Johnson, R. L., Chien, K. Y., Lin, S. C., Han, J., Avruch, J., Chen, L. & Zhou, D. Kinases Mst1 and Mst2 positively regulate phagocytic induction of reactive oxygen species and bactericidal activity. *Nat Immunol* **16**, 1142-1152 (2015).

75 Abdollahpour, H., Appaswamy, G., Kotlarz, D., Diestelhorst, J., Beier, R., Schaffer, A. A., Gertz, E. M., Schambach, A., Kreipe, H. H., Pfeifer, D., Engelhardt, K. R., Rezaei, N., Grimbacher, B., Lohrmann, S., Sherkat, R. & Klein, C. The phenotype of human STK4 deficiency. *Blood* **119**, 3450-3457 (2012).

76 Nehme, N. T., Schmid, J. P., Debeurme, F., Andre-Schmutz, I., Lim, A., Nitschke, P., Rieux-Laucat, F., Lutz, P., Picard, C., Mahlaoui, N., Fischer, A. & de Saint Basile, G. MST1 mutations in autosomal recessive primary

immunodeficiency characterized by defective naive T-cell survival. *Blood* **119**, 3458-3468 (2012).

77 Halacli, S. O., Ayvaz, D. C., Sun-Tan, C., Erman, B., Uz, E., Yilmaz, D. Y., Ozgul, K., Tezcan, I. & Sanal, O. STK4 (MST1) deficiency in two siblings with autoimmune cytopenias: A novel mutation. *Clin Immunol* **161**, 316-323 (2015).

78 Asada, S., Fujino, T., Goyama, S. & Kitamura, T. The role of ASXL1 in hematopoiesis and myeloid malignancies. *Cell. Mol. Life Sci.* **76**, 2511-2523, doi:10.1007/s00018-019-03084-7 (2019).

79 Abdel-Wahab, O., Gao, J., Adli, M., Dey, A., Trimarchi, T., Chung, Y. R., Kuscu, C., Hricik, T., Ndiaye-Lobry, D., Lafave, L. M., Koche, R., Shih, A. H., Guryanova, O. A., Kim, E., Li, S., Pandey, S., Shin, J. Y., Telis, L., Liu, J., Bhatt, P. K., Monette, S., Zhao, X., Mason, C. E., Park, C. Y., Bernstein, B. E., Aifantis, I. & Levine, R. L. Deletion of Asxl1 results in myelodysplasia and severe developmental defects in vivo. *J. Exp. Med.* **210**, 2641-2659, doi:10.1084/jem.20131141 (2013).

80 Abdel-Wahab, O., Adli, M., LaFave, L. M., Gao, J., Hricik, T., Shih, A. H., Pandey, S., Patel, J. P., Chung, Y. R., Koche, R., Perna, F., Zhao, X., Taylor, J. E., Park, C. Y., Carroll, M., Melnick, A., Nimer, S. D., Jaffe, J. D., Aifantis, I., Bernstein, B. E. & Levine, R. L. ASXL1 mutations promote myeloid transformation through loss of PRC2-mediated gene repression. *Cancer Cell* **22**, 180-193, doi:10.1016/j.ccr.2012.06.032 (2012).

81 Gerstung, M., Pellagatti, A., Malcovati, L., Giagounidis, A., Porta, M. G., Jadersten, M., Dolatshad, H., Verma, A., Cross, N. C., Vyas, P., Killick, S., Hellstrom-Lindberg, E., Cazzola, M., Papaemmanuil, E., Campbell, P. J. & Boultwood, J. Combining gene mutation with gene expression data improves outcome prediction in myelodysplastic syndromes. *Nat Commun* **6** (2015).

82 Estey, E. H. Acute myeloid leukemia: 2013 update on risk-stratification and management. *Am J Hematol* **88**, 318-327 (2013).

83 Estey, E. & Dohner, H. Acute myeloid leukaemia. *Lancet* **368**, 1894-1907 (2006).

84 Tenen, D. G., Hromas, R., Licht, J. D. & Zhang, D. E. Transcription factors, normal myeloid development, and leukemia. *Blood* **90**, 489-519 (1997).

85 Zandstra, P. W., Lauffenburger, D. A. & Eaves, C. J. A ligand-receptor signaling threshold model of stem cell differentiation control: a biologically conserved mechanism applicable to hematopoiesis. *Blood* **96**, 1215-1222 (2000).

86 Look, A. T. Oncogenic transcription factors in the human acute leukemias. *Science* **278**, 1059-1064 (1997).

87 Erickson, P., Gao, J., Chang, K. S., Look, T., Whisenant, E., Raimondi, S., Lasher, R., Trujillo, J., Rowley, J. & Drabkin, H. Identification of breakpoints in t(8;21) acute myelogenous leukemia and isolation of a fusion transcript, AML1/ETO, with similarity to Drosophila segmentation gene, runt. *Blood* **80**, 1825-1831 (1992).

88 Chuang, L. S., Ito, K. & Ito, Y. RUNX family: Regulation and diversification of roles through interacting proteins. *Int J Cancer* **132**, 1260-1271 (2013).

89 Okuda, T., van Deursen, J., Hiebert, S. W., Grosveld, G. & Downing, J. R. AML1, the target of multiple chromosomal translocations in human leukemia, is essential for normal fetal liver hematopoiesis. *Cell* **84**, 321-330 (1996).

90 Lam, K. & Zhang, D. E. RUNX1 and RUNX1-ETO: roles in hematopoiesis and leukemogenesis. *Front Biosci* **17**, 1120-1139 (2012).

91 Wolford, J. K. & Prochazka, M. Structure and expression of the human MTG8/ETO gene. *Gene* **212**, 103-109 (1998).

92 Wang, J., Hoshino, T., Redner, R. L., Kajigaya, S. & Liu, J. M. ETO, fusion partner in t(8;21) acute myeloid leukemia, represses transcription by interaction with the human N-CoR/mSin3/HDAC1 complex. *Proc Natl Acad Sci U S A* **95**, 10860-10865 (1998).

93 Amann, J. M., Nip, J., Strom, D. K., Lutterbach, B., Harada, H., Lenny, N., Downing, J. R., Meyers, S. & Hiebert, S. W. ETO, a target of t(8;21) in acute leukemia, makes distinct contacts with multiple histone deacetylases and binds mSin3A through its oligomerization domain. *Mol Cell Biol* **21**, 6470-6483 (2001).

94 Peterson, L. F. & Zhang, D.-E. The 8;21 translocation in leukemogenesis. *Oncogene* **23**, 4255-4262, doi:10.1038/sj.onc.1207727 (2004).

95 Ebert, B. L., Pretz, J., Bosco, J., Chang, C. Y., Tamayo, P., Galili, N., Raza, A., Root, D. E., Attar, E., Ellis, S. R. & Golub, T. R. Identification of RPS14 as a 5q- syndrome gene by RNA interference screen. *Nature* **451**, 335-339 (2008).

96 Starczynowski, D. T., Kuchenbauer, F., Argiropoulos, B., Sung, S., Morin, R., Muranyi, A., Hirst, M., Hogge, D., Marra, M., Wells, R. A., Buckstein, R., Lam, W., Humphries, R. K. & Karsan, A. Identification of miR-145 and miR-146a as mediators of the 5q- syndrome phenotype. *Nat Med* **16**, 49-58 (2010).

97 McNerney, M. E., Brown, C. D., Wang, X., Bartom, E. T., Karmakar, S., Bandlamudi, C., Yu, S., Ko, J., Sandall, B. P., Stricker, T., Anastasi, J., Grossman, R. L., Cunningham, J. M., Le Beau, M. M. & White, K. P. CUX1 is a haploinsufficient tumor suppressor gene on chromosome 7 frequently inactivated in acute myeloid leukemia. *Blood* **121**, 975-983 (2013).

98 List, A., Ebert, B. L. & Fenaux, P. A decade of progress in myelodysplastic syndrome with chromosome 5q deletion. *Leukemia* **32**, 1493-1499 (2018).

99 Rhyasen, G. W., Bolanos, L., Fang, J., Jerez, A., Wunderlich, M., Rigolino, C., Mathews, L., Ferrer, M., Southall, N., Guha, R., Keller, J., Thomas, C., Beverly, L. J., Cortelezzi, A., Oliva, E. N., Cuzzola, M., Maciejewski, J. P., Mulloy, J. C. & Starczynowski, D. T. Targeting IRAK1 as a therapeutic approach for myelodysplastic syndrome. *Cancer Cell* **24**, 90-104 (2013).

100 Schneider, R. K., Adema, V., Heckl, D., Jaras, M., Mallo, M., Lord, A. M., Chu, L. P., McConkey, M. E., Kramann, R., Mullally, A., Bejar, R., Sole, F. & Ebert, B. L. Role of casein kinase 1A1 in the biology and targeted therapy of del(5q) MDS. *Cancer Cell* **26**, 509-520 (2014).

101 Asimakopoulos, F. A. & Green, A. R. Deletions of chromosome 20q and the pathogenesis of myeloproliferative disorders. *Br J Haematol* **95**, 219-226 (1996).

102 Kralovics, R. & Skoda, R. C. Molecular pathogenesis of Philadelphia chromosome negative myeloproliferative disorders. *Blood Rev* **19**, 1-13 (2005).

103 Bejar, R., Levine, R. & Ebert, B. L. Unraveling the molecular pathophysiology of myelodysplastic syndromes. *J Clin Oncol* **29**, 504-515 (2011).

104 Yu, F. X., Zhao, B. & Guan, K. L. Hippo Pathway in Organ Size Control, Tissue Homeostasis, and Cancer. *Cell* **163**, 811-828 (2015).

105 Cottini, F., Hideshima, T., Xu, C., Sattler, M., Dori, M., Agnelli, L., ten Hacken, E., Bertilaccio, M. T., Antonini, E., Neri, A., Ponzoni, M., Marcatti, M., Richardson, P. G., Carrasco, R., Kimmelman, A. C., Wong, K. K., Caligaris-Cappio, F., Blandino, G., Kuehl, W. M., Anderson, K. C. & Tonon, G. Rescue of Hippo coactivator YAP1 triggers DNA damage-induced apoptosis in hematological cancers. *Nat Med* **20**, 599-606 (2014).

106 Jansson, L. & Larsson, J. Normal hematopoietic stem cell function in mice with enforced expression of the Hippo signaling effector YAP1. *PLoS One* **7**, 21 (2012).

107 Katagiri, K., Imamura, M. & Kinashi, T. Spatiotemporal regulation of the kinase Mst1 by binding protein RAPL is critical for lymphocyte polarity and adhesion. *Nat Immunol* **7**, 919-928 (2006).

108 Zhou, D., Medoff, B. D., Chen, L., Li, L., Zhang, X. F., Praskova, M., Liu, M., Landry, A., Blumberg, R. S., Boussiotis, V. A., Xavier, R. & Avruch, J. The Nore1B/Mst1 complex restrains antigen receptor-induced proliferation of naive T cells. *Proc Natl Acad Sci U S A* **105**, 20321-20326 (2008).

109 Ueda, Y., Katagiri, K., Tomiyama, T., Yasuda, K., Habiro, K., Katakai, T., Ikehara, S., Matsumoto, M. & Kinashi, T. Mst1 regulates integrin-dependent thymocyte trafficking and antigen recognition in the thymus. *Nat Commun* **3** (2012).

110 Mou, F., Praskova, M., Xia, F., Van Buren, D., Hock, H., Avruch, J. & Zhou, D. The Mst1 and Mst2 kinases control activation of rho family GTPases and thymic egress of mature thymocytes. *J Exp Med* **209**, 741-759 (2012).

111 Kurz, A. R., Pruenster, M., Rohwedder, I., Ramadass, M., Schafer, K., Harrison, U., Gouveia, G., Nussbaum, C., Immler, R., Wiessner, J. R., Margraf, A., Lim, D. S., Walzog, B., Dietzel, S., Moser, M., Klein, C., Vestweber, D., Haas, R., Catz, S. D. & Sperandio, M. MST1-dependent vesicle trafficking regulates neutrophil transmigration through the vascular basement membrane. *J Clin Invest* **126**, 4125-4139 (2016).

112 Li, C., Bi, Y., Li, Y., Yang, H., Yu, Q., Wang, J., Wang, Y., Su, H., Jia, A., Hu, Y., Han, L., Zhang, J., Li, S., Tao, W. & Liu, G. Dendritic cell MST1 inhibits Th17 differentiation. *Nat Commun* **8** (2017).

113 Du, X., Wen, J., Wang, Y., Karmaus, P. W. F., Khatamian, A., Tan, H., Li, Y., Guy, C., Nguyen, T. M., Dhungana, Y., Neale, G., Peng, J., Yu, J. & Chi, H. Hippo/Mst signalling couples metabolic state and immune function of CD8alpha(+) dendritic cells. *Nature* **30**, 018-0177 (2018).

114 Skov, V., Larsen, T. S., Thomassen, M., Riley, C. H., Jensen, M. K., Bjerrum, O. W., Kruse, T. A. & Hasselbalch, H. C. Whole-blood transcriptional profiling of interferon-inducible genes identifies highly upregulated IFI27 in primary myelofibrosis. *Eur J Haematol* **87**, 54-60 (2011).

115 Rampal, R., Al-Shahrour, F., Abdel-Wahab, O., Patel, J. P., Brunel, J. P., Mermel, C. H., Bass, A. J., Pretz, J., Ahn, J., Hricik, T., Kilpivaara, O., Wadleigh, M., Busque, L., Gilliland, D. G., Golub, T. R., Ebert, B. L. & Levine, R. L. Integrated genomic analysis illustrates the central role of JAK-STAT pathway activation in myeloproliferative neoplasm pathogenesis. *Blood* **123**, 2014-2002 (2014).

116 Meng, Z., Moroishi, T., Mottier-Pavie, V., Plouffe, S. W., Hansen, C. G., Hong, A. W., Park, H. W., Mo, J. S., Lu, W., Lu, S., Flores, F., Yu, F. X., Halder, G. & Guan, K. L. MAP4K family kinases act in parallel to MST1/2 to activate LATS1/2 in the Hippo pathway. *Nat Commun* **6** (2015).

117 Plouffe, S. W., Meng, Z., Lin, K. C., Lin, B., Hong, A. W., Chun, J. V. & Guan, K. L. Characterization of Hippo Pathway Components by Gene Inactivation. *Mol Cell* **64**, 993-1008 (2016).

118 Steensma, D. P., Bejar, R., Jaiswal, S., Lindsley, R. C., Sekeres, M. A., Hasserjian, R. P. & Ebert, B. L. Clonal hematopoiesis of indeterminate potential and its distinction from myelodysplastic syndromes. *Blood* **126**, 9-16 (2015).

119 Hirsch, P., Zhang, Y., Tang, R., Joulin, V., Boutroux, H., Pronier, E., Moatti, H., Flandrin, P., Marzac, C., Bories, D., Fava, F., Mokrani, H., Betems, A., Lorre, F., Favier, R., Feger, F., Mohty, M., Douay, L., Legrand, O., Bilhou-Nabera, C., Louache, F. & Delhommeau, F. Genetic hierarchy and temporal variegation in the clonal history of acute myeloid leukaemia. *Nat Commun* **7** (2016).

120 Li, J., Kent, D. G., Chen, E. & Green, A. R. Mouse models of myeloproliferative neoplasms: JAK of all grades. *Dis Model Mech* **4**, 311-317 (2011).

121 Mondet, J., Hussein, K. & Mossuz, P. Circulating Cytokine Levels as Markers of Inflammation in Philadelphia Negative Myeloproliferative Neoplasms: Diagnostic and Prognostic Interest. *Mediators Inflamm* **670580**, 7 (2015).

122 Kleppe, M., Kwak, M., Koppikar, P., Riester, M., Keller, M., Bastian, L., Hricik, T., Bhagwat, N., McKenney, A. S., Papalexi, E., Abdel-Wahab, O., Rampal, R., Marubayashi, S., Chen, J. J., Romanet, V., Fridman, J. S., Bromberg, J., Teruya-Feldstein, J., Murakami, M., Radimerski, T., Michor, F., Fan, R. & Levine, R. L. JAK-STAT pathway activation in malignant and nonmalignant cells contributes to MPN pathogenesis and therapeutic response. *Cancer Discov* **5**, 316-331 (2015).

123 Kleppe, M., Koche, R., Zou, L., van Galen, P., Hill, C. E., Dong, L., De Groote, S., Papalexi, E., Hanasoge Somasundara, A. V., Cordner, K., Keller, M., Farnoud, N., Medina, J., McGovern, E., Reyes, J., Roberts, J., Witkin, M., Rapaport, F., Teruya-Feldstein, J., Qi, J., Rampal, R., Bernstein, B. E., Bradner, J. E. & Levine, R. L. Dual Targeting of Oncogenic Activation and Inflammatory Signaling Increases Therapeutic Efficacy in Myeloproliferative Neoplasms. *Cancer Cell* **33**, 29-43 (2018).

124 Mao, Y., Yen, H., Sun, Y., Lv, Z. & Huang, R. Development of non-overlapping multiplex antibody arrays for the quantitative measurement of 400 human and 200 mouse proteins in parallel. *J Immunol* **192** (2014).

125 Tefferi, A., Vaidya, R., Caramazza, D., Finke, C., Lasho, T. & Pardanani, A. Circulating interleukin (IL)-8, IL-2R, IL-12, and IL-15 levels are independently prognostic in primary myelofibrosis: a comprehensive cytokine profiling study. *J Clin Oncol* **29**, 1356-1363 (2011).

126 Fang, J., Bolanos, L. C., Choi, K., Liu, X., Christie, S., Akunuru, S., Kumar, R., Wang, D., Chen, X., Greis, K. D., Stoilov, P., Filippi, M. D., Maciejewski, J. P., Garcia-Manero, G., Weirauch, M. T., Salomonis, N., Geiger, H., Zheng, Y. & Starczynowski, D. T. Ubiquitination of hnRNPA1 by TRAF6 links chronic innate immune signaling with myelodysplasia. *Nat Immunol* **18**, 236-245 (2017).

127 Varney, M. E., Niederkorn, M., Konno, H., Matsumura, T., Gohda, J., Yoshida, N., Akiyama, T., Christie, S., Fang, J., Miller, D., Jerez, A., Karsan, A., Maciejewski, J. P., Meetei, R. A., Inoue, J. & Starczynowski, D. T. Loss of Tifab, a del(5q) MDS gene, alters hematopoiesis through derepression of Toll-like receptor-TRAF6 signaling. *J Exp Med* **212**, 1967-1985 (2015).

128 Chen, Z. J. Ubiquitin signalling in the NF-kappaB pathway. *Nat Cell Biol* **7**, 758-765 (2005).

129 Barreyro, L., Chlon, T. M. & Starczynowski, D. T. Chronic immune response dysregulation in MDS pathogenesis. *Blood* **132**, 1553-1560 (2018).

130 Sallman, D. A. & List, A. The central role of inflammatory signaling in the pathogenesis of myelodysplastic syndromes. *Blood* **22**, 2018-2010 (2019).

131 Kristinsson, S. Y., Bjorkholm, M., Hultcrantz, M., Derolf, A. R., Landgren, O. & Goldin, L. R. Chronic immune stimulation might act as a trigger for the development of acute myeloid leukemia or myelodysplastic syndromes. *J Clin Oncol* **29**, 2897-2903 (2011).

132 Chen, X., Eksioglu, E. A., Zhou, J., Zhang, L., Djeu, J., Fortenbery, N., Epling-Burnette, P., Van Bijnen, S., Dolstra, H., Cannon, J., Youn, J. I., Donatelli, S. S., Qin, D., De Witte, T., Tao, J., Wang, H., Cheng, P., Gabrilovich, D. I., List, A. & Wei, S. Induction of myelodysplasia by myeloid-derived suppressor cells. *J Clin Invest* **123**, 4595-4611 (2013).

133 Lee, S. C., North, K., Kim, E., Jang, E., Obeng, E., Lu, S. X., Liu, B., Inoue, D., Yoshimi, A., Ki, M., Yeo, M., Zhang, X. J., Kim, M. K., Cho, H., Chung, Y. R., Taylor, J., Durham, B. H., Kim, Y. J., Pastore, A., Monette, S., Palacino, J., Seiler, M., Buonamici, S., Smith, P. G., Ebert, B. L., Bradley, R. K. & Abdel-

Wahab, O. Synthetic Lethal and Convergent Biological Effects of Cancer-Associated Spliceosomal Gene Mutations. *Cancer Cell* **34**, 225-241 (2018).

134 Basiorka, A. A., McGraw, K. L., Eksioglu, E. A., Chen, X., Johnson, J., Zhang, L., Zhang, Q., Irvine, B. A., Cluzeau, T., Sallman, D. A., Padron, E., Komrokji, R., Sokol, L., Coll, R. C., Robertson, A. A., Cooper, M. A., Cleveland, J. L., O'Neill, L. A., Wei, S. & List, A. F. The NLRP3 inflammasome functions as a driver of the myelodysplastic syndrome phenotype. *Blood* **128**, 2960-2975 (2016).

135 Varney, M. E., Choi, K., Bolanos, L., Christie, S., Fang, J., Grimes, H. L., Maciejewski, J. P., Inoue, J. I. & Starczynowski, D. T. *Epistasis between TIFAB and miR-146a: neighboring genes in del(5q) myelodysplastic syndrome*. (Leukemia. 2017 Feb;31(2):491-495. doi: 10.1038/leu.2016.276. Epub 2016 Oct 3.).

136 Tefferi, A. Primary myelofibrosis: 2019 update on diagnosis, risk-stratification and management. *Am J Hematol* **93**, 1551-1560 (2018).

137 Kramann, R. & Schneider, R. K. The identification of fibrosis-driving myofibroblast precursors reveals new therapeutic avenues in myelofibrosis. *Blood* **131**, 2111-2119 (2018).

138 Ogilvy, S., Metcalf, D., Gibson, L., Bath, M. L., Harris, A. W. & Adams, J. M. Promoter elements of vav drive transgene expression in vivo throughout the hematopoietic compartment. *Blood* **94**, 1855-1863 (1999).

139 Kuhn, R., Schwenk, F., Aguet, M. & Rajewsky, K. Inducible gene targeting in mice. *Science* **269**, 1427-1429 (1995).

140 Lu, L., Li, Y., Kim, S. M., Bossuyt, W., Liu, P., Qiu, Q., Wang, Y., Halder, G., Finegold, M. J., Lee, J. S. & Johnson, R. L. Hippo signaling is a potent in vivo growth and tumor suppressor pathway in the mammalian liver. *Proc Natl Acad Sci U S A* **107**, 1437-1442 (2010).

141 Metsalu, T. & Vilo, J. ClustVis: a web tool for visualizing clustering of multivariate data using Principal Component Analysis and heatmap. *Nucleic Acids Res* **43**, 12 (2015).

142 Ley, T. J., Miller, C., Ding, L., Raphael, B. J., Mungall, A. J., Robertson, A., Hoadley, K., Triche, T. J., Jr., Laird, P. W., Baty, J. D., Fulton, L. L., Fulton, R., Heath, S. E., Kalicki-Veizer, J., Kandoth, C., Klco, J. M., Koboldt, D. C., Kanchi, K. L., Kulkarni, S., Lamprecht, T. L., Larson, D. E., Lin, L., Lu, C., McLellan, M. D., McMichael, J. F., Payton, J., Schmidt, H., Spencer, D. H., Tomasson, M. H., Wallis, J. W., Wartman, L. D., Watson, M. A., Welch, J., Wendl, M. C., Ally, A., Balasundaram, M., Birol, I., Butterfield, Y., Chiu, R., Chu, A., Chuah, E., Chun, H. J., Corbett, R., Dhalla, N., Guin, R., He, A., Hirst,

C., Hirst, M., Holt, R. A., Jones, S., Karsan, A., Lee, D., Li, H. I., Marra, M. A., Mayo, M., Moore, R. A., Mungall, K., Parker, J., Pleasance, E., Plettner, P., Schein, J., Stoll, D., Swanson, L., Tam, A., Thiessen, N., Varhol, R., Wye, N., Zhao, Y., Gabriel, S., Getz, G., Sougnez, C., Zou, L., Leiserson, M. D., Vandin, F., Wu, H. T., Applebaum, F., Baylin, S. B., Akbani, R., Broom, B. M., Chen, K., Motter, T. C., Nguyen, K., Weinstein, J. N., Zhang, N., Ferguson, M. L., Adams, C., Black, A., Bowen, J., Gastier-Foster, J., Grossman, T., Lichtenberg, T., Wise, L., Davidsen, T., Demchok, J. A., Shaw, K. R., Sheth, M., Sofia, H. J., Yang, L., Downing, J. R. & Eley, G. Genomic and epigenomic landscapes of adult de novo acute myeloid leukemia. *N Engl J Med* **368**, 2059-2074 (2013).

143 Tyner, J. W., Tognon, C. E., Bottomly, D., Wilmot, B., Kurtz, S. E., Savage, S. L., Long, N., Schultz, A. R., Traer, E., Abel, M., Agarwal, A., Blucher, A., Borate, U., Bryant, J., Burke, R., Carlos, A., Carpenter, R., Carroll, J., Chang, B. H., Coblentz, C., d'Almeida, A., Cook, R., Danilov, A., Dao, K. T., Degnin, M., Devine, D., Dibb, J., Edwards, D. K. t., Eide, C. A., English, I., Glover, J., Henson, R., Ho, H., Jemal, A., Johnson, K., Johnson, R., Junio, B., Kaempf, A., Leonard, J., Lin, C., Liu, S. Q., Lo, P., Loriaux, M. M., Luty, S., Macey, T., MacManiman, J., Martinez, J., Mori, M., Nelson, D., Nichols, C., Peters, J., Ramsdill, J., Rofelty, A., Schuff, R., Searles, R., Segerdell, E., Smith, R. L., Spurgeon, S. E., Sweeney, T., Thapa, A., Visser, C., Wagner, J., Watanabe-Smith, K., Werth, K., Wolf, J., White, L., Yates, A., Zhang, H., Cogle, C. R., Collins, R. H., Connolly, D. C., Deininger, M. W., Drusbosky, L., Hourigan, C. S., Jordan, C. T., Kropf, P., Lin, T. L., Martinez, M. E., Medeiros, B. C., Pallapati, R. R., Pollyea, D. A., Swords, R. T., Watts, J. M., Weir, S. J., Wiest, D. L., Winters, R. M., McWeeney, S. K. & Druker, B. J. Functional genomic landscape of acute myeloid leukaemia. *Nature* **562**, 526-531 (2018).

144 Yoshida, K., Sanada, M., Shiraishi, Y., Nowak, D., Nagata, Y., Yamamoto, R., Sato, Y., Sato-Otsubo, A., Kon, A., Nagasaki, M., Chalkidis, G., Suzuki, Y., Shiosaka, M., Kawahata, R., Yamaguchi, T., Otsu, M., Obara, N., Sakata-Yanagimoto, M., Ishiyama, K., Mori, H., Nolte, F., Hofmann, W. K., Miyawaki, S., Sugano, S., Haferlach, C., Koeffler, H. P., Shih, L. Y., Haferlach, T., Chiba, S., Nakauchi, H., Miyano, S. & Ogawa, S. Frequent pathway mutations of splicing machinery in myelodysplasia. *Nature* **478**, 64-69 (2011).

145 Puente, X. S., Bea, S., Valdes-Mas, R., Villamor, N., Gutierrez-Abril, J., Martin-Subero, J. I., Munar, M., Rubio-Perez, C., Jares, P., Aymerich, M., Baumann, T., Beekman, R., Belver, L., Carrio, A., Castellano, G., Clot, G., Colado, E., Colomer, D., Costa, D., Delgado, J., Enjuanes, A., Estivill, X., Ferrando, A. A., Gelpi, J. L., Gonzalez, B., Gonzalez, S., Gonzalez, M., Gut, M., Hernandez-Rivas, J. M., Lopez-Guerra, M., Martin-Garcia, D., Navarro, A., Nicolas, P., Orozco, M., Payer, A. R., Pinyol, M., Pisano, D. G., Puente, D. A., Queiros, A. C., Quesada, V., Romeo-Casabona, C. M., Royo, C., Royo, R., Rozman, M., Russinol, N., Salaverria, I., Stamatopoulos, K., Stunnenberg, H.

G., Tamborero, D., Terol, M. J., Valencia, A., Lopez-Bigas, N., Torrents, D., Gut, I., Lopez-Guillermo, A., Lopez-Otin, C. & Campo, E. Non-coding recurrent mutations in chronic lymphocytic leukaemia. *Nature* **526**, 519-524 (2015).

146 Reddy, A., Zhang, J., Davis, N. S., Moffitt, A. B., Love, C. L., Waldrop, A., Leppa, S., Pasanen, A., Meriranta, L., Karjalainen-Lindsberg, M. L., Norgaard, P., Pedersen, M., Gang, A. O., Hogdall, E., Heavican, T. B., Lone, W., Iqbal, J., Qin, Q., Li, G., Kim, S. Y., Healy, J., Richards, K. L., Fedoriw, Y., Bernal-Mizrachi, L., Koff, J. L., Staton, A. D., Flowers, C. R., Paltiel, O., Goldschmidt, N., Calaminici, M., Clear, A., Gribben, J., Nguyen, E., Czader, M. B., Ondrejka, S. L., Collie, A., Hsi, E. D., Tse, E., Au-Yeung, R. K. H., Kwong, Y. L., Srivastava, G., Choi, W. W. L., Evens, A. M., Pilichowska, M., Sengar, M., Reddy, N., Li, S., Chadburn, A., Gordon, L. I., Jaffe, E. S., Levy, S., Rempel, R., Tzeng, T., Happ, L. E., Dave, T., Rajagopalan, D., Datta, J., Dunson, D. B. & Dave, S. S. Genetic and Functional Drivers of Diffuse Large B Cell Lymphoma. *Cell* **171**, 481-494 (2017).

147 Bradner, J. E., Hnisz, D. & Young, R. A. Transcriptional Addiction in Cancer. *Cell* **168**, 629-643 (2017).

148 Lo, M. C., Peterson, L. F., Yan, M., Cong, X., Jin, F., Shia, W. J., Matsuura, S., Ahn, E. Y., Komeno, Y., Ly, M., Ommen, H. B., Chen, I. M., Hokland, P., Willman, C. L., Ren, B. & Zhang, D. E. Combined gene expression and DNA occupancy profiling identifies potential therapeutic targets of t(8;21) AML. *Blood* **120**, 1473-1484 (2012).

149 Richter, A. M., Pfeifer, G. P. & Dammann, R. H. The RASSF proteins in cancer; from epigenetic silencing to functional characterization. *Biochim Biophys Acta* **2**, 114-128 (2009).

150 Iwasa, H., Hossain, S. & Hata, Y. Tumor suppressor C-RASSF proteins. *Cell Mol Life Sci* **75**, 1773-1787 (2018).

151 Dammann, R., Li, C., Yoon, J. H., Chin, P. L., Bates, S. & Pfeifer, G. P. Epigenetic inactivation of a RAS association domain family protein from the lung tumour suppressor locus 3p21.3. *Nat Genet* **25**, 315-319 (2000).

152 Dammann, R., Yang, G. & Pfeifer, G. P. Hypermethylation of the cpG island of Ras association domain family 1A (RASSF1A), a putative tumor suppressor gene from the 3p21.3 locus, occurs in a large percentage of human breast cancers. *Cancer Res* **61**, 3105-3109 (2001).

153 van der Weyden, L., Papaspyropoulos, A., Poulogiannis, G., Rust, A. G., Rashid, M., Adams, D. J., Arends, M. J. & O'Neill, E. Loss of RASSF1A synergizes with deregulated RUNX2 signaling in tumorigenesis. *Cancer Res* **72**, 3817-3827 (2012).

154 Pefani, D. E., Latusek, R., Pires, I., Grawenda, A. M., Yee, K. S., Hamilton, G., van der Weyden, L., Esashi, F., Hammond, E. M. & O'Neill, E. RASSF1A-LATS1 signalling stabilizes replication forks by restricting CDK2-mediated phosphorylation of BRCA2. *Nat Cell Biol* **16**, 962-971 (2014).

155 Schmidt, M. L., Hobbing, K. R., Donninger, H. & Clark, G. J. RASSF1A Deficiency Enhances RAS-Driven Lung Tumorigenesis. *Cancer Res* **78**, 2614-2623 (2018).

156 Song, H., Kim, H., Lee, K., Lee, D. H., Kim, T. S., Song, J. Y., Lee, D., Choi, D., Ko, C. Y., Kim, H. S., Shin, H. I., Choi, J., Park, H., Park, C., Jeong, D. & Lim, D. S. Ablation of Rassf2 induces bone defects and subsequent haematopoietic anomalies in mice. *Embo J* **31**, 1147-1159 (2012).

157 Vos, M. D., Ellis, C. A., Elam, C., Ulku, A. S., Taylor, B. J. & Clark, G. J. RASSF2 is a novel K-Ras-specific effector and potential tumor suppressor. *J Biol Chem* **278**, 28045-28051 (2003).

158 Yu, F. X. & Guan, K. L. The Hippo pathway: regulators and regulations. *Genes Dev* **27**, 355-371 (2013).

159 Heasman, S. J. & Ridley, A. J. Mammalian Rho GTPases: new insights into their functions from in vivo studies. *Nat Rev Mol Cell Biol* **9**, 690-701 (2008).

160 Jaffe, A. B. & Hall, A. Rho GTPases: biochemistry and biology. *Annu Rev Cell Dev Biol* **21**, 247-269 (2005).

161 Rossman, K. L., Der, C. J. & Sondek, J. GEF means go: turning on RHO GTPases with guanine nucleotide-exchange factors. *Nat Rev Mol Cell Biol* **6**, 167-180 (2005).

162 Garcia-Mata, R., Boulter, E. & Burridge, K. The 'invisible hand': regulation of RHO GTPases by RHOGDIs. *Nat Rev Mol Cell Biol* **12**, 493-504 (2011).

163 Maldonado, M. D. M. & Dharmawardhane, S. Targeting Rac and Cdc42 GTPases in Cancer. *Cancer Res* **78**, 3101-3111 (2018).

164 Qiu, R. G., Chen, J., Kirn, D., McCormick, F. & Symons, M. An essential role for Rac in Ras transformation. *Nature* **374**, 457-459 (1995).

165 Kazanietz, M. G. & Caloca, M. J. The Rac GTPase in Cancer: From Old Concepts to New Paradigms. *Cancer Res* **77**, 5445-5451 (2017).

166 Kawazu, M., Ueno, T., Kontani, K., Ogita, Y., Ando, M., Fukumura, K., Yamato, A., Soda, M., Takeuchi, K., Miki, Y., Yamaguchi, H., Yasuda, T., Naoe, T., Yamashita, Y., Katada, T., Choi, Y. L. & Mano, H. Transforming

mutations of RAC guanosine triphosphatases in human cancers. *Proc Natl Acad Sci U S A* **110**, 3029-3034 (2013).

167 Caye, A., Strullu, M., Guidez, F., Cassinat, B., Gazal, S., Fenneteau, O., Lainey, E., Nouri, K., Nakhaei-Rad, S., Dvorsky, R., Lachenaud, J., Pereira, S., Vivent, J., Verger, E., Vidaud, D., Galambrun, C., Picard, C., Petit, A., Contet, A., Poiree, M., Sirvent, N., Mechinaud, F., Adjaoud, D., Paillard, C., Nelken, B., Reguerre, Y., Bertrand, Y., Haussinger, D., Dalle, J. H., Ahmadian, M. R., Baruchel, A., Chomienne, C. & Cave, H. Juvenile myelomonocytic leukemia displays mutations in components of the RAS pathway and the PRC2 network. *Nat Genet* **47**, 1334-1340 (2015).

168 Mizukawa, B., Wei, J., Shrestha, M., Wunderlich, M., Chou, F. S., Griesinger, A., Harris, C. E., Kumar, A. R., Zheng, Y., Williams, D. A. & Mulloy, J. C. Inhibition of Rac GTPase signaling and downstream prosurvival Bcl-2 proteins as combination targeted therapy in MLL-AF9 leukemia. *Blood* **118**, 5235-5245 (2011).

169 Martin, H., Mali, R. S., Ma, P., Chatterjee, A., Ramdas, B., Sims, E., Munugalavadla, V., Ghosh, J., Mattingly, R. R., Visconte, V., Tiu, R. V., Vlaar, C. P., Dharmawardhane, S. & Kapur, R. Pak and Rac GTPases promote oncogenic KIT-induced neoplasms. *J Clin Invest* **123**, 4449-4463 (2013).

170 Muller, L. U., Schore, R. J., Zheng, Y., Thomas, E. K., Kim, M. O., Cancelas, J. A., Gu, Y. & Williams, D. A. *Rac guanosine triphosphatases represent a potential target in AML*. (Leukemia. 2008 Sep;22(9):1803-6. doi: 10.1038/leu.2008.196. Epub 2008 Jul 31.).

171 Lin, Y. & Zheng, Y. Approaches of targeting Rho GTPases in cancer drug discovery. *Expert Opin Drug Discov* **10**, 991-1010 (2015).

172 Haferlach, T., Kohlmann, A., Wieczorek, L., Basso, G., Kronnie, G. T., Bene, M. C., De Vos, J., Hernandez, J. M., Hofmann, W. K., Mills, K. I., Gilkes, A., Chiaretti, S., Shurtleff, S. A., Kipps, T. J., Rassenti, L. Z., Yeoh, A. E., Papenhausen, P. R., Liu, W. M., Williams, P. M. & Foa, R. Clinical utility of microarray-based gene expression profiling in the diagnosis and subclassification of leukemia: report from the International Microarray Innovations in Leukemia Study Group. *J Clin Oncol* **28**, 2529-2537 (2010).

173 Hesson, L. B., Wilson, R., Morton, D., Adams, C., Walker, M., Maher, E. R. & Latif, F. CpG island promoter hypermethylation of a novel Ras-effector gene RASSF2A is an early event in colon carcinogenesis and correlates inversely with K-ras mutations. *Oncogene* **24**, 3987-3994 (2005).

174 Sun, X. J., Wang, Z., Wang, L., Jiang, Y., Kost, N., Soong, T. D., Chen, W. Y., Tang, Z., Nakadai, T., Elemento, O., Fischle, W., Melnick, A., Patel, D. J.,

Nimer, S. D. & Roeder, R. G. A stable transcription factor complex nucleated by oligomeric AML1-ETO controls leukaemogenesis. *Nature* **500**, 93-97 (2013).

175 Beck, D., Thoms, J. A., Perera, D., Schutte, J., Unnikrishnan, A., Knezevic, K., Kinston, S. J., Wilson, N. K., O'Brien, T. A., Gottgens, B., Wong, J. W. & Pimanda, J. E. Genome-wide analysis of transcriptional regulators in human HSPCs reveals a densely interconnected network of coding and noncoding genes. *Blood* **122**, 2013-2003 (2013).

176 Heidenreich, O., Krauter, J., Riehle, H., Hadwiger, P., John, M., Heil, G., Vornlocher, H. P. & Nordheim, A. AML1/MTG8 oncogene suppression by small interfering RNAs supports myeloid differentiation of t(8;21)-positive leukemic cells. *Blood* **101**, 3157-3163 (2003).

177 Ben-Ami, O., Friedman, D., Leshkowitz, D., Goldenberg, D., Orlovsky, K., Pencovich, N., Lotem, J., Tanay, A. & Groner, Y. Addiction of t(8;21) and inv(16) acute myeloid leukemia to native RUNX1. *Cell Rep* **4**, 1131-1143 (2013).

178 Ptasinska, A., Assi, S. A., Martinez-Soria, N., Imperato, M. R., Piper, J., Cauchy, P., Pickin, A., James, S. R., Hoogenkamp, M., Williamson, D., Wu, M., Tenen, D. G., Ott, S., Westhead, D. R., Cockerill, P. N., Heidenreich, O. & Bonifer, C. Identification of a dynamic core transcriptional network in t(8;21) AML that regulates differentiation block and self-renewal. *Cell Rep* **8**, 1974-1988 (2014).

179 The Genotype-Tissue Expression (GTEx) project. *Nat Genet* **45**, 580-585 (2013).

180 Novershtern, N., Subramanian, A., Lawton, L. N., Mak, R. H., Haining, W. N., McConkey, M. E., Habib, N., Yosef, N., Chang, C. Y., Shay, T., Frampton, G. M., Drake, A. C., Leskov, I., Nilsson, B., Preffer, F., Dombkowski, D., Evans, J. W., Liefeld, T., Smutko, J. S., Chen, J., Friedman, N., Young, R. A., Golub, T. R., Regev, A. & Ebert, B. L. Densely interconnected transcriptional circuits control cell states in human hematopoiesis. *Cell* **144**, 296-309 (2011).

181 Bagger, F. O., Sasivarevic, D., Sohi, S. H., Laursen, L. G., Pundhir, S., Sonderby, C. K., Winther, O., Rapin, N. & Porse, B. T. BloodSpot: a database of gene expression profiles and transcriptional programs for healthy and malignant haematopoiesis. *Nucleic Acids Res* **44**, 26 (2016).

182 Yan, M., Kanbe, E., Peterson, L. F., Boyapati, A., Miao, Y., Wang, Y., Chen, I. M., Chen, Z., Rowley, J. D., Willman, C. L. & Zhang, D. E. A previously unidentified alternatively spliced isoform of t(8;21) transcript promotes leukemogenesis. *Nat Med* **12**, 945-949 (2006).

183 Donninger, H., Hesson, L., Vos, M., Beebe, K., Gordon, L., Sidransky, D., Liu, J. W., Schlegel, T., Payne, S., Hartmann, A., Latif, F. & Clark, G. J. The Ras effector RASSF2 controls the PAR-4 tumor suppressor. *Mol Cell Biol* **30**, 2608-2620 (2010).

184 Uhlen, M., Fagerberg, L., Hallstrom, B. M., Lindskog, C., Oksvold, P., Mardinoglu, A., Sivertsson, A., Kampf, C., Sjostedt, E., Asplund, A., Olsson, I., Edlund, K., Lundberg, E., Navani, S., Szigyarto, C. A., Odeberg, J., Djureinovic, D., Takanen, J. O., Hober, S., Alm, T., Edqvist, P. H., Berling, H., Tegel, H., Mulder, J., Rockberg, J., Nilsson, P., Schwenk, J. M., Hamsten, M., von Feilitzen, K., Forsberg, M., Persson, L., Johansson, F., Zwahlen, M., von Heijne, G., Nielsen, J. & Ponten, F. Proteomics. Tissue-based map of the human proteome. *Science* **347**, 1260419 (2015).

185 Faber, Z. J., Chen, X., Gedman, A. L., Boggs, K., Cheng, J., Ma, J., Radtke, I., Chao, J. R., Walsh, M. P., Song, G., Andersson, A. K., Dang, J., Dong, L., Liu, Y., Huether, R., Cai, Z., Mulder, H., Wu, G., Edmonson, M., Rusch, M., Qu, C., Li, Y., Vadodaria, B., Wang, J., Hedlund, E., Cao, X., Yergeau, D., Nakitandwe, J., Pounds, S. B., Shurtleff, S., Fulton, R. S., Fulton, L. L., Easton, J., Parganas, E., Pui, C. H., Rubnitz, J. E., Ding, L., Mardis, E. R., Wilson, R. K., Gruber, T. A., Mullighan, C. G., Schlenk, R. F., Paschka, P., Dohner, K., Dohner, H., Bullinger, L., Zhang, J., Klco, J. M. & Downing, J. R. The genomic landscape of core-binding factor acute myeloid leukemias. *Nat Genet* **48**, 1551-1556 (2016).

186 Kovalski, J. R., Bhaduri, A., Zehnder, A. M., Neela, P. H., Che, Y., Wozniak, G. G. & Khavari, P. A. The Functional Proximal Proteome of Oncogenic Ras Includes mTORC2. *Mol Cell* **73**, 830-844 (2019).

187 Hwang, E., Cheong, H. K., Ul Mushtaq, A., Kim, H. Y., Yeo, K. J., Kim, E., Lee, W. C., Hwang, K. Y., Cheong, C. & Jeon, Y. H. Structural basis of the heterodimerization of the MST and RASSF SARAH domains in the Hippo signalling pathway. *Acta Crystallogr D Biol Crystallogr* **70**, 1944-1953 (2014).

188 Song, H., Oh, S., Oh, H. J. & Lim, D. S. Role of the tumor suppressor RASSF2 in regulation of MST1 kinase activity. *Biochem Biophys Res Commun* **391**, 969-973 (2010).

189 Avruch, J., Zhou, D., Fitamant, J., Bardeesy, N., Mou, F. & Barrufet, L. R. Protein kinases of the Hippo pathway: regulation and substrates. *Semin Cell Dev Biol* **23**, 770-784 (2012).

190 Roux, K. J., Kim, D. I., Burke, B. & May, D. G. BioID: A Screen for Protein-Protein Interactions. *Curr Protoc Protein Sci* **91**, 1-19 (2018).

191 Kim, D. I., Jensen, S. C., Noble, K. A., Kc, B., Roux, K. H., Motamedchaboki, K. & Roux, K. J. An improved smaller biotin ligase for BioID proximity labeling. *Mol Biol Cell* **27**, 1188-1196 (2016).

192 Mellacheruvu, D., Wright, Z., Couzens, A. L., Lambert, J. P., St-Denis, N. A., Li, T., Miteva, Y. V., Hauri, S., Sardiu, M. E., Low, T. Y., Halim, V. A., Bagshaw, R. D., Hubner, N. C., Al-Hakim, A., Bouchard, A., Faubert, D., Fermin, D., Dunham, W. H., Goudreault, M., Lin, Z. Y., Badillo, B. G., Pawson, T., Durocher, D., Coulombe, B., Aebersold, R., Superti-Furga, G., Colinge, J., Heck, A. J., Choi, H., Gstaiger, M., Mohammed, S., Cristea, I. M., Bennett, K. L., Washburn, M. P., Raught, B., Ewing, R. M., Gingras, A. C. & Nesvizhskii, A. I. The CRAPome: a contaminant repository for affinity purification-mass spectrometry data. *Nat Methods* **10**, 730-736 (2013).

193 Subramanian, A., Tamayo, P., Mootha, V. K., Mukherjee, S., Ebert, B. L., Gillette, M. A., Paulovich, A., Pomeroy, S. L., Golub, T. R., Lander, E. S. & Mesirov, J. P. Gene set enrichment analysis: a knowledge-based approach for interpreting genome-wide expression profiles. *Proc Natl Acad Sci U S A* **102**, 15545-15550 (2005).

194 Valk, P. J., Verhaak, R. G., Beijen, M. A., Erpelinck, C. A., Barjesteh van Waalwijk van Doorn-Khosrovani, S., Boer, J. M., Beverloo, H. B., Moorhouse, M. J., van der Spek, P. J., Lowenberg, B. & Delwel, R. Prognostically useful gene-expression profiles in acute myeloid leukemia. *N Engl J Med* **350**, 1617-1628 (2004).

195 Tonks, A., Pearn, L., Musson, M., Gilkes, A., Mills, K. I., Burnett, A. K. & Darley, R. L. Transcriptional dysregulation mediated by RUNX1-RUNX1T1 in normal human progenitor cells and in acute myeloid leukaemia. *Leukemia* **21**, 2495-2505 (2007).

196 Kuleshov, M. V., Jones, M. R., Rouillard, A. D., Fernandez, N. F., Duan, Q., Wang, Z., Koplev, S., Jenkins, S. L., Jagodnik, K. M., Lachmann, A., McDermott, M. G., Monteiro, C. D., Gundersen, G. W. & Ma'ayan, A. Enrichr: a comprehensive gene set enrichment analysis web server 2016 update. *Nucleic Acids Res* **44**, 3 (2016).

197 Zaldua, N., Llavero, F., Artaso, A., Galvez, P., Lacerda, H. M., Parada, L. A. & Zugaza, J. L. Rac1/p21-activated kinase pathway controls retinoblastoma protein phosphorylation and E2F transcription factor activation in B lymphocytes. *Febs J* **283**, 647-661 (2016).

198 Viatour, P., Somervaille, T. C., Venkatasubrahmanyam, S., Kogan, S., McLaughlin, M. E., Weissman, I. L., Butte, A. J., Passegue, E. & Sage, J. Hematopoietic stem cell quiescence is maintained by compound contributions of the retinoblastoma gene family. *Cell Stem Cell* **3**, 416-428 (2008).

199 Nishikimi, A., Uruno, T., Duan, X., Cao, Q., Okamura, Y., Saitoh, T., Saito, N., Sakaoka, S., Du, Y., Suenaga, A., Kukimoto-Niino, M., Miyano, K., Gotoh, K., Okabe, T., Sanematsu, F., Tanaka, Y., Sumimoto, H., Honma, T., Yokoyama, S., Nagano, T., Kohda, D., Kanai, M. & Fukui, Y. Blockade of inflammatory responses by a small-molecule inhibitor of the Rac activator DOCK2. *Chem Biol* **19**, 488-497 (2012).

200 Zhang, Q., Davis, J. C., Lamborn, I. T., Freeman, A. F., Jing, H., Favreau, A. J., Matthews, H. F., Davis, J., Turner, M. L., Uzel, G., Holland, S. M. & Su, H. C. Combined immunodeficiency associated with DOCK8 mutations. *N Engl J Med* **361**, 2046-2055 (2009).

201 Dobbs, K., Dominguez Conde, C., Zhang, S. Y., Parolini, S., Audry, M., Chou, J., Haapaniemi, E., Keles, S., Bilic, I., Okada, S., Massaad, M. J., Rounioja, S., Alwahadneh, A. M., Serwas, N. K., Capuder, K., Ciftci, E., Felgentreff, K., Ohsumi, T. K., Pedergnana, V., Boisson, B., Haskologlu, S., Ensari, A., Schuster, M., Moretta, A., Itan, Y., Patrizi, O., Rozenberg, F., Lebon, P., Saarela, J., Knip, M., Petrovski, S., Goldstein, D. B., Parrott, R. E., Savas, B., Schambach, A., Tabellini, G., Bock, C., Chatila, T. A., Comeau, A. M., Geha, R. S., Abel, L., Buckley, R. H., Ikinciogullari, A., Al-Herz, W., Helminen, M., Dogu, F., Casanova, J. L., Boztug, K. & Notarangelo, L. D. Inherited DOCK2 Deficiency in Patients with Early-Onset Invasive Infections. *N Engl J Med* **372**, 2409-2422 (2015).

202 Shi, H., Liu, C., Tan, H., Li, Y., Nguyen, T. M., Dhungana, Y., Guy, C., Vogel, P., Neale, G., Rankin, S., Feng, Y., Peng, J., Tao, W. & Chi, H. Hippo Kinases Mst1 and Mst2 Sense and Amplify IL-2R-STAT5 Signaling in Regulatory T Cells to Establish Stable Regulatory Activity. *Immunity* **49**, 899-914 (2018).

203 Wang, T., Yu, H., Hughes, N. W., Liu, B., Kendirli, A., Klein, K., Chen, W. W., Lander, E. S. & Sabatini, D. M. Gene Essentiality Profiling Reveals Gene Networks and Synthetic Lethal Interactions with Oncogenic Ras. *Cell* **168**, 890-903 (2017).

204 Wu, M., Hamaker, M., Li, L., Small, D. & Duffield, A. S. DOCK2 interacts with FLT3 and modulates the survival of FLT3-expressing leukemia cells. *Leukemia* **31**, 688-696 (2017).

205 Stieglitz, B., Bee, C., Schwarz, D., Yildiz, O., Moshnikova, A., Khokhlatchev, A. & Herrmann, C. Novel type of Ras effector interaction established between tumour suppressor NORE1A and Ras switch II. *Embo J* **27**, 1995-2005 (2008).

206 Yang, J., Zhang, Z., Roe, S. M., Marshall, C. J. & Barford, D. Activation of Rho GTPases by DOCK exchange factors is mediated by a nucleotide sensor. *Science* **325**, 1398-1402 (2009).

207 Worthylake, D. K., Rossman, K. L. & Sondek, J. Crystal structure of Rac1 in complex with the guanine nucleotide exchange region of Tiam1. *Nature* **408**, 682-688 (2000).